Quantification of terrestrial weathering and contamination in meteorites recovered in the Sultanate of Oman

Inauguraldissertation
der Philosophisch-naturwissenschaftlichen Fakultät
der Universität Bern

Vorgelegt von

Florian Johann Zurfluh

von Isenthal, UR

Leiter der Arbeit: PD Dr. Beda A. Hofmann,
Naturhistorisches Museum der Burgergemeinde Bern

Ko-Leiter: PD Dr. Edwin Gnos,
Muséum d'Histoire Naturelle de la Ville de Genève

Ko-Leiter: Dr. Urs Eggenberger,
Institut für Geologie, Universität Bern

Koreferent: Prof. Dr. Jochen Schlüter,
Mineralogisches Museum, Universität Hamburg

Quantification of terrestrial weathering and contamination in meteorites recovered in the Sultanate of Oman

Inauguraldissertation
der Philosophisch-naturwissenschaftlichen Fakultät
der Universität Bern

Vorgelegt von

Florian Johann Zurfluh

von Isenthal, UR

Leiter der Arbeit: PD Dr. Beda A. Hofmann,
Naturhistorisches Museum der Burgergemeinde Bern

Ko-Leiter: PD Dr. Edwin Gnos,
Muséum d'Histoire Naturelle de la Ville de Genève

Ko-Leiter: Dr. Urs Eggenberger,
Institut für Geologie, Universität Bern

Koreferent: Prof. Dr. Jochen Schlüter,
Mineralogisches Museum, Universität Hamburg

Von der Philosophisch-naturwissenschaftlichen Fakultät angenommen.

Der Dekan:
Bern, 14.12.2012   Prof. Dr. Silvio Decurtins

Acknowledgments

I will fondly keep in mind the years I could participate in the Omani-Swiss meteorite search and research project with all those positive and informative moments. In this section I would like to thank all the people, who provided considerable help to my PhD-Thesis and thus are responsible for the *good vibrations*:

First of all, I have to thank the leader of the project and my main supervisor, Beda A. Hofmann. His infective inquisitiveness to understand every detail, his broad knowledge of mineralogy, optical microscopy and his creative way to solve problems helped to find a path out of many labyrinths. I'm especially grateful for his time and patience he invested in the extremely detailed corrections of my written work or the endless performance of HHXRF analyses on meteorites. I am also grateful for the possibility to participate at several events at the Natural History Museum such as the public nights at the museum.

My second supervisor, Edwin Gnos, is thanked for sharing his wide knowledge in geology of Oman, geology in general and electron microanalysis. His childish-funny, inquiring habit and well-trained eyes enriched the experience during field- and laboratory-work. I enjoyed also every working-visit at the Natural History Museum of Geneva.

The third supervisor, Urs Eggenberger, I thank for his confident behavior and since he was not a meteorite-researcher before, providing a view from another perspective. His critical comments, his immense experience in X-ray analytics, data logging and database expanded significantly the dimension of the project. I appreciate also the possibility to attend his coURSes, which widened my horizon.

A fundamental part of the thesis presented here is the fieldwork, which I could complete in 2009, 2009/2010 and 2012. I would like to thank the Directors of the Directorate General of Minerals, Ministry of Commerce and Industry: Salim Omar Abdullah Al-Ibrahim, Salim Al-Buseidi, Sami Al Zubaidy and Akram Hassan Abdullah Al-Murazza for the permission and aid during fieldwork. Mohammed Al-Suleimani and Khalid Al-Tobi are thanked for bureaucratic and logistical support. It was always pleasant to be a guest in the beautiful and friendly Sultanate of Oman.

I am grateful to the fieldwork participants for the help with finding meteorites, cooking delicious menus, disputes about all kind of topics and identification of stars at night. This includes:
Ali Al Rajhi, Ali Al-Kathiri, André Piuz, Annette Bretscher, Beda Hofmann, Christian Meister, Christoph Opitz, Edwin Gnos, Elise Wimmer, Emilie Janots, Frank Preusser, Jan Walbrecker, Karl Wimmer, Mariana Cosarinsky, Martin Fisch, Mathias M. M. Meier, Mohammed Al-Ayrami, Mohammed Al-Battashi, Musallam Al-Maashani, Nathalie Dalcher, Nicolas Greber, Reto Trappitsch, Salim Al-Shahri, Salim Bakhit Al-Kathiri, Silvio Lorenzetti, Thomas Rosenberg and Urs Eggenberger.

To my precursor, Ali Al-Kathiri, I would like to say shukran for the support in the field, answering my questions, placement of the temperature logger in mid June in the middle of

شكرا

Contents

Contents

Summary

This PhD thesis was realized within the frame of the joint Omani-Swiss meteorite search and research project, which was launched in 2001 and focuses on the quantification of weathering and contamination of ordinary chondrites. All meteorites found during the 2009 and 2010 campaigns were classified using optical and electron microscopy techniques. Terrestrial ^{14}C ages of 101 samples were determined by Prof. Dr. A. J. T. Jull, University of Arizona, Tucson. All ^{14}C dated samples and all meteorites found in 2009 and 2010 were examined macroscopically for weathering features and measured with non-destructive handheld X-ray fluorescence (HHXRF) for bulk chemical composition and terrestrial contamination. Thirty-one samples were studied for contamination with water-soluble salts by leaching experiments. In addition to meteorites from Oman, samples found in Saudi Arabia, the Sahara and Australia were investigated for macroscopic weathering features and chemical contamination by HHXRF. The large amount of data from this and previous studies has been compiled in a newly built FileMaker database. This database allows quick extraction of relevant data, e.g. for evaluation of weathering properties using geographical information systems (GIS).

A HHXRF (NITON XL3t-600) instrument was tested for precision, accuracy and suitability in meteoritics. With a measuring time of 300 s, it is possible to collect accurate data for K, Ca, Ti, Cr, Mn, Fe, Co, Ni, Sr and Ba that are needed for the identification and classification of meteorites as well as the quantification of terrestrial contamination. The instrument was calibrated with the use of well-analyzed meteorite standards. Relative errors of 10% to 20% are reached for the mentioned elements. The instrument was tested successfully during field- and laboratory-work.

Contamination and weathering features on meteorites from Oman and other hot deserts were studied. Meteorites from Oman showed high contamination of Sr and Ba (up to 100x initial concentration inside) and Sr/Ba ratios of >1.2. Australian and Saharan meteorites show also relatively high concentrations of Sr and Ba but have, in contrast, low Sr/Ba ratios. In Oman and Sahara Sr/Ba ratios of meteorites and soils from the same locality are similar, implying

the control of soil on meteorite Sr and Ba contamination. This is supported by Sr-isotope data showing that meteorite-soil pairs from Oman have similar $^{87}Sr/^{86}Sr$ isotope signatures. Due to wind ablation, Oman meteorites show only low enrichment of manganese on surfaces (desert varnish). Manganese was found in higher concentrations on Saharan and especially Australian meteorites.

The influence of water-soluble salts on weathering of ordinary chondrites (OC) from the hot desert of Oman was evaluated in a comprehensive study. This work includes leaching experiments to extract water-soluble ions from OC and from soil samples, petrographical studies on alteration features and pore space fillings, and in situ recording of temperature variation in an OC and soil. A strong chemical gradient exists between reduced phases in freshly fallen meteorites and the oxidizing atmosphere. Salts from carbonate-rich soil that are dissolved in rain or fog water are soaked into the meteorite by capillary forces. Daily heating and cooling (mean measured daily temperature variations is 34.3°C) of the meteorites cause a pumping effect resulting in a strong concentration of soluble ions in meteorites over time. Dominant soluble ions detected in soils (n=35) are Cl^-, Na^+, SO_4^{2-}, Ca^{2+} and HCO_3^- while the leachates of the OC samples from Oman (n=31) contain mainly SO_4^{2-}, Cl^-, Ca^{2+}, iron and Mg^{2+}. The median total concentration of water-soluble salts in soils is relatively low (~960 µg/g) but depends on geographical location. Median total concentration of water-soluble salts in bulk meteorites is 2500 µg/g, but reaches in extreme cases almost 9000 µg/g. The assemblages of water-soluble ions of the meteorites are a combination of ions infiltrated from the soil and ions mobilized during weathering of the meteorites. Thus, the salt contamination of OC depends on the degree of weathering and availability of water and not on the salt concentration in the soil. During initial stages of weathering alteration products close pore space but due to volume expansion and leaching of minerals new porosity is generated. Weathering processes are enhanced by sulfide (troilite) oxidation producing acidic conditions. When troilite is completely weathered the conditions in the meteorites getting less acidic and chemical weathering is slowed down.

Weathering features (macroscopic and microscopic) and chemical contamination patterns (e.g. Sr and Ba uptake) were recorded in over 100 ^{14}C-dated meteorites. They show a positive correlation with terrestrial residence time. For a better resolution of the weathering history, a

refined weathering scale based on thin sections and the current W0-W6 classification (Wlotzka 1993) was developed. It newly includes the intermediate steps WD3.0, WD3.3 and WD3.6 as well as WD4.0 and WD4.5. For 55 14C-dated meteorites, the terrestrial age was back calculated using macroscopic weathering features, refined weathering degree classification and amount of terrestrial elemental contamination. The resulted estimated terrestrial ages correlate well with the radiocarbon ages (r=0.77). This method for terrestrial age estimation was applied to all OC (n=295) found in 2009 and 2010. The resulting pattern shows a lack of young (<5 ka) and old (>30ka) samples, similar to the ^{14}C-dated population. The correlation between terrestrial age and the newly defined weathering subclasses W3.0-W4.5 demonstrates that the addition of these classes is meaningful and improves the terrestrial age estimation of OC found in Oman.

The detailed investigation of weathering and contamination features in meteorites linked with the study of the soil material, clarified the interaction of meteorites with hot desert environment and helped to reveal terrestrial histories of meteorites.

Urs and Al Huwaysah 005. Photo by Edwin Gnos.

ملخص

رسالة الدكتوراة هذه تم إعدادها ضمن إطار المشروع العماني–السويسري المشترك للبحث عن النيازك واستكشافها ودراستها والذي تم الشروع فيه منذ عام 2001م، وتركز هذه الدراسة على تقييم وحساب مدى تأثر النيازك الإعتيادية بعوامل التجوية وتلوثها بالعناصر الأرضية. جميع النيازك التي وجدت ضمن حملات البحث لعامي 2009 و2010م تم وصفها بإستخدام تقنيات الميكرسكوب البصري والميكروسكوب الألكتروني. وقد تم قياس العمر الأرضي لـ 101 عينة (منذ سقوطها على الأرض) بإستخدام الكربون المشع ^{14}C بالتعاون مع البروفسور A. J. T. Jull من جامعة أريزونا، توكسون، بالولايات المتحدة الأمريكية. جميع النيازك التي تم حساب عمرها الأرضي والتي وجدت في عامي 2009م و2010م تم فحصها يدويا لقياس مدى تعرضها للتجوية بإستخدام جهاز محمول يستخدم الأشعة السينية (HHXRF) دون الحاجة لتكسير العينات، ويقوم الجهاز بتحليل التركيبة الكيميائية للنيازك وتلوثها بالعناصر الأرضية. وقد تم دراسة واحدا وثلاثون عينة لقياس مستوى تلوثها بالعناصر التي تذوب في الماء وذلك بإستخدام تجارب الرشح. بالإضافة إلى النيازك العمانية، فقدم تم كذلك دراسة بعض النيازك من المملكة العربية السعودية، والصحراء الكبرى، وأستراليا للتحقق من مدى تأثرها بعوامل التجوية وتم تحليلها كيميائيا لقياس تلوثها بالعناصر الأرضية بإستخدام جهاز الأشعة السينية (HHXRF). هذا الكم الكبير من البيانات الناتجة عن الدراسات المشار إليها أعلاه والدراسات السابقة تم تجميعها في قاعدة بيانات تم تصميمها حديثا لهذا الغرض بإستخدام قاعدة بيانات الفايلميكر (FileMaker). وتسمح قاعدة البيانات هذه بسهولة إستخراج البيانات، فمثلا يمكن تقييم خواص عوامل التجوية بإستخدام نظام المعلومات الجغرافية (GIS).

تمت معايرة جهاز الأشعة السينية المحمول (HHXRF (NITON XL3t-600)) للتحقق من دقة قياساته ومدى ملائمتة لتحليل النيازك. بالإعتماد على مدة قياس تساوي 30 ثانية فإنه بالإمكان الحصول على نتائج دقيقة لعناصر الــ K, Ca, Ti, Cr, Mn, Fe, Co, Ni, Sr, Ba والتي نحتاجها لتمييز النيازك من الصخور الأخرى ووصفها، وكذلك لتقييم تلوثها بالعناصر الأرضية. وقد تمت معايرة الجهاز من خلال تحليل عينات مرجعية تم تحليلها مسبقا بدقة عالية. وقد أظهر التحاليل وجود

نسبة خطأ تتراوح بين 10% و 20% للعناصر المشار إليها. وقد تمت معايرة دقة الجهاز بنجاح أثناء العمل الميداني وفي المختبر.

تمت دراسة تأثير عوامل التجوية والتلوث الأرضي على النيازك في عمان والصحارى الحارة الأخرى. أظهرت نيازك سلطنة عمان إرتفاع كبير في تلوثها بـ Sr و Ba (قد يصل إلى 100 ضعف التركيز القياسي للنيازك) ومعدل Ba\Sr > 1.2. كذلك نيازك استراليا والصحراء الكبرى أظهرت إرتفاع في تركيز الـ Sr و Ba ولكنها على العكس أظهرت إنخفاض في معدل Ba\Sr. في عمان والصحراء الكبرى يتساوى تقريبا معدل Ba\Sr في النيازك والتربة المحيطة بها مما يدل على دور التربة في التأثير على تلوث النيازك بـ Sr و Ba، ويؤكد ذلك البيانات عن نظائر السترونشيوم (Sr) التي تظهر تطابق في تحاليل معدل $^{87}Sr\^{86}Ba$ في عينات النيازك والتربة من عمان. وتظهر النيازك العمانية إرتفاع طفيف فقط في المنجنيز على سطحها والذي عادة ينتج عن نحت الهواء لسطح النيازك في الصحراء (ورنيش الصحراء). يوجد المنجنيز بتركيز أكبر في نيازك الصحراء الكبرى و خصوصا في نيازك استراليا.

تم إجراء دراسة شاملة لتقييم تأثير الأملاح القابلة للذوبان في الماء على تجوية النيازك الإعتيادية من الصحاري الحارة في سلطنة عمان. وشمل هذا العمل أجراء تجارب الرشح لإستخلاص الأيونات الذائبة في الماء من النيازك الإعتيادية والتربة، ودراسة مظاهر تحلل الصخور والرواسب التي تتخلل الفجوات، وتسجيل مدى التغير في درجات الحرارة في أحد النيازك الذي ترك في الصحراء وفي التربة المجاورة له. لوحظ كيميائيا وجود علاقة ذات منحنى حاد بين المعادن الغير مؤكسدة وبين الغلاف الجوي المسبب للتأكسد وذلك في النيازك التي سقطت على الأرض حديثا. الأملاح، الموجودة في التربة الغنية بالكربونات، الذائبة بفعل الأمطار أو الندى سوف تمتصها النيازك بفعل الخاصية الشعرية. تسخين وتبريد النيازك خلال اليوم (يبلغ معدل التغير في درجات الحرارة اليوم 34.3 درجة مئوية) يؤدي إلى حدوث ظاهرة الضخ التي ينتج عنها حدوث تركيز عالي للأيونات الذائبة في النيازك مع مرور الوقت. الأيونات الأكثر تواجدا في التربة (35 عينة) هي $Cl^-, Na^+, SO_4^{2-}, Ca^{2+}$, HCO_3^- بينما وجد أن الأيونات التي رشحت من النيازك الإعتيادية (31 عينة) هي غالبا SO_4^{2-}, Cl^-, Ca^{2+} والحديد و Mg^{2+}. معدل مجموع تركيز الأملاح الذائبة في الماء منخفض نسبيا في عينات

التربة (~960 مايكروجرام/جرام)، ولكن هذا يعتمد على الموقع الجغرافي. معدل مجموع تركيز الأملاح الذائبة في الماء في عينات النيازك يساوي 2500 مايكروجرام/جرام، ولكن وصل التركيز إلى 9000 مايكروجرام/جرام كحد أقصى في بعض العينات. مجموعة الأيونات القابلة للذوبان في الماء الموجودة في النيازك هي عبارة عن تلك التي تسربت إلى النيازك من التربة المحيطة بالإضافة إلى تلك التي تحررت منها نتيجة لعوامل التجوية التي أثرت على النيازك. لذلك، فإن مقدار تلوث النيازك الاعتيادية بالأملاح يعتمد على درجة تجوية النيازك ووجود الماء وليس على مقدار تركيز الأملاح في التربة. في بداية تعرض النيازك لعوامل التجوية سوف يتم سد المسامات بفعل الرواسب الناتجة عنها ولكن زيادة حجم النيازك بالتمدد وإذابة المعادن سوف يؤدي إلى فتح مسامات جديدة. يتم تسريع عوامل التجوية عندما يتأكسد الكبريتيد (التروليت) الموجود في النيازك بسبب خلق بيئة حامضية. بعد أن يتأكسد التروليت بشكل كامل سوف تنخفض حامضية النيازك مما يؤدي إلى إبطاء عملية التجوية الكيميائية.

مظاهر التجوية (المشاهدة بالعين المجردة وبالمجهر) ومستويات التلوث الكيميائي (مثل إمتصاص الـ Sr و الـ Ba) تم رصدها ضمن أكثر من 100 عينة من النيازك تم تحديد عمرها الأرضي بإستخدام الكربون المشع C^{14}. وقد أظهرت علاقة طردية مع العمر الأرضي للنيازك. وفي سبيل الحصول على صورة أكثر وضوحا لتاريخ تجوية النيازك، فقد تمت مراجعة المقياس المعمول به حاليا لوصف مقدار التجوية والذي يعتمد على دراسة الشرائح الصخرية وتم تطوير التوصيف الحالي W0-W6 والذي أستحدثه فلوتسكا (Wlotzka 1993). وقد أدخلت هذه الدراسة بعض الخطوات الجديدة التي تتخلل التوصيف السابق مثل WD3.0 و WD3.3 و WD3.6 وكذلك WD4.0 و WD4.5. وبعد دراسة تفصيلية أجريت على 55 عينة من النيازك التي تم تحديد عمرها بإستخدام الكربون المشع C^{14}، فقد تم إعادة حساب عمرها الأرضي بإستخدام مظاهر التجوية المشاهدة بالعين المجردة وبتطبيق مقياس توصيف التجوية الجديد وبتحديد مدى تلوث النيازك بالعناصر الأرضية. وقد كانت نتيجة حساب العمر بهذه الطريقة متطابقة جدا مع تلك التي حسبت بإستخدام الكربون المشع. وقد تم تطبيق هذه الطريقة في حساب عمر النيازك الاعتيادية على 295 عينة وجدت في عامي 2009م و2010م. وقد أظهرت النتيجة إنخفاض عدد العينات الحديثة التي يبلغ عمرها أقل من 5000 سنة وتلك القديمة التي يزيد عمرها عن 30000 سنة، وهي متماثلة مع النتيجة التي أظهرها حساب العمر الأرضي بإستخدام

الكربون المشع. بالمقارنة بين حساب العمر الأرضي للنيازك والخطوات التي أدخلت على التوصيف الجديد للتجوية W3.0 إلى W4.5 فقد أظهرت النتائج بأن إضافة هذه الخطوات كان مفيدا جدا وقد أدى إلى تحسين تقديرات العمر الأرضي للنيازك الإعتيادية التي وجدت في سلطنة عمان.

الدراسة التفصيلية التي أجريت على التجوية وعوامل تلوث النيازك مقرونة بدراسة مواد التربة، أثبتت وجود تفاعل بين النيازك والبيئة الصحراوية الحارة وكذلك ساعدت على كشف التاريخ الأرضي للنيازك.

Abbreviations

Anh	Anhydrite
Ap	Apatite
AUS	Australia
Brt	Barite
BS	Buried surface
BSE	Back-scatter electron
Cal	Calcite
CL	Cathodo luminescence
Cls	Celestine
CP	Chemical parameter
CS	Cut surface
DB	Database
DV	Desert Varnish (rock varnish)
EMP	Electron micro probe
Eps	Epsomite
ES	Exposed surface
Fa	Fayalite
Fs	Ferrosilite
Fsp	Feldspar
Gp	Gypsum
Gth	Goethite
HHXRF	Handheld X-ray fluorescence
IC	Ion chromatography
ICP-OES	Inductive couple plasma optical emission spectroscopy
JaH	Jiddat al Harasis
Jrs	Jarosite
KSA	Kingdom of Saudi Arabia
Ksr	Kieserite
LOD	Limit of detection
Mrl	Merrillite
MWP	Macroscopic Weathering Parameter
MWPA	Macroscopic weathering parameter
NS	Natural surface
OC	Ordinary Chondrite
Ol	Olivine
OSMS	Oman-Swiss meteorite search (project)
QaM	Qarat al Milh
RaS	Ramlat as Sahmah
RaW	Ramlat al Wahibah
RFL	Reflected light
SaU	Sayh al Uhaymir
SDD	Silicon drift detector
SEM	Scanning electron microscopy
Tro	Troilite
UaS	Umm as Samim
Wo	Wolastinite

Introduction and background

1.1. Meteorites

Meteorites are natural, solid objects that have fallen to another body larger than itself (Rubin and Grossman, 2010). Most meteorites that have reached Earth have their origin in the asteroid belt between Mars and Jupiter. They provide a window to the early formation of the Solar System and are an important resource for science. Several types of meteorites exist, which are grouped using properties of their mineralogy, petrology, bulk chemistry or oxygen isotopes (e.g. Weisberg et al., 2006) as displayed in Figure 1.1. A general distinction is made between undifferentiated (chondrites, primitive achondrites) and differentiated meteorites (achondrites). For more details of classification and grouping of meteorites see recent summarizing literature (Bischoff, 2001a; Bischoff, 2001b; Mittlefehldt, 2008; Mittlefehldt et al., 1998; Norton and Chitwood, 2008; Weisberg et al., 2006).
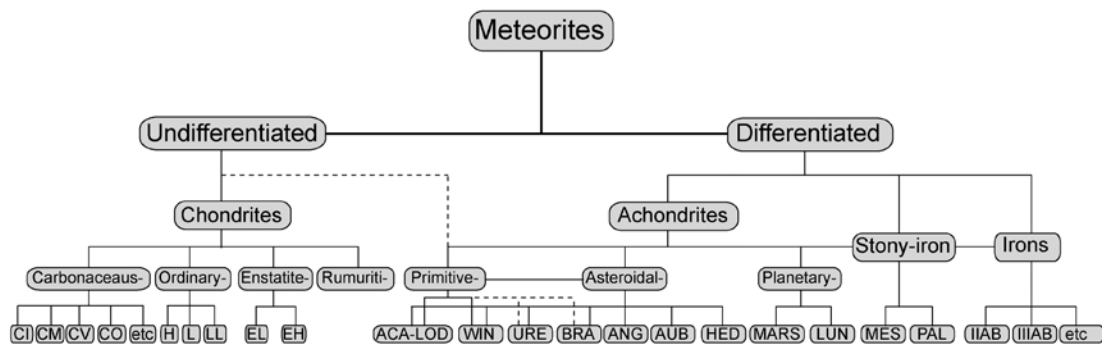
Figure 1.1. Meteorite classification tree. For simplification, not all groups are listed. If more groups are present, it is indicated by "etc". Ungrouped achondrites and chondrites (including the K chondrite grouplet) were excluded. Brachinites (BRA) and ureilites (URE) show characteristics of both, primitive and differentiated meteorites (indicated by dashed lines). HED summarizes howardites, eucrites and diogenites; MARS are meteorites from Mars and include shergotittes, nakhlites, chassingites ("SNC-group") and one orthopyroxenite. For other meteorite trees and abbreviations, which were used as basis, see Bischoff, (2001a; 2001b), Weisberg et al., (2006) and Norton and Chitwood, (2008).

The most abundant types of meteorites are chondrites (86.3 % of meteorite falls according to the Meteoritical Society database, http://www.lpi.usra.edu/meteor/metbul.php), which are dominated by ordinary chondrites (93.2% of chondrite falls). They are built of small silicate spherules called

chondrules, which are fast cooled melt droplets that were accreted in the protoplanetary disk at the beginning of the formation of the Solar System (e.g. Brearley and Jones, 1998; Hewins and Zanda, 2012). Chondrites are the most primitive meteorites, which are virtually unchanged since early solar system times. Because meteorites have formed in other environments than are present now on Earth, they are not stable when reaching our planet.

Meteorites can be observed to fall and be collected immediately afterwards. Such meteorites are called *falls* and show usually no terrestrial modification. However, most meteorites are found by chance, mostly during systematic searches. Such samples are called *finds* and are normally altered by terrestrial weathering. Ideal areas for systematic searches of meteorites are dry and geomorphologic stable environments, which lowers weathering rates and allow meteorite accumulation. Helpful for meteorite recovery are bright soils without vegetation. The central desert of the Sultanate of Oman on the Arabian Peninsula fulfills these criteria (Chapter 1.4, 1.5, 1.11). Other hot desert meteorite accumulation areas are listed in Chapter 1.2 and a more detailed characterization of meteorite accumulation surfaces form Oman in Chapter 1.11.

1.2. Weathering of hot desert meteorites

A large number of meteorites are recovered from Oman and other hot desert, which are now a major source of meteorites used for research. To understand which features are due to terrestrial residence and what is still original, the study of terrestrial weathering is important (e.g. Bland et al., 2006). Research with the focus of terrestrial weathering and contamination have been preformed including the study of alteration mineralogy (Al-Kathiri et al., 2005; Lee and Bland, 2004), quantification of chemical contamination (Al-Kathiri et al., 2005; Crozaz et al., 2003; Hezel et al., 2011), quantification of the degree of oxidation by Mössbauer spectroscopy (Bland et al., 1998) or iron isotope analyses (Saunier et al., 2010). The grade of weathering is classified by optical microscopy (Wlotzka, 1993). For weathering rate determination, the time span the meteorites have been on Earth is important. Such terrestrial ages of hot desert meteorites can be determined using the ^{14}C method (Jull, 2006).

In a precursor project (Al-Kathiri, 2006) the fundament for the current study was built. There, ordinary chondrites (OC) collected in Oman were studied for weathering effects, which were detected macroscopically, microscopically and in bulk chemistry (Al-Kathiri et al., 2005). They were investigated on their dependence on terrestrial age.

1.3. Goals of the study

The focus of this PhD is to study in detail selected weathering and contamination effects of meteorites (mainly ordinary chondrites) found in Oman by the Omani-Swiss meteorite search team (Chapter 1.7) and study the interaction of the terrestrial environment with the meteorites. Based on the results obtained from samples found in Oman, meteorites recovered in Saudi Arabia, Sahara and Australia were investigated for comparison. Quantification of chemical contamination was performed with a new type of handheld X-ray fluorescence (HHXRF) instrument, which was not used in meteoritics before. A major task was to test and calibrate a HHXRF for its precision, accuracy and evaluate possible applications for meteorite studies (Chapter 3). One valuable application is the quick quantification and location of Sr and Ba contamination (Chapters 3, 4 and 6), which is a prominent feature of hot desert meteorites (e.g. Al-Kathiri et al., 2005; Hezel et al., 2011; Saunier et al., 2010; Stelzner et al., 1999). Macroscopic weathering features were recorded for all meteorites analyzed by HHXRF to investigate whether variations of weathering intensity are linked to geographical provenance or terrestrial age (Chapter 4 and 6). A significant number of meteorites from Oman show hygroscopic behavior or efflorescence of water-soluble salts during storage. Such behavior has not been described previously and at the beginning of this study it was not clear what kind of salts are present, how their presence in meteorites can be explained and what their influence on weathering might be. In Chapter 5 a comprehensive investigation of these water-soluble salts within OC from Oman is presented. In a summarizing study, the dependence of chemical contamination, macroscopic weathering features (including salt contamination) and weathering classification on ^{14}C terrestrial ages was investigated and a relative simple method for terrestrial age estimation was developed (Chapter 6).

The current weathering classification was based on an abstract that was published nearly 20 years ago (Wlotzka, 1993). Even though it provides a relative simple and easy way to determine the degree of terrestrial alteration as seen in thin section, some weathering steps were not unambiguously defined. A goal of this study was also to refine the weathering classification and evaluate its correlation to terrestrial age, at least for OC from Oman (Chapter 6).

The investigations of chemical contamination and macroscopic weathering features (Chapters 4 and 6) as well as the study of water-soluble salts in meteorites from Oman (Chapter 5) used soil samples collected during the meteorite search campaigns to study the interaction of meteorites with the environment.

A basis for the proper research on meteorites and the organization of all related data, a Filemaker database described in Appendix A was established. The classification of all meteorites found during fieldwork related to this project was another prerequisite for this work (classification of 2009/2010 meteorites is in Appendix B).

The purpose of this dissertation is to evaluate how the macroscopic and microscopic investigation of meteorites combined with HHXRF and other complementary analyzes can be used for an estimation of terrestrial ages and how these data can give an indication in which geographic area a specific meteorite was recovered. The interaction between meteorites and soil is crucial for weathering studies. Therefore, a special focus was put on the contamination of meteorites from Oman by Sr and water-soluble salts.

1.4. Geographical and geological settings of Oman

The Sultanate of Oman, a country with an area of ~309'500 km^2 located at the south-eastern corner of the Arabian Peninsula (Fig. 1.2), is an ideal environment to collect meteorites for the study of weathering and contamination. It is bordered by Yemen in the south, Saudi Arabia in the west and United Arab Emirates in the north. The coast is flanked by the Arabian Sea in the east and the Arabian Gulf in the north (Fig. 1.2). In Miocene, the current land surface was covered by seawater and limestone rocks were deposited. After uplift and sea regression, they weathered and a desert pavement surface evolved, which is relatively stable and allowed meteorite accumulation over time.

In the north, due to the collision with the Eurasian plate, ophiolite material builds up the Oman Mountains (Fig. 1.2) with the highest point Jabel Akdahr (3000 m above Sea level) was reexposed to surface (e.g. Fookes and Lee, 2009; Le Métour et al., 1995); Le Métour et al., 1995). The eroded material from the Oman Mountains was transported towards south into the flat in land depression from late Miocene to Pliocene (Blechschmidt et al., 2009). These alluvial fans reach south to ~21°N and are composed of gravels of black ophiolitic material, dark grey limestones and black-weathering cherts. Even though these surfaces are now flat and homogeneous, it is very difficult to find meteorites, especially smaller sized ones, due to the high abundance of black rocks. Intense search for meteorites during mapping of alluvial fan area yielded only one meteorite find (Bühler et al., 2006).

The central Oman desert can be divided into further geomorphological areas such as the sand dune area (Rub al Khali, Wahiba sands), sabkha deposit (Umm as Samim) and desert pavement surfaces of Dhofar, Jiddat al Harasis and Sayh al Uhaymir areas (Fig. 1.2). The desert pavement surfaces are best suited for meteorite accumulation and meteorite recovery (Chapter 1.11).
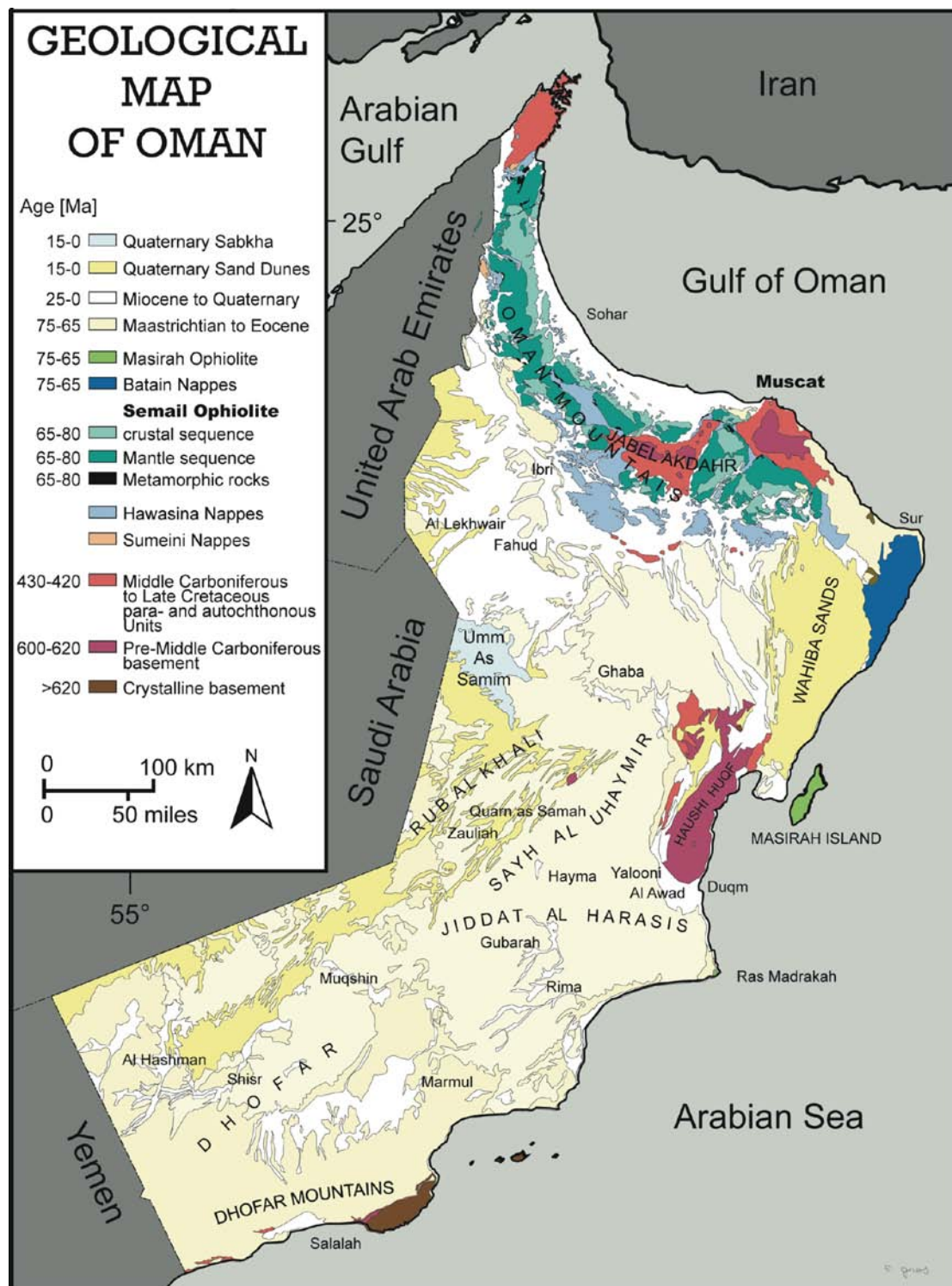
Figure 1.2. *Simplified geological overview map of Oman indicating the ages of the surfaces. Edwin Gnos has compiled and drawn the map based on Glennie et al., (1974), Le Métour et al., (1993), Peters et al., (1995) and Peters et al., (2001). FJZ made some modifications. Regional names are capitalized; for Meteoritical Society nomenclature names see Figure 1.4.*

1.5. Present climate and climate history of Oman

Present climate of Arabia is arid, especially in the inland desert where the meteorite accumulation surfaces are located. There, mean annual precipitation usually is below <70 mm (Edgell, 2006; Fisher, 1994), which is suited for meteorite preservation. However, during Quaternary history the climate conditions changed several times and episodes of more humid conditions occurred. Climate history was reconstructed using geological archives such as speleothem record (e.g. Fleitmann et al., 2003a; Fleitmann et al., 2003b), aeolian deposits (Preusser et al., 2002), lacustrine lake sediments (e.g. Parker et al., 2006) or event stratigraphy (Glennie and Singhvi, 2002). Relevant for the meteorites that are still present today is at least the more humid period between 10 to 5.5 ka ago and a probable time of more humid conditions at 35-20 ka (Preusser, 2009). Speleothem records date the pluvial conditions from 10.5 to 6.3 ka before present (Fleitmann and Matter, 2009). Today, the Indian Summer Monsoon (ISM) reaches only the costal region around Salalah in the south of Oman and is correlated to the intertropical convergence zone (ITCZ, Fig. 1.3). The ITCZ was moved about 500 km inland during the wetter periods (Burns et al., 2003; Burns et al., 2001; Fleitmann et al., 2011; Neff et al., 2001) and reached the Oman inland areas where most of the meteorites were found. Towards the coast, vegetation (small shrubs and acacia trees) is more abundant and rocks are more frequently covered with lichen (Chapters 2, 3 and 4), which is the result of higher humidity due to ISM or coastal winds (Edgell, 2006).
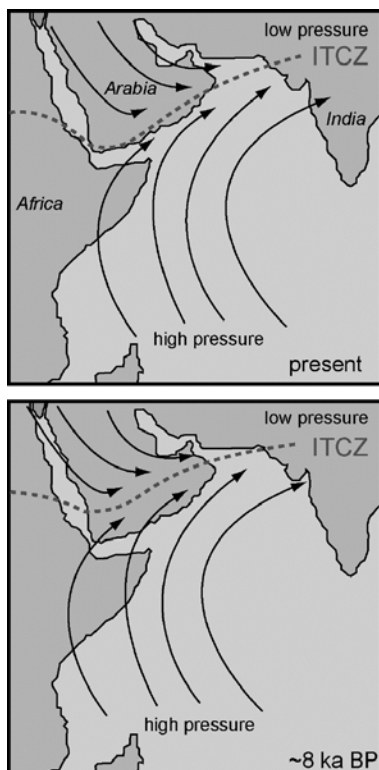
Figure 1.3. *Distribution of current summer ITCZ line and the situation about 7-8 ka ago. Today, only the costal regions of South Oman suffer monsoon precipitation. Redrawn after Fleitmann et al., (2007).*

Winds have a strong influence on landscape development of the desert. The current situation with large sand dunes in the Rub al Khali and deflation planes in between is

the result of long-term stable wind systems. Nowadays, the position of the dunes is stable (Edgell, 2006). Winds have blown out the fine-grained material between limestone pebbles, which lead to the formation of desert pavement surfaces. Current winds in central Oman are dominated either from north or south. Winds from north are usually dry whereas winds from south are humid (Chapter 1.12). Abundant wind and transported soil material are responsible for relative strong wind erosion features on meteorites from Oman (Chapters 2, 4 and 6).

Meteorites, especially ordinary chondrites, might have also the potential to be used as climate archives since their terrestrial ages can be determined and their pre-terrestrial compositions and properties are well defined from falls (Bland, 2006; Lee and Bland, 2003). Even though some studies focusing on climate conditions and meteorite weathering rates were preformed, no unambiguous parameter could be defined or was extracted so far (Bland et al., 1998). The investigations presented here focus on weathering history, which is partly controlled by climate. But no strong correlations between weathering or contamination features with the climate history were recognized (Chapter 6).

Terrestrial ages of meteorites are needed for climate studies. Chapter 6 presents a relative simple way to estimate the terrestrial ages of ordinary chondrites from Oman based on macroscopic observations, weathering degree and chemical composition.

1.6. Meteorite search areas

Systematic searches for meteorites started in the mid 1970s in Antarctica, where meteorites are accumulated on stranding areas due to glacier movement and ice ablation (Harvey, 2003). In addition, due to low temperatures and restricted exposure to liquid water, weathering rates are extremely low, which allows meteorite preservation. Most of meteorite stranding areas contain nearly no terrestrial rocks, which makes meteorite spotting relatively easy. However, logistics for Antarctic meteorite search is complex and expensive. More simple are searches in hot and dry environments. Soon after the start of Antarctic programs, meteorites were systematically searched on dry lakes in western US (Rubin et al., 2000; Zolensky et al., 1992; Zolensky et al., 1990) and on calcareous (clay) desert of South Western

Australia (Bevan and Binns, 1989a; Bevan and Binns, 1989b; Bevan and Binns, 1989c; Bevan et al., 1998; Bevan et al., 2001). Then, searches were performed in the Sahara desert (Bischoff and Geiger, 1995; Otto, 1992; Ouazaa et al., 2009; Schlüter et al., 2002) and the Arabian Peninsula (Al-Kathiri et al., 2005; Franchi et al., 1996; Franchi et al., 1995; Gnos et al., 2009a; Hezel et al., 2011; Holm, 1960). A more detailed history of meteorite search in Arabia is presented in Chapter 1.7. Due to the high aridity, the Atacama Desert in South America is also well suited for meteorite accumulation (Gattacceca et al., 2011; Munoz et al., 2007). Beside scientific searches, a lot of meteorites, especially from the Sahara, are found by private meteorite hunters and local inhabitants. The big advantage of hot desert meteorites as compared to the situation in Antarctica is that they are found on the site of fall. This allows, if documentation is done properly, recognizing strewn fields and helps to estimate pairing corrected fall rates.

1.7 Meteorites from Oman

Before this century, not many meteorites were known from Arabia, with the exception of the iron fragments found at the Wabar craters, which were discovered by Philby, (1933). Holm (1962) has described some meteorite finds in the Rub al Khali (Saudi Arabia), which were made due to oil exploration. In Oman, one of the earliest found meteorites is the L5 chondrite Ghubara, that was found in 1954 (Krinov, 1959). (Franchi et al., 1995) made an evaluation of the meteorite find potential of the JaH and Rub al Khali areas in Oman. The found samples of this short expedition were analyzed and compared with meteorites from other localities. Meteorites from Oman were slightly stronger oxidized as compared to those from Australia and Libya but at similar rates as such from Roosevelt County (Franchi et al., 1996), which lead them to conclude, Oman to be a good accumulation area for meteorites. After some calm years, meteorite rush started about 1999, where a lot of meteorites were found with an incredible amount of special meteorites such as lunar and Martian meteorites (Grossman, 2000; Grossman and Zipfel, 2001; Russell et al., 2002; 2003; 2004). Then, in 2001 the Omani-Swiss meteorite search and research project was initiated (for more details see Chapters 1.8 and 2).

1.8. General goals of the Omani-Swiss meteorite project

Between 2001 and 2012, 11 campaigns of the joint Omani-Swiss meteorite search group took place, which yielded 5637 samples that represent at least 759 fall events. Further details of the individual campaigns are listed in Table 1.1. Meteorites collected during the project are classified and curated at the Natural History Museum Bern where also some pieces are on exhibition. So far, most of the investigations were performed in laboratories outside of Oman. It is planned to keep up the transfer of knowledge to Oman and to build up museum(s) for public outreach in Oman.

Table 1.1. Summary of Oman-Swiss meteorite search campaigns, 2001-2012.

Year	Number of meteorites	Unpaired samples	Mass [kg]	Duration [d]	Man days [d]	Search [km]	km/find	Finds by foot*
2001	186	41	42	24	59	1773	39	0
2002	1066	32	531	26	83	2717	65	0
2002/03	2460	136	661	93	209	7618	36	2
2005	204	68	235	41	151	3114	42	15
2006	515	42	2088	30	96	1668	30	3
2007	554	56	295	30	104	2667	37	1
2008	108	50	59	15	58	2661	29	2
2009	143	92	123	39	177	6604	48	2
2009/10	165	107	130	40	176	4479	36	39
2011	96	75	52	23	117	2597	39	12
2012	140	60	71	24	133	4099	55	10
Total	5637	759	4287	385	1363	39997	41[§]	86

*Not including obviously paired strewn field samples.

[§] Mean km/find of all campaigns.

The main intend of the OSMS-project it to collect a significant number of well-documented meteorites for research. This provides the basis for (i) statistics of meteorite find density and abundance of types, (ii) understanding accumulation and destruction mechanisms in the hot desert of Oman, (iii) study of rare meteorites, and (iv) the study of abundance and dynamics of strewn fields.

(i) Statistics

This task includes (a) the meteorite density or find density and (b) the abundance of meteorite types.

(a) Based on long-term experience and systematic searches, mainly by foot, find density for central Oman is about 1 to 4 fall/km^2. Find density can be reached from

searched kilometers and the number of finds. In average, one has to drive approximately 41 km to find a meteorite (Table 1.1).

(b) Beside the question of how many meteorites falling to Earth (a) it is also interesting to study, which type hit in which frequency Earth. As for falls, the population of Oman is dominated by ordinary chondrites. Since achondrites have lower weathering rates due to the lack of metallic minerals that are very susceptible to weathering (Chapters 5 and 6), they can survive longer times and therefore occur in higher proportions (Korotev, 2012). As for example the meteorites with the oldest terrestrial ages from Oman are the lunar meteorite Dhofar 025 with 500-600 ka (Nishiizumi and Caffee, 2001) and the shergottite Dhofar 019 with 360 ka (Nishiizumi et al., 2002). Oman has a high abundance of lunar meteorites over chondrites as compared to other accumulation areas, which might be the result of higher accumulation due to higher resistance against weathering, or a result of selected search for rare meteorites and/or not classification or officialisation of most ordinary chondrites (Korotev, 2012, references therein).

(ii) Accumulation/destruction

Goal (i), the find density, takes mostly the mechanisms of accumulation into account and is a result of recovery rate. To understand this process, the mechanisms of preservation are important to know. But it is also crucial to recognize, how a meteorite is destroyed. Chapters 4, 5 and 6 provide details about aspects of weathering of meteorites from Oman. Chapter 2 gives a general overview of weathering and contamination of meteorites from Oman.

(iii) Rare meteorites

Rare meteorite types such as the martian shergottite SaU 094 (Gnos et al., 2002), the unique lunar (regolith) breccia SaU 169 , the first meteorite where the provenance on the parent body could be determined (e.g. Al-Kathiri et al., 2007; Gnos et al., 2004), the ureilitic impact melt breccia JaH 422 (Janots et al., 2011), the iron poor mesosiderite JaH 203 (Bretscher, 2011), the only iron meteorite found so far in Oman, Shisr 043 (Al-Kathiri et al., 2006) are subject for detailed studies. In Appendix B the meteorites that are classified during this PhD project are listed. Separate entries for rare meteorites are available from the database of the Meteoritic Society.

(iv) Strewn fields/strewnfields.

Most meteorites break into several fragments in the atmosphere and the pieces are distributed in so-called strewn fields. Such meteorites are paired and generally share

relevant properties crucial for classification. Since hot desert meteorites are usually found at the place of their fall, the mass distribution of such meteorite showers can be studied and allows reconstruction of fall dynamics (e.g. Wimmer et al., 2009; 2012). Large strewn fields found in Oman are JaH 073, L6 S4 (Gnos et al., 2009b; Huber et al., 2008); JaH 091, L5 S2 (Boschetti, 2011; Gnos et al., 2006; Zurfluh, 2008); SaU 001, L4-5 S2 (Korochantsev et al., 2003); Dhofar 020 (H4/5 S4), Shisr 015 (L5 S2) and RaS 418 (L6 S5).

Some samples of one of the largest strewn fields on Earth, the JaH 091 shower (Gnos et al., 2006; Zurfluh, 2008), were investigated for their content of water-soluble salts (Chapter 5). We found a large diversity of weathering grades and amounts of salts within meteorites from a single fall event that implies local condition to control weathering and not only the terrestrial residence time.

1.9. Meteorite names

A unique label for each meteorite find is used that is composed of the year of the campaign, the moth of recovery and a serial number, e.g. 0901_010 was found during the campaign in 2009 (**09**01_010) in January (09**01**_010) and was the tenth sample (0901_**010**). When a meteorite is fully characterized the classification is submitted to the Meteoritical Society with the coordinates from where the meteorite gets the official name (Appendix B). For falls, the name usually is derived from the closest post-office. For finds from dense accumulation areas, a name of the recovery area followed by a serial number is introduced. Nomenclature areas for Oman are defined in Al-Kathiri et al., (2005), an overview including the find locations of meteorites in Oman is given in Figure 1.4. For this reason, meteorite 0901_010 obtains the official name Umm as Samim 011 (or shortened UaS 011). All data of the meteorites is collected in a FileMaker database (Appendix A).
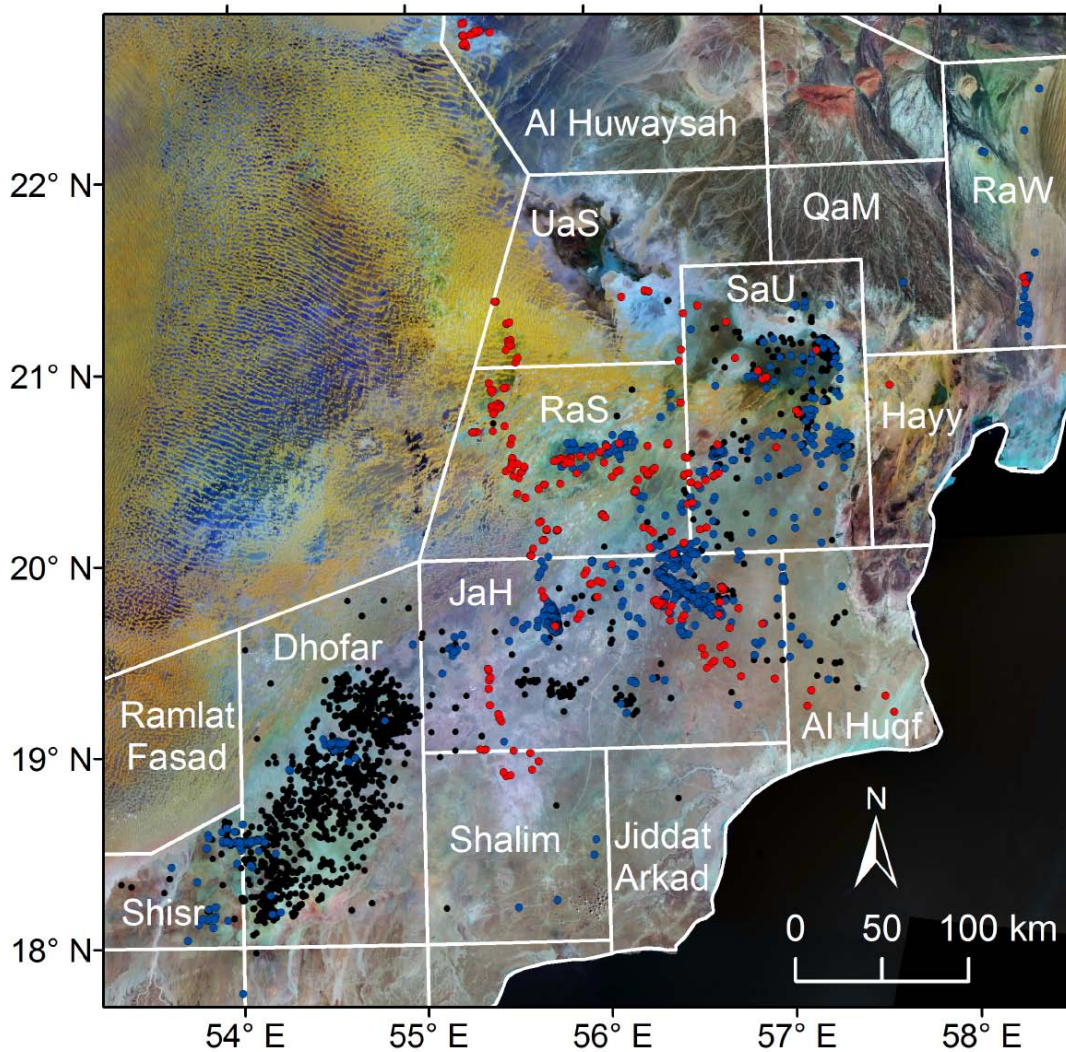
Figure 1.4. *Meteorite nomenclature areas and meteorite finds from Oman on false-color Landsat 7 images. Black dots are meteorite finds from Meteoritical Society database; blue dots are finds from Oman-Swiss team (OSMS) and red dots are meteorite finds from 2009 and 2010 campaigns of OSMS. Not displayed are meteorite finds of the Oman-Swiss group from 2011 and 2012.*
Nomenclature areas:
JaH: Jiddat al Harasis, QaM: Qarat al Milh, RaW: Ramlat al Wahibah, RaS: Ramlat as Sahmah, SaU: Sayh al Uhaymir and UaS: Umm as Samim.

1.10. Suited surfaces for meteorite recovery in central Oman

Beside meteorites 47 soil samples were collected and 273 surfaces characterized during the campaigns 2009 and 2010. The way of sampling or description and further results are incorporated in Chapters 4, 5 and 6.

Ideal for meteorite recovery are desert pavement surfaces where most of the fine material is deflated and no chert or other dark rocks are present. Such surfaces occur in central Oman of an area of approximately 200 x 600 km, at altitudes of 50 – 250 m and lacking an active drainage system. Although locally affected by salt tectonics and some mild erosion that has produced some relief, the area has become peneplenized by wind activity. The desert surface is composed of rocks, which is most dominantly weathered limestone and fine-grained, windblown material. This layer is usually 5 to 30 cm thick and can be relatively soft when the limestone fragments are small. Below this, normally a layer of caliche occurs, which can reach a thickness of several decimeters. Thus, actual bedrock with carst surface is only exposed on cliffs or in diggings for example due to road construction. A schematic profile of this general description of central Oman desert surface is given in Figure 1.5, which is drawn based on own observations that are in agreement with other observations (Adelsberger and Smith, 2009; Fookes and Lee, 2009). Normally, meteorites are found lying just on the surface (Fig. 1.6a). But since the top part of the soil is soft and mobile (after rain events or daily temperature variation), and the meteorites have relative high densities, they can be buried to a certain degree in the soil (Fig. 1.6b).

Figure 1.5. Simplified schematic profile through a typical Oman desert soil. The top 20-50 cm are composed of limestone pebbles and fine-grained, wind blown material. Below, caliche horizon is found and bedrock, which is weathered on the top, appears after 50-100 cm.
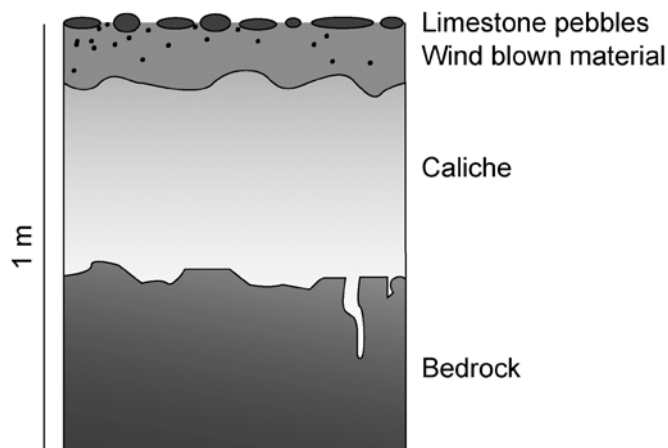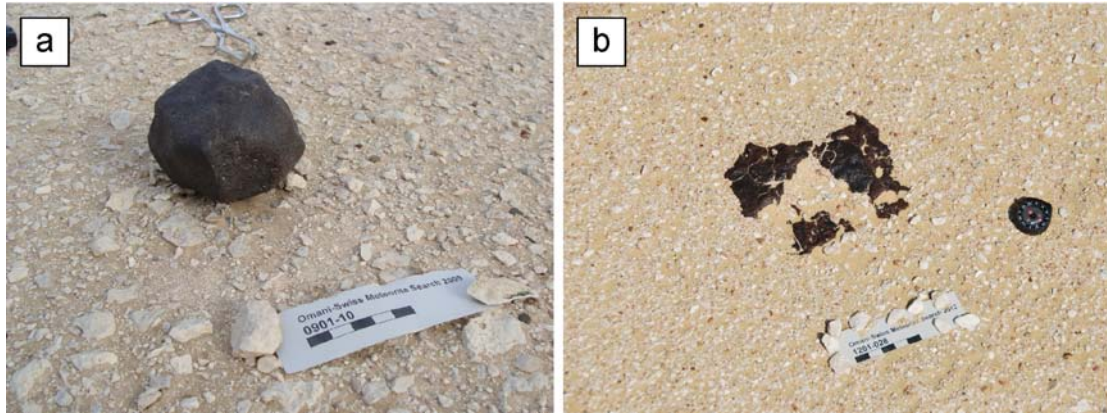
Figure 1.6. *Find situations of meteorites from Oman*
a) Meteorite UaS 011 was found completely on the surface.
b) A meteorite fragment is nearly completely buried into the soil.

Most of the high-density meteorite recovery areas are on Miocene limestones. Some Eocene surfaces are also suitable for meteorite search, but most of them contain a lot of dark cherts that make meteorite recovery extremely difficult. For simplification, the ideal surfaces for meteorite search in Oman visited during campaigns 2009 and 2010 can be divided in four types: (i) surface type typical for Ramlat as Samah (RaS) region, (ii) typical western Jiddat al Harasis (JaH) surface, (iii) the eastern JaH – Al Huqf type and (iv) the Sayh al Uhaymir type. Figure 1.7 shows photos of the surface types and location of the areas is given in Figure 1.4.

(i) The RaS soil is relatively homogeneous and composed of Early to Middle Miocene lower Fars group sediments, dominantly of Dam Formation limestone (Le Métour et al., 1993). It occurs between the dunes of the Rub al Khali and contains a significant proportion of dune material. Therefore, the amount of fine-grained material (<0.15 mm) is highest (Fig. 1.8). The soils are free of lichen, have relatively fine limestone pebbles (commonly <3 cm), are homogeneous, have nearly no disturbing cherts and vegetation is sparse (Fig. 1.7a). These factors make such surfaces very suitable for meteorite recovery. Salt content is also slightly below the mean of studied Oman soils (Chapter 5). Since dune sand is available, wind erosion is slightly stronger on terrestrial rocks and meteorites (Chapter 4) as compared to, for example, E JaH-Al Huqf area (Fig. 1.4).
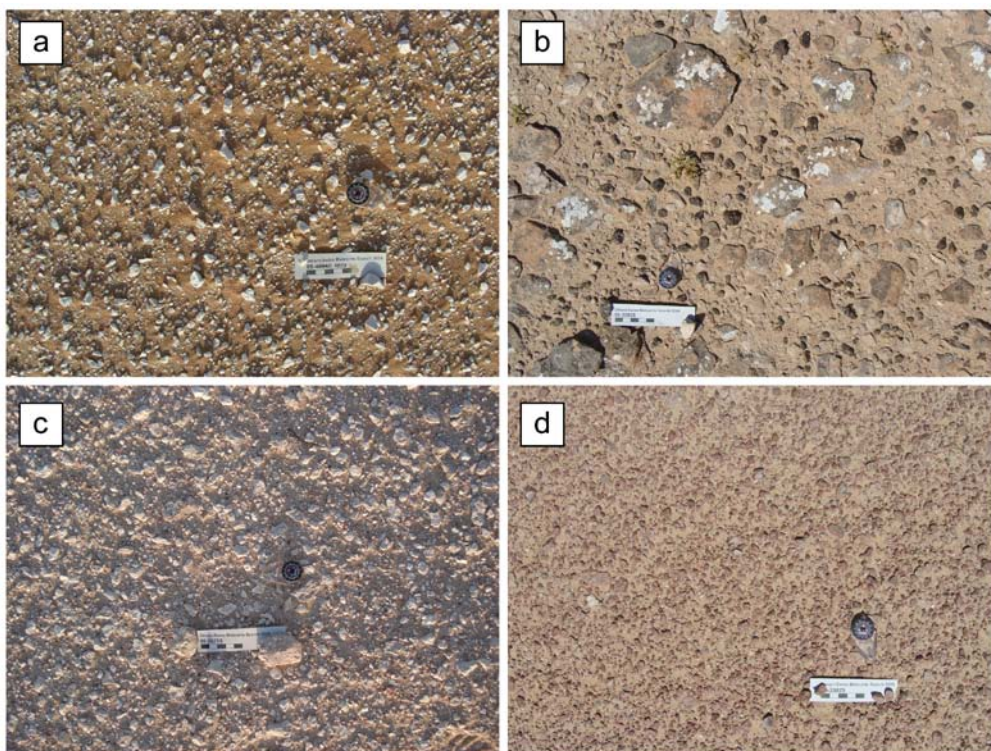
Figure 1.7. *Overview of the four main surface types well suited for meteorite search. Scale on label is 5 cm.*
a) In the RaS area surfaces are often similarly to W JaH (Fig. 1.4) but have slightly higher contents of fine-grained components, which is mainly sand from the dunes.
b) Most of the surface of eastern JaH and Al Huqf (Fig. 1.4) area is composed of relatively coarse limestone pebbles that are covered by lichen. Dark coated cherts make meteorite search difficult.
c) Typical surface of western JaH (Fig. 1.4) is very homogeneous and composed of whitish to slightly reddish limestone pebbles.
d) Surfaces in the SaU region (Fig. 4) are fine-grained and reddish.

(ii) The eastern part of the JaH area and the Al Huqf area (Fig. 1.4) is build of Middle Miocene limestones of the Middle Fars group, shelf facies (Le Métour et al., 1993). Dominantly, the rocks belong to the Gubbhara formation. The surface has relative large limestone pebbles, which are regularly covered by lichen (Fig. 1.7b). Towards the coast, vegetation (shrubs, small acacia trees) increases. Fine-grained material is relatively sparse and limestones show dissolution by moisture that has formed rillenkarren (Smith et al., 2000) and lichens have attacked some of the rocks. Wind erosion is minor but not absent. All these criteria make meteorite search in these areas more difficult. In addition, dark coated cherts (Chapter 4) occur frequently and complicate meteorite searches. However, it is possible to spot even small meteorites,

when the eyes are trained. No systematic higher degree of weathering was observed on meteorites from areas close to the coast (Chapters 4 and 6)

(iii) The region of the western JaH (Fig. 1.4), mostly around the small town of Hayma, is composed of surfaces with relative small and homogeneous limestone pebbles (Fig. 1.7c) of Early to Middle Miocene lower Fars group sediments, mainly Dam formation (Le Métour et al., 1993). Sometimes, the normally whitish limestones have reddish to rose staining due to ferruginization. In general, cherts, vegetation and lichens are absent, what makes such surfaces to excellent meteorite finding areas. The percentage of fine-grained material is high (Fig. 1.8).

(iv) Just south of the alluvial fans, there is a very homogenous red surface that gives the region its name (Fig. 1.7d). "Sayh al Uhaymir" (SaU, Fig. 1.4) means "slightly reddish plain" (Al-Kathiri, personal communication). In the dune free region of RaS similar surface type is present. The reddish soil is composed of Middle Miocene Fars group sediments from the lacustrine facies (Le Métour et al., 1993). The meteorite find density is highest in this homogeneous, nearly chert and vegetation free area. Similar meteorite density is present in on the lacustrine sediments of the Dhofar area, but in contrast, there the soils are white.
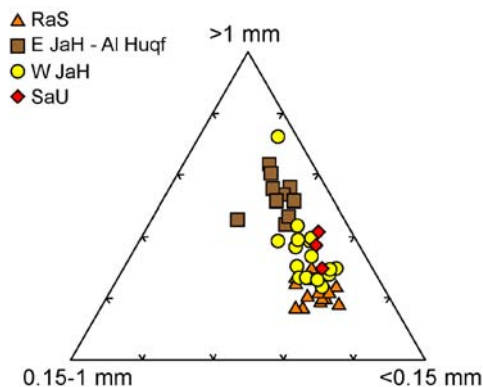
Figure 1.8. *Ternary diagram showing the amounts of the sieved fraction of typical Oman soil samples. Soils from W JaH, SaU and RaS (Fig. 1.4) have relatively high amounts of fine-grained material (<0.15 mm) whereas soils from eastern JaH and Al-Huqf (Fig. 1.4) have higher contents of coarse components (>1 mm). The fraction 0.15 – 1 mm is nearly absent in all soils.*

In general, the best plains for meteorite search are composed of bright limestone pebbles with equal pebble sizes, preferentially small diameters of <3 cm, have no disturbing cherts, the rocks are not covered by lichen and vegetation is virtually absent.

The influence of the soil composition and surface characteristics on meteorite weathering and contamination is given in Chapters 4, 5 and 6.

1.11. Weather observations

During the field campaigns, which took place in January and February, climatic and weather data was recorded in the morning after breakfast, mostly 1h after sunrise at 8 am; at lunch, normally at 1 pm and in the evening, approximately 1h after sunset at 7 pm. Air temperature and humidity were measured with simple, commercially available devices that were placed about 0.5 m above ground. Determination of wind direction and relative force (weak, strong) and description of the weather (clear sky, cloudy, rain etc.) was noted. In addition to these three measuring intervals, the minimal temperature was also recorded. It usually occurs just before sunrise at ~7 am. The temperatures during the campaigns 2009, 2010 and 2012 ranged between 0°C (06:50 am) and 33°C (1:45 pm). Temperature variations recorded in a meteorite and in soil are presented in Chapter 5. Humidity is dependent on wind direction. Winds from S(E) transporting humidity from Arabian Sea and are usually warm, wet and relatively strong. They often cause fog in the morning, which can stay until 10 am. Fog can wet the meteorites. Winds from N deliver air from Rub al Khali, and are, in contrast, generally "cold" and dry.

In both campaigns, 2009 and 2010, we were witnesses of sparse rain events in Oman. Rain occurred in the 2009 campaign during preparation of logistics for fieldwork when we were in Muscat region. When we started fieldwork, the desert area was already dry. Some usually dry plants were green. While doing fieldwork in 2010 slight rainfall occurred in central desert during the last night. A sample of rainwater was analyzed during the study of salt contamination of ordinary chondrites from Oman (Chapter 5). Rain stopped in early morning and the clouds disappeared until noon. In early afternoon, the top surface was completely dry.

The recording of weather conditions help to interpret the temperature variations recorded in a meteorite and in soil (Chapter 5).

1.12. References

Adelsberger, K. A. and Smith, J. R., 2009. Desert pavement development and landscape stability on the Eastern Libyan Plateau, Egypt. *Geomorphology* 107:178-194.

Al-Kathiri, A., 2006. Studies on Oman Meteorites. PhD Thesis, University of Bern.

Al-Kathiri, A., Gnos, E., and Hofmann, B. A., 2007. The regolith portion of the lunar meteorite Sayh al Uhaymir 169. *Meteoritics & Planetary Science* 42:2137-2152.

Al-Kathiri, A., Hofmann, B. A., Gnos, E., Eugster, O., Welten, K. C., and Krähenbühl, U., 2006. Shisr 043 (IIIAB medium octahedrite): The first iron meteorite from the Oman desert. *Meteoritics & Planetary Science* 41:A217-A230.

Al-Kathiri, A., Hofmann, B. A., Jull, A. J. T., and Gnos, E., 2005. Weathering of meteorites from Oman: Correlation of chemical and mineralogical weathering proxies with ^{14}C terrestrial ages and the influence of soil chemistry. *Meteoritics & Planetary Science* 40:1215-1239.

Bevan, A. W. R. and Binns, R. A., 1989a. Further meteorite recoveries from the Nullarbor region Western-Australia. *Meteoritics* 24:251-251.

Bevan, A. W. R. and Binns, R. A., 1989b. Meteorites from the Nullarbor Region, Western Australia. 1. A review of past recoveries and a procedure for naming new finds. *Meteoritics* 24:127-133.

Bevan, A. W. R. and Binns, R. A., 1989c. Meteorites from the Nullarbor region, Western Australia. 2. Recovery and classification of 34 new meteorite finds from the Mundrabilla, Forrest, Reid and Deakin areas. *Meteoritics* 24:135-141.

Bevan, A. W. R., Bland, P. A., and Jull, A. J. T., 1998. Meteorite flux on the Nullarbor Region, Australia. In: Grady, M. M., Hutchinson, R., McCall, R., and Rothery, D. A. Eds., *Meteorites: Flux with time and impact effects*. Special Publications. Geological Society of London, London.

Bevan, A. W. R., Downes, P. J., and Thompson, M., 2001. Little Minnie Creek, a L4(S2) ordinary chondritic meteorite from Western Australia. *Journal of the Royal Society of Western Australia* 84:149-152.

Bischoff, A., 2001a. Fantastic new chondrites, achondrites, and lunar meteorites as the result of recent meteorite search expeditions in hot and cold deserts. *Earth Moon and Planets* 85-6:87-97.

Bischoff, A., 2001b. Meteorite classification and the definition of new chondrite classes as a result of successful meteorite search in hot and cold deserts. *Planetary and Space Science* 49:769-776.

Bischoff, A. and Geiger, T., 1995. Meteorites from the Sahara: Find locations, shock, classification, degree of weathering and pairing. *Meteoritics* 30:113-122.

Bland, P. A., 2006. Terrestrial weathering rates defined by extraterrestrial materials. *Journal of Geochemical Exploration* 88:257-261.

Bland, P. A., Sexton, A. S., Jull, A. J. T., Bevan, A. W. R., Berry, F. J., Thornley, D. M., Astin, T. R., Britt, D. T., and Pillinger, C. T., 1998. Climate and rock weathering: A study of terrestrial age dated ordinary chondritic meteorites from hot desert regions. *Geochimica et Cosmochimica Acta* 62:3169-3184.

Bland, P. A., Zolensky, M. E., Benedix, G. K., and Sephton, M. A., 2006. Weathering of chondritic meteorites. In: Lauretta, D. S. and McSween, H. Y. (Eds.), *Meteorites and the Early Solar System II*. University of Arizona Press, Tucson.

Blechschmidt, I., Matter, A., Preusser, F., and Rieke-Zapp, D., 2009. Monsoon triggered formation of Quaternary alluvial megafans in the interior of Oman. *Geomorphology* 110:128-139.

Boschetti, S., 2011. Geomagnetic characterizations of meteorite impact sites in the desert of Oman. Master Thesis, ETHZ.

Brearley, A. J. and Jones, R. H., 1998. Chondritic meteorites. In: Papike, J. J. (Ed.), *Planetary Materials*. Mineralogical Society of America, Washington D. C.

Bretscher, A., 2011. The mesosiderite JaH 203 from the Sultanate of Oman - An extraterrestrial breccia containing igneous clast. Master Thesis, University of Bern.

Bühler, J., Gnos, E., Hofmann, B. A., Jull, A. J. T., and Al-Kathiri, A., 2006. Mapping meteorite distribution as a function of soil characteristics, central Oman desert. *Meteoritics & Planetary Science* 41 Suppl.:A30.

Burns, S. J., Fleitmann, D., Matter, A., Kramers, J., and Al-Subbary, A. A., 2003. Indian Ocean climate and an absolute chronology over Dansgaard/Oeschger events 9 to 13. *Science* 301:1365-1367.

Burns, S. J., Fleitmann, D., Matter, A., Neff, U., and Mangini, A., 2001. Speleothem evidence from Oman for continental pluvial events during interglacial periods. *Geology* 29:623-626.

Crozaz, G., Floss, C., and Wadhwa, M., 2003. Chemical alteration and REE mobilization in meteorites from hot and cold deserts. *Geochimica et Cosmochimica Acta* 67:4727-4741.

Edgell, H. S., 2006. *Arabian deserts*. Springer, Dordrecht.

Fisher, M., 1994. Another look at the variability of desert climates, using examples from Oman. *Global Ecology and Biogeography Letters* 4:79-87.

Fleitmann, D., Burns, S. J., Mangini, A., Mudelsee, M., Kramers, J., Villa, I., Neff, U., Al-Subbary, A. A., Buettner, A., Hippler, D., and Matter, A., 2007. Holocene ITCZ and Indian monsoon dynamics recorded in stalagmites from Oman and Yemen (Socotra). *Quaternary Science Reviews* 26:170-188.

Fleitmann, D., Burns, S. J., Mudelsee, M., Neff, U., Kramers, J., Mangini, A., and Matter, A., 2003a. Holocene forcing of the Indian monsoon recorded in a stalagmite from Southern Oman. *Science* 300:1737-1739.

Fleitmann, D., Burns, S. J., Neff, U., Mangini, A., and Matter, A., 2003b. Changing moisture sources over the Last 330,000 Years in Northern Oman from fluid-inclusion evidence in speleothems. *Quaternary Research* 60:223-232.

Fleitmann, D., Burns, S. J., Pekala, M., Mangini, A., Al-Subbary, A., Al-Aowah, M., Kramers, J., and Matter, A., 2011. Holocene and Pleistocene pluvial periods in Yemen, southern Arabia. *Quaternary Science Reviews* 30:783-787.

Fleitmann, D. and Matter, A., 2009. The speleothem record of climate variability in Southern Arabia. *Comptes Rendus Geoscience* 341:633-642.

Fookes, P. G. and Lee, M. E., 2009. Desert environments of inland Oman. *Geology Today* 25:226-231.

Franchi, I. A., Bland, P. A., Jull, A. J. T., Cloudt, S., Berry, F. J., and Pillinger, C. T., 1996. An assessment of the meteorite recover potential of southeast Arabia form meteorite weathering patterns. *Meteoritics & Planetary Science* vol. 31:A46.

Franchi, I. A., Delisle, G., Jull, A. T., Hutchison, R., and Oukkubger, C. T., 1995. An evaluation of the meteorite potential of the Jiddat al Harasis and the Rub al Khali regions of southern Arabia. *LPI Technical Report #95-02*:29-30.

Gattacceca, J., Valenzuela, M., Uehara, M., Jull, A. J. T., Giscard, M., Rochette, P., Braucher, R., Suavet, C., Gounelle, M., Morata, D., Munayco, P., Bourot-Denise, M., Bourles, D., and Demory, F., 2011. The densest meteorite collection area in hot deserts: The San Juan meteorite field (Atacama Desert, Chile). *Meteoritics & Planetary Science* 46:1276-1287.

Glennie, K. W., Boeuf, M. G. A., Hughes-Clark, M. W., Moody-Stuart, M., Pillar, W. F. H., and Reinhardt, B. M., 1974. Geology of the Oman Mountains. *Verh. K. Ned. Geol. Mijnbouwkd. Genoot. Ged.* 31:1-423.

Glennie, K. W. and Singhvi, A. K., 2002. Event stratigraphy, paleoenvironment and chronology of SE Arabian deserts. *Quaternary Science Reviews* 21:853-869.

Gnos, E., Eggimann, M., Al-Kathiri, A., and Hofmann, B. A., 2006. The JaH 091 strewnfield. *Meteoritics & Planetary Science* 41 Suppl.:A64.

Gnos, E., Hofmann, B., Franchi, I. A., Al-Kathiri, A., Hauser, M., and Moser, L., 2002. Sayh al Uhaymir 094: A new martian meteorite from the Oman desert. *Meteoritics & Planetary Science* 37:835-854.

Gnos, E., Hofmann, B. A., Al-Kathiri, A., Lorenzetti, S., Eugster, O., Whitehouse, M. J., Villa, I. M., Jull, A. J. T., Eikenberg, J., Spettel, B., Krahenbuhl, U., Franchi, I. A., and Greenwood, R. C., 2004. Pinpointing the source of a lunar meteorite: Implications for the evolution of the moon. *Science* 305:657-659.

Gnos, E., Hofmann, B. A., Al-Shanti, M., and Al-Halawani, M., 2009a. Meteorite exploration in Saudi Arabia 2008: Yabrin area and a visit to the Wabar craters. *Meteoritics & Planetary Science* 44:A79-A79.

Gnos, E., Lorenzetti, S., Eugster, O., Jull, A. J. T., Hofmann, B. A., Al-Kathiri, A., and Eggimann, M., 2009b. The Jiddat al Harasis 073 strewn field, Sultanate of Oman. *Meteoritics & Planetary Science* 44:375-387.

Grossman, J. N., 2000. The Meteoritical Bulletin, No. 84, 2000 August. *Meteoritics & Planetary Science* 35:A199-A225.

Grossman, J. N. and Zipfel, J., 2001. The Meteoritical Bulletin, No. 85, 2001 September. *Meteoritics & Planetary Science* 36:A293-A322.

Harvey, R., 2003. The origin and significance of Antarctic meteorites. *Chemie Der Erde-Geochemistry* 63:93-147.

Hewins, R. H. and Zanda, B., 2012. Chondrules: Precursors and interactions with the nebular gas. *Meteoritics & Planetary Science* 47:1120-1138.

Hezel, D. C., Schlüter, J., Kallweit, H., Jull, A. J. T., Al-Fakeer, O. Y., Al-Shamsi, M., and Strekopytov, S., 2011. Meteorites form the United Arab Emirates: Description, weathering, and terrestrial ages. *Meteoritics & Planetary Science* 46:327-336.

Holm, D. A., 1960. Desert geomorphology in the Arabian peninsula. *Science* 132:1369-1379.

Holm, D. A., 1962. New meteorite localities in the Rub' Al Khali, Saudi Arabia. *American Journal of Science* 260:303-309.

Huber, L., Gnos, E., Hofmann, B., Welten, K. C., Nishiizumi, K., Caffee, M. W., Hillegonds, D. J., and Leya, I., 2008. The complex exposure history of the Jiddat al Harasis 073 L-chondrite shower. *Meteoritics & Planetary Science* 43:1691-1708.

Janots, E., Gnos, E., Hofmann, B. A., Greenwood, R. C., Franchi, I. A., and Bischoff, A., 2011. Jiddat al Harasis 422: A ureilite with an extremely high degree of shock melting. *Meteoritics & Planetary Science* 46:134-148.

Jull, A. J. T., 2006. Terrestrial ages of meteorites. In: Lauretta, D. S. and McSween, H. Y. Eds., *Meteorites and the Early Solar System II*. University of Arizona Press, Tucson.

Korochantsev, A. V., Sadilenko, D. A., Ivanova, M. A., Lorentz, C. A., and Zabalueva, E. V., 2003. A study of the fragment dispersal and trajectory of the Sayh al Uhaymir 001 meteorite shower. *Meteoritics & Planetary Science* 38:A5049w.

Korotev, R. L., 2012. Lunar meteorites from Oman. *Meteoritics & Planetary Science* 47:1365-1402.

Krinov, E. L., 1959. *The Meteoritical Bulletin No. 13*, Moscow, USSR.

Le Métour, J., Michel, J. C., Béchennec, F., Platel, J. P., and Roger, J., 1995. *Geology and mineral wealth of the Sultanate of Oman*. Ministry of Petroleum and Minerals, Directorate General of Minerals, Sultanate of Oman, Muscat.

Le Métour, J., Platel, J. P., Béchennec, F., Berthiaux, A., Chevrel, S., Dubreuilh, J., Roger, J., and Wyns, R., 1993. Geological map of the Sultanate of Oman, 1:1'000'000, with explanatory notes, Sultanate of Oman. Ministry of Petroleum and Minerals, Directorate General of Minerals, Muscat.

Lee, M. R. and Bland, P. A., 2003. Dating climatic change in hot deserts using desert varnish on meteorite finds. *Earth and Planetary Science Letters* 206:187-198.

Lee, M. R. and Bland, P. A., 2004. Mechanisms of weathering of meteorites recovered from hot and cold deserts and the formation of phyllosilicates. *Geochimica et Cosmochimica Acta* 68:893-916.

Mittlefehldt, D. W., 2008. Appendix: Meteorites - A brief tutorial, *Oxygen in the Solar System*. Mineralogical Society of America, Washington D. C.

Mittlefehldt, D. W., McCoy, T. J., Goodrich, C. A., and Kracher, A., 1998. Non-chondritic meteorites from asteroidal bodies. In: Papike, J. J. (Ed.), *Planetary Materials*. Mineralogical Society of America, Washinton D.C.

Munoz, C., Guerra, N., Martinez-Frias, J., Lunar, R., and Cerda, J., 2007. The Atacama Desert: A preferential arid region for the recovery of meteorites - Find location features and strewnfield distribution patterns. *Journal of Arid Environments* 71:188-200.

Neff, U., Burns, S. J., Mangini, A., Mudelsee, M., Fleitmann, D., and Matter, A., 2001. Strong coherence between solar variability and the monsoon in Oman between 9 and 6 kyr ago. *Nature* 411:290-293.

Nishiizumi, K. and Caffee, M. W., 2001. Exposure histories of Lunar meteorites Dhofar 025, 026, and Northwest Africa 482. *Meteoritics & Planetary Science*.

Nishiizumi, K., Okazaki, R., Park, J., Nagao, K., Masarik, J., and Finkel, R., 2002. Exposure and terrestrial history of Dhofar 019 Martian meteorite (abstract #1366). *33rd Lunar and Planetary Science Conference,*

Norton, O. R. and Chitwood, L. A., 2008. *Field Guide to Meteors and Meteorites*. Patrick Moore's Practical Astronomy Series, Springer, London.

Otto, J., 1992. New meteorite finds from the Algerian Sahara desert. *Chemie der Erde* 52:33-40.

Ouazaa, N. L., Perchiazzi, N., Kassaa, S., Zeoli, A., Ghanmi, M., and Folco, L., 2009. Meteorite finds from southern Tunisia. *Meteoritics & Planetary Science* 44:955 - 960.

Parker, A. G., Goudie, A. S., Stokes, S., White, K., Hodson, M. J., Manning, M., and Kennet, D., 2006. A record of Holocene climate change from lake geochemical analyses in southeastern Arabia. *Quaternary Research* 66:465-476.

Peters, T., Battashy, M., Bläsi, H., Hauser, M., Immenhauser, A., Moser, L., and Al-Rajhi, A., 2001. Explanatory notes to the geological maps of Sur an Al Ashkharah, Sheets NF 40-8F and NF 40-12C. Ministry of Commerce and Industry, Directorate General of Minerals, Muscat.

Peters, T., Immenhauser, A., Mercolli, I., and Meyer, J., 1995. Explanatory notes to geological map of Masirah Island North and Masirah South, Sheet K768-North and sheet K768-South. Ministry of Petroleum and Minerals, Directorate general of Minerals, Muscat.

Philby, H. S. J. B., 1933. Rub al Khali. *The Geographical Journal* 81:1-26.

Preusser, F., 2009. Chronology of the impact of Quaternary climate change on continental environments in the Arabian Peninsula. *Comptes Rendus Geoscience* 341:621-632.

Preusser, F., Radies, D., and Matter, A., 2002. A 160'000-year record of dune development and atmospheric circulation in southern Arabia. *Science* 296:2018-2020.

Rubin, A. E. and Grossman, J. N., 2010. Meteorite and meteoroid: New comprehensive definitions. *Meteoritics & Planetary Science* 45:114-122.

Rubin, A. E., Verish, R. S., Moore, C. B., and Oriti, R. A., 2000. Numerous unpaired meteorites exposed on a deflating playa lake at Lucerne Valley, California. *Meteoritics & Planetary Science* 35:A181-A183.

Russell, S. S., Folco, L., Grady, M. M., Zolensky, M. E., Jones, R., Righter, K., Zipfel, J., and Grossman, J. N., 2004. The Meteoritical Bulletin, No. 88, 2004 July. *Meteoritics & Planetary Science* 39:A215-A272.

Russell, S. S., Zipfel, J., Folco, L., Jones, R. H., Grady, M. M., McCoy, T. J., and Grossman, J. N., 2003. The Meteoritical Bulletin, No. 87, 2003 July. *Meteoritics & Planetary Science* 38:A189-A248.

Russell, S. S., Zipfel, J., Grossman, J. N., and Grady, M. M., 2002. The Meteoritical Bulletin, No. 86, 2002 July. *Meteoritics & Planetary Science* 37:A157-A184.

Saunier, G., Poitrasson, F., Moine, B., Gregoire, M., and Seddiki, A., 2010. Effect of hot desert weathering on the bulk-rock iron isotope composition of L6 and H5 ordinary chondrites. *Meteoritics & Planetary Science* 45:195-209.

Schlüter, J., Schultz, L., Thiedig, F., Al-Mahdi, B. O., and Abu Aghreb, A. E., 2002. The Dar al Gani meteorite field (Libyan Sahara): Geological setting, pairing of meteorites, and recovery density. *Meteoritics & Planetary Science* 37:1079-1093.

Smith, B. J., Warke, P. A., and Moses, C. A., 2000. Limestone weathering in contemporary arid environments: A case study from southern Tunisia. *Earth Surface Processes and Landforms* 25:1343-1354.

Stelzner, T., Heide, K., Bischoff, A., Weber, D., Scherer, P., Schultz, L., Happel, M., Schron, W., Neupert, U., Michel, R., Clayton, R. N., Mayeda, T. K., Bonani, G., Haidas, I., Ivy-Ochs, S., and Suter, M., 1999. An interdisciplinary study of weathering effects in ordinary chondrites from the Acfer region, Algeria. *Meteoritics & Planetary Science* 34:787-794.

Weisberg, M. K., McCoy, T. J., and Krot, A. N., 2006. Systematics and Evaluation of Meteorite Classification. In: Lauretta, D. S. and McSween, H. Y. (Eds.),

Meteorites and the Early Solar System II. University of Arizona Press, Tucson.

Wimmer, K., Gnos, E., and Hofmann, B. A., 2012. Cimate of prehistoric Oman - Information from the meteorite strewn field Jiddat al Harasis 073. *International Conference on the Geology of the Arabian Plate and the Oman Mountains,*

Wimmer, K., Gnos, E., Hofmann, B. A., Al-Kathiri, A., Huber, L., and Leya, I., 2009. From 2 dimensions to 4 dimensions: Modelling the JaH 073 strewn field, Sultanate of Oman. *Bolides and Meteorite Falls, Abstracts,*

Wlotzka, F., 1993. A Weathering scale for the ordinary chondrites. *Meteoritics* 28:460.

Zolensky, M. E., Rendell, H. M., Wilson, I., and Wells, G. L., 1992. The age of the meteorite recovery surfaces of Roosvelt County, New Mexico, USA. *Meteoritics* 27:460-462.

Zolensky, M. E., Wells, G. L., and Rendell, H. M., 1990. The accumulation rate of meteorite falls at the Earths surface - The view from Roosevelt Country, New-Mexico. *Meteoritics* 25:11-17.

Zurfluh, F. J., 2008. Meteorites in the Sultanate of Oman - Effects of terrestrial weathering in the Jiddat al Harasis (JaH) 091 strewn field. Master Thesis, University of Bern.

A small fragment of a meteorite with a macroscopically visible chondrule (diameter ~3 mm). Sample 1001_117, paired with RaS 387, H4 S1.
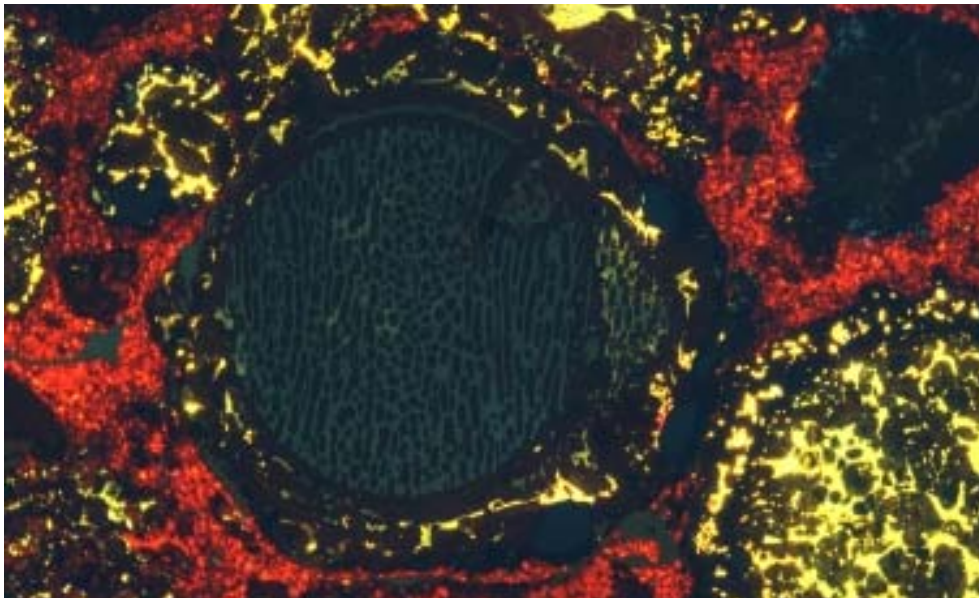
Cathodo luminescence image of a chondrule with a diameter of 2 mm. Shisr 033, CR chondrite.

About the weathering and strontium contamination of meteorites recovered in the Sultanate of Oman

Published in *Meteorite*, February 2012, Volume 18, No. 1.[*]

---

[*]The text and figures presented here have been adjusted to fit the layout of this thesis. This includes the numbering of titles and figures. Meteorites that were not named at the time of publication are now labeled with the official name. The unit "ppm" was changed to "µg/g".

Weathering and strontium contamination of meteorites recovered in the Sultanate of Oman

Florian J. ZURFLUH[1*], Beda A. HOFMANN[1,2], Edwin GNOS[3], Urs EGGENBERGER[1], Nicolas D. GREBER[1,2] and Igor M. VILLA[1,4]

[1]Institut für Geologie, Universität Bern, Baltzerstrasse 1 + 3, CH-3012 Bern, Switzerland
[2]Naturhistorisches Museum der Burgergemeinde Bern, Bernastrasse 15, CH-3005 Bern, Switzerland
[3]Muséum d'histoire naturelle de la Ville de Genève, 1 Route de Malagnou, CP 6434 CH-1211 Genève 6, Switzerland
[4]Università di Milano Bicocca, Milano, Italy.
* Corresponding author. E-mail address: florian.zurfluh@geo.unibe.ch

Nico and the fragmented (not his fault) RaS 343, H5 S2 WD3.3.

2.1. Introduction

Meteorites are fascinating rocks from outer space. Their study in thin section lets us travel to foreign worlds. Actually, they provide a lot of essential information to understand the evolution of the early Solar System. However, because meteorites are formed under conditions very different from those prevailing on Earth today, they are chemically not stable and change during their residence in terrestrial environments. Meteorites can be collected after falls or searched systematically in regions where favorable conditions for accumulation and preservation occur. The three most important regions nowadays are Antarctica, the Saharan desert and Oman. The ways of meteorite accumulation, methods of recovery and collection, and the resulting availability for science is different for these three sources. A report of the Antarctic meteorite search by ANSMET was presented in an earlier issue of this magazine (Righter et al., 2011). In this article we would like to present our approach to search for meteorites and some observations of terrestrial alteration we have made on meteorites we have collected in Oman. Some of these signatures are similar to other recovery areas while others are unique.

2.2. The Omani-Swiss meteorite search and research project

Before 2000, only a few meteorites were known from Oman. This changed dramatically with the Meteoritic Bulletin 84 in 2000 (Grossman, 2000) where 39 meteorites from Oman were described. More than 30 years ago the Institute of Geology at the University of Bern established partnership with the Sultanate of Oman. Due to this long-term collaboration with Oman, two of us (BAH and EG) initiated the Omani-Swiss meteorite search and research project with the help of Tjerk Peters (1936-2009), former professor of mineralogy, University of Bern. Ali Al-Kathiri was the first Omani PhD-student at the University of Bern and the Natural History Museum of Bern. Since 2001 ten field campaigns were conducted which resulted in approximately 5500 meteorite finds belonging to ~690 meteorite falls (Hofmann et al., 2011).

A careful planning of the fieldwork is fundamental. Suitable surfaces for meteorite recovery are selected using satellite images available from Google Earth and other sources. Based on our experience from former campaigns, we have learned to interpret the satellite images to plan our routes along the most suitable surfaces. During the campaigns 2009 and 2010 we mainly followed routes from the coast towards the interior of the country. The idea behind this was to find meteorites at various distances from the sea to study its influence on the weathering. Search for meteorites is performed visually by car or by foot. For security reasons we search with at least two cars. To obtain quantitative information for the meteorite find density we systematically search by foot numerous quadrangles of one quarter of a square kilometer each. Such a foot search takes about ~2 hours when 4-6 persons are involved and it is conducted in the morning hours. We perform our field campaigns in winter (between January and March) in view of the fact that the temperatures are relatively pleasant (typical daytime temperatures 25-30°C).

When a meteorite is found the finders give signs to the other searchers and all members of the search group meet at the find location. Usually, searches are performed in sight distance but often one is very concentrated and the eyes are fixed to the ground with the consequence that one looses the beckons from the other team when they have found a meteorite. Our procedure of meteorite collection is standardized according to the following routine: record the coordinates by GPS (Fig. 2.1a), take photographs with a label containing the field number and a scale bar (Fig 2.1b), estimate the degree of burial, perform analyses for identification (magnetic susceptibility or handheld X-ray fluorescence, HHXRF, measurement, Fig 2.1c), collect all fragments without touching (Fig. 2.1d), weight all, or at least the largest fragments, note the number of fragments and the total weight. In some cases we also measure distance and direction (with a compass) of the fragments with respect to the largest fragment. All data are recorded in field books and recently also on a tablet computer. Samples are then wrapped in polypropylene bags, labeled several times and stored in metal boxes for transport. For small to medium sized samples the large bags help to build up a kind of soft shield around the samples to avoid further fragmentation or damage during transport. For selected meteorites we additionally collect soil samples beneath and near the meteorite. The recording of the coordinates is essential for studies on find density and to answer questions of pairing, i.e. the identification of samples belonging to the same fall event. In hot deserts, meteorites usually

are found on the place where they have fallen. This allows us to reconstruct meteorite strewn fields (e.g. Gnos et al., 2009).

Figure 2.1. Work that has to be done during meteorite recovery:
a) Mohammed Al-Batashi points to a newly found meteorite (RaS 304, H6 S2 WD3.3) in the flat desert of Oman. The GPS (device visible in front of the meteorite) coordinates are recorded and noted into the field book (photo courtesy of Silvio R. Lorenzetti).
b) Don't be afraid, this picture is a fake! This meteorite (Shalim 009, L6 S5 WD3.0) was already fragmented due to weathering. A look inside a rock for identification is best done using a hammer. However, meteorites are too valuable and therefore we use non-destructive methods for meteorite identification, as it is visible e.g. in Fig. 2.1c. Anyhow, Edwin Gnos will take a serious picture of the meteorite with a label for identification and a compass for orientation to document the find situation.
c) Urs Eggenberger performs a HHXRF measurement on a dark rock in the desert. We were able to identify this rock as a meteorite and could even determine its class using elemental ratios and bulk concentrations (RaS 309, brachinite). Based on the Sr and Ba content we can also estimate, how long the rock lay there.
d) To avoid contamination samples are collected without touching and wrapped in polypropylene bags. Beda Hofmann collects here samples with tweezers for microbial studies. The meteorite visible here is RaS 418, a 28.79 kg L6 S5 WD4.0 chondrite (paired with 1002-157, Fig. 2.3b) weathered into 917 fragments.

When the meteorites have reached the Natural History Museum Bern, we unpack them without touching, clean them with pressurized air and count the number of fragments and take the accurate weight. Based on an agreement, the samples are on loan for study while remaining property of the Sultanate of Oman. After a macroscopic description of weathering features such as wind ablation and salt efflorescence, a sample is cut off using isopropanol as coolant, and thin sections for classification are prepared. The main masses are stored in a rock archive in the basement of the Natural History Museum Bern at constant temperature and relative humidity of 40% maximum. The degree of shock (Stöffler et al., 1991), weathering grade (Wlotzka, 1993, with modifications: Weathering degree, Chapter 6) and the petrologic type (Van Schmus and Wood, 1967) of the chondrites are determined for each individual find by the use of optical microscopy in reflected and transmitted light. Those investigations have to be performed by at least two persons for verification. Afterwards, the composition of the minerals is analyzed with the electron microprobe and X-ray diffraction to assign the group (Brearley and Jones, 1998). Most of the meteorites are ordinary chondrites belonging to the H or L groups. After classification, the pairing of meteorites is resolved by direct comparison of meteorites which have a similar classifications and close geographical provenance. The whole procedure of classification and check for pairing is very time consuming and non-trivial, but it is necessary for a proper statistic evaluation of the find population.

2.3. Weathering

When we find meteorites in Oman, they usually lack a black fusion crust, the typical characteristics of meteorites, and are strongly weathered, i.e. they have a rusty color and/or are sometimes broken up into several fragments. Which processes are responsible for the damage of meteorites? Air, water and salts from soil are the enemies of meteorites and are the main agents to decompose the primary constituents of the extraterrestrial rocks. Even though the climate in Oman is relatively hot and dry, the daily temperatures vary over several tens of degrees and water is present more one would expect. Winds from SE bring humidity from the Arabian Sea inland with the result of fog and dew on the rocks. Today, rain is rare but occurs normally at least once per year (inland desert usually <70 mm). In ordinary chondrites

metallic (nickel-) iron grains usually are affected first, followed by the iron sulfide troilite. Both minerals are replaced by a mixture of iron oxides and iron hydroxides ("rust"), which causes the brown-reddish staining of the meteorites. These newly formed minerals need more space than the original minerals and form a network of veins (Fig. 2.2) and cracks can evolve. Frequent winds transport sand and salts into the cracks, which enhance weathering (Fig. 2.3a). These processes eventually cause fragmentation of meteorites at advanced stages of weathering (Fig. 2.3a and b). Another important enemy of meteorites is sandblasting. Sand grains transported by the wind impact on the surface of the rocks and chip small fragments. In extreme cases, ventifacts are formed (Fig. 2.3c). Close to the coast, humidity is highest and the rocks, including meteorites, are covered by lichen. Consequently, the recognition of these meteorites is very difficult (Fig. 2.3d). In addition, the soil surfaces in these areas are mostly made up of larger rocks and cherts commonly covered with black desert varnish, rendering meteorite recognition even more difficult. Biology is also involved in the decomposition of meteorites. Lichen, mosses, fungi and bacteria can inhabit meteorites and use their constituents as nutrients and source of energy. Also higher forms of live are a source of contamination of meteorites as we found bird excrements on several meteorites (Fig. 2.3b).

Figure 2.2. Backscatter electron (BSE) image of a large terrestrial celestine (SrSO$_4$) crystal occupying a (former) pore space in UaS 016, a H5 S2 WD4.5 chondrite. The dark minerals are the silicates olivine and pyroxene, the bright veins are iron hydroxides produced by weathering.

Figure 2.3. *The change of meteorites during their stay in the hot desert:*
a) Due to the replacement of iron-nickel metal by iron (oxi)hydroxides, which need more space, meteorites can swell and fragment. Salt weathering and input of sand into the cracks enhance fragmentation, as it is visible on the "crocodile" meteorite RaS 354, a H6 S1 WD3.0. Since H chondrites have high metal contents they have an increased tendency to fragment during weathering.
b) Effects of weathering and contamination are visible on meteorite Hayy 001, a H5 S3 WD3.6 chondrite. Sand, cemented by Fe-hydroxides sticks to the meteorite surface. The whitish spot on the meteorite is guano.
c) Wind ablation can modify the surface of the meteorites. Meteorite 1002-157 (not named, paired with RaS 418), L6 S5 WD3.3, was shaped into a ventifact over thousands of years similar to the surrounding stones.
d) The main fragment of Al Huqf 070, L3.7-3.9 S3 WD4.0, at the find site. This highly weathered chondrite is fragmented into several pieces, some of them completely covered by lichen.

2.4. Strontium in hot desert meteorites

With this background in weathering of meteorites, we will now look at the strontium contamination in ordinary chondrites found in Oman. To quantify the amount of contamination we measured a large number of meteorites using a handheld X-ray fluorescence (HHXRF) device (Zurfluh et al., 2011). This instrument, resembling a taser we

know from science fiction movies (Fig. 2.1c), allows us to perform a lot of nondestructive chemical analyses of our samples within short time. We observed strontium accumulations up to 200 times the value of an unweathered ordinary chondrite which lies between 9 and 11 µg/g (Wasson and Kallemeyn, 1988). We measured up to 2200 µg/g! Even in the core of meteorites the concentrations reached up to 888 µg/g. It is clear that the Sr derived from outside. But from where? To solve this question we performed ^{87}Sr/^{86}Sr isotopic analyses of three meteorites found at different distances to the sea. In addition, corresponding soil samples were analyzed. The results showed the local soil as source of the strontium. The ^{87}Sr/^{86}Sr ratio of the three soil samples is different but always similar to the corresponding meteorite. For this reason we can exclude sea spray, which also contents Sr, to be an important source of contamination of meteorites in Oman. Moreover, the contamination with Sr increases terrestrial residence time in the meteorite. Strontium links to sulfur, to produce the strontium sulfate mineral celestine (Fig. 2.2), a mineral with a low solubility in water. This fact allows an accumulation of terrestrial Sr in the meteorite over time.

Beside meteorites from Oman, we have also measured meteorites from Saudi Arabia, Sahara and Australia. Interestingly, meteorites found on the Arabian Peninsula have the tendency to preferentially accumulate strontium whereas the Saharan and Australian meteorites have a stronger barium signal (Fig. 2.4). It is likely possible to estimate the terrestrial residence time of the meteorites based on Sr and Ba uptake and degree of weathering. But it has to be calibrated for each collection individually since the rate of uptake varies with geographical provenance.
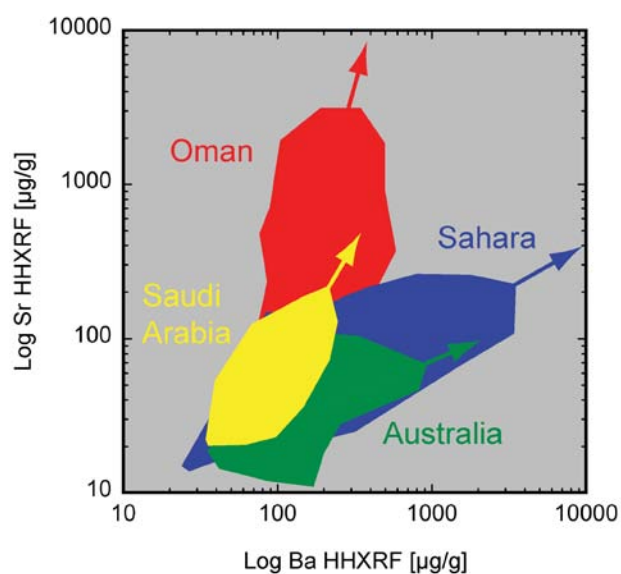
Figure 2.4. Logarithmic plot of Sr versus Ba obtained by HHXRF measurements of ordinary chondrites from various classical recovery areas. Note that meteorites from Sahara and Australia tend to preferentially accumulate Ba whereas Arabian meteorites (Oman and Saudi Arabia) are Sr-dominated.

Although a high percentage of the meteorites from Oman are badly weathered, all of them are worth to be studied, as these features contain important and interesting information. Beside the fascinating stories they can tell from their journey through time and space, it is also worth and necessary to listen to their terrestrial anecdotes.

2.5 Acknowledgments

2.6 References

Brearley A. J. and Jones R. H. (1998) Chondritic meteorites. In *Planetary Materials* (ed. J. J. Papike). Mineralogical Society of America, Washington D. C.

Gnos E., Lorenzetti S., Eugster O., Jull A. J. T., Hofmann B. A., Al-Kathiri A., and Eggimann M. (2009) The Jiddat al Harasis 073 strewn field, Sultanate of Oman. *Meteoritics & Planetary Science*, 44:375-387.

Grossman J. N. (2000) The Meteoritical Bulletin, No. 84, 2000 August. *Meteoritics & Planetary Science*, A199-A225.

Hofmann B. A., Gnos E., Eggenberger U., Zurfluh F. J., Boschetti S., and Al-Rajhi A. (2011) The Omani-Swiss meteorite search project-recent campaigns and outlook. *Meteoritics & Planetary Science* 46:A97-A97.

Righter K., Satterwhite C., McBride K., and Harrington R. (2011) The NASA Antarctic Meteorite Curation Laboratories. *Meteorite* 17:7-11.

Stöffler D., Keil K., and Scott E. R. D. (1991) Shock metamorphism of ordinary chondrites. *Geochimica et Cosmochimica Acta* 55:3845-3867.

Van Schmus W. R. and Wood J. A. (1967) A chemical-petrologic classification for the chondritic meteorites. *Geochimica et Cosmochimica Acta* Acta, 31:747-765.

Wasson J. T. and Kallemeyn G. W. (1988) Compositions of chondrites. *Philosophical Transactions of the Royal Society of London Series a-Mathematical Physical and Engineering Sciences* 325:535-544.

Wlotzka F. (1993) A Weathering scale for the ordinary chondrites (abstract). *Meteoritics* 28:460

Zurfluh F. J., Hofmann B. A., Gnos E., and Eggenberger U. (2011) Evaluation of the utility of handheld XRF in meteoritics. *X-Ray Spectrometry* 40:449-463.

Evaluation of the utility of handheld XRF in meteoritics

Keywords:
Handheld XRF, meteorite, terrestrial contamination, bulk composition, classification

*The text presented here hax been adjusted to fit the layout of this thesis. This includes: Numbering of chapters, figures and tables, style of references, unit "ppm" was changed to "μg/g", "DL" (detection limit) was replaced by "LOD" (limit of detection), the order of elements in chapter 3.4.3.5 and the conclusion was changed according to their Z number ("Ba and Sr" to "Sr and Ba", "Sr, Ba and Mn" to "Mn, Sr and Ba" and errors in display of decimals of Ti, Mn and Fe in Table 3.2 were fixed.

Evaluation of the utility of handheld XRF in meteoritics

Florian J. ZURFLUH[1]*, Beda A. HOFMANN[2], Edwin GNOS[3], Urs EGGENBERGER[1]

[1]Institut für Geologie, Baltzerstrasse 1 + 3, CH-3012 Bern, Switzerland.
florian.zurfluh@geo.unibe.ch.
[2]Naturhistorisches Museum der Burgergemeinde Bern, Bernastrasse 15, CH-3005 Bern,
Switzerland
[3]Muséum d'histoire naturelle de la Ville de Genève, 1 Route de Malagnou, CH-1211 Genève
6, Switzerland
* Correspondence to: Florian Zurfluh, Institute of Geological Sciences, Baltzerstrasse 1 + 3,
CH-3012 Bern, Switzerland E-mail: florian.zurfluh@geo.unibe.ch

Abstract - We tested a handheld XRF instrument with adaptable matrix correction for its suitability in meteoritics. We report here the instrument set up, precision and accuracy and present examples of applications. With a measuring time of 300 s it is possible to collect accurate data for K, Ca, Ti, Cr, Mn, Fe, Co, Ni, Sr and Ba that are needed for the identification of doubtful meteorites and the non-destructive classification of chondrites and achondrites. The factory supplied calibration curve of the instrument is fine tuned for our purposes using well-analyzed meteorite powders, pressed pellets and meteorite hand specimens as standards. Relative errors of 10% to 20 % are reached for the mentioned elements. The instrument was tested in the hot desert of Oman while searching for meteorites and also in the laboratory while doing research on meteorites. The main applications of the instrument are the identification and classification of meteorites, the quantification of terrestrial elemental contamination (Sr, Ba) and detection of Mn-rich desert varnish. It is possible to discriminate the major meteorite groups using Fe/Mn and Ni values. Handheld XRF is also useful to identify meteorites belonging to the same fall event.

The diogenite RaS 287 with the HHXRF and the field book where its classification is noted.

3.1. INTRODUCTION

The determination of bulk chemical composition is essential for the identification and classification of rocks. Since nearly half a century X-ray fluorescence (XRF) is used as a standard analytical method in the Earth sciences. The advantages of XRF, i.e. speed and non-destructive, were recognized early in meteoritics (Reed, 1972). Whereas typically X-ray tubes are used to provide excitation X-rays, early portable instruments used radioactive sources instead, having the disadvantages of safety problems and an unavoidable degradation of the source activity over time. In the last ten years the availability of miniature X-ray tubes has allowed the development of field portable XRF devices and a number of instruments are now commercially available. Handheld XRF (here abbreviated to HHXRF, the most popular; also known as field portable XRF [FPXRF] or portable XRF [PXRF]) instruments are now widely used by the industry, academia and government agencies. Prominent applications are the determination of heavy metal elements at contaminated sites, ore exploration, investigation of archaeological artifacts, determination of pigments in paints and by far the most popular of them analysis of metals and alloys (e.g. Bonizzoni et al., 2010; Goldstein et al., 1996; Hou et al., 2004; Radu and Diamond, 2009; Roldan et al., 2009; Szokefalvi-Nagy et al., 2004). Reasons for the success of HHXRF are its easy handling, speed of analysis and portability. Another important factor, especially in dealing with rare samples, is the possibility to perform non-destructive, reproducible analyses.

Meteorites are rock fragments fallen to the surface of solar system bodies. For a definition of the term meteorite see Rubin and Grossman, (2010); for general information e.g. Norton and Chitwood, (2008). Most commonly meteorites are derived from the asteroid belt. In some rare instances, meteorites from Mars and Moon reach Earth. All these extraterrestrial materials are of high potential value for science, as they provide the vast majority of information about bodies in our solar system. The work presented here was performed as part of a meteorite search and research project in collaboration with the Ministry of Commerce, Sultanate of Oman. Our institution has a long-term partnership with Oman. In the frame of this project, meteorites are searched, documented and collected in the hot desert of Oman and classified and investigated in laboratories mainly in Switzerland.

Notwithstanding the large number of meteorites found in cold deserts (Antarctica, e.g. Harvey, 2003) and hot deserts (e.g. Arabia: Al-Kathiri, 2006; Hezel et al., 2011; Atacama:

Munoz et al., 2007; Australia: Bevan and Binns, 1989a; Bevan and Binns, 1989b; Jull et al., 2010; Sahara: Bischoff and Geiger, 1995; Otto, 1992; Ouazaa et al., 2009; Schlüter et al., 2002 and USA: Jull et al., 1993; Zolensky et al., 1990) these space rocks remain unique, rare and precious samples helping us to understand the early evolution of the Solar system. Since we have to take care of these valuable samples, fast and non-destructive methods for determination of meteorite types are needed. One such method is the measurement of the magnetic susceptibility (Rochette et al., 2008; Rochette et al., 2009; Rochette et al., 2003). Although very powerful for meteorites with a low degree of alteration, this method is unreliable when terrestrial weathering changes the magnetic signal.

The aim of our study is to test the suitability of HHXRF in terms of analytical precision and accuracy and to demonstrate its usefulness in several branches of meteoritics, including meteorite identification, classification and the quantification of terrestrial elemental contamination. We tested the instrument as an "average user" without the ability to influence the internal data processing procedure. We show that an identification and classification of many common meteorite types based on element ratios (Fe/Mn) and bulk concentrations (Ni, Ca, K and Ti) is possible whereas Ba and Sr are the most important elemental indicators of terrestrial weathering and contamination. Here we present our findings obtained with the optimized calibration set up.

3.2. METHODS

3.2.1. The instrument

The instrument used for this study is a NITON XL3t-600 (Thermo Fisher Scientific, Billerica, MA, USA) energy dispersive XRF (EDX) analyzer calibrated for geological samples. It is equipped with a miniature X-ray tube with an Au anode (maximum 50 kV, 2 W and 40 μA) and three primary beam filters to provide optimized excitation energies for different elements (Table 3.1) (NITON, 2008). Their task is to reduce spectral background under analytes lines and selectively filter primary beam of X-rays from the tube. The instrument we have used in this study was equipped with silicon p-i-n diode detector (PIN) with typical energy resolution better than 200 eV. The latest (2011) version of the analyzer is

equipped with silicon drift detector (SDD), which can sustain much higher count rates and offers better energy resolution (typically 175 eV). The diameter of measured area on sample is about 8 mm, but it can be reduced to 3 mm using built-in small spot collimator. Normally, the measurements are performed using the 8 mm spot. The small spot collimator is sparsely used, for example to measure inclusions or larger grains. A build in camera helps to fix the position. The detector operating temperature is thermoelectrically stabilized with a Peltier element to -25 °C. The detector signal is processed by a central processing unit (CPU) and stored in the form of an X-ray spectrum with 4000 channels corresponding to 60 keV. The spectra of the measurements are overlaid on computer using Niton data transfer software. During a single analysis, data are sequentially collected, first using the "main filter" (excitation 40 kV, 50 µA; material: Al/Fe), followed by the "low filter" (20 kV, 100 µA; Cu) and the "high filter" (50 kV, 40 µA; Mo) (Table 3.1). Counting times of each filter are adjustable. Table 3.1 lists the elements for which the instrument was delivered with factory calibrations for

Table 3.1. List of element lines measured with the three filters at different X-ray tube energies.

Soil Mode	Mining Mode	Measuring time
Main, 40 kV, 50 µA		F[3]: 30 s; L[4]: 120 s
	Ag	
As	As	
	Bal[2]	
	Bi	
	Cd	
Co	Co	
Cu	Cu	
Fe	Fe	
	Hf	
Hg[1]		
Mn	Mn	
Mo	Mo	
	Nb	
Ni	Ni	
Pb	Pb	
	Pd	
Rb	Rb	
	Re	
	Sb	
Se	*Se*	
	Sn	
Sr	Sr	
	Ta	
	Ti	
Th		
U		
	V	
W	*W*	
Zn	Zn	
Zr	Zr	
Low, 20 kV, 100 µA		F: 30 s L: 60 S
Ca	Ca	
Cr	Cr	
K	K	
S	S	
Sc		
Ti	Ti	
V	V	
High, 50 kV, 40 µA		F: 0 s; L 120 s
Ag	*Ag*	
Ba	Ba	
Cd	Cd	
Cs		
Pd	Pd	
Sb	Sb	
Sn	Sn	
Te		

[1]*Italic: usually bellow limit of detection.*
[2]Bal: "balance", virtual element for balance.
[3]F: Field.
[4]L: Laboratory.

ambient conditions i.e. without He gas flushing. About 30 elements ranging from S to U are detectable but some of them usually are below limit of detection (LOD) in typical geological samples. It is possible to flush the chamber between the sample and the detector with helium gas for the analysis of low energy characteristic X-rays of Mg, Al, Si and P. The latest

generations of HHXRF devices that are currently on the market have silicon drift detectors (SDD) and are able to detect these light elements also under ambient (w/o He flush) conditions.

Two measuring modes are available: "Soil" mode and "Mining" mode. The main difference between these two modes is the type of algorithms used for quantifying the elements. "Soil mode" uses the element-to-Compton peak ratio method in which the intensity of the region of interest (ROI) of a given element is divided by the intensity of the Compton peak and then quantification is calculated using a calibration curve. ROI is an integral of spectrum between two boundary channels (energies). At low concentrations, the X-ray intensities of the analytes and the intensity of Compton scattered X-rays are mainly affected by their absorption in the sample. Therefore, the rationing analyte intensity (ROI) to Compton peak intensity linearizes the calibration curve for that analyte. For this reason the "Soil" mode is preferred for quantifying heavy metal contamination in soils where contaminants typically are present at low concentration levels. However, when analyzing ores and minerals, we are faced with very large variations in composition of samples which are the source of severe absorption and enhancement effects, and which cannot be corrected by the element-to-Compton ratio method. In such a situation the "Mining mode" based on a fundamental parameter (FP) approach is effective. Fundamental parameters based algorithms account for all matrix effects taking place in analyzed materials since they are nonlinear, transcendental equations, they are solved numerically by iteration. The intensity of the Compton backscattered radiation is used to represent the sum of all elements that are not measured directly via their characteristic X-rays (such as oxygen, nitrogen etc.) but which contribute to the intensity of the Compton scattered radiation. We exclusively used the "mining" mode for this study, because preliminary tests showed it to be more robust and more accurate than the "Soil" mode for our sample types. The use of the "mining" mode also allowed us to adjust the calibration curve. This is particularly important since the matrix of meteorites differs from common terrestrial rocks.

The user has no access to the detailed algorithms used for quantification including inter-element corrections. For this reason we are not able to treat these issues here in detail. But the instrument user can optimize the accuracy by adjusting the calibration curves as discussed in section 3.3.4.

The instrument was originally designed for field use but it can also be mounted in a portable test stand and be controlled by an external computer for non-destructive "laboratory" analyses. The values of the measured elements appear in real time on the instrument's LCD-display (touch screen) or on the screen of a connected computer. All concentrations are displayed as elements, not oxides, as commonly used in geology. Therefore all data are listed here in elemental form.

3.2.2. Standard samples

In order to define optimal analytical conditions and to test the quality of the instrument a set of standard samples was analyzed using alternating measuring times. In a first step we used international (TILL-4, NCS DC 73308, NIST 2780 and RCRA) and in house (KAI 230 R, MPI olivine sand, MPI norite, MPI diabase and Desert Soil 0603-062b) standards to test the accuracy of the method (Table 3.2). Meteorites are richer in iron and denser (higher average Z) in comparison to soils and most terrestrial rocks. Therefore a modification of the

Table 3.2. List of international and in-house standards.

Sample	Class	Source	K	Ca	Ti	Cr	Mn	Fe	Co	Ni	Sr	Sr[1]	Ba
TILL-4	Int STD	Niton Manual	27000	8900	4840	53	490	39700	8	17	109		395
NCS DC 73308	Int STD	Niton Manual	1041	2800	1270	136	1010	27000	15.3	30	25		42
NIST 2780	Int STD	Niton Manual	33800	1950	6990	44	462	27840	2.2	12	217		993
RCRA	Int STD	Niton Manual				500							100
KAI 230 R, soil sample	Inhouse STD	Actlab, MPI	49850	19767	4967	119	612	45475	17	54	166		461
MPI olivine sand	Inhouse STD	MPI	166	2644	119	2090	820	54133	194	2620	12		20
MPI norite	Inhouse STD	MPI	2491	89123	893	30	999	42943	125	100	316		101
MPI diabase	Inhouse STD	MPI	3487	51673	9681	270	1425	82739	86	140	476		130
Desert Soil 0603-62b	Inhouse STD	Actlab	8551	146299	5647	2870	596	20002	16	110	382	363	240

All values in µg/g.
[1]XRF.

calibration of the instrument is needed; this can easily be achieved by adjustment of the slope of the calibration curve for the "mining" mode of our instrument. For this purpose, a series of

meteorites with well-known compositions were measured with "factory settings" and compared with values obtained by other methods such as ICP-MS, ICP-OES or XRF mainly done by Activation Laboratories (Ancaster, Ontario, Canada [actlab]), (Table 3.3), in order to test the applicability of the "factory" settings for meteorite analysis. This allows the calculation of correction factors for each element of interest for a proper calibration. We used meteorite powders mounted in standard X-ray sample cups, meteorite powders prepared as pressed pellets and meteorite hand specimens for calibration and for testing the robustness of our procedure. By measuring hand specimens of meteorites we tested the degree of natural variation within single samples. As meteorite standard samples we mainly used ordinary chondrites found in Oman (JaH 091, Shalim 004, AH 010 and UaH 001) since these are the main objects for future studies. Additionally, three achondrites, were tested: ureilite SaU 511, martian meteorite SaU 094 (Gnos et al., 2002) and lunar meteorite SaU 169 (Gnos et al., 2004) because their compositions are distinct from chondrites. Finally, we also included powders and hand specimens of Allende, a carbonaceous chondrite (type CV3) that fell on February 8 1969 (Clarke et al., 1971). This is one of the best studied meteorites with well-established concentration ranges, used in several laboratories as standard material (Jarosewich et al., 1987). Elements of main interest for our study are K, Ca, Ti, Cr, Mn, Fe and Ni as important primary elements in meteorites that can be used for identification and chemical classification of meteorites (Mittlefehldt et al., 1998; Weisberg et al., 2006), and Sr and Ba, as important contaminants from the soil in hot desert meteorites (e.g. Al-Kathiri et al., 2005; Stelzner et al., 1999). For the test measurements, meteorites with the highest available variability in composition were used with the intention to cover the whole range of meteoritic compositions. For Sr and Ba, spiked chondrite pressed pellets were produced in addition to natural samples to enlarge the concentration range. Finely ground JaH 091, a L5 ordinary chondrite (Gnos et al., 2006; Russell et al., 2004), was used as matrix material. Pure Sr- and Ba-carbonates were used for spiking and sodium glass (water glass, which bears Na and K) as cement in the pressed pellets.

Table 3.3. List of the meteorites and element concentrations used as standards for instrument calibration.

Sample	Class	Source	K			Ca			Ti			Cr			Cr [1]
AH_010 (0201_791)	L	Al-Kathiri 2005	996	±	100	12579	±	800	611	±	100	3050	±	200	3590
AH_011 (0201_0788)	L	Al-Kathiri 2005	779	±	100	12506	±	800	678	±	100	4000	±	200	
Allende [2010]	CV	Actlab	415	±	100	17081	±	800	803	±	100	3390	±	200	
Allende [2009]	CV	Actlab	830	±	100	16438	±	800	791	±	100	3360	±	200	
Allende Jarosewich	CV	Jarosewich 1987	332	±	100	18439	±	700	899	±	100	3626	±	200	
Dho_813 (0101_163)	L	Al-Kathiri 2005	1085	±	100	16249	±	800	705	±	100	4180	±	200	
JaH_069 (0101_008)	H	Al-Kathiri 2005	963	±	100	14789	±	800	684	±	100	4410	±	200	
JaH_091 Med	L	Calc [2]	1328	±	100	12865	±	800	647	±	100	3310	±	200	
JaH_091 (0201_011) [2009]	L	Actlab	996	±	100	12007	±	800	594	±	100	3430	±	200	3890
JaH_091 (0210_0011B)	L	Al-Kathiri 2005	789	±	100	11037	±	800	519	±	100	3360	±	200	
JaH_091 (0210_011) [2010]	L	Actlab	830	±	100	12436	±	800	629	±	100	3400	±	200	
JaH_091 AM	Spiked L	Calc													
JaH_091 M1	Spiked L	Calc													
JaH_091 M2	Spiked L	Calc													
JaH_091 M3	Spiked L	Calc													
JaH_091 STD	Spiked L	Calc													
JaH_091 ZMV	Spiked L	Calc													
SaU_194 (0102_227)	L	Al-Kathiri 2005	991	±	100	13672	±	800	665	±	100	3630	±	200	
SaU_511 (0902_018)	Ureilite	Al-Kathiri 2005	83	±	100	13508	±	800	264	±	100	4260	±	200	
Shalim _003	H	Al-Kathiri 2005	619	±	100	12259	±	800	659	±	100	3500	±	200	
Shalim_004 (0103_259)	H	Al-Kathiri 2005	1411	±	100	11864	±	800	540	±	100	2540	±	200	3770
Shalim_004 am	Spiked H	Calc													
Shalim_004 m1	Spiked H	Calc													
Shalim_004 m2	Spiked H	Calc													
Shisr_020 (0102_256)	H	Actlab	818	±	100	14749	±	800	653	±	100	4160	±	200	
UaH_001 (0301_0003)	LL	Actlab	1245	±	100	13222	±	800	695	±	100	3500	±	200	
SaU_169 IMB	Lunar	Gnos 2004	4480	±	100	72614	±	800	13249	±	200	975	±	200	
SaU_169 Rego	Lunar	Gnos 2004	7310	±	100	75758	±	800	8813	±	200	816	±	200	
SaU_094	Martian	Actlab	747	±	100	43954	±	800	2332	±	200	5650	±	200	

All values in μg/g
1 XRF
2 Calc = calculated

Table 3.3. Continued.

Mn	Fe	Co	Ni	Sr	Sr [1]	Ba
2517 ± 100	200380 ± 1000	560 ± 100	11500 ± 200	14 ± 3	11 ± 3	9 ± 3
2151 ± 100	230000 ± 1000	571 ± 100	10800 ± 200	25 ± 3		7 ± 3
1456 ± 100	234580 ± 1000	435 ± 100	2790 ± 200	14 ± 3		7 ± 3
1441 ± 100	236820 ± 1000	570 ± 100	9390 ± 200	15 ± 3		6 ± 3
1472 ± 100	235700 ± 800	600 ± 100	14200 ± 200	12 ± 3		4 ± 1
2295 ± 100	238000 ± 1000	601 ± 100	10000 ± 200	1140 ± 3		150 ± 20
1974 ± 100	303000 ± 1000	750 ± 100	13200 ± 200	594 ± 3		150 ± 20
2494 ± 100	207440 ± 1000	567 ± 100	± 200	15 ± 3		7 ± 3
2432 ± 100	214580 ± 1000	580 ± 100	11900 ± 200	13 ± 3	14 ± 3	4 ± 3
1982 ± 100	204000 ± 1000	550 ± 100	11900 ± 200	14 ± 3		3 ± 3
2517 ± 100	204710 ± 1000	432 ± 100	5100 ± 200	12 ± 3		8 ± 3
				21818		3285 ± 300
				670		105 ± 10
				233		39 ± 15
				123		22 ± 8
				14		6 ± 3
				2008		306 ± 15
2001 ± 100	240000 ± 1000	644 ± 100	13600 ± 200	181 ± 3		73 ± 15
3059 ± 100	145970 ± 1000	125 ± 30	1380 ± 200	86 ± 3		32 ± 7
2066 ± 100	241000 ± 1000	780 ± 100	14500 ± 200	19 ± 3		5 ± 3
2308 ± 100	229260 ± 1000	700 ± 100	14800 ± 200	13 ± 3	11 ± 3	5 ± 3
				100010	10015	
				3014	357	
				1014	156	
1874 ± 100	296000 ± 1000	733 ± 100	13200 ± 200	938 ± 3		265 ± 20
2688 ± 100	175830 ± 1000	459 ± 100	8660 ± 200	22 ± 3		5 ± 3
1084 ± 100	82938 ± 1000	31 ± 10	204 ± 50	359 ± 20		1520 ± 40
929 ± 100	68402 ± 1000	19 ± 8	58 ± 15	214 ± 15		593 ± 30
3570 ± 100	140070 ± 1000	63 ± 12	311 ± 50	83 ± 3		68 ± 15

3.2.3. Shielding depth experiments

Most meteorites are medium- to fine-grained rocks with typical mineral grain diameters of 0.01 to 1 mm. Variations in composition can occur within a few millimeters, either due to primary inhomogeneities, especially the presence of up to mm-sized grains of Fe-Ni metal and Fe-sulfide, or to the presence of contamination-rich surface rinds when measuring meteorite surfaces. It is important to know the effective depth of analysis and its consequences for analytical results. To explore this issue, a test series has been designed. Natural minerals extremely rich in certain key elements (i.e. not pure chemical end members) were selected and the X-ray intensities of these elements were measured through a pile of 1 up to 15 slices of ordinary chondrite (unclassified chondrite from Northwest Africa, H-type) with thicknesses ranging from 0.40 to 0.75 mm, summing up to a total chondrite thickness of 8.32 mm (Table 3.4 and 3.5). Counting times of 300 s were used in case of Ba to put down the detection limit of Ba to ~100 µg/g; all other elements were measured for 180 s since the high filter is not used.

Table 3.4. Thicknesses of slices used for the shielding experiments (MJA).

MJA label	Thickness of slice [mm]	Shielding thickness[1] [mm]
A	0.40	0.40
B	0.43	0.83
C	0.50	1.33
D	0.50	1.83
E	0.54	2.37
F	0.55	2.92
G	0.55	3.47
H	0.55	4.02
I	0.55	4.57
J	0.57	5.14
K	0.60	5.74
L	0.60	6.34
M	0.60	6.94
N	0.63	7.57
O	0.75	8.32

[1] During the experiments the slices were placed in alphabetical order. Shielding thickness is the resulting cumulative thickness of meteorite slices between the HHXRF and the test mineral.

Table 3.5. Minerals and instrument conditions used for determination of depth of interaction for different elements (contaminants).

Element	Tube conditions	Mineral	Idealized chemical formula	Signal depth [mm]
Cr	20 kVp, 100 µA	Chromite	$FeCr_2O_4$	<1
Mn	40 kVp, 50 µA	Mn-ore	MnO_2	<1
Fe	40 kVp, 50 µA	Magnetite	Fe_3O_4	<1
Sr	40 kVp, 50 µA	Celestine	$SrSO_4$	<2
Ba	50 kVp, 40 µA	Barite	$BaSO_4$	<5

3.3. RESULTS

3.3.1. Influence of the sample type

Most standards used are samples with at least one flat surface: powders mounted in standard XRF cups or as pressed pellets and hand specimens with cut surfaces. Nevertheless, some irregularly shaped samples were also measured, especially hand specimens from Allende and the convex side of pressed pellets. No significant or specific differences were observed between powdered samples (pressed into pellets and loose in sample cups) and hand specimens, both using flat and rough surfaces on the latter. In hand specimens, variations can occur on irregular or rough surfaces but are interpreted as natural inhomogeneities. Repeated measurements on uniform samples with the 8 mm window mode and subsequent 3 mm small spot mode yielded similar concentrations within two sigma error. The variation of accuracies of the different sample types is listed in Table 3.6.

Table 3.6. The elements of interest

Element	Correction factor: "factory"	Correction factor "meteorite"	Correction factor "desert soil"	Precision[1] HHXRF [%]	Accuracy[2] HHXRF [%]	Accuracy HHXRF HS[3] [%]	Accuracy HHXRF PH[4] [%]	Accuracy HHXRF pp[5] [%]	Detection limits[6] [µg/g]
K	1	0.98	1.08	8.4	18.0	11.4	18.0	-	500
Ca	1	1.13	0.87	2.8	15.1	16.6	12.1	-	-
Ti	1	1.40	1.55	0.3	10.8	14.2	6.4	-	200
Cr	1	1.13	1.50	0.9	17.8	22.0	12.0	(19.5)	80
Mn	1	0.98	0.99	0.8	16.1	16.1	8.3	(16.2)	70
Fe	1	1.04	1.10	0.8	7.0	8.8	7.0	(1.4)	300
Co	1	1.20	-	-	30.5	12.4	29.5	(40)	400
Ni	1	1.36	1.03	2.5	9.1	17.3	5.0	-	20
Sr	1	1.60	1.70	2.7	11.2	20.3	6.0	19.4	6
Ba	1	1.04	2.20	-	16.3	26.5	71.2	5.3	100
Average all	1	1.19	1.34	2.4	15.2	16.6	17.5		

Correction factors used for meteorite and desert soil samples, precision, accuracies and detection limit for the element of Interest at 300 s measurements.
[1] Precision: Three to five repeated measurements at the very same spot from two different samples; deviation in % to the median value of measurements.
[2] Accuracy: Deviation of HHXRF (y) from standard/reference value (x) (literature, ICP-MS, XRF), ((x-y)/x)*100), medians from 5 to 51 measurements, including all kind of samples,
[3] HS: Hand specimen, measurements mainly at cut surface (CS),
[4] PH: Measurements of powder in XRF standard cups,
[5] pp: Spiked powder press pellets, standard values for Ba and Sr are calculated,
[6] Detection limits observed measuring standard samples, meteorites, soil samples or marbles.

3.3.2. Signal depth of contaminants

The experiments measuring the maximum depth from which a characteristic X-ray signal of a contaminant can be obtained while shielded with meteorite material yielded some interesting results. Since meteorites have a very dense matrix small critical depths are expected. Indeed, calculations of penetration depth (minimum thickness of sample to obtain correct values) using H-chondrite composition (Jarosewich, 1990) and a density of 3.4 g/cm^3 (Consolmagno et al., 2008) yield values below or around 1 mm for chromium ($K\alpha_1$ at 5.4 keV), manganese ($K\alpha_1$ at 5.9 keV), iron ($K\alpha_1$ at 6.4 keV) and Sr ($K\alpha_1$ at 14.2 keV). Barium ($K\alpha_1$ at 32.2 keV) has a calculated penetration depth of about 3 mm. This is also visible in the shielding experiment (Fig. 3.1) but the contribution of the contaminants behind the meteorite slices seems to be derived from a greater depth, especially in case of Ba, where it is still overestimated behind about 5 mm of meteorite material. Strontium is also measured from
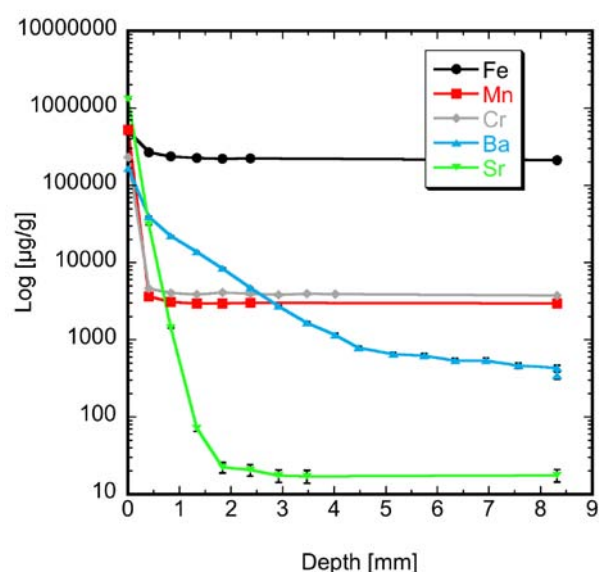
Figure 3.1. Maximum depth of contaminant signal provenance for Fe Kα_1, *Mn* Kα_1, *Cr* Kα_1, *Ba* Kα_1 *and Sr* Kα_1. *Minerals with high concentrations of the respective element were covered with thin meteorite slices of variable thickness. Excess Fe, Mn and Cr were detected through a meteorite cover of one millimeter, whereas excess Ba was still detected when 5 mm of meteorite shielding was present between the detector and the barite. A constant value is reached due to the contribution of the meteorite slices.*

greater depth. These two elements have higher penetration depths since they have also higher activation energies. They might be detected deeper because they are only present as traces in the chondrite, but highly concentrated in the material behind the meteorite slices. While the calculated penetration depth determines the minimum thickness of a sample to obtain correct values, our experiment delivers the maximum depth from which a specific element signal can be derived through a chondrite. The implication of our experiment is that signals of most of

the contaminants tested in the experiment are derived from low depths (<1 mm) with the exception of Sr and Ba, which contribute up to depths of 2 mm and 5 mm, respectively (Table 3.5).

3.3.3. Precision and required counting times

Precision is dependent on signal intensity and counting time and varies from element to element. The tested HHXRF instrument lists an element as detected when the standard deviation error of the result has decreased to <30% of the measured value. Most of the typical meteoritic elements (Ca, Ti, Mn, Fe, Ni and Sr) are detected at the expected range using counting times of about 10 to 25 s. Other elements like K, Co and Ba require longer measuring times. Since for field applications (as discussed in section 3.4.3.1.) only Ca, Mn, Fe, Ni and Sr are of key interest, the measuring time can be accordingly reduced for such applications. We recommend a "field set up" of at least 60 s total measuring time where 30 s are measured with the "main filter" and 30 s with the "low filter", respectively. Using this setup, the errors of the most important elements for field issues are in an acceptable range (<20% deviation). Because Ba is not needed for field applications, the "high filter" is switched off. In contrast, using a "lab set up" where also data for K, Ti, Co, and especially Ba are desired, a counting time of 300 s using the "mining mode" is recommended. A counting time of 120 s using the "main filter" is important since the background correction and the virtual element are calculated based on data collected with this filter. For "low filter" 60 s is sufficient while 120 s for "high filter" is needed to decrease the limit of detection (LOD) of barium particularly. 300 seconds is too long for a fatigue-proof handheld measurement (Fig. 3.2) on a small sample. For this reason the device is

Figure 3.2. *In situ HHXRF analysis of a meteorite (RaS 309) discovered in the desert of Oman. Note the high contrast between the dark meteorite and the light colored soil.*

mounted on a test stand with a shielded box protecting the user from stray radiation. Samples are set on a horizontal table and in the ideal case have a flat surface and do not exceed the dimensions of the 19 cm x 19 cm x 10 cm shielded box.

3.3.4. Calibration correction factors

Several meteorite samples, including powders, pressed pellets and hand specimens, were measured for 300 s and, based on the deviation of the HHXRF data from the "standard" value, correction factors were calculated (Table 3.6). Some results were excluded from the calculations, as they did not fit to the standard value for explicable reasons. For example, K contents measured on the pressed pellets were too high due to K from sodium silicate (water glass) used for cementation. At high Ba concentrations ($\sim$500 µg/g Ba) the Ti $K\alpha$ and Ba $L\alpha$ peak overlap has an influence, resulting in overestimated Ti concentrations (Fig. 3.3). This overlap cannot be corrected by adjustment of a calibration curve. Repeated measurements of the same powder of Allende by ICP-MS, ICP-OES and XRF yielded some slight but relevant differences for some elements (i.e. K and Ni concentrations of Allende [2009] and Allende [2010], table 3.3). When calculating the correction factors, such strong outliers were excluded. The production of meteorite powder is a difficult issue since most of meteorites contain metallic iron that is tricky to grind resulting in non-uniform powders sometimes containing metal "nuggets". Nickel and cobalt are concentrated in the iron metal grains and hence typically yield low values. When hand specimens are measured it has to be taken into account that minerals like chromite (Cr rich) or Ca-rich minerals such as feldspars or Ca-rich pyroxenes are not distributed homogeneously in a sample. This is also the case for terrestrial contamination minerals such as calcite, gypsum (both Ca-rich), celestine ($SrSO_4$) or barite ($BaSO_4$). Even with the spot size of 8 mm those effects can locally influence the measurement. The inhomogeneous distribution of Sr on a large cut slab of Allende is displayed in Figure 3.4. Since this is an observed meteorite fall unaffected by weathering, the variation of Sr is a primary effect and not due to contamination. Strontium is related to Ca-bearing minerals, such as Ca-rich pyroxene, feldspar (or feldspatic glass) Ca-phosphate and CAI (Calcium-Aluminium-rich) inclusions, which are not distributed homogeneous in the relatively coarse grained Allende meteorite.
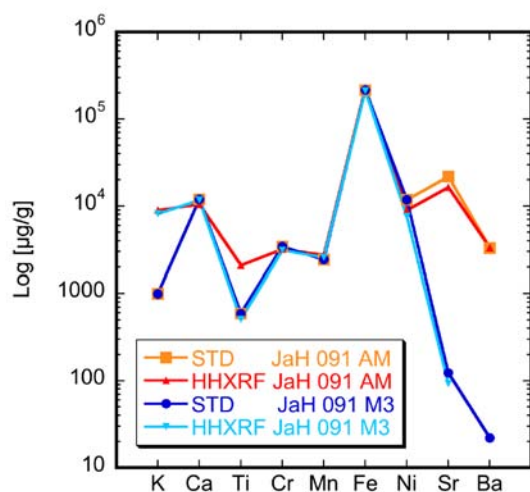
Figure 3.3. *Data for two samples (median values of four HHXRF measurements) of Sr- and Ba-spiked standard pressed pellets compared with expected values (STD). In the high Ba sample JaH 091 AM the Ti content is overestimated due to overlapping of Ti Kα and Ba Lα lines. Note the elevated K values observed in the pressed pellets produced with sodium silicate (water glass).*
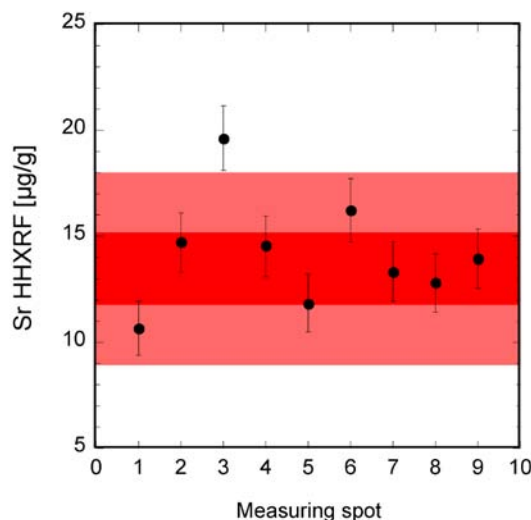
Figure 3.4. *Strontium variation in a large cut slab of the Allende CV3 meteorite. All data points represent measurements of 300 s. Dark red: all available reference values (Jarosewich et al., 1987; actlab 2009 & 2010), light red: corresponding error box. Sr is not homogeneously distributed in meteorites. Therefore we recommend using weighted mean values.*

The results of the corrected measurements are presented in Table 3.7. Most meteorites have comparable "chondritic" bulk compositions. Their mineralogy is dominated by olivine (Mg, Fe)$_2$SiO$_4$, Ca-poor pyroxene (Mg, Fe)SiO$_3$ and Ca-rich pyroxene (Ca, Mg, Fe)SiO$_3$, feldspar (Ca, Na, K)(Si, Al)$_4$O$_8$, Ca-phosphate Ca$_5$(PO$_4$)$_3$(F, OH, Cl), iron sulfide (FeS) and metallic iron-nickel, kamacite and taenite (Fe, Ni) and Cr-rich spinel (Fe, Mg)(Cr, Al)$_2$O$_4$, (e.g. McSween et al., 1991; Rubin, 1997). Therefore the correction factors are valid for most of the stony meteorite types.

In addition to meteorite samples, a series of soil samples from Oman were measured and correction factors were calculated for this type of samples (Table 3.6). Since the instrument is calibrated with a fundamental parameter for common geological samples, small calibration adjustments are required for desert soil samples to fit with standard values.

Table 3.7. HHXRF measurements of meteorite samples.

Sample	Sample status[1]	Sample surface[2]	Number of analyses	K			Ca			Ti			Cr		
AH_010	PH	P	2	n.d.	<	796	14044	±	474	628	±	75	3697	±	110
AH_010 std	pp	gp	3	n.d.	<	1390	11786	±	491	555	±	70	3160	±	100
AH_011 (0201_788)	HS	CS	5	494	±	621	13863	±	471	578	±	75	2924	±	101
Allende	HS	NS	5	n.d.	<	832	21219	±	594	906	±	87	4491	±	126
Allende M13	PH	P	3	n.d.	<	793	18429	±	563	752	±	85	4378	±	127
Dho_813 (0101_163)	cs	cs	3	672	±	607	21219	±	632	672	±	76	4378	±	92
JaH_069	HS	NS	5	n.d.	<	451	11240	±	428	855	±	81	2388	±	94
JaH_069 (0101_008D)	HS	CS	6	1073	±	403	14819	±	454	691	±	73	2940	±	99
JaH_091	PH	P	3	n.d.	<	849	14593	±	486	656	±	77	4083	±	117
JaH_091 AM	pp	gp	4	4784	±	595	11448	±	446	2742	±	124	3809	±	119
JaH_091 M1	pp	gp	4	3402	±	551	14421	±	491	701	±	79	3866	±	114
JaH_091 M2	pp	gp	4	20379	±	1017	12561	±	479	655	±	76	3540	±	109
JaH_091 M3	pp	gp	4	30239	±	1206	12948	±	502	652	±	76	3512	±	109
JaH_091 STD	pp	gp	4	7954	±	693	13435	±	467	568	±	72	3670	±	108
JaH_091 ZMV	pp	gp	4	6704	±	656	13610	±	471	797	±	79	3597	±	108
SaU_194	PS	P	3	n.d.	<	758	13362	±	445	591	±	70	3607	±	105
SaU_194	HS	CS	3	n.d.	<	785	17236	±	512	842	±	79	3377	±	103
SaU_194	HS	NS	5	n.d.	<	459	19708	±	552	n.d.	<	85	2786	±	95
SaU_194 (0102_227)	HS	CS	3	995	±	416	18037	±	537	723	±	75	3026	±	96
SaU_511 (0901_018)	HS	CS	3	n.d.	<	260	12743	±	171	267	±	22	5105	±	49
Shalim_004 (0203_259)	HS	CS	3	n.d.	<	638	15476	±	444	766	±	64	2983	±	99
Shalim_004 am	pp	gp	4	11683	±	982	10739	±	545	7697	±	274	3753	±	165
Shalim_004 m1	pp	gp	4	97672	±	2035	7609	±	519	452	±	68	2571	±	94
Shalim_004 m2	pp	gp	4	130900	±	2326	2419	±	504	340	±	65	2295	±	90
Shalim_004 oman	PH	P	3	n.d.	<	764	13517	±	472	663	±	78	3793	±	114
Shalim_004 std	pp	gp	4	66654	±	1695	6908	±	460	n.d.	<	66	3033	±	102
Shisr_020	PH	P	4	n.d.	<	859	17878	±	556	804	±	87	4061	±	123
Shisr_020 (0102_256)	cs	CS	3	n.d.	<	824	12365	±	467	714	±	79	3492	±	114
UaH_001 (0301_0003)	PH	P	3	1469	±	435	17398	±	507	771	±	74	4116	±	111
UaH_001 (0301_0003)	HS	CS	4	1162	±	406	17677	±	509	792	±	73	2629	±	90
SaU_169 IMB	HS	CS/NS	4	5059	±	320	74117	±	1050	16175	±	363	1201	±	64
SaU_169 Regolith	HS	CS/NS	6	6783	±	532	88320	±	1122	n.d.	<	367	1207	±	97
SaU_094	HS	CS	5	2033	±	1323	45091	±	810	2585	±	104	5346	±	125

[1] PH: Powder in standard XRF cup, pp: pressed pellet, HS: hand specimen, cs: small hand specimen.
[2] P: Powder, gp: water glass cemented powder, CS: cut surface, NS: natural surface.
All measurements with modified calibration factor (ModCF) for meteorites ("Meteorit") with a spot size of 8 mm.
n.d.: Not detected.
All values in μg/g.

Table 3.7. Continued.

Sample	Mn			Fe			Co			Ni			Sr			Ba		
AH_010	2614	±	135	217800	±	3050	n.d.	<	360	11549	±	226	11	±	1	n.d.	<	83
AH_010 std	2324	±	127	187260	±	2618	743	±	171	23152	±	388	12	±	1	n.d.	<	82
AH_011 (0201_788)	2725	±	135	210470	±	2922	n.d.	<	337	9290	±	187	12	±	1	n.d.	<	84
Allende	1498	±	117	245520	±	3495	n.d.	<	380	12308	±	247	17	±	1	n.d.	<	91
Allende M13	1560	±	121	252160	±	3668	583	±	198	13270	±	270	13	±	1	n.d.	<	89
Dho_813 (0101_163)	2345	±	130	258480	±	3737	578	±	195	10610	±	223	888	±	15	118	±	47
JaH_069	2889	±	141	267180	±	3829	n.d.	<	400	15926	±	318	548	±	10	99	±	47
JaH_069 (0101_008D)	2291	±	135	268830	±	3899	n.d.	<	407	12796	±	273	333	±	8	n.d.	<	98
JaH_091	2523	±	135	221230	±	3124	388	±	182	10087	±	205	15	±	1	n.d.	<	86
JaH_091 AM	2714	±	179	228080	±	3985	483	±	238	12186	±	300	27849	±	487	3400	±	136
JaH_091 M1	2722	±	139	223760	±	3161	n.d.	<	367	10800	±	217	733	±	12	107	±	45
JaH_091 M2	2494	±	133	215840	±	3059	483	±	181	10901	±	215	249	±	5	n.d.	<	85
JaH_091 M3	2512	±	134	216350	±	3086	553	±	182	10192	±	203	200	±	5	n.d.	<	84
JaH_091 STD	2418	±	130	212960	±	2943	n.d.	<	350	9681	±	192	15	±	1	n.d.	<	84
JaH_091 ZMV	2498	±	134	210400	±	2950	405	±	179	9796	±	197	2475	±	35	328	±	46
SaU_194	2418	±	130	254240	±	3503	n.d.	<	377	13490	±	262	178	±	4	125	±	51
SaU_194	2374	±	129	213760	±	2931	n.d.	<	348	5828	±	132	92	±	3	n.d.	<	85
SaU_194	3155	±	146	233110	±	3319	n.d.	<	375	7564	±	168	546	±	10	n.d.	<	46
SaU_194 (0102_227)	2449	±	131	223650	±	3136	n.d.	<	355	5138	±	124	87	±	3	n.d.	<	87
SaU_511 (0901_018)	2901	±	54	169900	±	900	n.d.	<	120	1715	±	25	76	±	1	125	±	17
Shalim_004 (0203_259)	2536	±	136	235980	±	3358	n.d.	<	380	10667	±	221	14	±	1	n.d.	<	100
Shalim_004 am	2747	±	320	252620	±	7190	1203	±	437	20210	±	747	164020	±	5063	13634	±	860
Shalim_004 m1	1977	±	128	194820	±	2931	1561	±	193	53144	±	896	3467	±	52	359	±	49
Shalim_004 m2	1968	±	127	198040	±	2982	1564	±	192	47401	±	794	1461	±	23	135	±	45
Shalim_004 oman	2437	±	133	242610	±	3431	520	±	191	14635	±	284	12	±	1	n.d.	<	90
Shalim_004 std	1935	±	124	226090	±	3270	980	±	190	27745	±	484	17	±	1	n.d.	<	88
Shisr_020	2278	±	136	273860	±	4039	637	±	208	13871	±	290	995	±	17	n.d.	<	92
Shisr_020 (0102_256)	2400	±	138	246060	±	3621	824	±	199	12373	±	259	16	±	1	n.d.	<	92
UaH_001 (0301_0003)	3158	±	144	189140	±	2613	n.d.	<	334	4178	±	104	24	±	1	n.d.	<	81
UaH_001 (0301_0003)	3123	±	140	175190	±	2377	n.d.	<	315	3513	±	89	26	±	1	n.d.	<	78
SaU_169 IMB	1280	±	37	90563	±	877	n.d.	<	325	216	±	31	356	±	6	1230	±	49
SaU_169 Regolith	1207	±	97	87407	±	1270	n.d.	<	348	78	±	41	261	±	5	515	±	37
SaU 094	3688	±	153	115130	±	2033	n.d.	<	305	281	±	35	85	±	3	n.d.	±	88

3.4. DISCUSSION

3.4.1. Accuracy, precision and detection limits

The instruments precision is of high quality for a field portable device. Precision was determined by three to five repeated measurements at the very same spot of two different international standards at counting times of 300 s each. Potassium has the lowest precision of 8.4%, all other studied elements range between 0.8 and 2.8%. The calculation of the accuracy is not an easy task. For example an offset of the standard value obtained by Activation Laboratories, in comparison to the values recommended by Jarosewich and coauthors (Jarosewich et al., 1987) was observed for the Allende standard samples. The powder used for the actlab analysis was from a small fragment (approximately 1.5 g) that might be biased since the components of Allende are relatively coarse. The mean chondrule diameter is around 1 mm (variance 0.5 – 2 mm) (Clarke et al., 1971), responding to the observed dependency of grain size of the contaminants in soils and the needed sample mass to get representative results, the mass should have been >6 g (Eggimann, 2008, references therein). Since we are interested mainly in the major and some trace elements that are distributed nearly homogeneous (with the exception of Cr) in the sample we believed to have an adequate sample mass. The used Oman meteorite standard samples were available in larger quantities and repeated measurements by actlab yielded similar concentrations. The accuracy was calculated using the deviation of the adjusted HHXRF measurements from the standard values. Each standard sample was measured with HHXRF for at least three times and the median out of these measurements was taken for the calculation. The relative errors for the elements of interest are 10% to 20 %, which is considered acceptable for a field portable instrument (Table 3.6) (Goldstein et al., 1996).

The best results are obtained for iron, which is the element occurring at the highest concentrations. The rather large errors for Co and Ni could be due to the inhomogeneous distribution of iron particles and the high absorption of X-rays within the metallic iron particles. Measuring pressed pellets with high concentrations of Sr, a large offset is observed. This is due to the large uncertainty on the standard value and the apparent non-linear behavior of Sr at concentrations exceeding 1000 µg/g. Only linear corrections are possible

with the used HHXRF analyzer. For Sr concentrations >1000 µg/g a second correction line is necessary. Accuracies for K, Co and Ba are to be taken with caution since these elements occur in meteorites in concentrations close to the detection limit of the used HHXRF. The other elements of interest (Ca, Ti, Cr, Mn, Fe, Ni and Sr) usually occur far above detection limit. Test on soil samples and other non-meteoritic standards yielded element-specific detection limits as noted in Table 3.6.

3.4.2. Evaluated elements

In the following section elements of interest for meteorites and the corresponding soils are discussed following their Z number (Fig. 3.5):

3.4.2.1. Potassium

In most stone meteorites potassium is a trace element (50 to 8000 µg/g), often occurring close to limit of detection (LOD) of the HHXRF of around 500 µg/g (Fig. 3.5a). Potassium is concentrated in feldspar. For precise results a minimum counting time of 60 s for the "low filter" is recommended. The accuracy for K is about 18 %, which is one of the worst. But K is the lightest detectable element with the PIN detector under ambient conditions. Therefore it is difficult to interpret K contents with respect to terrestrial contamination. For meteorite classification only the order of magnitude is relevant.

3.4.2.2. Calcium

Calcium typically occurs in meteorites at concentrations of 1 – 2 wt%. We find a good agreement of our measurements with the independently determined values (Fig. 3.5b). Calcium is concentrated in plagioclase, Ca-rich pyroxenes and Ca-phosphate that are inhomogeneously distributed within meteorites. Therefore some variation within a single sample is common. Additionally, Ca can occur as terrestrial contaminant in form of calcite or gypsum/anhydrite.
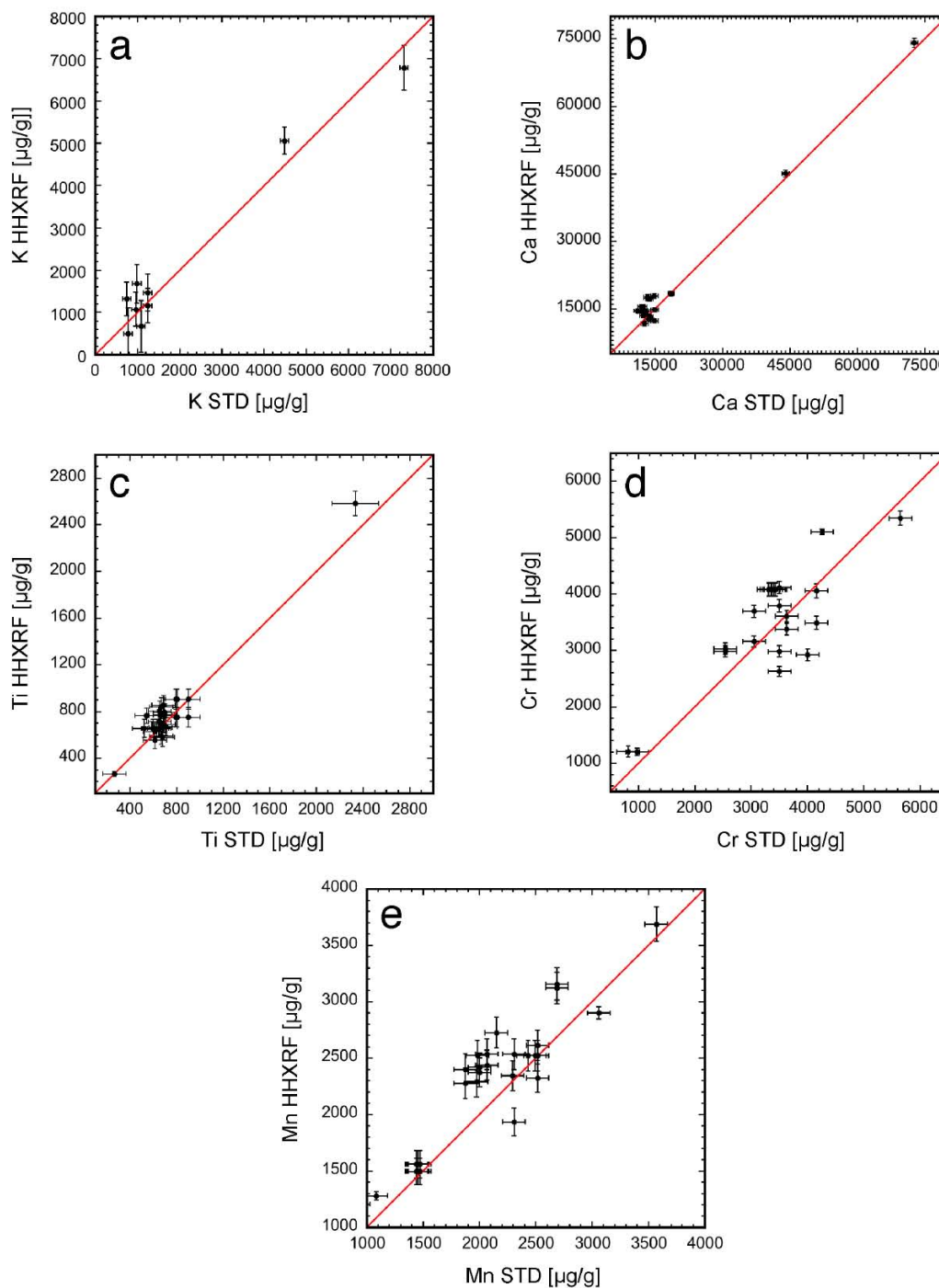
Figure 3.5. *HHXRF measurements on meteorite samples plotted versus reference (STD) values obtained by ICP-MS and XRF. a: K, b: Ca, c: Ti, d: Cr, e: Mn, f: Fe, g: Co, h: Ni, i: Sr, and j: Ba. The red line shows 1:1 linear correlation. Note the logarithmic scale in the Ba, Ni and Sr plots.*
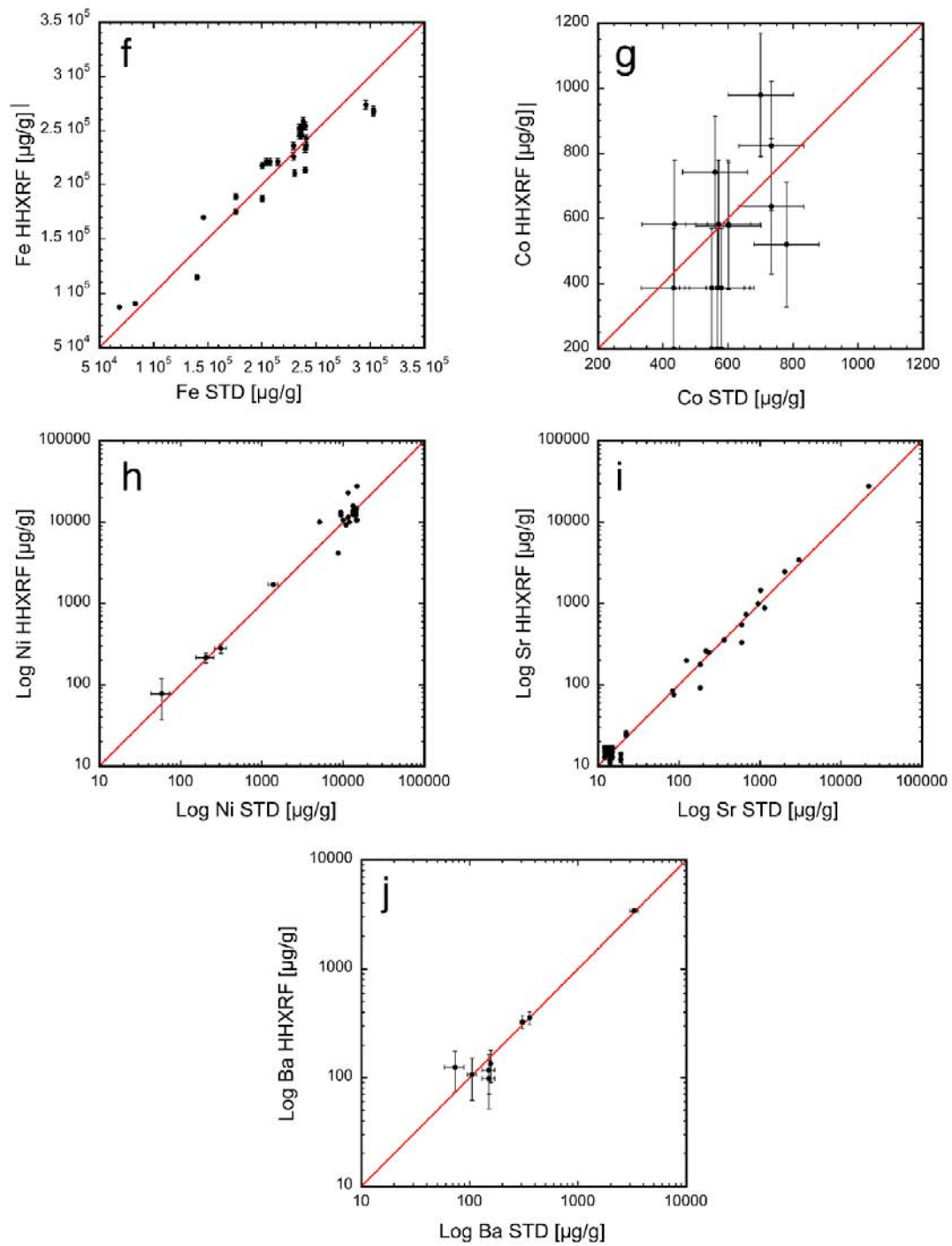
Figure 3.5. *Continued*

3.4.2.3. Titanium

In chondritic meteorites titanium is typically present at concentrations of 400 to 1200 µg/g, most commonly 700 - 1100 µg/g Ti (Fig. 3.5c). The outliners on Figure 3.5c are the measurements of the relative Ti-rich lunar meteorite SaU 169. Because of the methodology a well-known overlap exists for the Ti $K\alpha$ and Ba $L\alpha$ lines. For common meteoritic concentrations this is not a problem for the instrument used. Not until Ba exceeds concentrations of ~400 µg/g. This overlap results in over-estimated Ti values (Fig. 3.3).

3.4.2.4. Chromium

Meteorites generally have Cr concentrations of 1000 – 6000 µg/g with a peak of abundance at 3000 - 4000 µg/g (Fig. 3.5d). The main carrier phase is chromite, typically showing an irregular distribution in meteorites. Grain size is typically between 10 µm and 200 µm. In comparison with standard values, Cr measured by common XRF is mostly higher than the analysis by ICP-MS (Table 3.3). This could be due to insufficient leaching of chromite while sample preparation for ICP-MS. We often observe an overestimation of Cr with HHXRF measurements that supports this conclusion. Since chromite is not distributed uniformly in unprepared natural samples the Cr content often scatters by varying the measurement spot. The effective measuring depth for Cr is <1 mm. Therefore it is important to measure at least three spots in hand specimens, if proper Cr contents are required.

3.4.2.5. Manganese

Manganese is associated with Fe in silicate minerals while the metal fraction of meteorites is devoid of Mn. In combination with Fe, Mn is an important element for the classification of meteorites. Typical concentrations in silicate-rich meteorites are between 1000 and 4000 µg/g with a peak of values between 2200 and 2700 µg/g (ordinary chondrites and primitive achondrites) (Fig. 3.5e). No indications of a possible influence on analytical results of line interferences between Cr $K\beta$ and Mn $K\alpha$ were observed during our survey. Similar to Cr and Fe, the effective measuring depth of Mn is <1 mm.

3.4.2.6. Iron

Iron is one of the most abundant elements in meteorites, ranging from <1 wt% in aubrites to 90 wt% in iron meteorites. The most iron rich ordinary chondrites contain up to 30 wt%. Up to this value the instrument yields very good results (Fig. 3.5f). However, iron occurs partially in metallic form as "nuggets" up to several mm that can cause X-ray absorption when measuring cut surfaces of hand specimens and can be distributed irregularly in a meteorite powder due to the difficulty in milling metallic Fe. Other minerals carrying Fe are the silicates olivine and pyroxene and the iron sulfide troilite. During terrestrial weathering, metallic iron is replaced by iron oxides and iron hydroxides. The latter typically forms a dense network of veins. Where such veins reach the surface of the meteorite and form iron rich patches, this may yield increased Fe concentrations when measuring with HHXRF. One has to be aware that the measuring depth of Fe is <1 mm and since iron is a dense element it could cause shielding.

3.4.2.7. Cobalt

Cobalt concentrations in chondritic meteorites are in the range of 300 – 1000 µg/g, just above the instrument's LOD. This results in large error bars (Fig. 3.5g). However, the content of Co is not critical for chondrite classification, as it would be for iron meteorites, but is important to discriminate from artificial or terrestrials materials. The quantification of Co at high Fe concentrations, as is common in meteorites, is difficult due to an overlap of $K\alpha$ line of Co with the $K\beta$ line of Fe.

3.4.2.8. Nickel

Nickel concentrations range from 50 µg/g up to 2 wt% in the tested meteorites (Fig. 3.5h). Most meteorites have Ni contents of about 1.1 wt%. The most important nickel-bearing mineral is taenite, native iron nickel. During weathering of chondritic meteorites Fe-Ni-metal is preferentially weathered and some Ni get lost (Al-Kathiri et al., 2005; Lee and Bland, 2004). On meteorite surfaces in direct contact with soil often a pale green mineral is observed that was identified as Ni-serpentine (Al-Kathiri et al., 2005). HHXRF measurements on

buried surface of weathered meteorites often show an enrichment of Ni. Some of Ni remains within the meteorite in form of iron hydroxides (Lee and Bland, 2004).

3.4.2.9. Strontium

Freshly fallen chondritic meteorites have strontium concentrations of 9 ro 11 µg/g. Weathering and contamination in hot deserts can lead to Sr increases by a factor 10 to 1000 (Al-Kathiri et al., 2005). HHXRF provides reliable Sr data over the whole concentration range from fresh to weathered samples (Fig. 3.5i). The results from the experiments for signal depths of contaminants indicate that Sr can be traced up to 2 mm within a H chondrite (Fig. 3.1). The detection of Sr even at low concentrations requires only short measuring times. Mostly, it appears as the first element detected on the screen after 5 to 10 s.

3.4.2.10. Barium

Unaltered chondritic meteorites have low barium concentrations of about 3 to 5 µg/g (Wasson and Kallemeyn, 1988). During weathering and contamination in hot deserts Ba can be enriched by a factor of 100 (Al-Kathiri et al., 2005). With 300 s measuring time a limit of detection (LOD) of about 100 µg/g was found for Ba. In most of the samples Ba lies below or close to LOD. But in case of elevated concentrations and for the spiked pellets, the correlation is good (Fig. 3.5j). Another critical factor in Ba analysis is sample thickness. For samples thinner than 1 cm it is unlikely to obtain meaningful Ba concentrations since the instrument was calibrated using samples with a thickness of one centimeter. Barium is the only element of interest, which is measured using the "high filter" of the instrument. If Ba is not required, the "high filter" can be switched off, saving 120 seconds of measuring time with the settings used here. With the current instrument low Ba contaminations (5 to 100 µg/g) are thus not detectable.

3.4.2.11. Other elements

The concentrations of all other elements measurable with HHXRF mostly are below the limit of detection (LOD) in fresh and weathered meteorites. Elements at the LOD are S, V, Zn, As, Zr, Nb, Mo and Pb. In some cases they fit well to the standard value. But often they are

overestimated, especially S, V, As and Nb, since these elements are difficult to measure with a PIN detector at the concentration they appear in meteorites. Due to the lower precisions and accuracies, and their limited importance for meteoritics, these elements were not investigated systematically.

3.4.3. Applications of HHXRF in meteoritics

We have tested several applications in the field of meteorite analysis where HHXRF proved to be a powerful tool. Some of these take advantage of its portability and are thus specifically field-related applications while others profit from its simple handling and the possibility of the fast collection of large amounts of geochemical data in the laboratory for statistical studies.

3.4.3.1. Identification of doubtful meteorites

During the search for meteorites often materials of unidentified nature are encountered. Since most of the common meteorites contain metallic iron, a test with a magnet or a susceptibility meter can help in their recognition. However, several rare types of meteorites are not ferromagnetic and have a low susceptibility and may be missed. With a short HHXRF measurement it is possible to unequivocally identify most types of meteoritic materials, and distinguish them from terrestrial rocks and man-made artefacts. Magnetic meteorites typically have Ni contens >1 wt% and nonmagnetic meteorites (e.g. lunar or martian rocks) have characteristic element ratios (particularly Fe/Mn) distinguishable from terrestrial rocks. In addition to magnetic susceptibility measurements for the identification of meteorites (e.g., Folco et al., 2006), HHXRF is an instrument that allows the rapid identification of most types of meteorites in the field. As an example, we did identify meteorite Ramlat As Sahmah (RaS) 287 as diogenite (orthopyroxenite probably derived from asteroid Vesta) while still in find position in January 2009. This classification was later confirmed by mineralogical and oxygen isotopic analyses.

During terrestrial residence meteorites often break up into several rusty fragments (Al-Kathiri et al., 2005). In hot deserts environments, such small fragments are easily recognized but in

some cases cannot be discriminated from bits of corroded cans and other human waste, or terrestrial Fe-hydroxide nodules and magnetite pebbles. In such cases a short HHXRF measurement provides a reliable answer based on Ni concentration. Similarly, HHXRF was used in the prospection for fragments of the Twannberg meteorite (Hofmann et al., 2009) near Twann, Switzerland. Meteoritic fragments can easily be detected among large numbers of magnetic fragments extracted from a small stream, based on the presence of Fe, Ni and absence of Cr (present in Ni-Cr-steels).

3.4.3.2. Fast classification of meteorites

Although most chondrites have very similar compositions, they are distinguishable in terms of bulk chemistry, mainly by variations in Ca, Mn, Fe and Ni. The most robust method was found to be a plot of bulk Fe versus bulk Mn or bulk Ni versus Fe/Mn-ratio (Fig. 3.6). Fields in Figure 3.6 show the ranges of published compositional data for falls (achondrites and chondrites (Mittlefehldt et al., 1998, references therein; Mittlefehldt, 2003, references therein; Wasson and Kallemeyn, 1988; Jarosewich, 1990; Mason, 1962 and Kallemeyn et al., 1989) and finds (achondrites, Mittlefehldt et al., 1998, references therein; Mittlefehldt, 2003, references therein, actlab) for the most important and common meteorite classes. Ordinary chondrites are divided into LL, L and H chondrites based on the metal content and the degree of oxidation of Fe-Mg silicates i.e. H chondrites have higher bulk Fe and Ni contents and lower Mn contents and more magnesium-rich olivines and pyroxenes. The limit between LL and L chondrites is not sharp what makes it difficult for HHXRF analyses. Additionally, terrestrial weathering changes the bulk composition. Loss of Ni, S and to some extend Co is observed in strongly weathered meteorites recovered from Oman (Al-Kathiri et al., 2005). Iron is also mobilized during weathering and forms a dense network of Fe-oxide/hydroxide veins inside the meteorite and is also accumulated in the weathering rind in the outer parts of meteorites (Lee and Bland, 2004). Measurements by HHXRF on natural surfaces (NS) can thus result in overestimated bulk Fe contents while inside the meteorite, on cut surfaces (CS), it is underestimated, resulting in lower Fe/Mn ratios as observed in Figure 3.6.
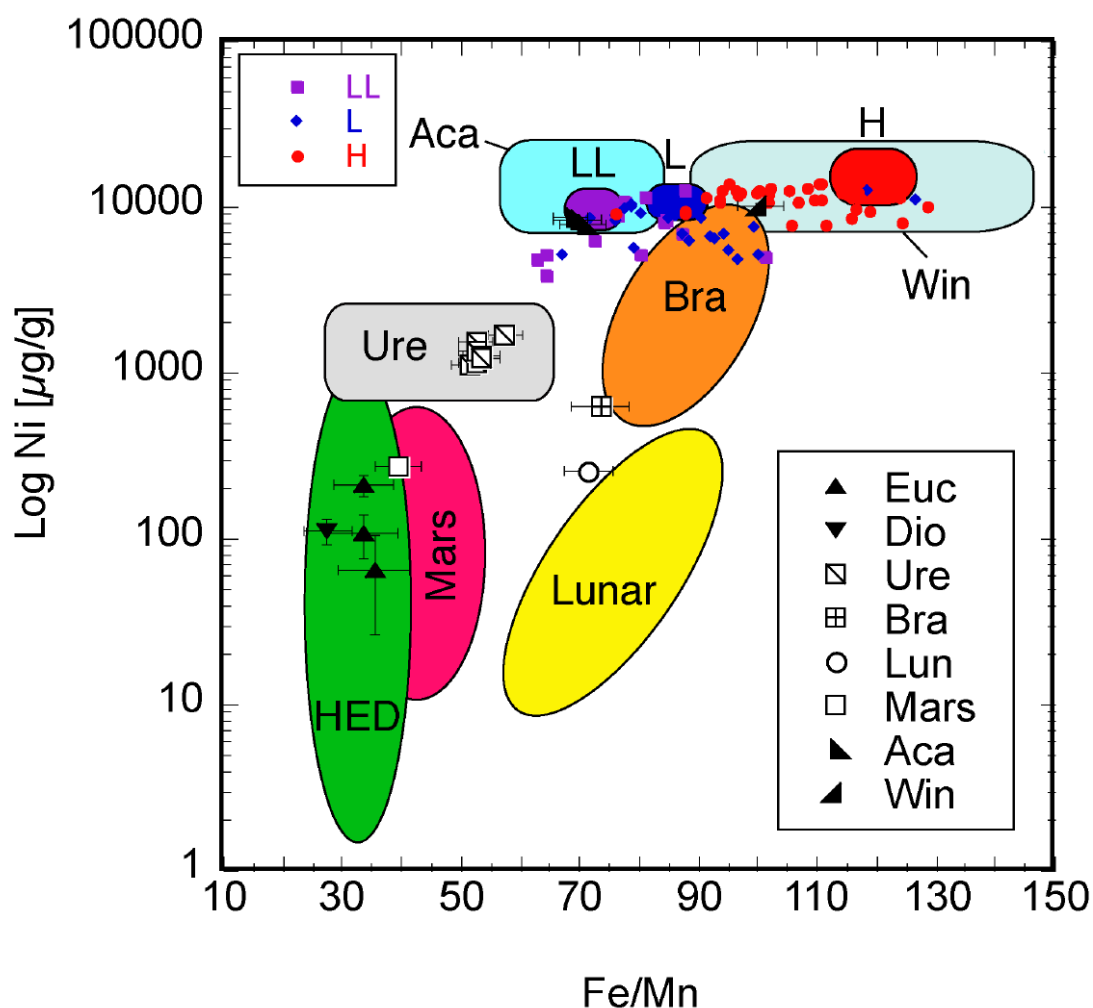
Figure 3.6. *Classification diagram for meteorites using bulk elemental data obtained by HHXRF. Fields show the ranges of published compositional data for falls and finds for the most important and common meteorite classes. Symbols represent 300 s HHXRF measurements obtained on cut surfaces of meteorite finds, mainly from the Sultanate of Oman.*

The displayed fields for the ordinary chondrites (LL, L and H) only include data from falls. Weathering effects lower the Ni content (Al-Kathiri et al., 2005).

Acapulcoites (Aca) and winonaites (Win) are primitive achondrites having chondritic bulk chemistry. Ureilites (Ure) and brachinites (Bra) are meteorites with near primitive bulk compositions but igneous textures. Eucrites (Euc) and diogenites (Dio) are differentiated meteorites probably derived from the asteroid 4 Vesta. Lunar (Lun) and martian (Mars) meteorites are also differentiated rocks derived from Earth's Moon and Mars, respectively.

The approximate classification of achondrites often is possible by visual inspection. Achondrites are meteorites with igneous textures and are in most cases chemically differentiated. Primitive achondrites (acapulcoites, lodranites and winonaites) have basically chondritic bulk compositions. From these meteorites only a few bulk chemical data are available and a lot of them are weathered finds resulting in large fields in Figure 3.6. Certain types of achondrites are linked to defined parent bodies that have distinct Fe/Mn ratios. For example lunar meteorites and eucrites (likely derived from asteroid 4 Vesta) can have very similar mineralogies and textures but have distinct Fe/Mn ratios of 60-90 (moon) or 28-35 (eucrites). We have routinely applied HHXRF analyses and derived Fe/Mn ratios for the discrimination of eucrites from lunar meteorites for samples brought to our lab by meteorite collectors. Meteorites probably derived from the differentiated asteroid Vesta 4 (howardites, eucrites and diogenites – summarized as HED) (e.g. Ruzicka et al., 1997) have basaltic/gabbroid compositions marginally overlapping with the field of martian meteorites. For a more profound classification, in addition to the Ni vs. Fe/Mn plot a discrimination of meteorites can be made based on Ca, K or Ti contents (Mittlefehldt et al., 1998). Combined with visual characteristics, it is possible to classify meteorites by nondestructive HHXRF measurements. However, best results are obtained on cut meteorite because the effect of terrestrial weathering and contamination is less pronounced than on natural surfaces. In addition, in fusion crusts of meteorites heavy elements such as Fe, Mn and Ni can be enriched whereas light elements like K can be depleted (e.g. Genge and Grady, 1999; Shirai et al., 2009).

For classification a 60 s measurement with the "field set up" yields satisfying results. However, a 300 s measurement in "lab set up" should be used to obtain lower errors and detection limits. At least three analyses at three different spots are recommended to obtain a representative result. Studies focused on chemical changes during magmatic differentiation will still have to rely on destructive chemical analyses in future. But HHXRF is a very suitable tool helping with the recognition and identification of meteorites.

3.4.3.3. Weathering effects in soils under meteorites

During oxidation of the Fe-Ni-phases kamacite and taenite, Ni is partially liberated and can be accumulated in the soil under meteorites (Al-Kathiri et al., 2005). Normally, soils in Oman have Ni contents in the range of 20 - 60 µg/g (size fraction <0.15 mm), close to LOD of the instrument used. Weathering of meteorites can result in an increase exceeding 10 times the pristine value in underlying soils (Fig. 3.7). Increased Ni contents under meteorites indicate stable position during the terrestrial history of the meteorite, consistent with stable desert surfaces that are required for meteorite accumulation.
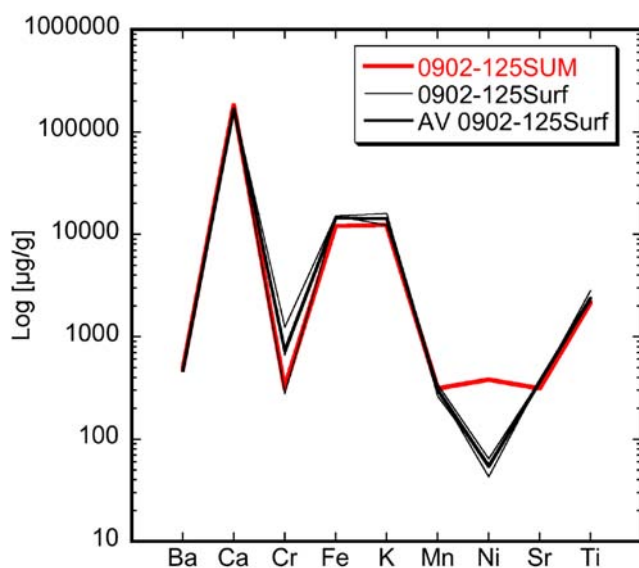
Figure 3.7. HHXRF measurements of soil samples from the find site of meteorite RaS 316 (field No. 0902-125) in Oman. Sample SUM refers to "soil under meteorite" and shows a strong enrichment of Ni as compared to measurements of reference soil samples from the surface (surf).

3.4.3.4. Desert varnish

A common feature on terrestrial rocks in hot deserts is a thin black coating called desert varnish (DV). The process of DV formation is not understood in detail but the main components are identified as clay minerals, often aeolian deposits, Fe-Mn-oxides, and organic components related to a suggested involvement of microbes and fungi in DV development (e.g. Dorn, 2009; Garvie et al., 2008; Perry et al., 2006). DVs are Mn rich and show traces of Ba, Sr and Ti (e.g. Engel and Sharp, 1958). The degree of evolution of a DV can give information on the terrestrial age. Archeologists have applied HHXRF in attempts to date petroglyphs by measurements comparing the DV surfaces with the scratched parts (Lytle, 2009; Lytle et al., 2000; Pingitore and Lytle, 2003; Pingitore et al., 2004). Desert varnish is reported on meteorites found in the US (Kring et al., 2001), Namibia (Fudali and Noonan, 1975) and Australia (Lee and Bland, 2003) with a typical thickness of 70-130 µm,

but it can reach 3 mm. By comparing HHXRF data obtained on cut surfaces (CS) of meteorites with exposed surfaces (preferably not fusion crusted), the relative enrichment of Mn and other elements is detectable and the presence of DV's can be inferred. As an example, analyses of the lunar meteorite SaU 169 (Gnos et al., 2004) are presented in Figure 3.8.
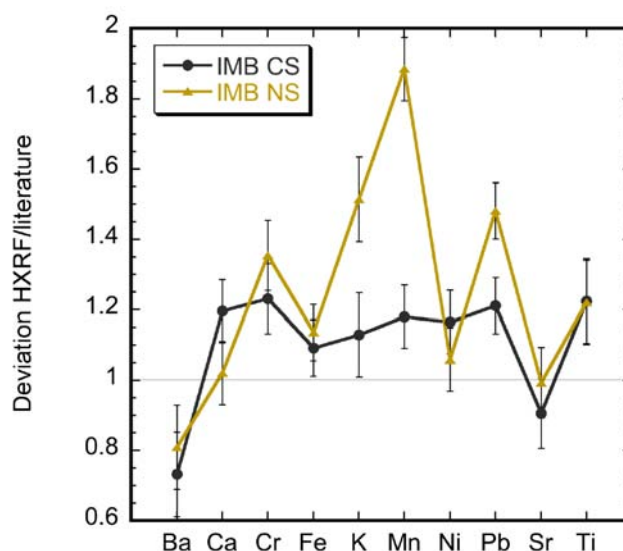
Figure 3.8. *HHXRF measurements of the impact melt breccia (IMB) portion of the lunar meteorite SaU 169 normalized to literature values of homogenized bulk samples (Gnos et al., 2004). Taking Into account the slightly different matrix of this sample as compared to the meteorites used for calibration, the HHXRF measurements are in good agreement with published values except for significantly elevated values of Mn, K and Pb on the natural surface (NS), indicating the development of a thin desert varnish enriched in these elements. Each data point represents the median of 4 to 11 measurements of 300 s.*

Measuring the degree of Mn enrichment on exposed surfaces can be used as proxy of the terrestrial history of the meteorite. A strong enrichment on medium to heavily weathered samples indicates a stable position on the soil implying the presence of an area ideal for the accumulation of meteorites over long periods. Potassium, lead and titanium that are enriched in the desert varnish could also be taken into account but are difficult to measure at the expected concentrations due to high LOD and low precision. The development of DV on meteorites likely is correlated with terrestrial age, but is also influenced by soil stability and sandblasting. We explore the suitability of regional DV abundance on meteorites as an indicator of surface stability and meteorite preservation potential.

3.4.3.5. Approximative terrestrial age dating based on Sr and Ba accumulation

For an estimation of the terrestrial residence time of a meteorite a number of parameters that change after arrival on Earth can be measured (degree of oxidation, water content). They are the result of interaction of meteorites with the terrestrial environment. Oxidative weathering and contamination from the soil are important factors.

In this context, our main application of HHXRF is to analyze natural and cut surfaces of meteorites from the Sultanate of Oman to study the effects of terrestrial contamination. The aim is to correlate the Sr and Ba enrichment in ordinary chondrites with the terrestrial age obtained by radiocarbon dating (e.g., Jull, 2006) to establish an approximative age scale. In the Oman case, Sr- and Ba-concentrations are independent indicators of a meteorite's terrestrial age. This allows the designation of a crude terrestrial age to each sample collected. The comparison of the large number of approximate ages with the smaller number of ^{14}C-dated samples provides a control to check for a bias in the samples selected for ^{14}C dating.

3.4.3.6. Pairing issues and recognition of find areas

In recent years, large amounts of meteorites have been recovered in hot deserts, especially in Northwest Africa (NWA, defined by the Meteoritical Society as "Morocco and parts of adjoining neighboring countries"). Due to the unknown find conditions, NWA meteorites may also include samples from other countries such as Mali, Niger, Libya and even Oman. By far the largest number is from "NWA" and lacks geographical information. Many meteorites, especially the ordinary chondrites, are not properly classified since this is time consuming and the scientific and commercial interest is mainly focused on achondrites and rare types of chondrites. Meteorites usually break up in the atmosphere and several fragments reach the earth forming strewn fields (e.g., Clarke et al., 1971; Gnos et al., 2009). A short measurement by HHXRF provides a fast first classification, which helps to recognize pairing groups (i.e. meteorites from the same fall event). The recognition of pairings is important for the determination of absolute fall abundances and statistical studies of the global meteorite influx derived from such data. Criteria applied include bulk compositional data (Fe/Mn, Ni, Cr and Ca) and the amount of terrestrial contamination (Ba, Sr and Mn) on natural surfaces.

3.5. CONCLUSIONS

The newly developed commercial HHXRF analyzers are powerful tools for simple and fast collection of element concentration data from meteorites and associated terrestrial materials. Since the method is non-destructive it is very helpful for the study of precious materials such as meteorites.

No sample preparation is needed, but since the measurement spot is 8 mm in diameter at least three measurements are recommended to get reliable results. The calibration curves of our HHXRF device were slightly adjusted for meteorite and desert soil matrices. Deviations between 10% and 20 % from standard values are reached for most important elements. The instrument is useful for the identification of doubtful meteorites in the field and for the chemical classification of the most abundant groups of chondrites and achondrites. Terrestrial contamination effects such as the accumulation of Mn, Sr and Ba or the loss of Ni are easily traceable with a 300 s HHXRF measurement. A combination of these two applications can help solving pairing issues. Due to the speed, easy handling and non-destructive character of analysis the instrument is a useful tool in meteoritics both in the field and in the laboratory. The latest generation of HHXRF instruments equipped with SDD detectors will yield much more precise analyses on more elements with lower LOD since they have a better energy resolution, which produces a better peak-to-background ratio.

3.6. Acknowledgments

3.7. REFERENCES

Al-Kathiri, A., 2006. Studies on Oman Meteorites. PhD Thesis, University of Bern.

Al-Kathiri, A., Hofmann, B. A., Jull, A. J. T., and Gnos, E., 2005. Weathering of meteorites from Oman: Correlation of chemical and mineralogical weathering proxies with ^{14}C terrestrial ages and the influence of soil chemistry. *Meteoritics & Planetary Science* 40:1215-1239.

Bevan, A. W. R. and Binns, R. A., 1989a. Meteorites from the Nullarbor Region, Western Australia. 1. A review of past recoveries and a procedure for naming new finds. *Meteoritics* 24:127-133.

Bevan, A. W. R. and Binns, R. A., 1989b. Meteorites from the Nullarbor region, Western Australia. 2. Recovery and classification of 34 new meteorite finds from the Mundrabilla, Forrest, Reid and Deakin areas. *Meteoritics* 24:135-141.

Bischoff, A. and Geiger, T., 1995. Meteorites from the Sahara: Find locations, shock, classification, degree of weathering and pairing. *Meteoritics* 30:113-122.

Bonizzoni, L., Caglio, S., Galli, A., and Poldi, G., 2010. Comparison of three portable EDXRF spectrometers for pigment characterization. *X-Ray Spectrometry* 39:233-242.

Clarke, J., Roy S., Jarosewich, E., Mason, B., Nelen, J., Gomez, M., and Hyde, J. R., 1971. The Allende, Mexico, meteorite shower. *Smithsonian Institution Press, City of Washington* 5.

Consolmagno, G. J., Britt, D. T., and Macke, R. J., 2008. The significance of meteorite density and porosity. *Chemie Der Erde-Geochemistry* 68:1-29.

Dorn, R. I., 2009. The rock varnish revolution: New insights from microlaminations and the contributions of Tanzhuo Liu. *Geography Compass* 3:1-20.

Eggimann, M., 2008. Geochemical aspects of municipal solid waste incineration bottom ash and implications for disposal. PhD Thesis, Institut für Geologie.

Engel, C. G. and Sharp, R. P., 1958. Chemical data on desert varnish. *Geological Society of America Bulletin* 69:487-&.

Folco, L., Rochette, P., Gattacceca, M., and Perchiazzi, N., 2006. In situ identification, pairing, and classification of meteorites from Antarctica through magnetic susceptibility measurements. *Meteoritics & Planetary Science* 41:343-353.

Fudali, R. F. and Noonan, A. F., 1975. Gobabeb, a new chondrite: The coexistence of equilibrated silicates and unequilibrated spinels. *Meteoritics* 10:31-39.

Garvie, L. A. J., Burt, D. M., and Buseck, P. R., 2008. Nanometer-scale complexity, growth, and diagenesis in desert varnish. *Geology* 36:215-218.

Genge, M. J. and Grady, M. M., 1999. The fusion crusts of stony meteorites: Implications for the atmospheric reprocessing of extraterrestrial materials. *Meteoritics & Planetary Science* 34:341-356.

Gnos, E., Eggimann, M., Al-Kathiri, A., and Hofmann, B. A., 2006. The JaH 091 strewnfield. *Meteoritics & Planetary Science* 41 Suppl.:A64.

Gnos, E., Hofmann, B., Franchi, I. A., Al-Kathiri, A., Hauser, M., and Moser, L., 2002. Sayh al Uhaymir 094: A new martian meteorite from the Oman desert. *Meteoritics & Planetary Science* 37:835-854.

Gnos, E., Hofmann, B. A., Al-Kathiri, A., Lorenzetti, S., Eugster, O., Whitehouse, M. J., Villa, I. M., Jull, A. J. T., Eikenberg, J., Spettel, B., Krähenbühl, U., Franchi, I. A., and Greenwood, R. C., 2004. Pinpointing the source of a lunar meteorite: Implications for the evolution of the moon. *Science* 305:657-659.

Gnos, E., Lorenzetti, S., Eugster, O., Jull, A. J. T., Hofmann, B. A., Al-Kathiri, A., and Eggimann, M., 2009. The Jiddat al Harasis 073 strewn field, Sultanate of Oman. *Meteoritics & Planetary Science* 44:375-387.

Goldstein, S. J., Slemmons, A. K., and Canavan, H. E., 1996. Energy-dispersive X-ray fluorescence methods for environmental characterization of soils. *Environmental Science & Technology* 30:2318-2321.

Harvey, R., 2003. The origin and significance of Antarctic meteorites. *Chemie Der Erde-Geochemistry* 63:93-147.

Hezel, D. C., Schlüter, J., Kallweit, H., Jull, A. J. T., Al-Fakeer, O. Y., Al-Shamsi, M., and Strekopytov, S., 2011. Meteorites form the United Arab Emirates: Description, weathering, and terrestrial ages. *Meteoritics & Planetary Science* 46:327-336.

Hofmann, B. A., Lorenzetti, S., Eugster, O., Krähenbühl, U., Herzog, G., Serefiddin, F., Gnos, E., Eggimann, M., and Wasson, J. T., 2009. The Twannberg (Switzerland) IIG iron meteorites: Mineralogy, chemistry, and CRE ages. *Meteoritics & Planetary Science* 44:187-199.

Hou, X., He, Y., and Jones, B. T., 2004. Recent advances in portable X-ray fluorescence spectrometry. *Applied Spectroscopy Reviews* 39:1-25.

Jarosewich, E., 1990. Chemical-analyses of meteorites - A compilation of stony and iron meteorite analyses. *Meteoritics* 25:323-337.

Jarosewich, E., Roy S. Clarke, J., and Barrows, J. N., 1987. The Allende Meteorrite Reference Sample. *Smithsonian Institution Press, City of Washington* 27.

Jull, A. J. T., 2006. *Terrestrial ages of meteorites*. The University of Arizona Press, Tucson, AZ.

Jull, A. J. T., Donahue, D. J., Cielaszyk, E., and Wlotzka, F., 1993. Carbon-14 terrestrial ages and weathering of 27 meteorites from the southern high-plains and adjacent areas (USA). *Meteoritics* 28:188-195.

Jull, A. J. T., McHargue, L. R., Bland, P. A., Greenwood, R. C., Bevan, A. W. R., Kim, K. J., LaMotta, S. E., and Johnson, J. A., 2010. Terrestrial ages of meteorites from the Nullarbor region, Australia, based on ^{14}C and [14]C-[10]Be measurements. *Meteoritics & Planetary Science* 45:1271-1283.

Kallemeyn, G. W., Rubin, A. E., Wang, D., and Wasson, J. T., 1989. Ordinary chondrites - Bulk compositions, classification, lithophile-element fractionations, and composition-petrographic type relationships. *Geochimica et Cosmochimica Acta* 53:2747-2767.

Kring, D. A., Jull, A. J. T., McHargue, L. R., Bland, P. A., Hill, D. H., and Berry, F. J., 2001. Gold basin meteorite strewn field, Mojave Desert, northwestern Arizona: Relic of a small late pleistocene impact event. *Meteoritics & Planetary Science* 36:1057-1066.

Lee, M. R. and Bland, P. A., 2003. Dating climatic change in hot deserts using desert varnish on meteorite finds. *Earth and Planetary Science Letters* 206:187-198.

Lee, M. R. and Bland, P. A., 2004. Mechanisms of weathering of meteorites recovered from hot and cold deserts and the formation of phyllosilicates. *Geochimica et Cosmochimica Acta* 68:893-916.

Lytle, F., 2009. How old are petroglyphs? Prove it. *Nevada Rock Art Foundation meeting, Mesquite NV*.

Lytle, F. W., Pingitore, N. E., Lytle, N. W., Ferris-Rowley, D., and Reheis, M. C., 2000. Determination of growth rate of desert varnish: Application to dating petroglyphs. *Workshop on Synchrotron Radiation in Art and Archaeology, SSRL*.

Mason, B., 1962. The classification of chondritic meteorites. *American Museum Novitates, Published by the American Museum of Natural History Central Park West at 79th street, New York* 2085:429-455.

McSween, H. Y., Bennett, M. E., and Jarosewich, E., 1991. The mineralogy of ordinary chondrites and implications for asteroid spectrophotometry. *Icarus* 90:107-116.

Mittlefehldt, D. W., 2003. Achondrites. In: Davis, A. M. (Ed.), *Treatise on Geochemistry, Volume 1*. Elsevier.

Mittlefehldt, D. W., McCoy, T. J., Goodrich, C. A., and Kracher, A., 1998. Non-chondritic meteorites from asteroidal bodies. In: Papike, J. J. (Ed.), *Planetary Materials*. Mineralogical Society of America, Washinton D.C.

Munoz, C., Guerra, N., Martinez-Frias, J., Lunar, R., and Cerda, J., 2007. The Atacama Desert: A preferential arid region for the recovery of meteorites - Find location features and strewnfield distribution patterns. *Journal of Arid Environments* 71:188-200.

NITON, 2008. User's Guide XL3t-600-v6.3. *User's Guide*:202.

Norton, O. R. and Chitwood, L. A., 2008. *Field Guide to Meteors and Meteorites*. Patrick Moore's Practical Astronomy Series, Springer, London.

Otto, J., 1992. New meteorite finds from the Algerian Sahara desert. *Chemie der Erde* 52:33-40.

Ouazaa, N. L., Perchiazzi, N., Kassaa, S., Zeoli, A., Ghanmi, M., and Folco, L., 2009. Meteorite finds from southern Tunisia. *Meteoritics & Planetary Science* 44:955 - 960.

Perry, R. S., Lynne, B. Y., Sephton, M. A., Kolb, V. M., Perry, C. C., and Staley, J. T., 2006. Baking black opal in the desert sun: The importance of silica in desert varnish. *Geology* 34:537-540.

Pingitore, N. E. and Lytle, F. W., 2003. Desert varnish: Relative and absolute dating using portable X-ray fluorescence. *EOS Trans. AGU* 84.

Pingitore, N. E., Lytle, F. W., Rowley, P. D., and Ferris, D. E., 2004. Absolute dating of desert varnish using portable X-ray fluorescence: Calibration and testing. *American Geophysical Union, Fall Meeting 2004*:abstrct #B33B-0266.

Radu, T. and Diamond, D., 2009. Comparison of soil pollution concentrations determined using AAS and portable XRF techniques. *Journal of Hazardous Materials* 171:1168-1171.

Reed, S. J. B., 1972. Determination of Ni, Ga, and Ge in iron meteorites by X-ray fluorescence analysis. *Meteoritics* 7:257-262.

Rochette, P., Gattacceca, J., Bonal, L., Bourot-Denise, M., Chevrier, V., Clerc, J. P., Consolmagno, G., Folco, L., Gounelle, M., Kohout, T., Pesonen, L., Quirico, E., Sagnotti, L., and Skripnik, A., 2008. Magnetic classification of stony meteorites: 2. Non-ordinary chondrites. *Meteoritics & Planetary Science* 43:959-980.

Rochette, P., Gattacceca, J., Bourot-Denise, M., Consolmagno, G., Folco, L., Kohout, T., Pesonen, L., and Sagnotti, L., 2009. Magnetic classification of stony meteorites: 3. Achondrites. *Meteoritics & Planetary Science* 44:405-427.

Rochette, P., Sagnotti, L., Bourot-Denise, M., Consolmagno, G., Folco, L., Gattacceca, J., Osete, M. L., and Pesonen, L., 2003. Magnetic classification of stony meteorites: 1. Ordinary chondrites. *Meteoritics & Planetary Science* 38:251-268.

Roldan, C., Murcia-Mascaros, S., Ferrero, J., Villaverde, V., Lopez, E., Domingo, I., Martinez, R., and Guillem, P. M., 2009. Application of field portable EDXRF

spectrometry to analysis of pigments of Levantine rock art. *X-Ray Spectrometry* 39:243-250.

Rubin, A. E., 1997. Mineralogy of meteorite groups. *Meteoritics & Planetary Science* 32:733-734.

Rubin, A. E. and Grossman, J. N., 2010. Meteorite and meteoroid: New comprehensive definitions. *Meteoritics & Planetary Science* 45:114-122.

Russell, S. S., Folco, L., Grady, M. M., Zolensky, M. E., Jones, R., Righter, K., Zipfel, J., and Grossman, J. N., 2004. The Meteoritical Bulletin, No. 88, 2004 July. *Meteoritics & Planetary Science* 39:A215-A272.

Ruzicka, A., Snyder, G. A., and Taylor, L. A., 1997. Vesta as the howardite, eucrite and diogenite parent body: Implications for the size of a core and for large-scale differentiation. *Meteoritics & Planetary Science* 32:825-840.

Schlüter, J., Schultz, L., Thiedig, F., Al-Mahdi, B. O., and Abu Aghreb, A. E., 2002. The Dar al Gani meteorite field (Libyan Sahara): Geological setting, pairing of meteorites, and recovery density. *Meteoritics & Planetary Science* 37:1079-1093.

Shirai, N., Humayun, M., and Irving, A. J., 2009. The bulk composition of coarse-grained meteorites from laser ablation analysis of their fusion crusts. *40th Lunar and Planetary Science Conference,*

Stelzner, T., Heide, K., Bischoff, A., Weber, D., Scherer, P., Schultz, L., Happel, M., Schron, W., Neupert, U., Michel, R., Clayton, R. N., Mayeda, T. K., Bonani, G., Haidas, I., Ivy-Ochs, S., and Suter, M., 1999. An interdisciplinary study of weathering effects in ordinary chondrites from the Acfer region, Algeria. *Meteoritics & Planetary Science* 34:787-794.

Szokefalvi-Nagy, Z., Demeter, I., Kocsonya, A., and Kovacs, I., 2004. Non-destructive XRF analysis of paintings. *Nuclear Instruments & Methods in Physics Research Section B-Beam Interactions with Materials and Atoms* 226:53-59.

Wasson, J. T. and Kallemeyn, G. W., 1988. Compositions of chondrites. *Philosophical Transactions of the Royal Society of London Series a-Mathematical Physical and Engineering Sciences* 325:535-544.

Weisberg, M. K., McCoy, T. J., and Krot, A. N., 2006. Systematics and Evaluation of Meteorite Classification. In: Lauretta, D. S. and McSween, H. Y. (Eds.), *Meteorites and the Early Solar System II*. University of Arizona Press, Tucson.

Zolensky, M. E., Wells, G. L., and Rendell, H. M., 1990. The accumulation rate of meteorite falls at the Earths surface - The view from Roosevelt Country, New-Mexico. *Meteoritics* 25:11-17.

A spider on a wind-eroded meteorite. Photo by Beda Hofmann.

Chemical contamination and macroscopic weathering features in meteorites from Oman and other hot deserts

To be submitted to *Meteoritics & Planetary Science*

Chemical contamination and macroscopic weathering features in meteorites from Oman and other hot deserts

Florian J. ZURFLUH[1]*, Beda A. HOFMANN[2], Edwin GNOS[3], Urs EGGENBERGER[1], Nicolas D. GREBER[1,2] and Igor M. VILLA[1,4]

[1]Institut für Geologie, Universität Bern, Baltzerstrasse 1 + 3, CH-3012 Bern, Switzerland
[2]Naturhistorisches Museum der Burgergemeinde Bern, Bernastrasse 15, CH-3005 Bern, Switzerland
[3]Muséum d'histoire naturelle de la Ville de Genève, 1 Route de Malagnou, CP 6434 CH-1211 Genève 6, Switzerland
[4]Università di Milano Bicocca, Milano, Italy.
* Corresponding author. E-mail address: florian.zurfluh@geo.unibe.ch

Abstract - The chemical composition and physical state of meteorites is modified during their terrestrial residence, depending on climate and soil composition of the recovery site. We have investigated meteorites from Oman, Saudi Arabia, Sahara and Australia for their elemental contamination on natural and cut surfaces with handheld XRF and recorded standardized macroscopic weathering parameters. For comparison, soil samples from Oman and Sahara were analyzed. Meteorites from Oman are highly contaminated with Sr and Ba (up to 100x the initial concentration inside) and have generally Sr/Ba ratios >1.2, which is similar to the corresponding soil samples. Further evidence for origin of the Sr contamination from the soil is provided by the near identical ^{87}Sr/^{86}Sr ratios in contaminated meteorites and corresponding soil samples. In contrast to Oman, meteorites from Sahara and Australia show preferential uptake of Ba and therefore typically have low Sr/Ba ratios <1, similar to their corresponding soils.

Natural surfaces of meteorites show slight enrichment of Ti, V and Mn, which is assumed to be the result of desert varnish. The enrichment of these elements is highest for meteorites from Australia (2.5-3.4x), elevated in Sahara (1.2-3.1x) and low for Oman (1.2-1.8x). A reason might be the stronger influence of wind erosion we observed on samples from Oman and parts of Sahara as compared to Australia. The differences in weathering and contamination of meteorites from different hot deserts may be used to give an indication where a specific meteorite was recovered.

4.1. INTRODUCTION

Each meteorite belonging to a specific group has similar mineralogical and chemical properties and is unweathered when it reaches Earth, no matter where it falls. But since most of the meteorites are recovered a few days to several thousand of years after their fall to Earth, interaction with the environment occurs and modifies its chemical and physical properties. Weathering rates are dependent on climate (Bland et al., 1998) and are fast in humid areas, moderate in hot desert environments and slow in cold deserts. The general weathering processes and weathering products are similar in all environments: oxidation of metal and troilite (e.g. Al-Kathiri et al., 2005; Bell and Lee, 2009; Bland et al., 2006; Buchwald and Clarke, 1989; Lee and Bland, 2004). But the contamination patterns and styles of physical weathering are slightly different. Meteorites from hot deserts all over the world often show precipitation of terrestrial calcite and gypsum (Al-Kathiri et al., 2005; Barrat et al., 1998; Bevan and Binns, 1989a; 1989b). Another recognized feature is elemental uptake of Mo, Sr, Ba and U (e.g. Barrat et al., 1998; Folco et al., 2007; Gattacceca et al., 2011; Hezel et al., 2011; Saunier et al., 2010; Stelzner et al., 1999). The primary content of Sr and Ba in ordinary chondrites is well established from falls. Mean values for Sr are 9-11 µg/g and for Ba 3-5 µg/g (Wasson and Kallemeyn, 1988). The major carrier phase for both are feldspars (Sr: ~90 µg/g, Ba: ~60µg/g) or feldspatic glass and to a lesser extent phosphate minerals (Sr: ~75 µg/g, Ba: ~14µg/g; (Kovach and Jones, 2010; Mason and Graham, 1970). Minor amounts occur in Ca-rich pyroxene (Sr: ~14µg/g, Ba: ~4 µg/g), Ca-poor pyroxene (Sr: ~4µg/g, Ba: ~1.4 µg/g), olivine (Sr: ~0.6 µg/g, Ba: ~0.8 µg/g) and chromite (Sr: ~7 µg/g, Ba: ~1.3 µg/g). No Sr and Ba is observed in sulfides and metals (Kovach and Jones, 2010; Mason and Graham, 1970).

Beside the chemical effects, meteorites from hot deserts are also modified in their macroscopic appearance. Soil material is introduced into cracks of meteorites and can be attached to the meteorite surface as well. Weathering minerals on the other hand precipitate in the interior and on the surface of the meteorites (Al-Kathiri et al., 2005; Hezel et al., 2011) and desert varnish develops on the surface and darkens the meteorite in addition to the rusty staining from iron oxyhydroxides (Lee and Bland, 2003; Schlüter et al., 2002). Sand particles transported by wind impact on the meteorites surface, polishing and eroding them (Al-Kathiri et al., 2005).

These macroscopic and chemical features are the most characteristic for hot deserts. The use of attached soil or biological material (bacteria, lichen) and the products of weathering to verify the find locality was proposed first by Treiman (1992). Two meteorites reportedly found in Europe showed typical hot desert features such as Sr and Ba accumulation, calcite veining and input of rounded (dune-) sand-grains (Bartoschewitz et al., 2009; Folco et al., 2007), which actually questions their reported finding site. Folco et al., (2007) included in their study also some European finds for comparison and found no significant enrichment of Sr and Ba within the European finds whereas all Saharan samples as well as Castenazo had Sr and Ba enrichments. Thus it becomes more and more important to describe and define the individual weathering styles characteristic of certain areas. The geographical dependence of contamination of meteorites from Antarctica was studied either by halogen contamination (Langenauer and Krähenbühl, 1993) or abundance of visible evaporite deposits (Losiak and Velbel, 2011). A new tool that has a high potential to trace the chemical contamination features is handheld XRF (HHXRF). Such commercially available instruments are relative easy and quick in handling and are non-destructive, which is a great advantage when measuring sparse and precious materials. Due to these advantages, HHXRF is used for example in archeology. In meteoritics, the potential of the instrument is only recognized for classification (Daviau et al., 2012; Mayne et al., 2011; Zurfluh et al., 2011). The use for weathering studies was proposed by Zurfluh et al., (2011; in review-b).

The purpose of this study is to trace the origin of the contamination material in meteorites from Oman and find differences between meteorites recovered from other well-known meteorite recovery areas. Therefore, we investigated several meteorites from Oman, Saudi Arabia, Sahara desert and Australia in order to reveal differences in their chemical and macroscopic terrestrial modification and explored the specific characteristics of individual environments. Since we have access to a large number of meteorites from Oman, we also searched for differences within this confined geographical environment.

4.2. SAMPLES AND ANALYSES

4.2.1. Meteorites and HHXRF

Meteorites from Oman were collected by the Omani Swiss meteorite search and research project and treated as reported in (Al-Kathiri et al., 2005; Gnos et al., 2009b; Hofmann, 2004; Zurfluh et al., in review-a; in review-b). Due to careful handling contamination was avoided during fieldwork as well as during laboratory/conservation work. In this study, we investigated all ^{14}C terrestrial age dated meteorites from Oman and all samples found during fieldwork in 2009 and 2010 (Zurfluh et al., in review-b). Thin sections were prepared including at least one cut through a natural surface of the meteorite. During the classification procedure meteorites were investigated by optical microscopy (transmitted and reflected light) and electron microprobe (JEOL JXA-8200) at the Institute for Geological Sciences, University of Bern. The profiles through the natural surfaces were scanned in quest of a hypothetical desert varnish (DV). Selected samples were investigated for their alteration and contamination mineralogy with a Zeiss EVO50 scanning electron microscope (SEM) with attached energy dispersive X-ray spectroscope (EDS) at the Institute for Geology, University of Bern.

All meteorites, including samples from Saudi Arabia, the Sahara Desert (from Dar al Gani, Libya; Tunisia and unresolved parts of Sahara desert) and Australia, were analyzed with a non-destructive NITON XLt3-600 handheld XRF (HHXRF) device. Diameter of the analyzed spot is 8 mm. The contamination of Sr is well detectable with HHXRF while Ba is difficult to measure and has a high limit of detection (Zurfluh et al., 2011). Besides these two elements, also Mn, Ti and V were studied in more detail. Calibration details of the instrument and the measurement routine is noted elsewhere (Zurfluh et al., 2011; in review-b). The meteorites were analyzed on their cut surface (CS), exposed surface (ES) and buried surface (BS). In cases where it was uncertain if the surface was exposed or buried, the measured surface was named natural surface (NS), which is, integrated over a complete meteorite, equal to the mean of ES and BS. In addition to the routine measurements of CS, ES and BS, on selected samples also profiles from ES to BS were analyzed on cut and natural surfaces.

All meteorites were macroscopically investigated for weathering parameters such as wind erosion, attached sand, attached caliche or calcite, greenish staining on BS due to Ni-serpentine precipitation (Al-Kathiri et al., 2005), surface coatings ("desert varnish") and cracks due to weathering. A detailed description of these parameters is given in Zurfluh et al., (in review-b).

To reconstruct the source of the Sr contamination we have investigated three meteorite/soil pairs from three distinct geographical meteorite recovery areas from Oman for their ^{87}Sr/^{86}Sr ratios.

4.2.2. Strontium isotope analyses

The strontium isotopic composition was determined on three complete individual ordinary chondrites from three different geographical locations in Oman and three corresponding soil samples collected within a few meters of the meteorites. The fragments of the analyzed meteorites are part of strongly weathered (WD≥4.0; (Zurfluh et al., in review-b), fragmented and strongly strontium contaminated samples. All visible attached terrestrial contamination was removed mechanically from the meteorites under a binocular before leaching. The soil samples were leached in MilliQ water for 9h and in 6.4M HCl for 20h in Savillex$^{®}$ PFA beakers. The meteorite fragments were leached in MilliQ water for 5h, in 0.18M HCl for 4h and in 6.4M HCl for 20h. All leachates were performed using open PTFE beakers under room temperature with the exception of the 6.4M HCl leaching of the meteorite, which were performed with closed PTFE beakers on a heating plate at 110°C. Strontium was separated from the sample matrix using Sr Spec™ in hand-made miniaturized PTFE columns. The ^{87}Sr/^{86}Sr isotope ratios were measured on a Nu-Instruments^{TM} multicollector inductively coupled plasma mass spectrometer (MC-ICP-MS, Wrexham, Wales, UK) at the Institute for Geological Sciences, University of Bern. Samples were analyzed in two distinct analytical sessions several weeks apart. The external reproducibility of the NIST SRM 987 analyzes of the two sessions were 0.710181 ± 29 and 0.710240 ± 10, respectively. The measured ^{87}Sr/^{86}Sr isotope ratios are normalized to a NIST SRM 987 value of 0.710245. Uncertainties (2σ standard errors) of the analyses are between $1.4*10^{-5}$ and $7.4*10^{-5}$ and include a propagation of the NIST SRM 987 uncertainty for the relevant analytical session.

4.2.3. Surface and soil samples characterization in Oman

Surfaces of meteorite recovery areas in Oman were described using average diameter of limestone pebbles, maximal grain size of limestone pebbles and the abundance lichen coverage on limestone (absent=no lichen; minor=a few isolated lichens are present; <20% coverage of limestone pebbles; present=area wide lichen covers the rock, 20-80% and strong=fully coverage of limestone pebbles by lichen, >80%). Wind ablation was recorded for surface description similar to meteorites. The criteria describe the state of the largest limestone clasts: absent=no wind ablation visible; minor=rock surface with cavities, mildly wind polished; present="monadnocks"/strong polishing and strong=ventifacts, striation visible.

Soil samples from Oman were taken at selected meteorite find sites and representative areas all over Oman. They were randomly taken from the top 5 cm over an area of about 10 m x 10 m, summing up about 1.5 kg in raw. The soil samples where sieved into >4 mm, 1-4 mm, 0.15-1 mm and <0.15 mm fractions. The <0.15 mm fraction was put in thin commercially available polyethylene (HDPE) bags and measured by HHXRF. The shielding effect of the plastic bag was found to be negligible as verified by comparison of analyzes of the same samples using standard sample cups with 0.6 μm Mylar foil and plastic bags. In addition to Omani soils, four soil samples from Saudi Arabia collected during a Saudi-Swiss meteorite expedition in 2008, two sieved samples from Dar al Gani, Sahara and four samples from recent meteorite search in Tunisia (Ouazaa et al., 2009) were investigated.

4.2.4. Terrestrial rocks

Varnished terrestrial cherts, limestones and volcanic rocks were measured by HHXRF on ES and CS to trace typical Omani desert varnish compositions. Although these rocks have a distinct matrix compared to meteorites, the same measuring setup was used since instrumental setting used for this work, "mining mode", was shown by Zurfluh et al., (2011) to provide robust results, independently of the matrix.

4.3. RESULTS

4.3.1. Elemental Sr and Ba contamination of Oman meteorites

As observed in previous studies, terrestrial Sr and Ba contamination in hot desert meteorites occurs mainly as Sr- and Ba-sulfates in pore space or fissures (Al-Kathiri et al., 2005; Stelzner et al., 1999). Inside Oman meteorites we have found relatively pure celestine with a semiquantitatively determined (EDS on a SEM) composition of 54 wt% SrO , 43% SO_3 and 2 wt% CaO. Small celestine (and/or barite) crystals are often found in (001) twin planes of weathered troilites (Fig. 4.1a), weathered metal grains (Fig. 4.1b), cracks (Fig. 4.1c), inside of newly formed pore space such as leached "boxwork" olivines (Lee and Bland, 2003; Lee and Bland, 2004) or within zoned iron hydroxide veins. Grain size is usually below 10 µm but can reach dimension up to 100 µm (Fig. 4.1d). Close to natural surfaces, barite and strontian barite are observed in addition to celestine. A typical semiquantitative composition is 29 wt%SrO, 40 wt% BaO, 1 wt% CaO and 30 wt% SO_3. Calcite is another common contamination mineral but usually has SrO concentrations of <1 wt%. Experimental leaching of highly Sr-contaminated chondrite fragments with 11.6M HCl followed by HHXRF analyses of the fragments demonstrated that Sr is strongly bound, consistent with an occurrence dominated by celestine, rather than in calcite.

Strontium and barium contamination is best recognized using bulk chemical analyses. The newly developed HHXRF instruments allow to measure surfaces with a spatial resolution of 0.5 cm^2 and spotting the place of contamination. Profiles on selected samples through the CS show relatively low Sr concentration inside the meteorite as compared to the outside (Fig. 4.2a). Enriched Sr concentrations occur either only on ES, only on BS, or in most of the cases, on both surfaces (Zurfluh et al., in review-b). Similar behavior was observed for other elements, as for example Mn (Fig. 4.2b). The profile measurement from ES to the BS on natural meteorite surface yielded highest Sr enrichment at the boundary where the meteorite started to be buried (Fig. 4.3). The behavior of Ba is similar. Strontium concentrations detected inside ordinary chondrites from Oman range from 10 to 888 µg/g. The mean CS Sr of 338 samples is 94 µg/g (median 49 µg/g; Table 4.1).

Table 4.1. Comparison of chemical contaminations of hot desert meteorites from different areas.

	Oman						Saudi Arabia						Sahara						Australia					
	Av.	Med.	Min	Max	STD	n	Av.	Med.	Min	Max	STD	n	Av.	Med.	Min	Max	STD	n	Av.	Med.	Min	Max	STD	n
Sr [CS]	94	49	10	888	120	338	31	24	10	53	17	5	25	19	10	104	21	42	22	18	13	55	10	15
Ba [CS]	109	101	65	186	26	30	n.a.	n.a.	n.a.	n.a.	n.a.	n.a.	195	170	52	386	154	4	101	100	54	149	40	4
Sr [BS]	438	238	13	4234	549	231	118	113	77	170	44	4	70	65	25	143	38	8	n.a.	n.a.	n.a.	n.a.	n.a.	n.a.
Ba [BS]	160	137	83	635	80	158	95	90	72	124	26	3	527	360	121	1311	478	5	n.a.	n.a.	n.a.	n.a.	n.a.	n.a.
Sr [ES]	318	208	21	3422	367	237	67	67	27	126	37	5	53	41	27	116	34	7	n.a.	n.a.	n.a.	n.a.	n.a.	n.a.
Ba [ES]	157	128	55	673	91	166	78	58	44	150	49	4	311	349	102	443	146	4	n.a.	n.a.	n.a.	n.a.	n.a.	n.a.
Sr [NS]	405	259	23	3231	417	362	76	72	26	133	44	4	65	50	16	226	43	94	38	33	12	95	21	15
Ba [NS]	161	137	73	646	79	295	117	108	90	153	32	3	338	236	47	2523	404	81	175	139	45	598	140	15
Mn [NS]/ Mn [CS]	1.2	1.1	0.7	3.9	0.5	61	1.0	1.0	0.8	1.2	0.1	5	1.4	1.2	0.8	4.2	0.7	39	2.5	2.7	0.8	5.3	1.4	15
Ti [NS]/ Ti [CS]	1.7	1.6	0.9	3.5	0.5	61	1.5	1.4	1.2	2.0	0.3	5	2.8	2.6	0.6	7.9	1.4	39	3.4	3.0	1.1	9.5	1.9	15
V [NS]/ V [CS]	1.8	1.5	0.9	4.8	0.9	47	1.8	1.4	1.4	2.6	0.7	3	3.1	2.6	1.0	12.3	2.4	35	2.9	3.0	0.6	6.5	1.5	13
Sr [CS]/ Ba [CS]	1.8	1.2	0.1	7.9	1.9	30	n.a.	n.a.	n.a.	n.a.	n.a.	n.a.	0.20	0.2	0.1	0.3	0.1	4	0.32	0.3	0.2	0.4	0.1	4
Sr [NS]/ Ba [NS]	2.9	2.21	0.2	20.4	2.5	295	0.8	0.8	0.7	0.9	0.1	3	0.34	0.3	0.1	1.3	0.3	81	0.26	0.2	0.1	0.6	0.1	15

Av.: Average.
Med.: Median.
STD: Standard deviation.
n: Number.
CS: Cut surface.
BS: Buried surface.
ES: Exposed surface.
NS: Natural surface.
n.a.: Not analyzed.
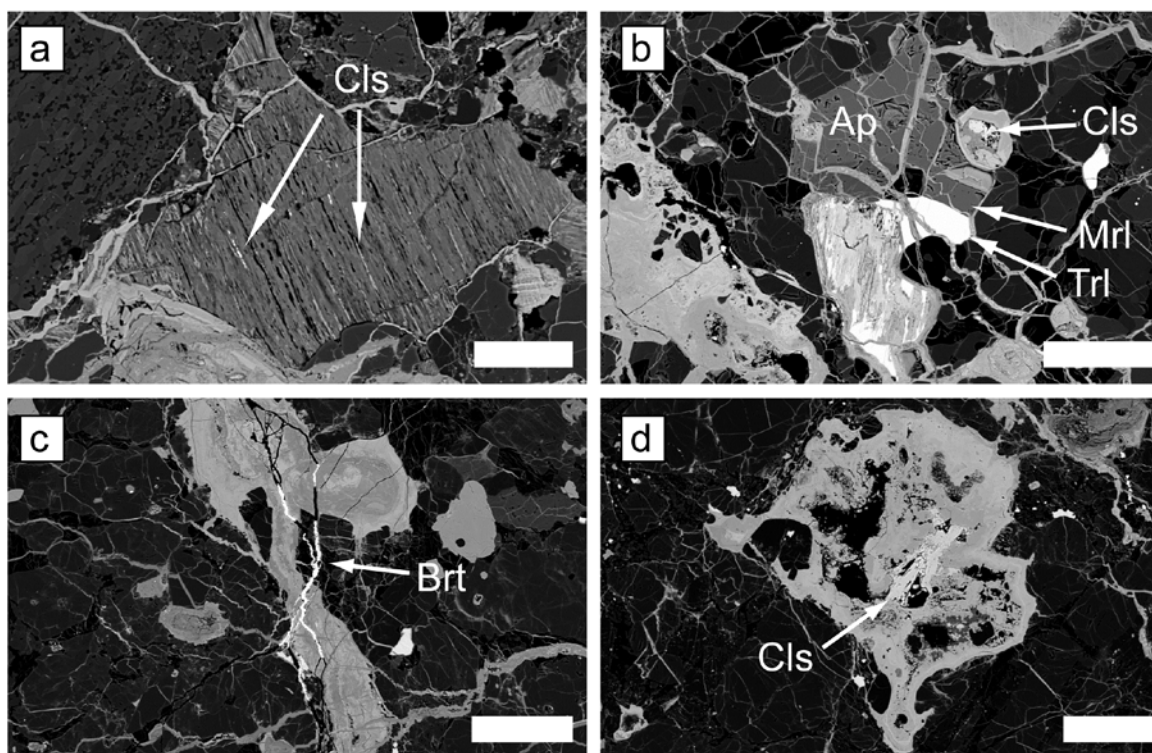
Figure 4.1. Occurrence of Sr and Ba contamination in ordinary chondrites from Oman. a) Celestine (SrSO₄), the most important terrestrial Sr precipitate, is visible here as bright streaks labeled Cls within fissures along (001) plains of a weathered troilite grain (iron hydroxides). Sample UaS 016, (H5 S2 WD4.5). Scale bar is 50 μm. b) In vicinity of weathered troilite (Troi) and partly weathered Ca-phosphates (Ap=apatite, Mrl=merrillite), celestine is present. Sample RaS 393 (H6 S2 W3.6). Scale bar is 50 μm. c) Barite (BaSO₄) can also occur within veins and is here visible as bright streaks labeled Brt. RaS 393, scale bar 100 μm. d) Large celestine grains are present within iron oxides and iron hydroxides of a weathered metal grain in RaS 302 (H4 S2 WD3.6). Scale bar is 100 μm.

4.3.2. Handheld XRF measurements on non-Omani meteorites

In addition to meteorites from Oman we have examined meteorites from other meteorite accumulation areas for their contamination signals: Five samples from Saudi Arabia found by a joint Saudi-Swiss expedition (Gnos et al., 2009a), 98 samples from Sahara desert and 16 from Australia. They were all described macroscopically and analyzed by HHXRF applying the same procedures as for the meteorites from Oman. The majority of the samples from Australia and Sahara were part slices and in most case it was not possible to reconstruct the find situation. Usually, either a BS or ES part was present. Similar to Oman, the samples are weathered and contaminated with Sr and Ba (Table 4.1). Meteorites from the Arabian

Peninsula (Oman and Saudi Arabia) show higher Sr concentrations compared to Ba whereas meteorites from Sahara and Australia show the opposite (Table 4.1). Mean Sr/Ba on NS of meteorites from Arabia is between 0.8 (Saudi Arabia) and 2.9 (Oman) whereas samples from Sahara (0.34) and Australia (0.26) have low Sr/Ba ratios (Table 4.1). Most of the analyzed hot desert meteorites show slight enrichments of Ti, V and Mn on natural surfaces as compared to concentrations in the interior (Table 4.1). Generally, the enrichment of these three elements is slightly higher for meteorites from Sahara and Australia (1.2-3.4x) relative to Saudi Arabia and Oman (1.2-1.8x).
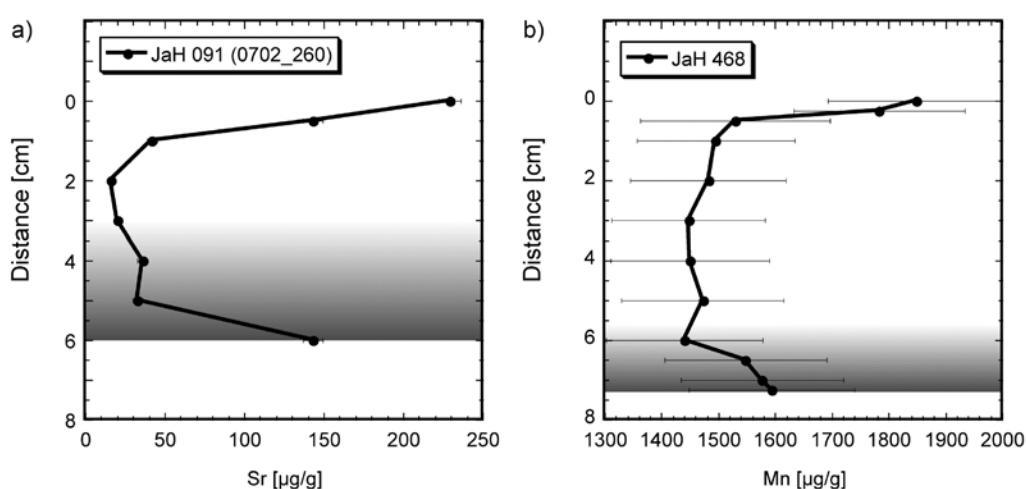
Figure 4.2. Profile measurements through cut slabs of ordinary chondrites from Oman. The top is the exposed surface (ES) where the bottom is the buried surface. The shaded part was buried into the soil. a) A fragment of the JaH 091 (L5) meteorite shower shows enrichments of Sr on ES as well as cut surface (CS). Analytical errors of Sr are smaller than the size of the symbols. b) Meteorite JaH 468 (L6) has resolvable enrichments of Mn on ES as compared to CS. The buried part of the meteorite shows also a slight Mn enrichment. Note the higher uncertainties of Mn measurements.
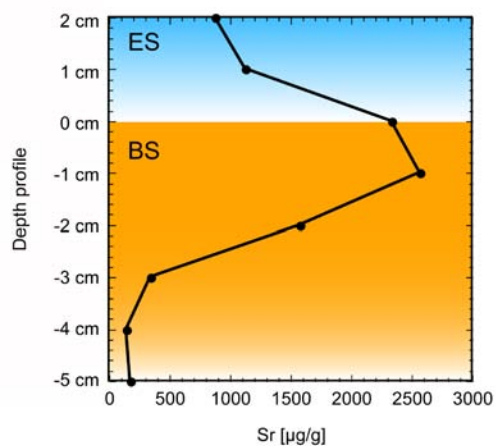
Figure 4.3. Profile of Sr measured on the natural surfaces of RaS 283 (H4 S1 WD4.0). The strongest enrichments of Sr occur at the boundary between the exposed (ES) and the buried (BS) surface. Error bars are smaller than symbols.

4.3.3. Strontium Isotopes

The three leachates of each meteorite using MilliQ water, 0.18M HCl and 6.4 M HCl yielded identical $^{87}Sr/^{86}Sr$ ratios within error for each individual measurement (Table 4.2, Fig. 4. 4). Meteorites Ras 316 and RaS 397 have similar isotope ratios (0.7084 to 0.7086) while Al Huqf 070 has a slightly elevated radiogenic signal (0.7086 to 0.7087). Results of water leachates of the associated soil samples are very close to that of the corresponding meteorite (Fig. 4.4b) whereas the acid leaches of the soil samples are different having a significantly less radiogenic $^{87}Sr/^{86}Sr$ ratio (Fig. 4.4a). While the $^{87}Sr/^{86}Sr$ ratios are internally very similar for each of the three sample suites (excluding the 6.4M HCl leaching), the three different suites show significant differences between each other.
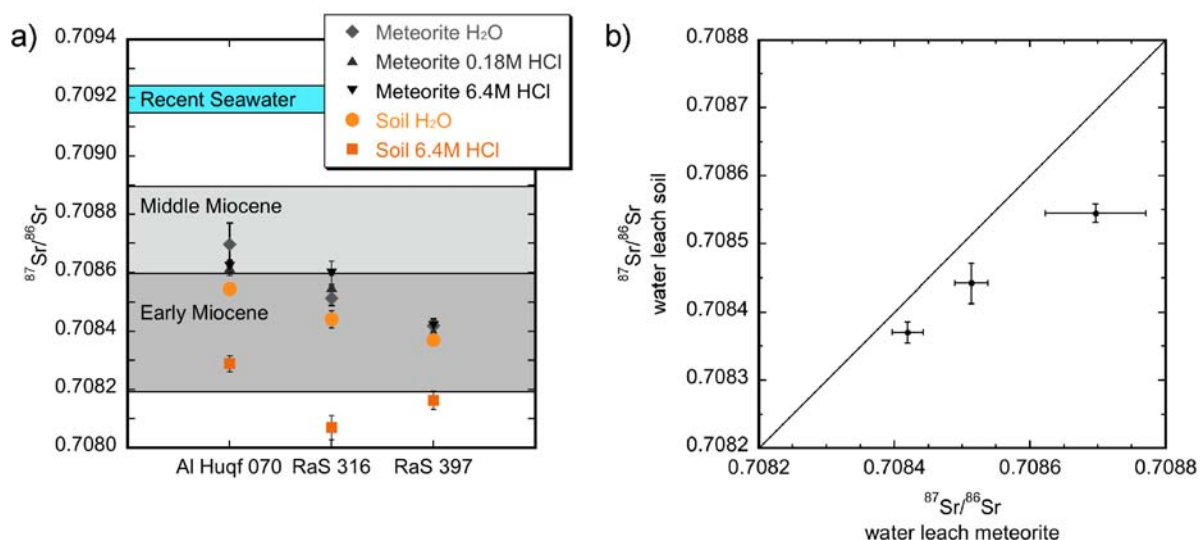
Figure 4.4. *Strontium isotope data for meteorite leachates and corresponding soil samples. a) The $^{87}Sr/^{86}Sr$ ratio of the meteorite leachates ("water"=leaches with water, 0.18M HCl=leaches with 0.18 molar hydrochloric acid and 6.4M HCl=leaches with 6.4 molar hydrochloric acid) are identical within errors for each leaching procedure and close to the water leaches of the local soil, which is of Middle Miocene (Al Huqf 070) and Early to Middle Miocene (RaS) age. b) Water leachates of soils and meteorites are closely corresponding for the three investigated pairs. The $^{87}Sr/^{86}Sr$ ratio of the meteorite leachates is slightly more radiogenic, probably due to leaching of radiogenic Sr from the meteorite.*

Table 4.2. Strontium isotope results.

Name	Sample type	Weight [g]	Leach procedure	$^{87}Sr/^{86}Sr$	Error
Al Huqf 070	L3.7-3.9 S3 WD4.0	0.822	0.18M HCl	0.70862	2.5E-05
Al Huqf 070	L3.7-3.9 S3 WD4.0	0.822	6.4M HCl	0.70862	2.2E-05
Al Huqf 070	L3.7-3.9 S3 WD4.0	0.822	H_2O	0.70870	7.4E-05
Al Huqf 070 soil	Surface soil <0.15 mm	0.518	6.4M HCl	0.70829	2.8E-05
Al Huqf 070 soil	Surface soil <0.15 mm	0.518	H_2O	0.70854	1.4E-05
RaS 316	L5 S3 WD4.5	1.786	0.18M HCl	0.70855	4.0E-05
RaS 316	L5 S3 WD4.5	1.786	6.4M HCl	0.70860	3.9E-05
RaS 316	L5 S3 WD4.5	1.786	H_2O	0.70851	2.5E-05
RaS 316 soil	Surface soil <0.15 mm	0.464	6.4M HCl	0.70807	4.2E-05
RaS 316 soil	Surface soil <0.15 mm	0.464	H_2O	0.70844	2.9E-05
RaS 397	L6 S5 WD4.0	2.819	0.18M HCl	0.70840	2.3E-05
RaS 397	L6 S5 WD4.0	2.819	6.4M HCl	0.70842	2.0E-05
RaS 397	L6 S5 WD4.0	2.819	H_2O	0.70842	2.3E-05
RaS 397 soil	Surface soil <0.15 mm	0.513	6.4M HCl	0.70816	3.1E-05
RaS 397 soil	Surface soil <0.15 mm	0.513	H_2O	0.70837	1.5E-05

4.3.4. Macroscopic weathering features

During collection of chemical data of the analyzed meteorites macroscopically visible weathering features were recorded. Table 4.3 summarizes to the results for the meteorites from Oman, Sahara and Australia. Salt contamination was only visible in about a fourth of the meteorites from Oman and Sahara whereas just 7% of the Australian meteorites showed efflorescence of salts. Salt contamination in Saharan and Australian samples was noted as brown hydroxide powder on CS or as whitish precipitation of probably gypsum or calcite. Extreme contamination with hygroscopic salts as described in Zurfluh et al., (in review-a; in review-b), occurred in 2.6% of the inspected samples from Oman but was not observed in meteorites from Sahara or Australia. A difference in color of ES to a more reddish BS was observed on 20-30% of samples from all three meteorite recovery areas. Meteorites from Australia appear often reddish due to attached soil material. Attached sand was not observed in the small number of investigated meteorites from Australia. A quarter of the Saharan meteorites had attached sand whereas nearly half of the Oman samples show cemented sand on their natural surfaces. Wind ablation features were recognized on samples from all localities. About half of the Australian samples had traces of wind erosion. 76% of the meteorites from Sahara desert are affected by sand blasting while even 86% of the Oman samples show modification of the surface due to the force of wind and wind transported particles. From 11 investigated Dar al Gani meteorites, 82% of the samples had wind erosion

features. Greenish staining due to precipitation of Ni-serpentine was found on 18% of the Oman samples but is essentially lacking on Saharan or Australian meteorites (Table 4.3).

Table 4.3. Comparison of macroscopic weathering features of hot desert meteorites.

Macroscopic feature	Oman	Sahara	AUS
Salt contamination [CS]	*n=269*	*n=35*	*n=15*
absent	75%	79%	93%
Minor	22%	21%	7%
Strong	3%	n.o.	n.o.
Red [BS]§	*n=318*	*n=66*	*n=7*
Absent	69%	80%	71%
Minor	28%	20%	29%
Strong	3%	n.o.	n.o.
Attached sand [ES]	*n=371*	*n=60*	*n=9*
Absent	58%	75%	100%
Minor	36%	25%	n.o.
strong	6%	n.o.	n.o.
Wind ersosion [ES]	*n=379*	*n=66*	*n=9*
absent	14%	24%	45%
minor	80%	73%	55%
strong	6%	3%	n.o.
*Ni-serpentines [BS]**	*n=332*	*n=76*	*n=7*
absent	82%	97%	100%
minor	17%	3%	n.o.
strong	1%	n.o.	n.o.

AUS: Australia.
CS: Cut surface.
BS: Buried surface.
ES: Exposed surface.
*: Greenish staining due to Ni-serpentine precipitation.
§: Color difference between ES and BS.
n.o.: not observed.

4.3.5. Surface characterization and soil chemistry

Surfaces from typical meteorite recovery areas in Oman were characterized and compared. Al Huqf, Jiddat al Harrasis (JaH), Jiddat Arkad and Shalim area have, in general, coarser grained limestone pebbles and lower amounts of <0.15 mm fraction as compared to the other meteorite recovery areas in Oman. The pebbles are usually covered by lichen and show minor traces of wind ablation. This description belongs to areas that are geologically mapped as being of Middle Miocene middle Fars group (Le Métour et al., 1993). Around Hayma (parts of JaH; parts of Ramlat as Sahmah, RaS; and parts of Sayh al Uhaymir, SaU), the surfaces are mainly composed of desert pavements with relative fine grained pebble, are dune free and belong to Early to Middle Miocene lower Fars group (Le Métour et al., 1993). Lichens are sparse to absent on terrestrial rocks. Meteorites found in the RaS areas are found on surfaces with fine to medium grained lime stone pebbles, often on deflated plains between stationary

dunes. Limestones are also of Early to Middle Miocene age (Le Métour et al., 1993). No lichens cover the limestone pebbles, which are often affected by wind ablation. Geochemistry of Oman soil is relatively homogeneous over the whole study area. HHXRF analyses of soil samples are in agreement with previous investigations, where samples were analyzed by INNA, ICP-MS and ICP-OES (Al-Kathiri et al., 2005). The Sr concentration varies from 267 µg/g to 529 µg/g and has a mean of 387 µg/g (median: 374 µg/g, n=48). For Ba, a range from 114 µg/g to 359 µg/g was observed and the mean concentration is 234 µg/g (median: 245 µg/g). The mean Sr/Ba ratios are: Oman (HHXRF): 2.5, Oman (Al-Kathiri et al., 2005) 1.4, Saudi Arabia (HHXRF): 2.3 and UAE (Hezel et al., 2011): around 8. Thus, Arabian soils have relatively high Sr/Ba ratios >1.3. In contrast, soils analyzed from Sahara have relatively low Sr/Ba ratios: 1.3 for Tunisia (HHXRF) and 0.7 for DaG (HHXRF). Soil samples from Sahara appear chemically and macroscopically similar to soil samples from Oman. The samples obtained from Tunisia contain a higher proportion of dune sand.

4.3.6. Desert varnish on terrestrial rocks from Oman

In order to better understand the proposed desert varnish (DV) formation on meteorites, 12 terrestrial samples with remarkable DV, found in typical meteorite recovery areas in Oman were measured by HHXRF. The most prominent varnished rocks are cherts. Since on CS of cherts most of the elements constituting DV are below the HHXRF detection limit, the chemical composition of the DV of cherts is easily characterized by HHXRF. Manganese for example is often not detectable (<50 µg/g) on CS whereas on ES it can reach concentrations up to 17000 µg/g. Typical Omani DV surfaces, commonly ES, show strong enrichments of Sr, Mn, Ti and to some extent V (Fig. 4.5). Enrichment on ES compared to CS is also observed for Ba, Pb and to some extent for K. These elements are also often below limit of detection on CS, which are Ba: <100 µg/g, Pb: <5 µg/g and K: <500 µg/g. Median concentrations as measured on ES are Ba: 700 µg/g, Pb: 20 µg/g and K: 1700 µg/g. Partial enrichment (i.e. not in all measured samples) was observed for Ni, and less pronounced for Zn, Zr and Fe. Arsenic can also be slightly enriched, but lies usually just below limit of detection of HHXRF.
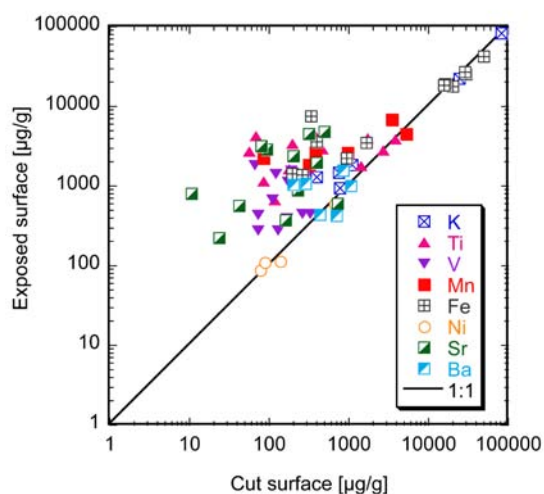
Figure 4.5. *Logarithmic plot of typical desert varnish elements measured on exposed and cut surfaces by HHXRF of 11 desert varnish-crusted terrestrial cherts and basalts found in the Oman desert. The black line shows the 1 to 1 correlation, i.e. no surface enrichment. Desert varnish shows strong enrichment of Ti, V, Mn, Fe, Sr and Ba. Potassium and Ni contents are almost similar for cut surfaces and exposed surfaces.*

4.4. DISCUSSION

4.4.1. Strontium and barium contamination of Oman meteorites

Strontium and barium are highly mobile elements. The process of the contamination of meteorites with Sr and Ba is therefore comparable to that of salt contamination (Zurfluh et al., in review-a). But in contrast to the Cl⁻ contamination, Sr and Ba are not dependent on the weathering of iron metal, iron sulfide and pH condition inside the meteorite. The precipitation of Sr and Ba sulfates might be coupled to the oxidative alteration of troilite. Celestine and barite are often found within altered troilite grains (Fig. 4.1a) and Sr and Ba might have combined with sulfur from troilite oxidation. However, Sr and Ba contamination occurs also in troilite poor meteorites such as lunar meteorites (e.g. Korotev, 2012; Korotev et al., 2009). The strong enrichment of Sr (and Ba) on the NS compared to the CS is the result of terrestrial Sr contamination, which is discussed in more detail in the Sr isotope section (4.4.3.). Similarly to Cl⁻ contamination, there is no enrichment of meteorites with Sr or Ba at areas where soils have Sr and Ba concentrations in the range of mean Oman composition. The main part of the Sr and Ba contamination is present in form of the sulfate minerals celestine and barite. The precipitation of Sr sulfates was observed in the vicinity of meteoritic Ca-phosphates (Fig. 4.1b), an important primary Sr carrier phase. But since the Sr (and Ba)

concentrations within meteorites can reach about 100x the initial value, the contamination by terrestrial Sr (and Ba) is obvious. Both elements are transported with water into the meteorite along micro-crack by capillary forces. The fact that Sr (and Ba) contamination occurs on ES and BS (and not only on BS) might be the result of creeping and overturning of meteorites and meteorite fragments during soil movement or strong winds. Pebbles on soil surface can move/creep during and after rain events, due to expansion and consolidation of soil caused by high daily temperature difference, strong winds or displacement caused by animals or human activity. Supporting evidence for unstable positions of rocks on desert surface comes from long term weathering experiments: Rock and meteorite pieces placed in the desert show evidence of movement within 1-2 years. Also, fragments of highly weathered meteorites dispersed over several meters from the original mass are common evidence for such movements (Al-Kathiri et al., 2005; Gnos et al., 2009b). Paleomagnetic studies of meteorites found on the Atacama desert support our observations that samples with masses <150 g have unstable positions in the desert environment. Weathering products of altered samples with masses >150 g have paleomagnetic directions close to the present Earth field (Uehara et al., 2012).

4.4.2. Strontium and barium contamination of meteorites from hot deserts

The contamination of meteorites from various hot deserts with Sr and Ba is well documented (e.g. Al-Kathiri et al., 2005; Folco et al., 2007; Gibson and Bogard, 1978; Stelzner et al., 1999). The most prominent difference observed in this study for the different hot desert areas is the preferential accumulation of Sr in meteorites from the Arabian Peninsula whereas meteorites from Sahara and Australia show a more Ba-dominated contamination (Fig. 4.6). This is in agreement with the types of identified contamination minerals, in case of Oman dominantly celestine (Al-Kathiri et al., 2005) while for meteorites from the Sahara barite is dominant and occurs in ordinary chondrites (Stelzner et al., 1999), in carbonaceous chondrites (Huber et al., 2006; Ash et al., 2011) as well as achondrites such as shergottites (Hui et al., 2011; Symes et al., 2008). In contrast, celestine is nearly nowhere mentioned in meteorites from Sahara and Australia. These mineralogical observations are in agreement

with bulk chemical contamination patterns that are dominated in Sr for Arabian meteorites (Al-Kathiri et al., 2005; Hezel et al., 2011) and Ba for Saharan meteorites (Folco et al., 2007; Saunier et al., 2010; Stelzner et al., 1999). A possible reason for this effect might be the local soil chemistry. Soil sample analyses from Oman plus a few from Tunisia and Dar al Gani (DaG, Libya) show higher Sr concentrations in Arabian samples than in those from the other areas (Fig. 4.7). The geology of both Arabian and Saharan desert areas are similar, being composed of Tertiary limestones with desert pavement composed of limestone clasts and fine grained windblown material with some heavy minerals. Therefore, the elemental pattern of both soils is similar. However, a detailed look at the Sr and Ba concentrations reveals differences in the Sr/Ba ratios of geographically distinct regions. Meteorites and soils from Oman have in general Sr/Ba >1 whereas Saharan samples have <1. Meteorites from Australia have Sr/Ba <0.55. Atmospheric dust particles collected in three different regions in Australia have Sr/Ba <0.5 (Moreno et al., 2009). In line with the results of the Sr isotopes from Omani desert and the observed slight correlation between the Sr/Ba ratios in soil samples and their corresponding meteorites (Fig. 4.8a), it is interpreted that the soil chemistry is mainly responsible for the observed differences in the Sr-Ba patterns of meteorites.
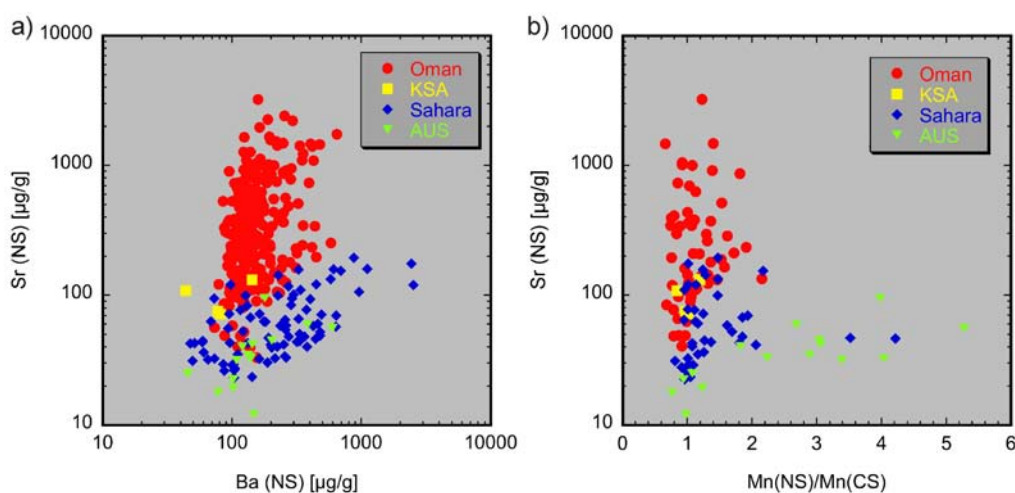
Figure 4.6. Contamination signals of ordinary chondrites from major hot desert meteorite recovery areas measured by HHXRF. a) Meteorites from the Arabian Peninsula (Oman and Saudi Arabia [KSA]) are preferentially enriched in Sr as compared with Ba whereas meteorites from the Sahara and Australia (AUS) have higher Ba concentrations. Limit of detection for Ba is around 100 µg/g for HHXRF. b) Ordinary chondrites from Australia have higher Mn on natural surface to Mn on cut surface ratios, labeled as Mn(NS)/Mn(CS), implying the evolution of desert varnish. Also some Saharan samples have the tendency of Mn accumulation on natural surfaces, which could be due to desert varnish. Meteorites from the Arabian Peninsula show only limited Mn accumulation.
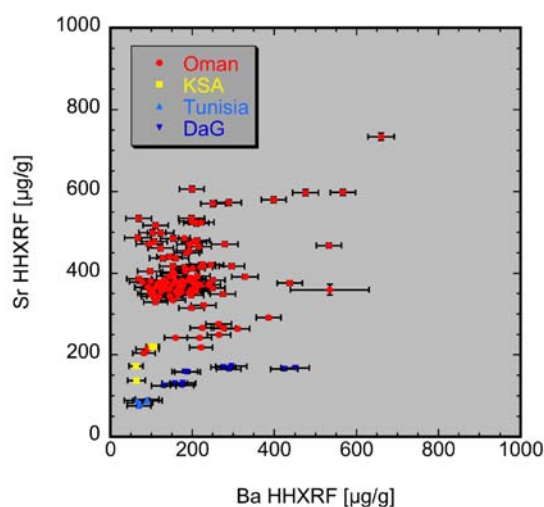
Figure 4.7. *HHXRF measurements of soil samples from four recovery areas of hot desert meteorites. Soils from Oman and Saudi Arabia (KSA) have relatively high Sr concentrations while soil samples from Sahara, Tunisia and Dar al Gani (DaG) show lower Sr concentrations.*

Geochemical characterization of soils from all high-density meteorite recovery areas would help to understand in more detail the contamination and the weathering processes. So far, studies comparing meteorites and corresponding soils are sparse (Al-Kathiri et al., 2005; Dreibus et al., 2001; Dreibus et al., 2000; Hezel et al., 2011; Struempler, 1990). It is noted that in contrast to our results, Bevan et al., (2001) suggest climate condition to be more important in the style of weathering than the local soil composition. They have studied an L4 chondrite, which showed an unusual preferential weathering of troilite relative to metal. The sample was found on potassium rich soil on weathered granite, which is different to the calcareous clay soil from Nullarbor region. But since a similar weathering pattern was observed in the L6 chondrite Nullarbor 018 (Ruzicka, 1995), Bevan et al., (2001) conclude the climate to be more important in weathering style.

Weathering and contamination of meteorites is a complex process, which is influenced by climate but also soil chemistry. Since no significant difference in weathering style or Sr and Ba contamination pattern was observed in meteorites that have fallen in either more humid or more arid periods on chemical homogenous soil of Oman, we tend to propose soil composition to control more dominantly weathering style and Sr and Ba contamination pattern than climate.

4.4.3. Strontium isotopes – source of the strontium and implications for Rb-Sr systematics

Freshly fallen ordinary chondrites have low Sr concentrations. Samples from Oman with higher terrestrial ages can reach high concentrations of Sr with a preferential accumulation on natural surfaces, which implies contamination with terrestrial Sr. The strontium isotope analyses were performed to trace the origin of the strontium. Leachings with water and acids were performed to identify the distinct Sr reservoirs. Water leaches yielded reservoirs that are accessible by rainwater and HCl leachates tapped all leachable minerals (e.g. calcite or apatite). Possible sources include sea spray (salts from aerosol) or local soil. Sea spray would have a Sr isotope signature similar to recent Sea water which is 0.7092 (Veizer, 1989, references therein). Sea spray transports water loaded with ions into the central Oman desert. Since all leaches of the meteorites show $^{87}Sr/^{86}Sr$ ratios close to the water leach of the corresponding soil samples, the contamination of the meteorites with Sr from the local soil is obvious (Fig. 4.4a). $^{87}Sr/^{86}Sr$ ratios of the water leaches of meteorites and of corresponding soil show a good correlation (R=0.99; Fig. 4.4b), which is a definitive proof of the transport of relatively mobile soil Sr into the meteorite by water, for example after a rain event. When Sr is inside the meteorites it precipitates as highly insoluble Sr-sulfate or as trace in the soluble Ca-carbonates, which defines the Sr isotope ratio signal in the water leachates. Meteorites have a slightly more radiogenic $^{87}Sr/^{86}Sr$ signal compared to water leachates of the corresponding soil. The Sr ratio in the meteorites is likely influenced by meteorite Sr, which is isotopically heterogeneous due to highly variable Rb/Sr ratios of the different mineral phases. The main original Sr carrier phases within ordinary chondrites are plagioclase and phosphates (Mason and Graham, 1970) that might have been leached to some extent during the strong acid leach. Mean $^{87}Sr/^{86}Sr$ for ordinary chondrites is about 0.75 (Minster et al., 1982) leading to considerably more radiogenic composition of the meteorite leaches as compared to soil. The water leaches of the soil samples are distinct from the acid leaches of the soil samples, which have lower $^{87}Sr/^{86}Sr$ ratios. All the water leaches and the acid leach of the soil sample collected beneath the Al Huqf 070 meteorite have a $^{87}Sr/^{86}Sr$ ratio that would be consistent with expected $^{87}Sr/^{86}Sr$ ratios of the Middle Miocene bedrock where the meteorites are found on. Al Huqf 070 was recovered close to the Arabian Sea on a surface

belonging to the Middle Miocene lower Fars group, which is a shelf limestone (Le Métour et al., 1993). Middle Miocene $^{87}Sr/^{86}Sr$ ratios are 0.7086 to 0.7089 (DePaolo and Ingram, 1985; McArthur et al., 2001). The other two meteorites, Ras 316 and RaS 397, were recovered on Early to Middle Miocene limestone of the lower Fars group from shelf, fore-reef and slope facies (Le Métour et al., 1993). Early Miocene $^{87}Sr/^{86}Sr$ ratios are 0.7082 to 0.7086 (DePaolo and Ingram, 1985; McArthur et al., 2001). The acid leaches of the soil samples have much lower $^{87}Sr/^{86}Sr$ ratios. The reason for this effect might be leaching of ophiolitic components that are present in the Oman desert soils, as indicated e.g. by high Cr-concentrations (Al-Kathiri et al., 2005). Whole rocks from the Semail ophiolite have a $^{87}Sr/^{86}Sr$ signature of 0.702-0.705 (Lanphere et al., 1981; Weyhenmeyer, 2000) . The soil sample of RaS 316, which is the closest to the alluvial fans with abundant ophiolitic rocks, has the lowest $^{87}Sr/^{86}Sr$ signature obtained from the 6.4M HCl leach. The content of ophiolitic components in the soil samples is determinable by HHXRF analyses. Soil samples close to the alluvial fans have higher concentrations of Ni and Cr as compared to soil samples far away, e.g. the Dhofar/Shisr region. This supports the hypothesis that ophiolitic components in the soil influence the Sr isotope signature of strong acid leachates.

Due to the extensive Sr contamination, Rb-Sr-dating of meteorites from Oman would be a very difficult task. Whole rock analyses of lunar and martian meteorites from hot deserts are usually disturbed and show a trend towards present day seawater (Borg et al., 2001; Shih et al., 2002). Especially the water leachates show contamination show terrestrial $^{87}Sr/^{86}Sr$ signatures. Even though samples were treated with HCl and cleaned in an ultrasonic bath, pyroxene and olivine yielded isotope signals influenced by terrestrial contamination (e.g. Borg et al., 2001) as earlier suggested earlier by Crozaz et al., (2003). Strontium contamination can occur within partly leached meteoritic minerals and can thus escape detection, both macroscopically and with an optical microscope. Only BSE (Fig. 4.1) shows μm-scale contaminants. Therefore, even careful handpicking of visually unaltered minerals does not eliminate the contamination. Since most of the Sr in our samples from Oman and presumably in other hot desert meteorites is present as celestine, which is very resistant against water and acids, it is difficult to clean the sample completely and obtain undisturbed results.

4.4.4. The influence of the desert environment on weathering features

In a previous study, Al-Kathiri et al., (2005) noted the homogeneous bulk chemistry of the soil in Oman and therefore the constant influence on meteorite weathering. However, differences in weathering of a single fall event was observed due to local surface topography, e.g. meteorites found on softer soil (depressions) are more affected by weathering than samples on hard bedrock hills (Al-Kathiri et al., 2005; Gnos et al., 2009b). We have evaluated the recorded macroscopically visible weathering effects with respect to their location. Salt contamination is abundant in meteorites from Oman. Many samples with terrestrial ages 5 ka to 20 ka and at WD3.0 to WD3.3 bear hygroscopic Mg-Cl-brines, an effect that is absent in meteorites from other localities (Zurfluh et al., in review-a; in review-b). Wind ablation is one of the most important weathering features in Oman as 86% of the meteorites show traces of wind erosion (Table 4.3). The effect of sand blasting is also well visible on terrestrial rocks. During surface characterization, the degree of wind erosion was recorded for limestone pebbles covering a profile from the coast to the Arabian Sea to the inland desert. Terrestrial rocks are most affected in the eastern RaS region (Fig. 4.6b). A similar distribution was observed for meteorites. The strongest wind-eroded rocks are found on a dune-free plain north of Zauliah in the central RaS area and at the boarder of the RaS and SaU meteorite recovery areas (Fig. 4.6b). The reason for this higher abundance of wind erosion is the presence of dunes close to these areas. In addition, the soil has a relative large amount of fine grained (<0.15 mm) material that is transported by wind (Fig. 4.8b). This fine grained material contains quartz, which is mainly responsible for sand blasting. Such sand grains can be cemented on meteorites due to efflorescence of iron hydroxides on meteorite surface (Zurfluh et al., in review-a; in review-b). Attached sand on meteorites is mainly found on meteorites close to dunes (RaS area) or where soil has higher relative amount of fine-grained material (Fig. 4.8b). Due to the strong force of wind erosion the attached sand is removed on meteorites from areas with stronger wind ablation (Fig. 4.8b and c). The mineralogical composition of the fine-grained soil material is relatively homogeneous over the whole study area. Even though the bulk chemistry of soil is relatively homogenous, slight differences are notable. Soil samples collected closer to the costal areas (Shisr, Dhofar, Shalim, parts of JaH, Al Huqf and partly SaU) have slightly lower Sr concentrations than

mean Oman soil. This is reflected by lower Sr/Ba ratios (Fig. 4.8a). Soil samples from dune areas in JaH and RaS have in general higher Sr/Ba ratios. A similar trend is observed for the meteorites. However, there are some meteorites with high Sr/Ba ratios in regions with low soil Sr/Ba ratios. Most of these samples are relatively young meteorites with Ba concentrations just above limit of detection of the HHXRF, which causes higher uncertainties.
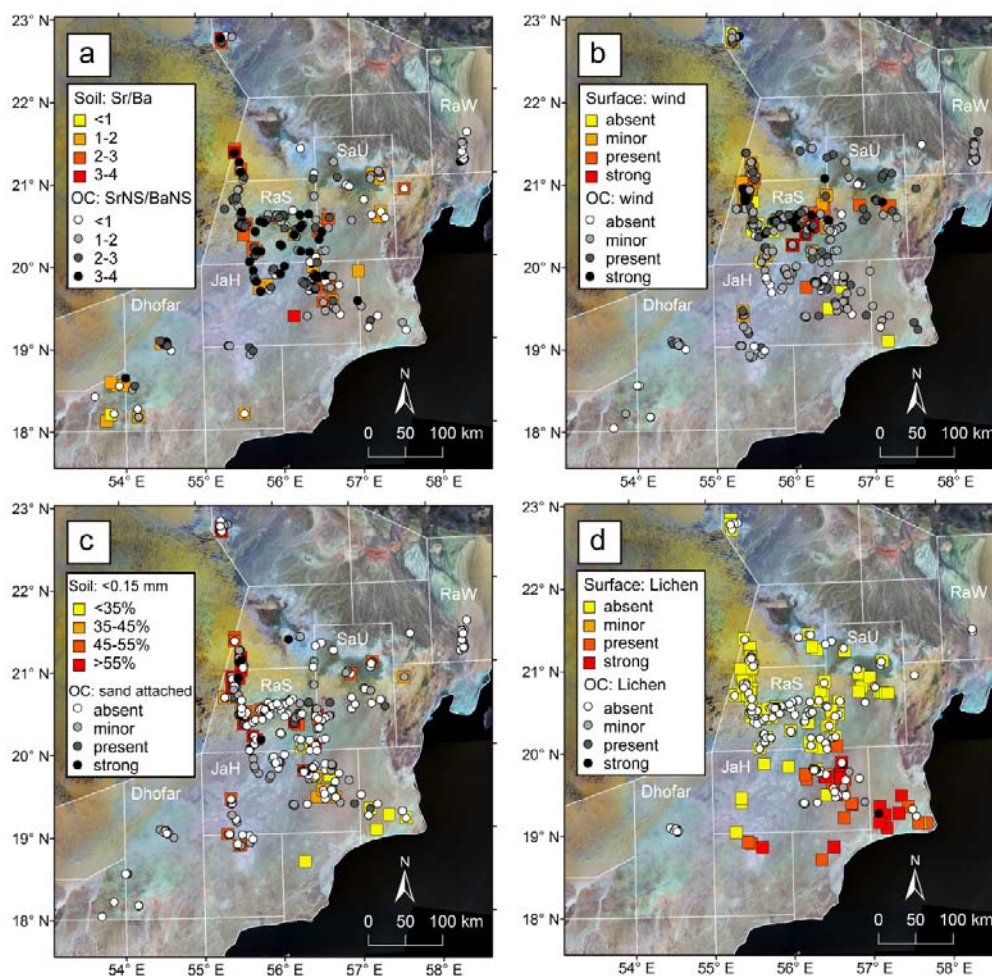
Figure 4.8. *Geographical dependence of weathering and contamination features in ordinary chondrites (OC) and soils/surfaces from central Oman. Nomenclature areas are defined by the Meteoritical Society; JaH: Jiddat al Harasis, RaW: Ramlat al Wahiba, RaS: Ramlat as Sahmah and SaU: Sayh al Uhaymir. a) Wind ablation features recognized on limestones and OCs. Strongest wind erosion is recognized in the RaS area where dune sand is available. b) The amount of fine-grained soil material (<0.15 mm) in percentage and the amount of attached sand on meteorites. Soils in the dune areas (RaS) have higher contents of fine-grained material and attached sand is slightly more present in meteorites from those regions. c) Sr/Ba ratios in soils (<0.15 mm fraction) and meteorites. Data from meteorites is collected by HHXRF on natural surfaces. d) Lichen on terrestrial rocks and meteorites are only present to a distance of about 150 km from the coast.*

Terrestrial rocks closer to the coast are covered by lichen indicating higher air humidity (Fig. 4.8d). Lichens were found only on a few meteorites, all recovered in areas towards the coast in the southeastern JaH and Al Huqf areas (Fig. 4.6d). Some of the lichen-produced pits on terrestrial rocks are found more inland than the present growth of lichen on rocks. Maybe they formed under stronger influence of the Indian monsoon ~10 to 6 ka ago as proposed by climate reconstructions based on speleothems, lake sediments or dune activity (e.g. Fleitmann and Matter, 2009; Preusser, 2009). We find no significant accelerated meteorite weathering on samples found near the coast as compared to meteorites found in lichen-free areas.

4.4.5. Desert varnish on terrestrial rocks and meteorites from Oman

In central Oman, desert varnish is found on terrestrial rocks such as cherts, basalts, quartzites and some other exotic rocks. The color of the DV on chert is dark olive (HUE 5Y 2/2) or black (N2-3) according to rock color chart (Goddard, 1948). The varnish never exceeds a few hundred micrometers in thickness and is mostly a near-surface impregnation of small cavities or micro pore space. Terrestrial desert varnish have mean Mn ES/Mn CS ratios >5, if Mn was detectable on CS. On meteorites from Oman we have never observed a DV in thin section even though thin sections of a large number of potentially crusted meteorites were produced and investigated. In cases where a layered crust was present it was due to an iron hydroxide vein that cracked the sample and was therefore exposed on surface (Fig. 4.9). Or, in the other prominent case, it was due to attached sand on efflorescence of iron (oxy)hydroxides on meteorites surface (Fig. 4.9a). Ordinary chondrites from Oman are rather covered by iron hydroxide crust due to weathering than coated with desert varnish. A slight Mn enrichment on ES is observed in old meteorites. But the same trend is also detected on BS of most meteorites (Fig. 4.2). Since most of the meteorites do not have a stable position during their residence time or are completely buried into the soil for long periods no remarkable DV can evolve. Due to the relatively strong wind erosion, DV seems to be continuously eroded from the exposed parts of meteorites. DV on chert can grow since they are usually relatively flat and less exposed to erosion. Therefore the attackable area is smaller as compared to large rocks. In addition, cherts have very low porosity and have a high hardness, which are factors for a successful DV evolution (e.g. Dorn, 2009).

The lunar meteorite SaU 169 (Gnos et al., 2004) shows a slight enrichment of Mn, K and Pb on natural surfaces as compared to cut surface (Zurfluh et al., 2011) that might be the result of beginning desert varnish coating. However, the enrichment factor of (Mn on ES)/(Mn on CS) never exceeds a factor of 2, which is far below terrestrial desert varnish. We conclude that meteorites from Oman are virtually free of DV and are coated, instead, by "weathering rinds" composed of layered iron oxide and iron hydroxide veins formed by weathering of meteoritic minerals. This weathering rind can incorporate contamination elements such as Sr (Fig. 4.9b).
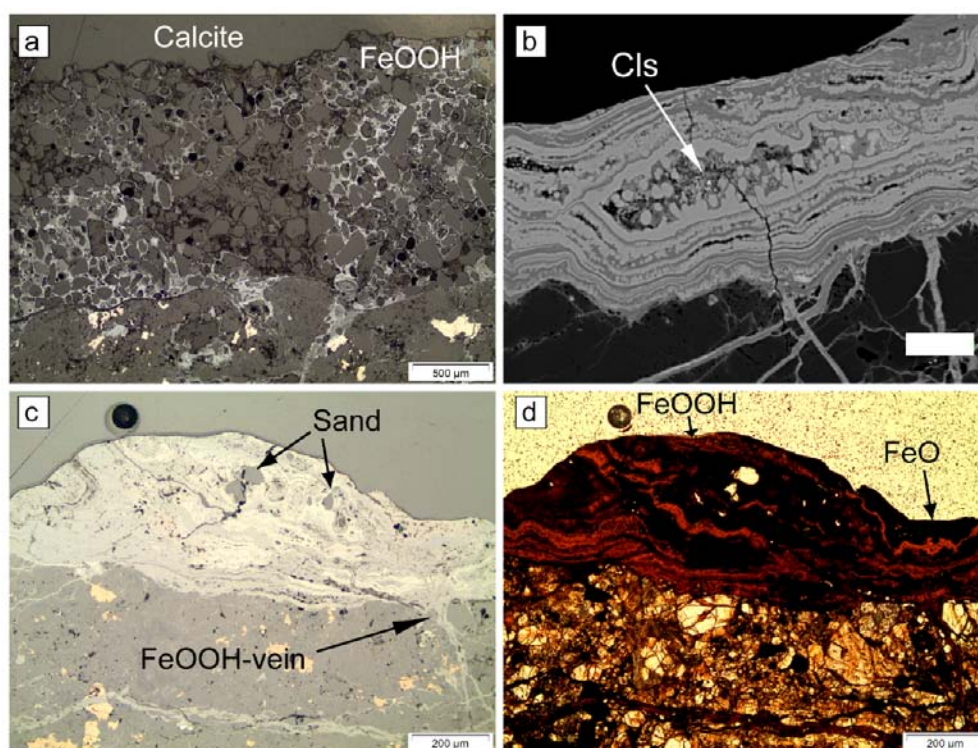
Figure 4.9. Micrographs of attached material on surfaces of ordinary chondrites from Oman: a) Sand grains, dominantly quartz, are cemented by calcite or iron oxyhydroxides (labeled with FeOOH) on Al Huwaysah 004 (H5 S2 WD3.3). Scale bar is 500 µm. Some wind erosion is present. b) RaS 400 (H6 S4 WD4.0) is partly coated with layered iron hydroxides and iron oxides. One small bright celestine crystal is shown by the arrow labeled with Cls. Scale bar is 20 µm. This coating might be called desert varnish, but it actually is composed of several generations of veins from weathering, which have precipitated on the meteorite surface. The veins are mostly mixtures of diverse iron oxyhydroxides. BSE image. c) Reflected light image of RaS 423 (H3-5 S3 WD3.6) that has a coating of layered iron oxide (FeO) and iron hydroxide (FeOOH) veins, which have enclosed some sand grains (quartz). Scale bar is 200 µm. d) Transmitted light image of c). The vein is zoned and appears similarly like a DV. Since the coating is of meteoritic origin we would call it weathering rind instead of desert varnish.

4.4.6. Desert varnish on meteorites from other localities

Desert varnish or rock varnish on meteorites is described only for a few meteorites from Australia (Lee and Bland, 2003; Smith et al., 2012), on Gobabed, Namibia (Fudali and Noonan, 1975), Gold Basin, USA (Kring et al., 2001) and supposed for meteorites from Sahara (Folco et al., 2000; Schlüter et al., 2002). Typical desert varnish composition includes clay minerals (Al, Si) and Mn- and Fe-(hydr)oxides. Elements that can be enriched in desert varnish and are detectable with HHXRF include Ti, V, Mn, Fe, Sr and Ba (e.g. Dorn, 2009; Engel and Sharp, 1958). Due to the iron rich nature of meteorites, iron is not a useful proxy. The instrument used in this study was not able to detect Al and Si. Meteorites from Oman show only a slight enrichment of Ti, V and Mn on NS as compared to CS whereas Saharan and especially the Australian samples have significant higher values of those elements on the natural surfaces (Fig. 4.6, Table 4.1). Since the elements were analyzed with HHXRF one has to be careful due to line overlaps of Ti $K\beta1$ (4.9 keV), V $K\alpha1$ (4.9 keV) and Ba Lβ1 (4.8 keV). In addition, Ti $K\alpha1$ and Ba $L\alpha1$ (4.5 keV) might also produce line interferences, as well as V $K\beta1$ (5.4 keV), Cr $K\alpha1$ (5.4 keV) and Ba $L\gamma1$ (5.5. keV). The Ti-Ba peak overlap is problematic when Ba concentrations exceeding about 500 µg/g, (Zurfluh et al., 2011), which is the case in some Saharan meteorites, but in none of the Australian meteorites. Since elevated Ti or V concentrations were observed in meteorites with high Ba concentrations but also in meteorites with Ba concentrations below limit of detection (<100 µg/g), the accumulation of these elements in some meteorites seem to be the result of desert varnish. The origin of Ti (and V) enrichment in desert varnish is most likely due to incorporation of detrital mineral grains (Garvie et al., 2008; Reneau et al., 1992). This lets us conclude that the desert environment of Australia and partially the Saharan desert is better suited for DV accumulation than Arabia. A reason might be the omnipresent wind and the availability of sand for wind erosion in Oman that suppresses the formation of DV. Sediment material sticking on meteorites from central Nullabor is reported to be free of quartz and is build nearly entirely of clay-sized particles (Treiman, 1992), indicating that soil in Australia is composed of much finer and softer components that erode to a lesser degree the meteorite surfaces. Wind ablation features are present on the investigated samples from Sahara and Australia but no ventifacts are reported among the Australian samples. However, most of the

pieces were not complete, which did not allow a full description. Wind ablation is present on meteorites from sand-rich areas in Sahara such as Niger, whereas meteorites and desert rocks from Dar al Gani plateau (DaG) are only weakly exposed to sand blasting (Schlüter et al., 2002). However, we found on 8 of 11 meteorites inspected from DaG samples minor to strong wind erosion features similar as for the total Saharan population (76%). Thus the presence of wind ablation features cannot be used to discriminate meteorites from Sahara and Oman. Wind erosion is also strong in the Atacama Desert, where terrestrial rocks and meteorites are shaped by wind (Gattacceca et al., 2011). Therefore, well-developed desert varnish is only excepted on meteorite finds from areas with low wind erosion such as Australia or dry lakes from US.

4.4.7. Attached sand and soil material as tracer of find locality

Cracks of meteorites from hot deserts are often filled with windblown material. In addition, due to the blooming of iron hydroxides on natural surfaces, sand grains from the environment can be attached to the meteorite (e.g. Hezel et al., 2011). Alternatively, precipitation of calcite or a combination of calcite and iron hydroxides can act as cement for the sand (Fig. 4.9). The attached suite of grains is characteristic for the find locality. Meteorites from Oman contain rounded quartz, feldspar and calcite grains from dune sand and local soil (Fig. 4.9). This pattern can also be used for forensic investigations, such as for example the meteorite reportedly from Castenazo (Italy), which included sand grains similar to meteorites from Sahara implying its origin from Saharan desert (Folco et al., 2007). This meteorite is also free of DV.

Attached soil might also be used for extended forensic investigations. Whole rock leachates of DaG 476, a shergottite from Lybia, have a $^{87}Sr/^{86}Sr$ ratio strongly influenced by present day seawater (Borg et al., 2003) and are therefore slightly distinct from our results. But they have applied another leach procedure and the type of meteorite is different. The same authors have compared martian meteorites from Dhofar and DaG and found similar whole rock Rb-Sr systematics, even though the DaG region is composed mainly of Eocene carbonates (Schlüter et al., 2002, references therein) where a distinct $^{87}Sr/^{86}Sr$ signal is expected. $^{87}Sr/^{86}Sr$ ratios of Libyan sandstones are much more radiogenic compared to Oman soil (Schaaf and Muller-

Sohnius, 2002). Anyhow, it might be possible to trace back the find origin of the meteorite if a larger data set of soil samples e.g. form Oman or DaG will be available and when the same leaching procedures are applied. The shergottite Los Angeles (Grossman, 2000), allegedly from the Mojave desert, had attached caliche, which yielded a very distinct ^{87}Sr/^{86}Sr signal than meteorites from DaG or Oman (Nyquist et al., 2000). Therefore, the find region of meteorites can be traced by use of Sr isotope determinations.

4.5. CONCLUSIONS

Meteorites with elevated degrees of weathering are strongly contaminated by Sr and Ba, whereby Sr enrichment in nearly all samples from Oman (and Saudi Arabia) are higher than those of Ba. The Sr and Ba contamination occurs as μm-sized celestine or barite in cracks within iron hydroxides, pore space, cracks or leached minerals. Meteorites from Sahara and Australia show also contamination with Sr and Ba, but in these samples Ba is dominant. A reason for the difference in Sr/Ba ratios of the contamination might be the soil, which has higher Sr/Ba ratios in Oman compared to Sahara. Strontium isotope analyses of soil and meteorite samples from Oman indicate the local soil as source of the contamination. Since Sr is present as small and insoluble celestine, Rb/Sr isotope analyses can be strongly affected. The natural surfaces of the analyzed hot desert meteorites show higher values of Ti, V, Mn, Sr and Ba compared to cut surfaces; elements that are typically detected in desert varnish. However, in none of the investigated Omani meteorite thin sections we found a rock coating of desert varnish sensu stricto; instead, we observed layered iron oxyhydroxides that are veins having precipitated on the surface of meteorites and build a local weathering rind. Meteorites from Sahara and especially Australia show stronger enrichment of Mn on natural surfaces relative to inside compared to Oman meteorites. Meteorites from sand-poor plains in Sahara (e.g. DaG) and Australia can accumulate higher elemental contamination, since wind ablation appears to be weaker in the regions where the desert soil contains lower amounts of abrasive quartz grains compared to Oman.

Thus, based on macroscopic inspection of weathering and contamination features and chemical analysis with non-destructive HHXRF the provenance of a meteorite find can be narrowed to specific hot deserts by excluding others.

4.6. Acknowledgments

4.7. REFERENCES

Al-Kathiri, A., Hofmann, B. A., Jull, A. J. T., and Gnos, E., 2005. Weathering of meteorites from Oman: Correlation of chemical and mineralogical weathering proxies with ^{14}C terrestrial ages and the influence of soil chemistry. *Meteoritics & Planetary Science* 40:1215-1239.

Ash, R. D., Walker, R. J., Puchtel, I. S., McDonough, W. F., and Irving, A. J., 2011. The trace element chemistry of Northweat Africa 5958, a curious primitive carbonaceous chondrite. *42nd Lunar and Planetary Science Conference,*

Barrat, J. A., Gillet, P., Lecuyer, C., Sheppard, S. M. F., and Lesourd, M., 1998. Formation of carbonates in the Tatahouine meteorite. *Science* 280:412-414.

Bartoschewitz, R., Appel, P., Mader, B., Greshake, A., and Kurtz, M., 2009. Königsbrück - Mineralogy and petrology. *Meteoritics & Planetary Science* 44:A29-A29.

Bell, A. and Lee, M. R., 2009. Weathering of the Glenrothes meteorite (H5), the first Scottish find. *Meteoritics & Planetary Science* 44:A32-A32.

Bevan, A. W. R. and Binns, R. A., 1989a. Meteorites from the Nullarbor Region, Western Australia. 1. A review of past recoveries and a procedure for naming new finds. *Meteoritics* 24:127-133.

Bevan, A. W. R. and Binns, R. A., 1989b. Meteorites from the Nullarbor region, Western Australia. 2. Recovery and classification of 34 new meteorite finds from the Mundrabilla, Forrest, Reid and Deakin areas. *Meteoritics* 24:135-141.

Bevan, A. W. R., Downes, P. J., and Thompson, M., 2001. Little Minnie Creek, a L4(S2) ordinary chondritic meteorite from Western Australia. *Journal of the Royal Society of Western Australia* 84:149-152.

Bland, P. A., Sexton, A. S., Jull, A. J. T., Bevan, A. W. R., Berry, F. J., Thornley, D. M., Astin, T. R., Britt, D. T., and Pillinger, C. T., 1998. Climate and rock weathering: A study of terrestrial age dated ordinary chondritic meteorites from hot desert regions. *Geochimica et Cosmochimica Acta* 62:3169-3184.

Bland, P. A., Zolensky, M. E., Benedix, G. K., and Sephton, M. A., 2006. Weathering of chondritic meteorites. In: Lauretta, D. S. and McSween, H. Y. (Eds.), *Meteorites and the Early Solar System II*. University of Arizona Press, Tucson.

Borg, L. E., Nyquist, L. E., Reese, Y., Wiesmann, H., Shih, C. Y., Taylor, L. A., and Ivanova, M., 2001. The age of Dhofar 019 and its relationship to the other martian meteorites (abstract). *Lunar and Planetary Science XXXII,*

Borg, L. E., Nyquist, L. E., Wiesmann, H., Shih, C. Y., and Reese, Y., 2003. The age of Dar al Gani 476 and the differentiation history of the martian meteorites inferred from their radiogenic isotopic systematics. *Geochimica et Cosmochimica Acta* 67:3519-3536.

Buchwald, V. F. and Clarke, R. S., 1989. Corrosion of Fe-Ni alloys by Cl-containing akaganéite (beta-FeOOH) - The Antarctic meteorite case. *American Mineralogist* 74:656-667.

Crozaz, G., Floss, C., and Wadhwa, M., 2003. Chemical alteration and REE mobilization in meteorites from hot and cold deserts. *Geochimica et Cosmochimica Acta* 67:4727-4741.

Daviau, K. C., Mayne, R. G., and Ehlmann, A. J., 2012. An XRF study of meteorites. *43rd Lunar and Planetary Science Conference,*

DePaolo, D. J. and Ingram, B. L., 1985. High-resolution stratigraphy with strontium isotopes. *Science* 227:938-941.

Dorn, R. I., 2009. The rock varnish revolution: New insights from microlaminations and the contributions of Tanzhuo Liu. *Geography Compass* 3:1-20.

Dreibus, G., Huisl, W., Haubold, T., and Jagouz, E., 2001. Influence of terrestrial desert weathering in martian meteorites. *Meteoritics & Planetary Science* 36:A50.

Dreibus, G., Spettel, B., Haubold, R., Jochum, K. P., Palme, H., Wolf, D., and Zipfel, J., 2000. Chemistry of a new shergottite: Sayh al Uhaymir 005. *Meteoritics & Planetary Science* 35:A49-A49.

Engel, C. G. and Sharp, R. P., 1958. Chemical data on desert varnish. *Geological Society of America Bulletin* 69:487-&.

Fleitmann, D. and Matter, A., 2009. The speleothem record of climate variability in Southern Arabia. *Comptes Rendus Geoscience* 341:633-642.

Folco, L., D'Orazio, M., and Perchiazzi, N., 2007. Authenticating the recovery location of meteorites: The case of Castenaso. *Meteoritics & Planetary Science* 42:321-330.

Folco, L., Franchi, I. A., D'Orazio, M., Rocchi, S., and Schultz, L., 2000. A new martian meteorite from the Sahara: The shergottite Dar al Gani 489. *Meteoritics & Planetary Science* 35:827-839.

Fudali, R. F. and Noonan, A. F., 1975. Gobabeb, a new chondrite: the coexistence of equilibrated silicates and unequilibrated spinels. *Meteoritics* 10:31-39.

Garvie, L. A. J., Burt, D. M., and Buseck, P. R., 2008. Nanometer-scale complexity, growth, and diagenesis in desert varnish. *Geology* 36:215-218.

Gattacceca, J., Valenzuela, M., Uehara, M., Jull, A. J. T., Giscard, M., Rochette, P., Braucher, R., Suavet, C., Gounelle, M., Morata, D., Munayco, P., Bourot-Denise, M., Bourles, D., and Demory, F., 2011. The densest meteorite collection area in hot deserts: The San Juan meteorite field (Atacama Desert, Chile). *Meteoritics & Planetary Science* 46:1276-1287.

Gibson, E. K., Jr. and Bogard, D. D., 1978. Chemical alterations of the Holbrook chondrite resulting from terrestrial weathering. *Meteoritics* 13.

Gnos, E., Hofmann, B. A., Al-Kathiri, A., Lorenzetti, S., Eugster, O., Whitehouse, M. J., Villa, I. M., Jull, A. J. T., Eikenberg, J., Spettel, B., Krähenbühl, U., Franchi, I. A.,

and Greenwood, R. C., 2004. Pinpointing the source of a lunar meteorite: Implications for the evolution of the moon. *Science* 305:657-659.

Gnos, E., Hofmann, B. A., Al-Shanti, M., and Al-Halawani, M., 2009a. Meteorite exploration in Saudi Arabia 2008: Yabrin area and a visit to the Wabar craters. *Meteoritics & Planetary Science* 44:A79-A79.

Gnos, E., Lorenzetti, S., Eugster, O., Jull, A. J. T., Hofmann, B. A., Al-Kathiri, A., and Eggimann, M., 2009b. The Jiddat al Harasis 073 strewn field, Sultanate of Oman. *Meteoritics & Planetary Science* 44:375-387.

Goddard, E. N., Trask, P. D:, De Ford, R. K., Rove, O. N., Singewald, J. T., Jr., and Overbeck, R. M., 1948. Rock-color chart. Boulder, Colorado. *Geological Society of America.* 11 p.

Grossman, J. N., 2000. The Meteoritical Bulletin, No. 84, 2000 August. *Meteoritics & Planetary Science* 35:A199-A225.

Hezel, D. C., Schlüter, J., Kallweit, H., Jull, A. J. T., Al-Fakeer, O. Y., Al-Shamsi, M., and Strekopytov, S., 2011. Meteorites form the United Arab Emirates: Description, weathering, and terrestrial ages. *Meteoritics & Planetary Science* 46:327-336.

Hofmann, B. A., Gnos, E. Al-Kathiri, A., 2004. Harvesting meteorites in the Omani desert: Implications for astrobiology. *Proceedings of the Third European Workshop on Exo-Astrobiology.* 73-76.

Huber, H., Rubin, A. E., Kallemeyn, G. W., and Wasson, J. T., 2006. Siderophile-element anomalies in CK carbonaceous chondrites: Implications for parent-body aqueous alteration and terrestrial weathering of sulfides. *Geochimica et Cosmochimica Acta* 70:4019-4037.

Hui, H., Peslier, A. H., Lapen, T. J., Shafer, J. T., Brandon, A. D., and Irving, A. J., 2011. Petrogenesis of basaltic shergottite Northwest Africa 5298: Closed-system crystallization of an oxidized mafic melt. *Meteoritics & Planetary Science* 46:1313-1328.

Korotev, R. L., 2012. Lunar meteorites from Oman. *Meteoritics & Planetary Science* 47:1365-1402.

Korotev, R. L., Zeigler, R. A., Jolliff, B. L., Irving, A. J., and Bunch, T. E., 2009. Compositional and lithological diversity among brecciated lunar meteorites of intermediate iron concentration. *Meteoritics & Planetary Science* 44:1287-1322.

Kovach, H. A. and Jones, R. H., 2010. Feldspar in type 4-6 ordinary chondrites: Metamorphic processing on the H and LL chondrite parent bodies. *Meteoritics & Planetary Science* 45:246-264.

Kring, D. A., Jull, A. J. T., McHargue, L. R., Bland, P. A., Hill, D. H., and Berry, F. J., 2001. Gold basin meteorite strewn field, Mojave Desert, northwestern Arizona: Relic of a small late pleistocene impact event. *Meteoritics & Planetary Science* 36:1057-1066.

Langenauer, M. and Krähenbühl, U., 1993. Halogen contamination in antarctic H5 and H6 chondrites and relation to sites of recovery. *Earth and Planetary Science Letters* 120:431-442.

Lanphere, M. A., Coleman, R. G., and Hopson, C. A., 1981. Sr isotopic tracer study of the Samail ophiolite, Oman. *Journal of Geophysical Research* 86:2709-2720.

Le Métour, J., Platel, J. P., Béchennec, F., Berthiaux, A., Chevrel, S., Dubreuilh, J., Roger, J., and Wyns, R., 1993. Geological map of the Sultanate of Oman, 1:1'000'000, with explanatory notes, Sultanate of Oman. Ministry of Petroleum and Minerals, Directorate General of Minerals, Muscat.

Lee, M. R. and Bland, P. A., 2003. Dating climatic change in hot deserts using desert varnish on meteorite finds. *Earth and Planetary Science Letters* 206:187-198.

Lee, M. R. and Bland, P. A., 2004. Mechanisms of weathering of meteorites recovered from hot and cold deserts and the formation of phyllosilicates. *Geochimica et Cosmochimica Acta* 68:893-916.

Losiak, A. and Velbel, M. A., 2011. Evaporite formation during weathering of Antarctic meteorites--A weathering census analysis based on the ANSMET database. *Meteoritics & Planetary Science* 46:443-458.

Mason, B. and Graham, A. L., 1970. Minor and trace elements in meteoritic minerals. *Smithsonian Institution Press, City of Washington* 3:19.

Mayne, R. G., Ehlmann, A. J., and Daviau, K. C., 2011. Exploring XRF as a new technique for basic meteorite classifications. *Meteoritics & Planetary Science* 46:A150.

McArthur, J. M., Howarth, R. J., and Bailey, T. R., 2001. Strontium isotope stratigraphy: LOWESS version 3: Best fit to the marine Sr-isotope curve for 0-509 Ma and accompanying look-up table for deriving numerical age. *Journal of Geology* 109:155-170.

Minster, J. F., Birck, J. L., and Allegre, C. J., 1982. Absolute age of formation of chondrites studied by the ^{87}Rb-^{87}Sr method. *Nature* 300:414-419.

Moreno, T., Amato, F., Querol, X., Alastuey, A., Elvira, J., and Gibbons, W., 2009. Bedrock controls on the mineralogy and chemistry of PM10 extracted from Australian desert sediments. *Environmental Geology* 57:411-420.

Nyquist, L. E., Reese, Y. D., Wiesmann, H., Shih, C. Y., and Schwandt, C., 2000. Rubidium-strontium age of the Los Angeles shergotitite. *Meteoritics & Planetary Science* 35:A121-A122.

Ouazaa, N. L., Perchiazzi, N., Kassaa, S., Zeoli, A., Ghanmi, M., and Folco, L., 2009. Meteorite finds from southern Tunisia. *Meteoritics & Planetary Science* 44:955 - 960.

Preusser, F., 2009. Chronology of the impact of Quaternary climate change on continental environments in the Arabian Peninsula. *Comptes Rendus Geoscience* 341:621-632.

Reneau, S. L., Raymond, R., and Harrington, C. D., 1992. Elemental relationships in rock varnish stratigraphic layers, Cima volcanic field, Valifornia - implications for varnish development and the interpretation of varnish chemistry. *American Journal of Science* 292:684-723.

Ruzicka, A., 1995. Nullarbor-018 - A new L6 chondrite from Australia. *Meteoritics* 30:102-105.

Saunier, G., Poitrasson, F., Moine, B., Gregoire, M., and Seddiki, A., 2010. Effect of hot desert weathering on the bulk-rock iron isotope composition of L6 and H5 ordinary chondrites. *Meteoritics & Planetary Science* 45:195-209.

Schaaf, P. and Muller-Sohnius, D., 2002. Strontium and neodymium isotopic study of Libyan Desert Glass: Inherited Pan-African age signatures and new evidence for target material. *Meteoritics & Planetary Science* 37:565-576.

Schlüter, J., Schultz, L., Thiedig, F., Al-Mahdi, B. O., and Abu Aghreb, A. E., 2002. The Dar al Gani meteorite field (Libyan Sahara): Geological setting, pairing of meteorites, and recovery density. *Meteoritics & Planetary Science* 37:1079-1093.

Shih, C.-Y., Nyquist, L. E., Reese, Y., Wiesmann, H., Nazarov, M. A., and Taylor, L. A., 2002. The choronology and petrogenesis of the mare basalt clast from lunar meteorite Dhofar 287: Rb-Sr and Sm-Nd isotopic studies. *Lunar and Planetary Science XXXIII, Abstract #1344,*

Smith, C. L., Kearsley, A. T., Bermingham, K. R., Deacon, G. L., Kurahashi, E., Franchi, I. A., and Bevan, A. W. R., 2012. Lynch 002: a new lunar meteorite from the Nullarbor desert, Western Australia. *75th Anual Meteoritical Society Meeting*

Stelzner, T., Heide, K., Bischoff, A., Weber, D., Scherer, P., Schultz, L., Happel, M., Schron, W., Neupert, U., Michel, R., Clayton, R. N., Mayeda, T. K., Bonani, G., Haidas, I., Ivy-Ochs, S., and Suter, M., 1999. An interdisciplinary study of weathering effects in ordinary chondrites from the Acfer region, Algeria. *Meteoritics & Planetary Science* 34:787-794.

Struempler, A. W., 1990. Element mobility due to weathering in the L5 Bayard chondrite. *Meteoritics* 25:185-186.

Symes, S. J. K., Borg, L. E., Shearer, C. K., and Irving, A. J., 2008. The age of the martian meteorite Northwest Africa 1195 and the differentiation history of the shergottites. *Geochimica et Cosmochimica Acta* 72:1696-1710.

Treiman, A. H., 1992. Foundation of forensic meteoritics. *Meteoritics* 27:298-299.

Uehara, M., Gattacceca, J., Rochette, P., Demory, F., and Millarca Valenzuela, E., 2012. Magnetic study of meteorites recovered in the Atacama desert (Chile): Implications for meteorite paleomagnetism and the stability of hot desert surfaces. *Physics of the Earth and Planetary Interiors* 200:113-123.

Veizer, J., 1989. Strontium isotopes in Seawater through time. *Annual Review of Earth and Planetary Sciences* 17:141-167.

Wasson, J. T. and Kallemeyn, G. W., 1988. Compositions of chondrites. *Philosophical Transactions of the Royal Society of London Series a-Mathematical Physical and Engineering Sciences* 325:535-544.

Weyhenmeyer, C. E., 2000. Origin and Evolution of Groundwater in the Alluvial Aquifer of the Eastern Batinah Coastal Plain, Sultanate of Oman. PhD Thesis, University of Bern.

Zurfluh, F. J., Hofmann, B. A., Gnos, E., and Eggenberger, U., 2011. Evaluation of the utility of handheld XRF in meteoritics. *X-Ray Spectrometry* 40:449-463.

Zurfluh, F. J., Hofmann, B. A., Gnos, E., and Eggenberger, U., in review-a. "Sweating meteorites" - water-soluble salts and temperature variation in ordinary chondrites and soil from the hot desert of Oman. *Meteoritics & Planetary Science*.

Zurfluh, F. J., Hofmann, B. A., Gnos, E., Eggenberger, U., and Jull, A. J. T., in review-b. Terrestrial age estimation of ordinary chondrites from Oman based on a refined weathering scale and other pysical and chemical weathering parameters. *Meteoritics & Planetary Science*.
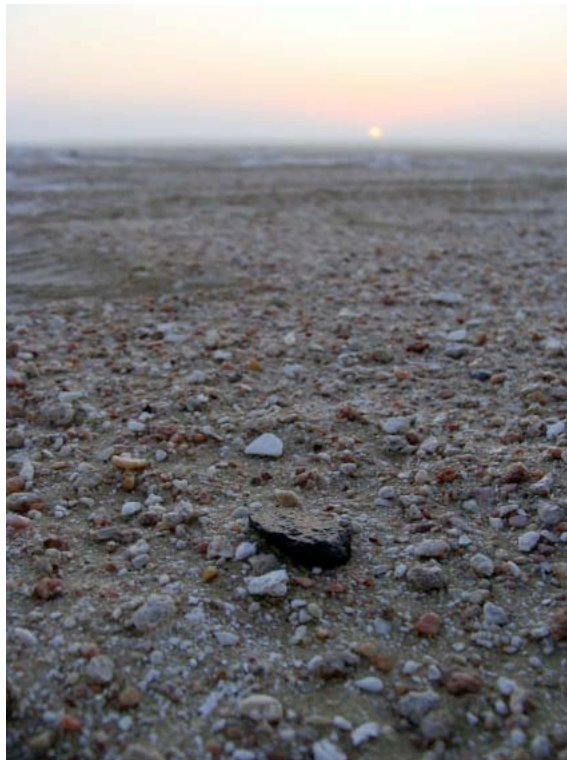
A wet JaH 073, L6 S4, fragment at sunrise at a foggy morning day in Oman.

Chapter 5

"Sweating meteorites" – water-soluble salts and temperature variation in ordinary chondrites and soil from the hot desert of Oman

"Sweating meteorites" – water-soluble salts and temperature variation in ordinary chondrites and soil from the hot desert of Oman

Florian J. ZURFLUH[1]*, Beda A. HOFMANN[2], Edwin GNOS[3], Urs EGGENBERGER[1],

[1]Institut für Geologie, Universität Bern, Baltzerstrasse 1 + 3, CH-3012 Bern, Switzerland
[2]Naturhistorisches Museum der Burgergemeinde Bern, Bernastrasse 15, CH-3005 Bern, Switzerland
[3]Muséum d'histoire naturelle de la Ville de Genève, 1 Route de Malagnou, CP 6434 CH-1211 Genève 6, Switzerland
* Corresponding author. E-mail address: florian.zurfluh@geo.unibe.ch

Abstract - To evaluate the influence of water-soluble salts in weathering of ordinary chondrites (OC) from the hot desert of Oman we performed a comprehensive study including leach experiments to extract water-soluble ions from OC and soil samples, petrographical studies on alteration features and pore space fillings, and in situ recording of temperature variation in an OC and soil. A strong chemical gradient exists between freshly fallen meteorites containing reduced phases and the oxidizing atmosphere. Oman desert soils are carbonate-rich and contain salts that are dissolved in rain or fog water and are soaked into the meteorite by capillary forces. Daily heating and cooling of the meteorites cause a pumping effect resulting in a strong concentration of soluble ions in meteorites over time. Dominant soluble ions detected in soils (n=35) are Ca^{2+}, SO_4^{2-}, HCO_3^-, Na^+ and Cl^- while the leachates of the OC samples from Oman (n=31) contain mainly Mg^{2+}, Ca^{2+}, Cl^- and SO_4^{2-} and iron. Reactions take place where ions introduced from soil react with ions leached from the meteorite. Thus, the concentration of water-soluble ions in meteorites depends on the degree of weathering. The median total concentration of salts in bulk meteorites is 2500 µg/g. Extreme samples had concentrations of nearly 9000 µg/g. During initial stages of weathering porosity is closed due to the precipitation of alteration minerals but due to volume expansion and leaching of minerals new pore space is generated. Weathering processes are enhanced by sulfide oxidation producing acidic conditions. When troilite is completely weathered neutralization occurs and chemical weathering is slowed down.

5.1. INTRODUCTION

Aqueous alteration products in meteorites are a key for the presence of water outside Earth in our solar system. So far, studies focused on Martian meteorites with Nakhla being one of the most studied samples (e.g. Gooding et al., 1991; Changela and Bridges, 2010). Water-soluble ions were determined in Nakhla in a pioneering work, yielding significant concentrations of Cl, S, Mg, Na, Ca and K (Sawyer et al., 2000). Water-soluble salts were also found in the ordinary chondrites (OC) Monahans and Zag that both fell in 1998 (Grossman, 1998; Grossman, 1999). The halite and sylvite grains found in these meteorites were identified to be of extraterrestrial origin (e.g. Rubin et al., 2002). So far, these are the only OC where extraterrestrial salts were described. However, meteorites are subject to terrestrial alteration and contamination from the first moment they reach Earth. Weathering in the cold desert of Antarctica can be used as analogue for preterrestrial low temperature aqueous alteration of carbonaceous chondrites (e.g. Bland et al., 2006). A few studies focused on the halogen contamination of meteorites from Antarctica (e.g. Langenauer and Krähenbühl, 1993b) and the efflorescence of salts on meteorite surfaces (e.g. Velbel, 1988). Liquid water is needed to produce the salt contamination. To study the temperature range meteorites are exposed to in Antarctica, a fragment of the Allende meteorite was equipped with a temperature dependent resistor, detecting temperatures above 0°C in the black meteorite (Schultz, 1986). In hot deserts, daily temperatures variations are much larger and water and water-soluble salts are much more abundant and play an important role in the history of weathering of meteorites (e.g. Al-Kathiri et al., 2005). However, the only investigation where salt contamination in hot desert meteorites was studied focused on the halogen contamination of eucrites and OC from western Australia (Krähenbühl and Langenauer, 1994b; Krähenbühl and Langenauer, 1995). The influence of geographical position, i.e. the distance to the sea and salt contamination was previously studied in meteorites from Antarctica (e.g. Langenauer and Krähenbühl, 1993b; Losiak and Velbel, 2011). But no study was done so far focusing on samples from hot deserts and a systematic survey of salts within hot desert meteorites is missing.

To fill this gap we have analyzed the water-soluble salts concentration of 15 samples from the JaH 091 meteorite shower (Gnos et al., 2006) and 16 individual OC samples collected in the hot desert of Oman during the Omani-Swiss meteorite search project. This study was

initiated after the common observation of a hygroscopic behavior ("sweating") of freshly sawn surfaces of Oman meteorites (Fig. 5.1). We selected samples from various geographical locations and different macroscopic appearances to be able to interpret the variability of salt concentrations. We recognized several types of salt contaminations in meteorites (Fig. 5.2): (i) hygroscopic ("sweating") meteorites as shown in Figures 5.1, 5.2a and 5.2b. In a relatively humid environment (room condition, 50-60% rh) their salts attract water and droplets appear on the surface; (ii) "dark green and dry" meteorites, which look relatively unaltered (no brown hydroxides) but generally belong to W≥3 weathering grade (Wlotzka, 1993) showing only minor efflorescence of salts (Fig. 5.2c); (iii) "dry rusty meteorites", typically of weathering degree W4 (Wlotzka, 1993) often showing macroscopically visible white pore space fillings (Fig. 5.2d).

Figure 5.1. *Cut surface of meteorite JaH 091 (individual 0703-703) showing prominent sweating caused by the presence of hygroscopic brine and salts. Fresh droplets (indicated by arrows) are clear and Mg^{2+} and Cl^- rich. Some ferrous iron is mobilized from the meteorite interior and oxidized to iron hydroxides on the surface to form a rusty precipitate as recognizable for example in the large drops in the middle of the sample. Note only minor hygroscopic behavior on the dark, slightly leached outermost rim of the meteorite.*
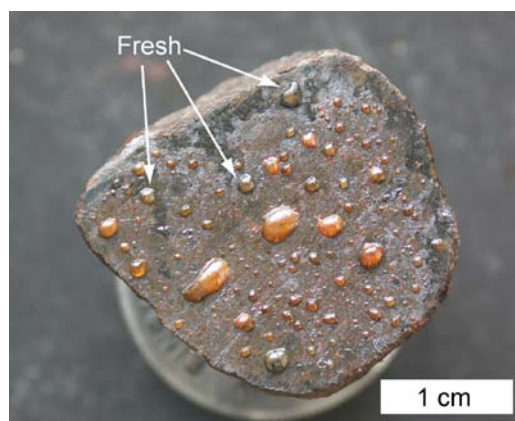
Liquid water is a prerequisite to mobilize salts in meteorites and initiate weathering. Precipitation in the Oman inland desert is sparse but occurs nearly annually. Maps displaying the distribution of precipitation show a gradual decrease of mean annual precipitation from the costal regions of Oman towards inland. Typical meteorite recovery surfaces receive precipitation of less than 70 mm per year (Edgell, 2006). Meteorological data from Yalooni station (19°56'N, 57°06'E), the only inland station in the cited study, yielded a mean annual precipitation of 38.9 mm for 1979 to 1990, which is the lowest out of 10 recording stations all over the Oman (Fisher, 1994). During our fieldwork we often observed fog in mornings, causing wetting of the desert soil surface, especially with wind from southerly directions, i.e. the Arabian Sea.
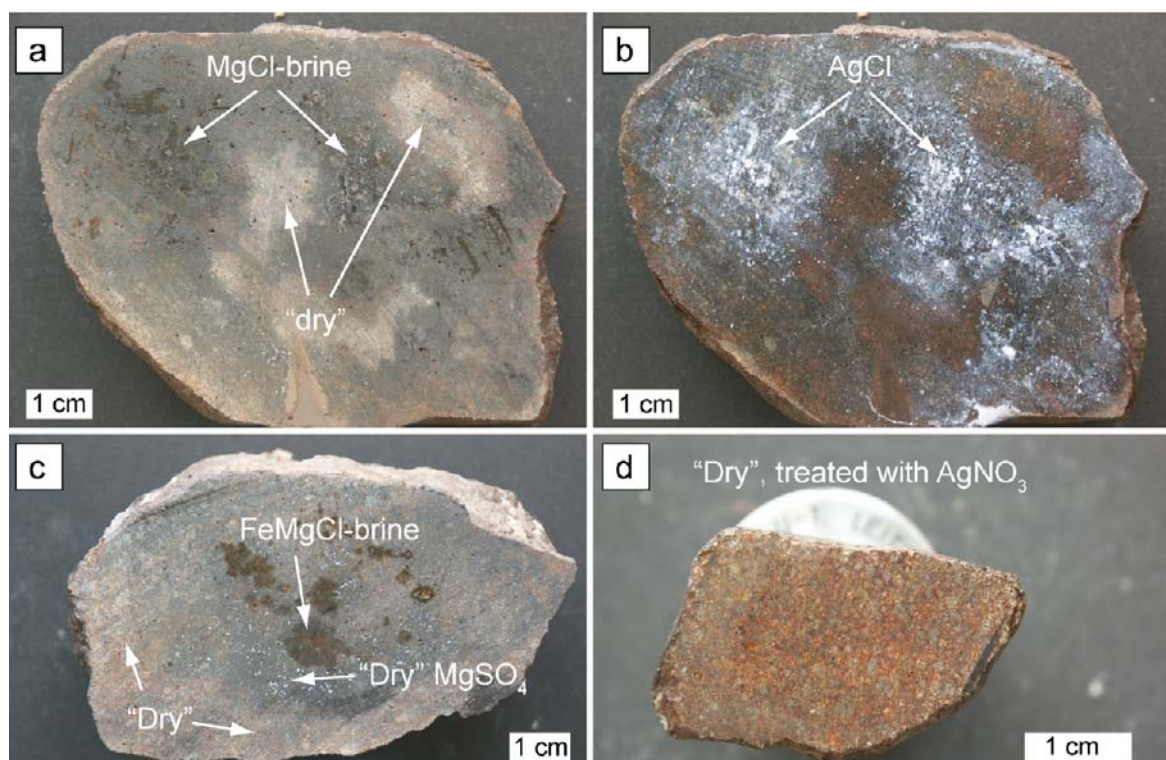
Figure 5.2. *Cut slabs of JaH 091 samples showing the distribution of salts. Images (a) and (b) are from sample 0703-331. (a) The major part shows presence of MgCl-rich brine with only minor iron hydroxide. Some spots are free of brine, as indicated by "dry". (b) The same cut surface as (a) but treated with AgNO₃. White precipitation of AgCl shows distribution of Cl⁻. (c) Sample 0603-239 (JaH 091) has a zoned occurrence of different types of salts. In the middle of the sample a hygroscopic MgFeCl-rich brine is present. It is surrounded by a greenish area with efflorescence of whitish, hairy MgSO₄, which is not hygroscopic. The outermost part shows no salt efflorescence or hygroscopic behavior and displays a rusty color. (d) Meteorite 0702-241 (JaH 091) is a typical W4 sample with white minerals, most likely Ca-sulfates, in pores. After treatment with AgNO₃ no Cl⁻ rich spots are observed.*

The daily temperature fluctuations are essential for the observed salt contamination. We therefore equipped a meteorite with a temperature logger and placed it in a typical meteorite recovery area for nearly one year (Fig. 5.3).

Special attention was paid to solve the enigma of the "sweating meteorites", i.e. the appearance of hygroscopic salts on meteorite surfaces (Fig. 5.1), an effect described by Nininger (1929) on iron meteorites, but otherwise apparently unobserved. The "sweating" of iron meteorites is linked to the presence of the mythic mineral lawrencite ($FeCl_2$) that was claimed to be inexistent (Buchwald and Clarke, 1988). Extreme hygroscopic behavior as seen in Figure 5.1 is commonly observed on OCs recovered from Oman but has not been reported

from deserts like the Sahara, Roosevelt County or Australia (personal communication with several people who have investigated meteorites from these provenance). In this study we present data for water-soluble salts in OC from Oman and discuss their role in the weathering of Omani meteorites.
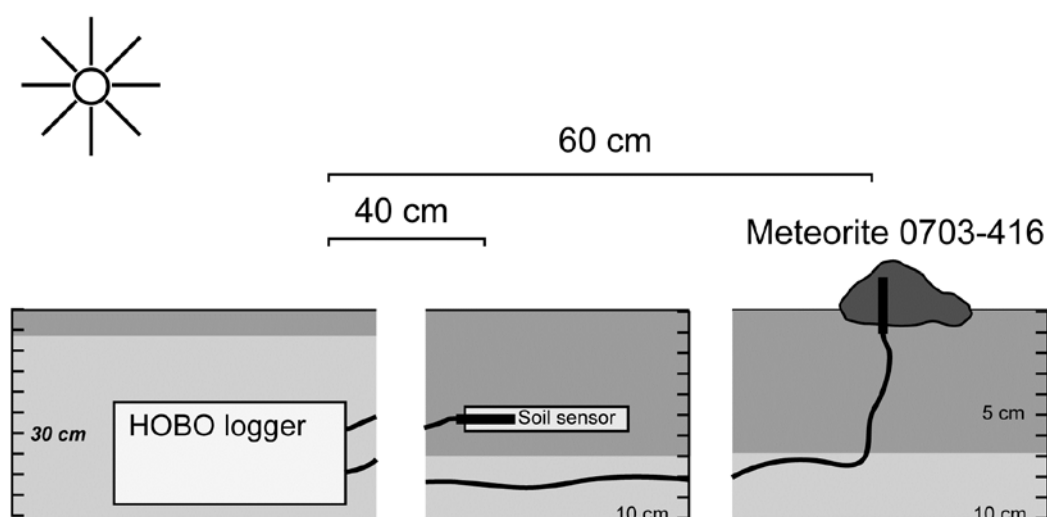
Figure 5.3. *Schematic drawing showing the emplacement of the thermocouples and temperature logger. The soil sensor was placed about 5 cm below surface, just above a caliche horizon. The meteorite was placed in a slightly buried (about 20% of the volume) position, typical for many find situations.*

5.2. SAMPLES AND ANALYTICAL TECHNIQUES

5.2.1. Temperature logging

We used a 173.7 g stone from the JaH 091 L5 S2 strewn field (stone 0703-416) (Gnos et al., 2006) for temperature logging (dimensions 7 cm x 5.5 cm x 4 cm). A thermocouple was placed in a borehole of 6 mm diameter and 3 cm depth so that the thermocouple was placed 1 cm below the outer surface of the meteorite, and connected with a temperature HOBO U23-003 version 1.0.9 data logger (Fig. 5.3). This experiment was placed in the Jiddat al Harasis near Hayma (19°49'N, 55°50'E) with the lower fifth of the meteorite buried in soil. The temperature dependent resistor was fixed with thermo conductive paste. A second

temperature sensor was placed in an aluminum disc and buried at a depth of 30 cm in the soil for recording the temperature variation in the soil (Fig. 5.3). Temperature was recorded at a rate of one record every 20 minutes in the first measuring period and one record every 30 minutes in the second.

5.2.2. Sample selection and leaching experiments

5.2.2.1. Soil samples

Thirty-five surface soil samples from Oman (fraction <0.15 mm) providing the source of ions introduced into the meteorites (Al-Kathiri et al., 2005;16 collected in 2007, SL091 series, 19 in 2009/2010, SLO1 and SLO2 series, Table 5.1 and 5.2) were studied by leaching experiments. Leaching was performed under laboratory atmosphere during 7 days in automatic shakers. Most samples were leached with solid to liquid ratios of 1:1, i.e. 30 g of soil sample and 30 g by weight of deionized Milli-Q water.

In addition to the leaching experiments of soil samples, which were analyzed by ion chromatography, the Cl⁻ concentration was tested in 63 soil samples by use of Aquamerck and Merck Mikroquant® fast tests. Approximately 10 g of soil (fraction <0.15 mm) was mixed with 10 g deionized water and stirred for one minute. After 5 minutes of sedimentation the supernatant was used for the test.

Table 5.1. Compilation of experimental work.

Label	Samples	Goal	Leach time [d]	Analyses	Year of sampling	Year of experiment
ML091	L5 S2 (JaH 091)	Water-soluble salts contamination in samples with identical terrestrial age (strewn field)	15	IC, alkalinity, microscopy, SEM	2007	2007/2008
SL091	soil samples, JaH 091 region	Variation of salts in soil over a small area	7	IC, alkalinity, sieve	2007	2007/2008
MLT	L5 S2 (JaH 091)	Test of leaching experiment set up (time)	variable	IC, alkalinity, ICP-OES	2010	2010
SLO1	soil samples	Salts in soils from Oman	7	IC, alkalinity, sieve	2009/2010	2011
SLO2	soil samples	Salts in soils from Oman	7	IC, alkalinity, sieve	2009/2010	2011
MLO	Ordinary chondrites, Oman, Tamdakht, H chondrite fall	Water-soluble salts in OC from Oman and Tamdakht	48	IC, alkalinity, ICP-OES, microscopy, SEM	2009/2010	2011

IC: Ion chromatography.
ICP-OES: Inductively coupled plsama - optical emission spectroscopy.
SEM: Scanning electron microscope.

5.2.2.2. Water samples

Complementary, surface water samples from central Oman desert were analyzed. Two samples are from artificial pools between dunes fed by shallow groundwater, one of reddish color that showed active precipitation of gypsum and one form a greenish part (Table 5.2). Three samples were collected at the natural oasis of Wadi Muqshin (Abed et al., 2011; Jupp et al., 2008), one sample from the surface of a brine pool, another at a depth of 20 cm in the same pool and the third at the bottom of a shallow irrigation well (Table 5.2). Rainwater was collected at Al Awad (20°52.696'N 58°11.631'E) during night of February 7, 2010, on a clean plastic canvas and filled in small plastic (PP) flasks for transportation.

Table 5.2. Oman water composition.

Label IC	OM-1	OM-2	OM-3	OM-4	OM-5	OM-21
Field number	080120G	080120R	080121b	080121t	080121w	Rain 7-2-10
N [°]	19.72177	19.72177	19.59525	19.59525	19.59180	20.87827
E [°]	55.09815	55.09815	54.89503	54.89503	54.89478	58.19358
Sample type	Water pool green	Water pool red	Water pool bottom	Water pool top	Water well	Rain water
pH	8.27	7.91	7.6	8.08	8.01	7.58
Temperature [°C]	17	17	32	16	19.4	-
Na^+	7700	38600	75000	30900	940	0.6
K^+	243	1350	1980	988	36	<1
Mg^{2+}	815	3394	9095	4201	213	<1
Ca^{2+}	1250	1140	278	692	724	7.3
Sr^{2+}	<0.5	<0.5	<0.5	<0.5	<0.5	<1
NH_4^+	na	na	na	na	na	na
F^-	4.1	14.2	19.0	11.0	1.9	0.2
Cl^-	12200	61100	87000	50800	1370	2.1
Br^-	8.6	31.3	30.3	10.4	<0.5	<0.5
SO_4^{2-}	5555	13300	76700	18900	2500	1.9
NO_3^-	20.8	52.1	16.1	9.0	16.8	<0.5
HCO_3^-	102	322	207	268	156	23

All IC data in [mg/L].

5.2.2.3. Meteorite samples

All Oman meteorites used here were collected in the field using tweezers and packed into polypropylene bags, and unpacked in the lab wearing gloves to avoid contamination. Samples were cleaned from attached soil material with pressured air and stored under controlled conditions (20°C, ~40 % air humidity) at the Natural History Museum Bern. The samples were cut using isopropanol as cooling agent to reduce leaching of the soluble pore minerals. Besides the meteorites selected for the aqueous leaching study other samples collected in Oman were investigated during classification procedure for their terrestrial minerals.

During a first study (ML091; Table 5.1) the range of water-soluble salts of 15 meteorites covering the whole ~50 km long JaH 091 L5 strewn field (Gnos et al., 2006) were selected for the leaching experiment. The size of the individuals varied from 47.7 g to 8.8 kg with an average mass of about 120 g. Representative test blocks were produced from meteorite interiors at least one centimeter below natural surfaces. Parts of the meteorites free of calcite veins or cracks were selected. The samples for the leaching experiment had a size of about 2 cm x 1 cm x 0.8 cm (weight between 2.02 to 7.17 g, mean 4.60 g). After weighing, samples were transferred to small Teflon flasks and filled with deionized Millipore-Q water (meteorite/water ratio approximate 1 to 4 by mass). The meteorites were leached over a period of 15 days at room temperature and agitated occasionally to reach equilibrium between the rock and water.

In a second run, fourteen subsamples from one individual stone of the JaH 091 strewn field were leached for 10 minutes, 1 hour, 8 h, 24 h, 4 days, 15 d and 30 d (MLT; Table 5.1). For each time span, two samples were leached and analyzed in parallel for control. To limit the oxidation of iron the meteorite cubes were vacuum-sealed immediately after cutting and transported into a N_2-filled glove box where they were transferred to the Teflon flasks. In addition, oxygen-free deionized Millipore-Q water was used as solvent.

In a third batch, 15 samples from meteorites with a total mass of 144.4 to 4700 g, covering a large spread of find localities, soil types, weathering grades and meteorite types were selected. The sampled meteorites were found along a profile from the coast to the interior. The aim of this selection was to study the geographical influence on the salt contamination (MLO; Table 5.1). Although many ordinary chondrites from all over Oman were accessible, some classes, petrologic types and shock stages are underrepresented (e.g. weathering grades below W2). A W0 sample from H5 S3 chondrite fall Tamdakht in 2008 to South Morocco (Chennaoui-Aoudjehane et al., 2009; Weisberg et al., 2009) was also included in the test series. The samples of the MLO series were leached for 48d under same conditions as MLT samples.

To visualize the chloride distribution in 16 cut meteorites of L5 JaH 091, cut surfaces were treated with a solution of $AgNO_3$. Ag^+ reacts with Cl^- to form a white precipitate of AgCl (Figs. 5.2b and 5.2c). The same procedure was applied to dark terrestrial rocks (sandstones, desert varnish coated cherts, gabbros, serpentinites, rhyolites and basalts).

5.2.3. Measurements of water-soluble ions

The leachates from soil and meteorite samples were measured by ion chromatography (IC) on a Metrohm 861 compact ion-chromatograph in the laboratory for rock-water interaction at the Institute for Geological Sciences, University of Bern using appropriate standards and blanks for each ion. Highly concentrated samples had to be diluted 1:2, 1:10 or 1:100. Before dilution, the samples were filtered (0.2 μm). The soil, meteorite and water samples were measured for the cations Na^+, Mg^{2+}, K^+, Ca^{2+} and Sr^{2+} and the anions F^-, Cl^-, Br^-, SO_4^{2-} and NO_3^-. In two meteorite samples a peak corresponding to NH_4^+ was observed and the concentration was determined semiquantitatively. The analytical error is about 5% based on repeated measurements of standard solutions. Detection limit for most of the anions and cations is 0.5 mg/l. The pH and alkalinity (by titration with HCl, alkalinity is later in the text specified as HCO_3^-) were measured using a Metrohm 785 DMP Titrino. Some selected samples were additionally measured by inductively coupled plasma-optical emission spectroscopy (ICP-OES) with a Varian 720 ES instrument. Meteorite leachates from the time series were analyzed for Na, Mg, Ca, Fe, Co, Ni and Sr; meteorites from ML series for Al, Si, Mn, Fe, Co, Ni, Sr and Ba. Even though the experiments were performed in a glove box flushed with N_2, iron hydroxides precipitated in several samples. All ML samples were treated with 5% HNO_3 before ICP-OES measurement. Blank samples treated the same way as the experimental samples were measured in the same run for control.

The weights of the solid material, the water for the soil leaches, the wet weights of the meteorites were determined with exact balances (±0.01 g). After the experiments the meteorites were dried at 105°C to constant weight and the (connective) porosity was calculated using wet and dry weights of the sample. For the calculation of the concentration of the ions in the pore space the solid to liquid ratio (S:L) corrected values were adjusted using the determined porosity and an assumed density of the occupied pore space of 1.2 g/cm^3. For simplification, we used a bulk density of 3.3 g/cm^3 for all meteorites, a mean of unaltered H and L chondrites (Consolmagno et al., 2008).

5.2.4. Determination of pore filling minerals

Secondary minerals in pores were identified by optical microscopy and a Zeiss EVO50 scanning electron microscope (SEM) with attached energy dispersive X-ray spectroscope (EDS) at the Institute for Geological Sciences at the University of Bern.

Some of the pore space fillings, salt efflorescence on the meteorite surface and brine drops were mounted on a sample carrier for SEM study. JaH 478 contained sufficient secondary material for X-ray diffractometric determination. The finely powdered material was mounted on a silicon wafer and measured with a Philips PW1800 diffractometer.

5.3. RESULTS

5.3.1. Temperature fluctuations in meteorite and soil

The first period of temperature measurements was from June 20, 2009 to January 13, 2010 with 14'900 temperature readings in the meteorite and the same amount the soil. The second period was from January 13, 2010 to January 22, 2011 with 17950 temperature readings in the soil. The cable leading to the thermistor in the meteorite was damaged on May 13, 2010 by animal bite (probably fox); only 6460 temperature records are thus available for the meteorite from the second period. In total, we thus have 21360 temperature readings in the meteorite for nearly one year. The short gap between mid May to mid June is not dramatic since maximum temperatures occur in July and minimum temperatures in January. For the meteorite, the maximum temperature was 66.3°C, recorded on July 11, 2009 at 1:00 pm; for the soil 54.8°C on July 13, 2009 at 2:40 pm. Minimum temperatures were measured on January 7, 2010 with 4.8°C for the meteorite at 6:40 am and 9.1°C for the soil at 7:20 am. Since the meteorite was placed on the surface, it heated faster and reached daily peak temperature earlier than the soil resistor (Fig. 5.4a). The maximum temperatures in the meteorite were recorded around 1:30 pm, in the soil about one hour later, at 2:30 pm. Minimum temperatures show a similar behavior: in the meteorite they are recorded at 6:20 am, just before sunrise, about 20 minutes earlier than in the soil. The mean daily min-max

temperature differences are much larger in the meteorite (34.3°C) than in the soil (21.6°C) and remain similar over the whole measuring period (Fig. 5.4b). However, daily and monthly average temperatures in soil and meteorite are very similar (Fig. 5.4b). The largest monthly deviations are observed in summer (June: meteorite-soil 1.7°C) in winter they are almost similar (January: 0.1°C).
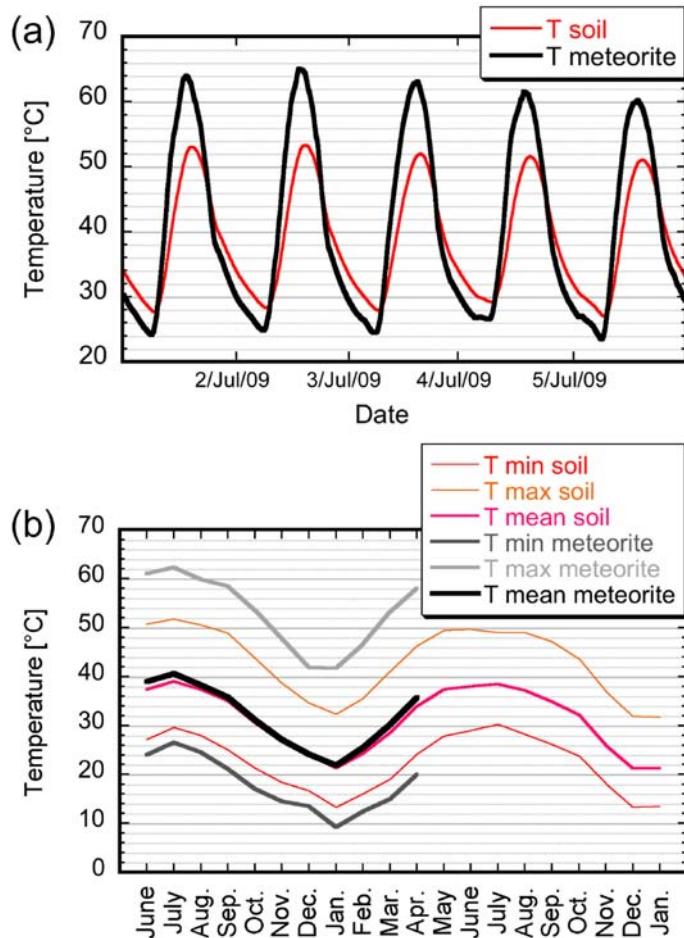
*Figure 5.4.*Temperatures recorded by the data logger.
a) Typical pattern of daily temperature evolution as recorded in July 2009. The meteorite is heated faster and cools down more rapid than the thermistor in the soil. The daily temperature difference can reach 34.3°C in the meteorite whereas in the soil it is about 21.6°C.
b) Monthly average temperatures of soil and meteorite temperatures show only small differences and are larger in summer. The meteorite reaches higher maximum and lower minimum temperatures. The thermistor of the meteorite was disconnected in May 2010 probably by an animal bite.

During fieldwork, we also measured surface temperatures with a thermometer coupled with a temperature sensor. On two days at the end of January 2010 with air temperatures reaching 28°C (1:15 pm) and 29°C (14:45 pm), surface temperatures of meteorite finds were 34°C and 41°C. The top 1 cm of the soil was at temperatures of 37 to 46°C. The temperatures measured on the surface of the soil are significantly higher than those measured at a depth of 5 cm. This indicates that the magnitude of diurnal temperature fluctuations rapidly decreases with increasing depth in the soil. On the other hand, the surface temperatures of the meteorite are within the range measured inside the meteorite at the same time.

5.3.2. Water-soluble salts in soils and saline waters

The Cl⁻ content was determined with the fast test method for 63 soil samples that were collected in all major meteorite recovery areas over much of Oman with a special focus on a cost-inland transect from Ras Madrakah via Hayma towards the dunes of the Rub al K'hali (Fig. 5.5). The results of the chlorine fast test are in good agreement with Cl⁻ concentration obtained by ion chromatography (Fig. 5.6). The analyzed values were corrected for solid to liquid ratio. The Cl⁻ concentration of the soils covers a range from 8 µg/g to 3297 µg/g (median) and varies with geographical provenance (Fig. 5.5).
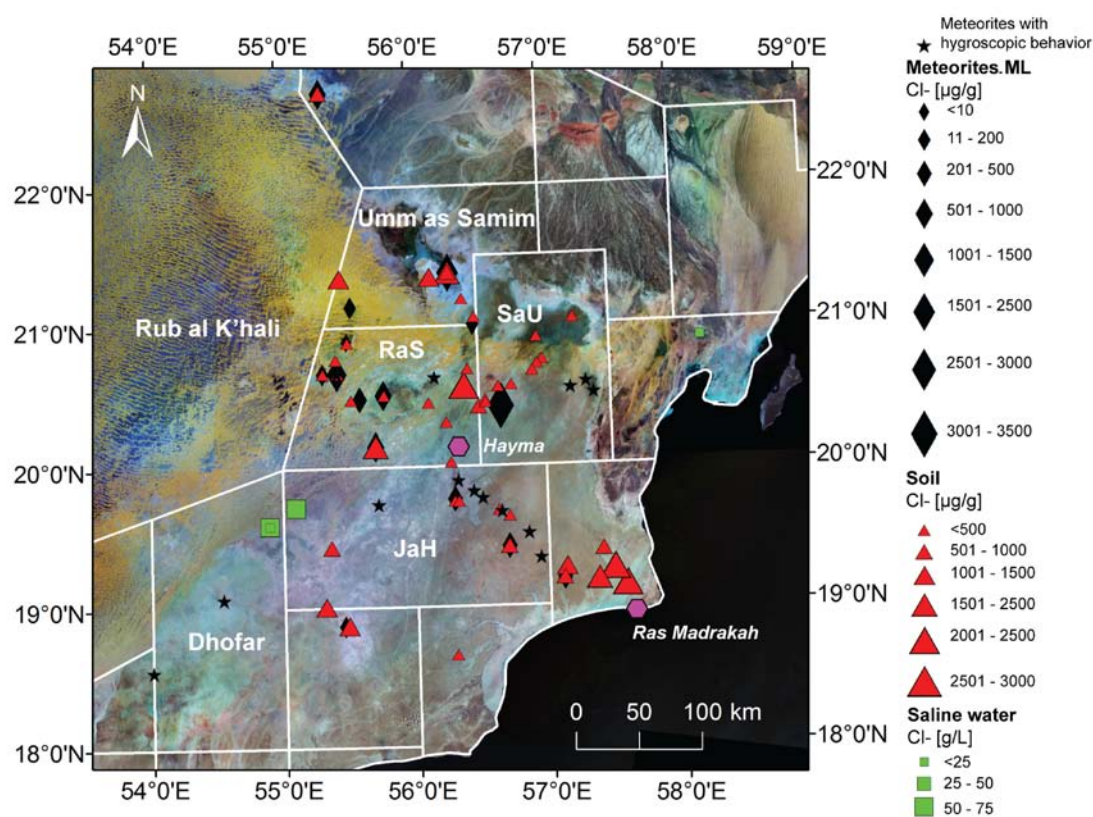
Figure 5.5. *Chloride concentration in soil, water and meteorite samples as function of geographical location. Stars represent meteorites with hygroscopic behavior as displayed in Figure 5.1. Diamonds show the find localities of the meteorites analyzed in the MLO series. The Cl⁻ content in solid is displayed. Pyramids represent the Cl⁻ concentration measured in soil samples as determined by fast tests. Locations of saline water sample locations are marked with circles with variable sizes depending on Cl⁻ content measured by ion chromatography. Towards the coast of the Arabian Sea (bottom right) the effect of salt derived by sea spray is well visible near Ras Madrakah. Inland depressions are also generally richer in salt (e.g. Umm as Samim). Hayma is a small town in the center of the study area. Areas with dense meteorite accumulations such as the Dhofar, JaH, RaS and SaU have relatively low concentrations of Cl⁻.*

Similar to soil bulk elemental composition (Al-Kathiri et al., 2005), the ionic composition of water-soluble salts from soils is fairly uniform (Fig. 5.7) but the concentrations are variable. A difference observed is that highly concentrated soil leaches have low Ca^{2+}/HCO_3^- ratios of about 0.3 while soils with low salt concentrations have high Ca^{2+}/HCO_3^- ratios up to 40. Usually, highly concentrated samples have higher sulfate content. Na^+/Cl^- ratio of higher concentrated samples is closer to the Na/Cl ratio of halite. Dominant ions are Ca^{2+}, SO_4^{2-}, HCO_3^-, Na^+ and Cl^- that can be interpreted as being derived from evaporite and bedrock minerals such as halite (NaCl), gypsum ($CaSO_4*2H_2O$) and calcite ($CaCO_3$). Potassium, magnesium, strontium and nitrate are present in minor amounts while bromine and fluorine are normally below detection. The soil samples of the first analyzed series (SL091) were quite uniform compared to the later analyzed (SLO1, SLO2; Table 5.3). Two explanations are plausible: (i) the covered geographical area was quite small for the SL091 samples and (ii) the way of sample collection was slightly different for the SLO1 and SLO2 samples.

Figure 5.6. *Comparison of the chlorine fast test to IC measurements. The agreement of a fast test to determine the concentration of chloride in soil samples with values determined by ion chromatography is generally good.*
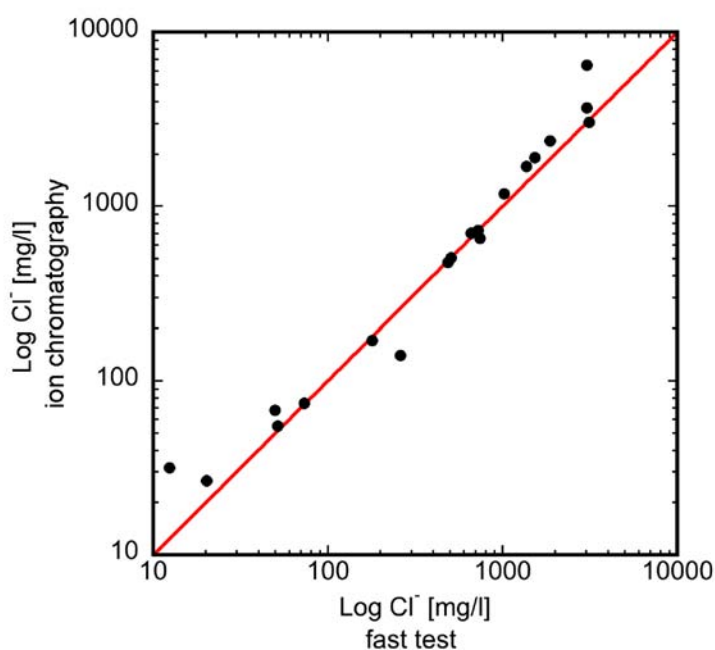
Concentrations of water-soluble salts (based on assumed filling of pore space during rain events, liquid to solid ~1:4) in soils are low compared to ocean water, saline waters and meteorites from Oman and range between 186 µg/g in solid to 14139 µg/g in solid. Excluding the SL091 samples, which are from a relatively small geographic region, the median value for the total dissolved ions is 1148 µg/g in solid. The content of water-soluble ions depends on geographical and geological factors. Close to the Arabic sea at Ras

Madrakah concentrations are higher due to the input of salts from sea spray (Fig. 5.5). Inland salt contents in the soil are higher close to depressions, where water accumulates during occasional rainstorms and evaporates. A prominent depression is the sabkhah Umm as Samim ("mother of poison"; e.g. Fookes and Lee, 2009). High-density meteorite recovery areas such as the Sayh al Uhaymir (SaU), Jiddat al Harasis (JaH), Dhofar or the Ramlat as Sahmah (RaS) are generally low in salt.

Saline waters have seawater like composition and Cl^- concentrations vary from 12000 mg/L to 87000 mg/L (Table 5.2). Our measurements of the pool water samples from Muqshin are comparable to data in literature (Abed et al., 2011; Jupp et al., 2008).
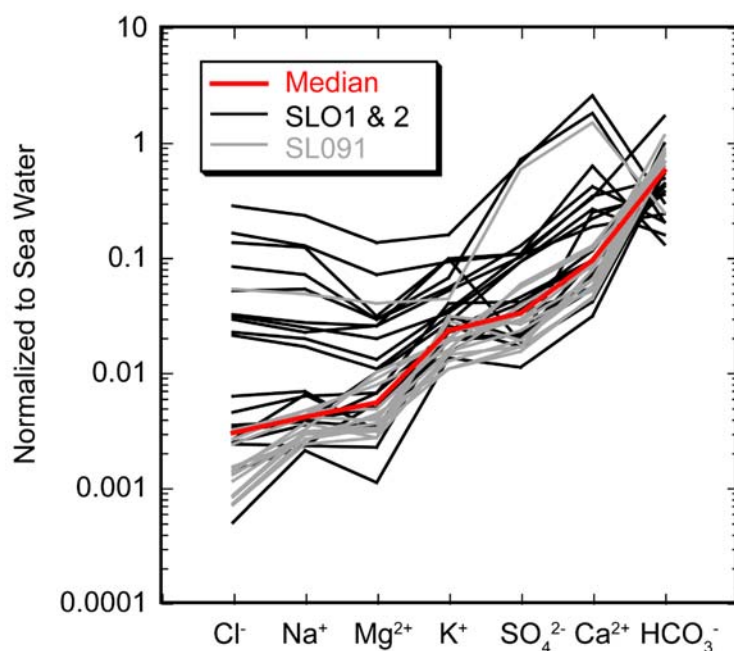
Figure 5.7. *Water-soluble salts in soil samples normalized to seawater. The elements are sorted by increasing median values to the right. Two types with relative uniform compositions occur. One type with generally higher concentrations and relative low Na^+/Cl^- and high Ca^{2+}/HCO_3^- ratios and soils with low concentrations and high Na^+/Cl^- and low Ca^{2+}/HCO_3^- ratios.*

To test for possible chloride accumulations within terrestrial rocks $AgNO_3$ tests were performed on broken surfaces of dark terrestrial rocks found during meteorite searches (sandstones, limestones and cherts with desert varnish, gabbros, rhyolites and basalts). None of the inspected samples showed obvious precipitation of AgCl, indicating that the accumulation of chloride is restricted to meteorites containing significant metal and troilite.

Table 5.3.a. Soil sample leaching results. SL091 series, soil samples from JaH 091 region.

IC label	SL091_01	SL091_02	SL091_03	SL091_04	SL091_05	SL091_06	SL091_07	SL091_08	SL091_09	SL091_10	SL091_11	SL091_12	SL091_13	SL091_4	SL091_15B	SL091_16B
FieldNo	FS38-235	239Soil	FS37-249	FS21-207	FS22-210	FS24-218	FS25-226	FS26-241	FS28-255	FS29-260	FS29-296	FS31-309	FS33-335	FS45-495	FS47-258	FS21_2 07U
Label	235B	239B	249B	207B	210B	218B	226B	241B	255B	260B	296B	309B	335B	495B	258B	207UB
pH	8.09	8.28	8.01	7.84	8.19	8.05	8.16	8.17	8.09	8.18	7.59	7.94	8.16	7.97	8.14	8.08
Na^+	102.8	45.4	74.1	65.6	40.8	37.3	50.3	67.2	41.7	45.4	749	74.1	56.8	48.8	45.4	64.6
K^+	10.2	12.6	8.4	10.5	5.0	6.5	8.7	9.1	4.8	6.9	20	7.2	14.3	6.5	5.7	10.8
Mg^{2+}	5.6	5.4	8.6	6.8	7.6	4.7	17.9	15.5	5.8	7.2	69	13.5	4.7	5.8	6.3	6.8
Ca^{2+}	27.6	31.8	46.8	32.1	38.7	21.8	42.2	59.0	22.9	26.2	729	62.8	25.5	40.7	28.2	31.7
Sr^{2+}	<0.5	2.6	<0.5	0.9	1.3	1.9	1.1	<0.5	<0.5	<0.5	9	6.2	0.6	<0.5	0.5	<0.5
F^-	<0.5	<0.5	<0.5	<0.5	<0.5	<0.5	<0.5	<0.5	<0.5	<0.5	<0.5	<0.5	<0.5	<0.5	<0.5	<0.5
Cl^-	60.1	26.0	71.0	54.7	35.4	16.2	34.2	73.9	16.6	18.9	1216	60.4	32.1	19.7	29.7	54.8
Br^-	<0.5	0.7	0.5	<0.5	<0.5	<0.5	0.7	<0.5	<0.5	<0.5	<0.5	<0.5	<0.5	<0.5	<0.5	<0.5
SO_4^{2-}	105	60.7	101	88.4	53.6	53.4	91.4	175	49.2	72.5	1889	189	83.1	124	61.6	89.0
NO_3^-	22.7	9.8	23.4	14.7	14.3	6.9	15.4	8.8	5.0	6.0	39	13.0	12.3	7.0	11.0	14.4
HCO_3^-	136	126	121	93.9	117	87.2	164	76.9	111	109	35	106	113	84.8	97.0	92.7

All IC data is corrected for S:L and displayed in [µg/g].
All samples were leached for 7 days.

Table 5.3.b. Soil sample leaching results. SLO1 series, soil samples from Oman.

IC label	SLO1_01	SLO1_03	SLO1_05	SLO1_06	SLO1_07	SLO1_11	SLO1_12	SLO1_13	SLO1_16	SLO1_17	SLO1_18	SLO1_19	SLO1_20
FieldNo	0901_007	0901_010	0901_033	0902_073	0902_125	0902_131	0902_139	1001_012	1001_021	1002_125	0902_098	0603_235	0603_235
	Surf	Surf	Surf	Surf	Surf	Surf	Surf	Surf	Surf	Surf	Surf	2010_Surf	2010_Surf
N [°]	21.06494	21.37603	20.66748	19.18798	20.89485	20.91903	20.37165	22.67752	21.34534	20.14650	18.86795	19.68365	19.68365
E [°]	56.48188	56.29112	55.31715	57.10978	55.50613	55.41193	56.51017	55.34026	55.46300	55.70913	55.45073	56.63440	56.63440
pH	8.35	8.03	8.19	7.41	8.24	8.32	7.81	8.03	7.99	7.83	7.74	7.94	8.35
Cl [µg/g][a]	260	507	51	721	12	3112	3018	660	1019	1524	3030	50	
Na^+	107	315	36	429	36	1910	2013	389	825	1123	3678	61	56
K^+	9	16	7	44	12	44	42	15	30	25	73	10	18
Mg^{2+}	5	23	10	44	4	54	125	35	51	51	234	9	12
Ca^{2+}	26	92	42	164	21	124	312	131	886	206	1271	57	47
Sr^{2+}	<1	5	2	4	<1	3	5	8	10	8	13	<1	1
NH_4^+	na	na	na	na	na	na	na	na	na	na	na	na	na
F^-	<0.5	<0.5	<0.5	<0.5	<0.5	<0.5	<0.5	<0.5	<0.5	<0.5	0.5	<0.5	<0.5
Cl^-	141	507	55.2	730	31.7	3053	3696	704	1180	1911	6509	68.0	56.3
Br^-	<0.5	<0.5	<0.5	<0.5	<0.5	<0.5	<0.5	<0.5	<0.5	<0.5	<0.5	<0.5	<0.5
SO_4^{2-}	66.0	330	111	340	53.1	59.3	338	290	2278	405	2139	127	131
NO_3^-	7.5	12.5	8.6	63.5	7.9	47.3	75.1	37.5	37.5	50.5	181	27.2	22.2
HCO_3^-	75.1	33.2	53.6	236	81.2	49.4	18.3	21.9	28.7	28.4	42.1	95.8	94.0

All IC data is corrected for L:S and displayed in [µg/g]
All samples were leached for 7 days
a Determined with quick tests

153

Table 5.3.c. Soil sample leaching results. SLO2 series, soil samples from Oman.

Label IC	SLO2_01	SLO2_02	SLO2_03	SLO2_04	SLO2_05	SLO2_06
FieldNo	0901_031Surf	0901_022Surf	0901_051Surf	0901_06XSurf	1001_071Surf	1001_030Surf
N [°]	20.66974	20.50789	19.75377	19.42066	20.48139	21.14270
E [°]	55.42814	55.77546	56.29692	56.69929	55.59514	55.53912
pH	7.89	8.45	7.93	7.98	8.21	7.93
Cl^- $[\mu g/g]^a$	484			73	740	
Na^+	268	33	59	348	99	60
K^+	14	6	13	23	11	9
Mg^{2+}	19	*2*	17	44	12	6
Ca^{2+}	47	15	108	171	48	35
Sr^{2+}	<5	<5	<5	<5	<5	<5
F^-	*1.2*	*1.3*	*1.1*	*1.2*	*1.3*	*1.3*
Cl^-	477	11.6	74.8	658	103	80.0
Br^-	<1	<1	<1	<1	<1	<1
SO_4^{2-}	62.8	35.3	288	324	146	68.1
NO_3^-	17.2	5.1	24.1	70.4	33.2	32.4
HCO_3^-	58.2	77.1	58.9	69.1	61.1	60.2

All IC data is corrected for L:S and displayed in [$\mu g/g$].

All samples were leached for 7 days.

Italic semiquantitative values.

a Determined with quick tests.

Table 5.4.a. Meteorite leaching experiment results. ML091 series, meteorites from JaH 091 L5 S2 shower.

Label IC	ML091_01	ML091_02	ML091_03	ML091_04	ML091_05	ML091_06	ML091_07	ML091_08
Field number	0603-235	0603-239	0603-249	0702-207	0702-210	0702-218	0702-226	0702-241
WD	3.3	3.0	3.0	3.3	3.3	3.3	3.3	4.5
Degree of burial [%]				80	50	20		50
Inital weight (solid, S) g]	2.97	4.34	3.17	2.02	5.4	4.39	3.26	2.98
Wet weight [g]	2.98	4.34	3.18	2.03	5.43	4.4	3.26	2.98
Water (liquid, L) [g]	9.402	5.356	8.922	9.536	5.346	4.714	5.057	9.852
Mass total [g]	>49000	>200000	>500000	8819	426.5	262.7	50.8	53.5
Fragments	>100	>50	>100	1	1	1	1	1
pH	7.7	4.73	7.65	7.16	7.52	7.67	7.44	6.69
Porosity [%]^a	3.4	1.9	3.8	2.6	3.9	3.3	4.2	5.2
Na^+	2	74	51	67	1	3	6	10
K^+	<1	2	3	5	4	7	35	3
Mg^{2+}	762	252	455	293	761	929	1695	55
Ca^{2+}	466	109^b	420	2054	366	311	490	906
Sr^{2+}	<1	<1	<1	<1	<1	<1	<1	7
NH_4^+	<1	14	<1	3	1	<1	<1	<1
F^-	3.2	<0.5	<0.5	<0.5	<0.5	<0.5	<0.5	<0.5
Cl^-	2015	1027	1142	4173	1839	1185	2427	201
Br^-	<0.5	<0.5	<0.5	<0.5	0.8	<0.5	1.8	<0.5
SO_4^{2-}	1187	383	1079	467	1101	2625	4572	2147
NO_3^-	<0.5	<0.5	2.5	<0.5	<0.5	<0.5	1.5	16.3
HCO_3^-	201	6.8	173	89.3	42.9	67.5	80.5	50.4

All IC data is corrected for L:S and displayed in [$\mu g/g$].

All samples were leached for 15 days.

WD: Weathering degree.

^{a} Porosity calculated by use of wet and dry weight of the meteorite cubes.

^{b} Ca^{2+} might be underestimated due to precipitation of a Ca phase.

Table 5.4.a. Continued.

Label IC Field number	ML091_09 0702-255	ML091_10 0702-260	ML091_11 0702-296	ML091_12 0702-309	ML091_13 0702-335	ML091_14 0703-495	ML091_15 0703-703	ML091_16 0702-331
WD	3.6	3.3	3.6	3.6	3.0	3.3	3.3	3.3
Degree of burial [%]		40	60	30	40	70	0	5
Inital weight (solid, S) g]	4	4.95	2.69	2.06	4.13	3.98	4.49	4.22
Wet weight [g]	3.99	4.96	2.71	2.06	4.15	3.98	4.46	4.23
Water (liquid, L) [g]	5.2713	5.336	9.067	9.658	4.974	9.212	4.947	9.58
Mass total [g]	217	180.8	336.4	103.7	5658	112	47.7	1216.6
Fragments	27	1	8	1	1	1	1	1
pH	4.37	7.4	4.95	6.05	7.08	7.63	4.3	7.52
Porosity [%]^a	3.7	2.8	5.5	2.7	2.2	3	3.4	2.2
Na^+	58	2	11	<1	39	3	52	23
K^+	26	4	13	2	5	7	40	1
Mg^{2+}	1834	622	557	671	318	781	1957	611
Ca^{2+}	399	225	523	<1	99	181	317	130
Sr^{2+}	1	<1	<1	<1	1	<1	<1	<1
NH_4^+	5	<1	<1	<1	<1	<1	<1	<1
F^-	<0.5	<0.5	<0.5	<0.5	<0.5	<0.5	<0.5	3.9
Cl^-	1472	1341	204	1319	41	1995	6037	1578
Br^-	<0.5	<0.5	<0.5	<0.5	<0.5	<0.5	8	2.6
SO_4^{2-}	6653	1053	3509	1824	1555	741	570	613
NO_3^-	0.9	<0.5	4.1	<0.5	<0.5	<0.5	2.2	2.1
HCO_3^-	0	46	16.5	28.6	25.7	140	<0.5	126

5.3.3. Water-soluble salts in ordinary chondrites

Although the extraction series of the meteorites were performed under different conditions, they are in agreement and provide a first data basis for a previously unrecognized effect. Some problems with the experiments concern the rock-water-ratio. Because meteorites are precious materials the mass of solid sample was limited, and the amount of added water should not be too large to obtain measurable ion concentrations. On the other hand, concentrations of some major ions such as magnesium, chloride and sulfate were expected to be very high based on experience from EDS analyzes of brines and the extracts from the ML091 series (Table 5.1, 5.4a). A critical parameter is the precipitation of minerals from oversaturated brines or the precipitation of iron hydroxides under oxidizing conditions.

Table 5.4.b. Meteorite leaching experiment results. MLT series, time series with samples from the JaH 091 L5 S2 shower

Label IC	MLT-01a	MLT-01b	MLT-02a	MLT-02b	MLT-03a	MLT-03b	MLT-04a	MLT-04b
Field number	0603_235a	0603_235a	0603_235a	0603_235a	0603_235a	0603_235a	0603_235a	0603_235a
Leach time [d]	0.007	0.007	0.04	0.04	0.3	0.3	1	1
Inital weight (solid, S) [g]	3.98	3.83	4.07	6.37	4.87	3.12	4.24	4.66
Wet weight [g]	3.98	3.83	4.08	6.38	4.87	3.14	4.26	4.69
Water (liquid, L) [g]	14.91	15.26	15.74	14.42	15.36	15.2	15.15	15.54
pH	5.84	5.58	6.33	6.32	6.05	6.04	6.31	3.16
Porosity [%][a]	2.2	1.9	2.1	2.2	2.2	3.4	3.2	4.1
Na^+	<1	<1	7	4	12	7	25	17
K^+	<1	<1	<1	<1	<1	<1	<1	<1
Mg^{2+}	4	6	8	4	9	18	18	107
Ca^{2+}	18	19	62	51	210	111	196	204
Sr^{2+}	<1	<1	<1	<1	<1	<1	<1	<1
NH_4^+	na	na	na	na	na	na	na	na
F^-	<0.5	<0.5	<0.5	<0.5	<0.5	<0.5	<0.5	<0.5
Cl^-	2.7	3.1	11.1	3.7	14.3	5.6	31.7	37.2
Br^-	<0.5	<0.5	<0.5	<0.5	<0.5	<0.5	<0.5	<0.5
SO_4^{2-}	52.1	65.8	167	136	496	347	522	1748
NO_3^-	<0.5	<0.5	<0.5	<0.5	<0.5	<0.5	<0.5	4.4
HCO_3^-	16.4	58.1	26.3	15.4	26.1	26	33	<0.5
Ba							<0.4	<0.3
Ca							203.7	226.8
Co							<0.1	5.7
Fe							14.3	626.9
Mg							25	113.4
Na							25	16.7
Ni							1.8	20
Sr							2.5	2

All IC and ICP-OES data is corrected for L:S and displayed in [$\mu g/g$].
[a] Porosity calculated by use of wet and dry weight of the meteorite cubes.

The time series experiment (MLT; Table 5.1, 5.4b) showed that even 30 d is at the low end for reaching equilibrium between rock and water, especially for Na^+, K^+ and Cl^- (Table 5.4b). The other species such as Mg^{2+}, Ca^{2+}, and SO_4^{2-} were in equilibrium. Therefore, during the mean experiments (MLO series; table 5.1, 5.4c) the meteorite samples were leached for 48 d. By then, most of the samples showed precipitates and the leaching procedure was stopped. For all meteorites F, Br, Cr, Cu, Co and Zn are below detection (Table 5.4c). Sr and Ba are also mostly below detection. Close to the detection limit are Si, Al, Mn and Ni. The values of Si and Al have to be treated with caution as these elements are known to occur in colloids depending on pH condition. An important element difficult to determine is iron. In meteorites it occurs in its zerovalent state in taenite and kamacite and in ferrous form in troilite and the mafic silicates olivine and pyroxene. During aqueous extraction experiments one might also

leach primary material in addition to the contaminants. Leachates of RaS 295 and RaS 316 showed a greenish precipitation, probably "green rust", i.e. ferrous (mixed with some ferric) iron hydroxides produced during leaching of metallic iron.

Table 5.4.b. Continued.

Label IC Field number	MLT-05a 0603_ 235a	MLT-05b 0603_ 235a	MLT-06a 0603_ 235a	MLT-06b 0603_ 235a	MLT-07a 0603_ 235a	MLT-07b 0603_ 235a	MLT-08a 0603_ 235b	MLT-08b 0603_ 235b	MLT-09 Blank
Leach time [d]	4	4	15	15	30	30	15	15	30
Inital weight (solid, S) [g]	3.96	4.17	5.75	4.5	5.94	5.91	4.89	5.85	
Wet weight [g]	3.98	4.18	5.77	4.52	5.97	5.95	4.91	5.86	
Water (liquid, L) [g]	15.71	15.76	*15.19*	*15.28*	14.7	14.94	*15.23*	*14.86*	
pH	6.53	4.61	6.78	6.45	6.83	6.82	5.08	5.63	6.17
Porosity [%][a]	3.3	3	2.8	3.6	4.1	4	3.1	3	
Na^+	17	12	21	32	104	129	<1	<1	<1
K^+	<1	<1	3	<1	5	6	<1	<1	<1
Mg^{2+}	81	41	29	65	54	41	216	193	<1
Ca^{2+}	242	275	394	623	623	581	258	206	<1
Sr^{2+}	<1	<1	5	9	8	9	<1	<1	<1
NH_4^+	na	na	na	na	na	na	na	na	na
F^-	<0.5	<0.5	<0.5	<0.5	<0.5	<0.5	<0.5	<0.5	<0.5
Cl^-	22.7	25.1	56	70.8	226	209	120	116	<0.5
Br^-	<0.5	<0.5	<0.5	<0.5	<0.5	<0.5	<0.5	<0.5	<0.5
SO_4^{2-}	885	826	990	1670	1735	1500	1355	1037	4
NO_3^-	<0.5	<0.5	4.7	<0.5	<0.5	2.5	<0.5	<0.5	<0.5
HCO_3^-	40.5	9.2	36	28.1	31.3	38.1	12.1	14.8	8.3
Ba	<0.2	<0.1	<0.1	<0.1	<0.1	<0.1	<0.1	<0.1	<0.1
Ca	269.8	291	425.3	641.8	678.1	604.2	289.7	210.8	3.1
Co	0.8	1.5	0.2	<0.1	<0.1	<0.1	0.3	0.1	<0.1
Fe	71.4	60.5	23.8	34	20.8	20.2	68.5	33	3
Mg	119	60.5	42.3	81.5	64.3	50.6	230.5	198.1	2
Na	15.9	15.1	21.1	34	99	126.4	1.9	1.3	0.1
Ni	11.9	22.7	3.4	6.8	4.9	5.1	12.5	7.6	0.6
Sr	1.98	3.4	3.17	10.19	8.91	7.58	0.62	0.25	<0.01

The patterns of relative and absolute ion concentrations in meteorites are quite heterogeneous. The total concentrations range from low levels of 596 µg/g in solid to high levels of 8817 µg/g (Table 5.4c). The Tamdakht meteorite, a fresh fall, yielded a total of 851 µg/g of soluble salts, obviously due to leaching of primary minerals and not due to terrestrials contamination. The reason of taking a fresh meteorite sample was to determine the amount of ions that might be leached out of the meteorite during the experiments in order to obtain values for non-terrestrial correction. Tamdakht yielded indeed the lowest concentrations for Mg^{2+}, SO_4^{2-} and Ca^{2+} that are very abundant in weathered samples. The measured values of Na^+ in Oman meteorites are in the range of 10 µg/g to 485 µg/g with a mean of 48 µg/g (Table 5.4c). From Tamdakht, 151 µg/g were leached. Calcium varies between 11 µg/g and 656 µg/g with a mean of 217 µg/g; here, Tamdakht is among the lowest with 17 µg/g and was relatively high

in Na^+. Magnesium, an abundant element in meteorites, shows strong variations. But it seems that the contribution of Mg^{2+} from artificial weathering during the experiment is minor since Tamdakht yielded with 4 µg/g by far the lowest value. The same is true for the anions SO_4^{2-} (58 µg/g) and Cl^- (8 µg/g), which are low in Tamdakht. These anions can be enriched during weathering and are especially high in SaU 523, a W3 chondrite, where 3367 µg/g Cl^- was analyzed. The sample with the highest total dissolved ions (UaS 011, W3) has 3939 µg/g SO_4^{2-} and 1461 µg/g Mg^{2+}. The elemental pattern shows scatter but a slight trend to either Cl^- or SO_4^{2-} dominated accumulation is observed (Fig. 5.8). Depending on the degree of weathering, the extractions are dominated either by Mg^{2+} or Ca^{2+} with low contents of Na^+ (Fig. 5.8). Oxidation of kamacite and taenite provides some Ni and Co detected in the solutions.
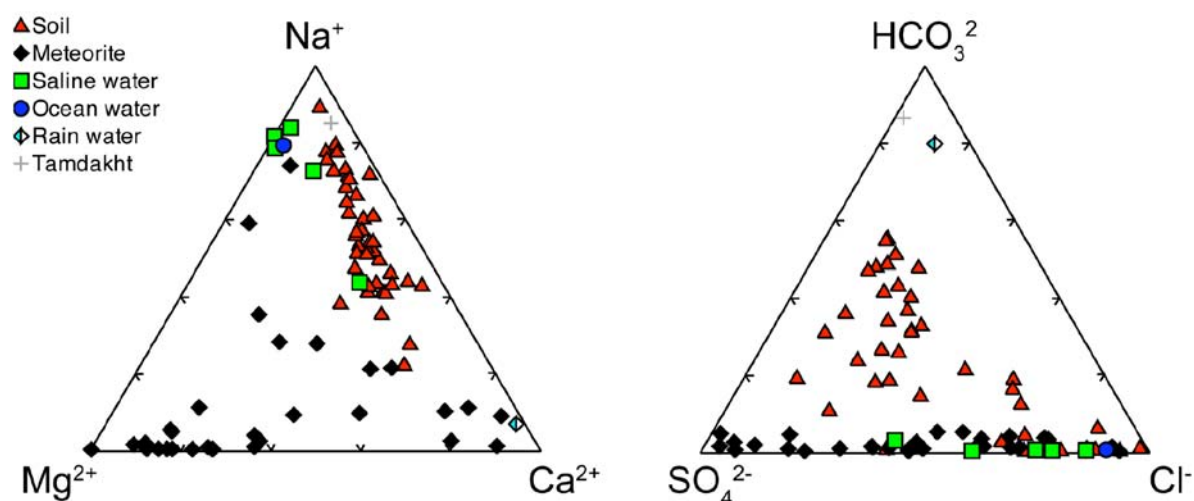
Figure 5.8. Ternary diagrams of the main cations and anions in meq/l. Data from the water extractions of soil- and meteorite-samples and the composition of saline and rain water are from this study. Ocean water values are from Pilson (1998). The saline waters are interpreted as soil salts mobilized by rain water and concentrated through evaporation. The trend for terrestrial samples is from Ca^{2+} to Na^+ and HCO_3^- to Cl^- respectively and is indicated by the soil leachates. Meteorites have distinct salt compositions, dominated by the cations Mg^{2+} and Ca^{2+}. Among the anions either Cl^- or/and SO_4^{2-} are dominant.

Macroscopically the salt contamination is well visible as described in the introduction (Fig. 5.1, 5.2). Samples with hygroscopic behavior (Fig. 5.1, 5.2a, b) are rich in Mg^{2+} and Cl^-, while the extractions of rusty samples (Fig. 5.2d) are dominated by Ca^{2+}, SO_4^{2-} and some Mg^{2+}. Sixteen cut surfaces of L5 chondrites from the JaH 091 strewn field treated with

AgNO$_3$ (Fig. 5.2b, d) showed that hygroscopic salts (Cl$^-$) occur normally at the parts of the meteorites that were not buried into soil during the find situation. According to the visible appearance of weathering with the contamination pattern the influence of type (H or L) is minor. Indeed, the 15 most extreme samples that show similar hygroscopic behavior as in Figure 5.1 are 8 H chondrites and 7 L chondrites, range from petrographic grade 4 to 6 (Van Schmus and Wood, 1967), are shocked from S1 to S5 (Stöffler et al., 1991) and have weathering grades from W2 to W4 (Wlotzka, 1993), dominated by W3. The weights of the sampled meteorite individuals show a wide range from 47.682 g to 8.2 kg and salt efflorescence and hygroscopic behavior was observed in small and big samples. Therefore the size of the meteorites has no influence on salt contamination. The degree of weathering of individual samples can vary within a single meteorite shower (Gnos et al., 2009). In the 15 analyzed samples of the JaH 091 meteorite shower we observe a high variation of absolute and relative concentrations of water-soluble salts. The concentration range of the ML091 series is similar compared to the samples from the MLO series.

During visual inspection of some NWA and Australian OC samples used for another study only minor amounts of possible salt efflorescence were observed. An OC sent for classification to one of us (BAH), reportedly found on a dune in Iran had some efflorescence of rust as seen in typical salt bearing meteorites from Oman (Fig. 5.2c). Climate histories of the three most important hot desert find sites (NWA, Australia and Oman) are similar, from a general view: Present-day hot and dry climate with some intervals of more humid periods in the past, mainly around 10ka before present (Fleitmann and Matter, 2009; Goede et al., 1990; Pachur, 1980). Salt concentrations of desert soils from Sahara are also expected in the same range as in Oman since geology is very similar (cf. Al-Kathiri et al., 2005; Schlüter et al., 2002). The concentration of water-soluble ions in meteorites is not primarily dependent on the concentration of the ions in the soil, but more so on the stage of weathering.

Table 5.4.c. Meteorite leaching experiment results. MLO series, Ordinary chondrites from Oman and Tamdakht.

Label IC	MLO-01	MLO-02	MLO-03	MLO-04	MLO-05	MLO-06	MLO-07	MLO-08
Field number	0901_006	0901_010	0901_022	0901_031	0901_033	0901_055	0902_064	0902_073
Name	UaS 008	UaS 011	RaS 286	RaS 295	RaS 297	JaH 578	JaH 583	Al Huqf 070
N [°]	21.00579	21.37603	20.50789	20.66974	20.66748	19.7642	19.42066	19.18798
E [°]	56.46919	56.29112	55.77546	55.42814	55.31715	56.29889	56.69929	57.10978
Class	L	H	H	H	L	H	H	L
P	6	4	4-5	4	6	6	5	3.7-3.9
S	3	1	1	2	4	2	2	3
WD	4.0	3.0	3.0	3.0	4.5	1.0	4.0	4.0
Leach Time [d]	48	48	48	48	48	48	48	48
Inital weight (solid, S) [g]	3.967	7.072	5.619	5.828	6.229	4.516	6.505	4.61
Wet weight [g]	3.99	7.05	5.66	5.85	6.28	4.53	6.52	4.6
Water (liquid, L) [g]	15.88	14.66	15.27	16.02	15.06	15.62	15.08	15.73
Burial [vol%]	3	0	95	30	40	85	60	0
Mass total [g]	290.271	790.5	4445.2	227.695	706.937	1064.3	1272.547	2632.834
Frag	3	1	>100	1	20	1	20	61
pH	7.07	5.88	3.84	4.66	7.03	4.62	5.29	5.41
Porosity [%]^a	3.3	3.3	3.8	3.2	4.2	1.3	2.1	2.2
Na^+	76	162	210	485	75	*30*	33	*26*
K^+	<1	<1	*11*	*12*	8	<1	8	<1
Mg^{2+}	*39*	1461	175	156	*19*	*21*	98	392
Ca^{2+}	484	473	184	43	656	*15*	131	383
Sr^{2+}	<1	<1	<1	<1	27	<1	<1	<1
NH_4^+	n.a.	n.a.	n.a.	n.a.	n.a.	n.a.	n.a.	n.a.
F^-	<0.5	<0.5	*4.6*	*4.8*	<0.5	*5.9*	<0.5	<0.5
Cl^-	174	2498	841	1279	79	401	261	384
Br^-	<0.5	<0.5	<0.5	<0.5	<0.5	<0.5	<0.5	<0.5
SO_4^{2-}	1051	3939	1318	1091	1610	219	574	2188
NO_3^-	27.9	<0.5	<0.5	<0.5	<0.5	<0.5	<0.5	<0.5
HCO_3^-	73.3	21.5	<0.5	3.4	51.6	8.4	11.3	20.8
Al	1	0.4	0.7	0.7	0.9	0.8	0.5	0.6
Ba	<0.02	<0.02	<0.02	<0.02	0.1	<0.02	<0.02	<0.02
Ca	n.a.	n.a.	n.a.	n.a.	n.a.	n.a.	n.a.	n.a.
Co	<0.05	4.4	2.3	5	<0.05	1.9	1.1	2.8
Fe	19.5	73.4	782.7	1061	24.4	553.4	126.8	117.7
Mg	n.a.	n.a.	n.a.	n.a.	n.a.	n.a.	n.a.	n.a.
Mn	<0.05	13.5	0.8	1.2	0.2	0.4	1.8	6.6
Na	n.a.	n.a.	n.a.	n.a.	n.a.	n.a.	n.a.	n.a.
Ni	1.4	141.4	22.5	66	1.3	13.3	38.7	97.2
Si	37.7	24.5	16.2	16.8	40.1	16	14.8	35.5
Sr	8.7	4.6	2.6	<0.01	21.7	<0.01	1.5	1.8

All IC and ICP-OES data is corrected for L:S and displayed in [µg/g]; All samples were leached for 48 d.
P: Petrologic type, S: Shock, WD: Weathering degree.
^{a} Porosity calculated by use of wet and dry weight of the meteorite cubes.
Italic below calibration limit, **Bold** above calibration limit.
<: Below detection limit.
n.a.: not analyzed.

Table 5.4.c. Continued.

Label IC	MLO-09	MLO-10	MLO-11	MLO-12	MLO-13	MLO-14	MLO-15	MLO-16	MLO-17
Field number	0902_098	0902_125	0902_146	1001_012	1001_030	1001_071	1002_125	Tamdakht	Blank
Name	Shalim 008	RaS 316	SaU 523	Al Huwaysah 012	UaS 023	RaS 361	RaS 397	Tamdakht	Blank
N [°]	18.86795	20.89485	20.41533	22.67752	21.1427	20.48139	20.1465	31.16333	
E [°]	55.45073	55.50613	56.6655	55.34026	55.53912	55.59514	55.70913	-7.015	
Class	H	L	L	H	L	L	L	H	
P	5	5	6	5	6	5	6	5	
S	3	3	4	1	4	3	5	3	
WD	2.0	4.5	3.3	4.0	2.0	3.3	4.0	0.0	
Leach time [d]	48	48	48	48	48	48	48	48	48
Inital weight (solid, S) [g]	6.33	4.615	5.614	6.464	5.686	5.379	5.215	7.17	
Wet weight [g]	6.35	4.66	5.6	6.51	5.7	5.39	5.24	7.24	
Water (liquid, L) [g]	15.08	15.64	15.54	15.28	15.32	15.25	15.6	14.96	
Burial [vol%]	50		20		10	25			
Mass total [g]	323.489	2706.034	265.209	4694.9	144.383	229.648	1118.758		
Frag	1	>1000	1	1125	1	2	273		
pH	6.63	7.03	4.39	7.03	5.13	4.93	7.01	10.21	5.94
Porosity [%][a]	2	2.8	2.4	4	1.7	1.9	3.8	4.3	
Na^+	124	38	*10*	91	*16*	155	185	152	*3*
K^+	<1	*12*	<1	*13*	<1	<1	*22*	*14*	<1
Mg^{2+}	*17*	*33*	659	181	*11*	107	104	*4*	<1
Ca^{2+}	*11*	251	380	462	35	180	432	*18*	5
Sr^{2+}	<1	<1	<1	<1	<1	<1	58	<1	<1
NH_4^+	n.a.	n.a.	n.a.	n.a.	n.a.	n.a.	n.a.	n.a.	
F^-	*3.9*	<0.5	*4.8*	<0.5	<0.5	<0.5	<0.5	*7.1*	<0.5
Cl^-	128	11	3367	866	95	327	809	*8*	*1*
Br^-	<0.5	<0.5	<0.5	<0.5	<0.5	<0.5	<0.5	<0.5	<0.5
SO_4^{2-}	154	703	742	687	139	994	669	58	<0.5
NO_3^-	<0.5	<0.5	<0.5	**121**	<0.5	<0.5	53.4	*7.8*	<0.5
HCO_3^-	21.8	43.4	5.1	79.3	8.2	12.1	36.5	532.2	<0.5
Al	1	2.9	0.9	0.9	0.8	1	1.3	1	<0.05
Ba	<0.02	<0.02	<0.02	0.1	<0.02	<0.02	0.1	<0.02	<0.02
Ca	n.a.	n.a.	n.a.	n.a.	n.a.	n.a.	n.a.	n.a.	n.a.
Co	1.9	<0.05	2.9	<0.05	1.5	2.1	<0.05	<0.05	<0.05
Fe	421.7	67.4	1312.1	23.6	253.3	323.2	34.4	11.4	<0.05
Mg	n.a.	n.a.	n.a.	n.a.	n.a.	n.a.	n.a.	n.a.	n.a.
Mn	0.2	0.5	7.6	0.3	0.2	0.7	0.3	0.1	<0.05
Na	n.a.	n.a.	n.a.	n.a.	n.a.	n.a.	n.a.	n.a.	n.a.
Ni	23	5.6	10.2	1.7	17.4	28.9	1.8	0.3	<0.05
Si	13.9	71.5	26	38.8	17.9	22.5	47	38.2	<0.3
Sr	<0.01	4.5	5.3	19.5	0.3	3.6	28.5	<0.01	<0.01

5.3.4. Mineralogy of pore fillings

A wide variety of secondary minerals formed in pore space of weathered meteorites are known. Minerals found in meteorites from Oman during this study are compiled in Table 5.5. The secondary minerals can be classified as contamination minerals (main element source from outside the meteorite) and alteration minerals (main element source are primary meteorite minerals). Some of the secondary minerals are typical alteration products of iron metal or troilite whereas others are salts from evaporation of brines. The most abundant phases, besides iron hydroxides and iron oxides, are Ca-sulfates (most important is gypsum) and calcite, which normally occur as relatively pure phases (Table 5.5). Carbonates may contain a few wt% of Sr, Mg or Fe. Ca-sulfates typically occupy pore spaces whereas calcite mostly forms veins penetrating the meteorite specimen. Iron- oxides and -hydroxides occupy the pore space as intimate mixtures of different phases, typically associated with gypsum. They often show some Si content or visible inclusions of opal or quartz. Magnesium salts are also abundant and often visible by naked eye. The most dominant phases are Mg-sulfates such as epsomite, $MgSO_4 * 7H_2O$, and kieserite, $MgSO_4 * H_2O$, that tend to efflorescence on the meteorite surfaces or in the pore space (Fig. 5.9a). Additional identified minerals in pore space are magnesite, celestine and barite. Jarosite, $(K,Na)Fe_3(SO_4)_2(OH)_6$, was observed in a few samples, mostly in cleavages of weathered troilites (Fig. 5.9b). Some jarosite occurs also in vein fillings (Fig. 5.9c) or in pore space (Fig. 5.9d).

Most contamination minerals are easily dissolved in water and do not survive water-assisted thin section preparation. Due to its deliquescent behavior the presence of bischofite as crystalline phase could not be verified. However, semi quantitative analysis of brine droplets removed from "sweating meteorites" (Fig. 5.1) yielded Mg/Cl ratios known from bischofite. Iron chloride with traces of Ni is also part of the suite of salts identified in dried brine droplets. A dried iron hydroxide rich residue of brine from meteorite Dhofar 1010, analyzed by XRD, yielded akaganéite as main phase, similar to observations by Buchwald and Clarke (1989). Halite was not observed within the studied meteorites.

Table 5.5. Secondary minerals in OCs from Oman.

Mineral	Chemical composition	RLM	TLM	SEM (EDS)	Raman	XRD	EMP
Akaganéite	$\beta\text{-}[Fe^{(III)}{}_7Ni][O, OH]_{16}(Cl, H)_{<2}$	x				x	
Anhydrite	$CaSO_4$		x	x		x	
Ankerite	$Ca(Fe, Mg)(CO_3)_2$					x	
Aragonite	$CaCO_3$			x		x	
Barite	$BaSO_4$			x			
Bassanite	$CaSO_4{*}0.5H_2O$			x	x		
"Bischofite"[a]	$MgCl_2{*}6H_2O$			x			
Calcite	$CaCO_3$		x	x			
Celestine	$SrSO_4$			x			
Dolomite	$CaMg(CO_3)_2$		x	x			
Ferrihydrite	$Fe^{(III)}{}_2O_3{*}0.5(H_2O)$			x			
Epsomite	$MgSO_4{*}7H_2O$			x			
Goethite	$a\text{-}Fe^{(III)}O(OH)$	x	x	x	x	x	
Gypsum	$CaSO_4{*}H_2O$		x	x			
Hematite	$a\text{-}Fe^{(III)}{}_2O_3$	x		x		x	
Hexahydrite	$MgSO_4{*}6H_2O$					x	
Jarosite	$KFe^{(III)}{}_3(SO_4)_2(OH)_6$			x		x	
Kieserite	$MgSO_4{*}H_2O$			x		x	
"Lawrencite"[b]	$(Fe^{(II)},Ni)Cl_2$			x			
Lepidocrocite	$g\text{-}Fe^{(III)}O(OH)$	x		x	x		
Maghemite	$g\text{-}Fe^{(III)}{}_2O_3$	x		x			
Magnesite	$MgCO_3$			x			
Magnetite	$Fe^{(II)}Fe^{(III)}{}_2O_4$	x		x			x
Natrojarosite	$NaFe^{(III)}{}_3(SO_4)_2(OH)_6$			x			
Nepouite	$Ni_3Si_2O_5(OH_4)$			x		x	
Nickel-bischofite	$NiCl_2{*}6H_2O$			x			
Opal	$SiO_2{*}xH_2O$		x	x			
Pecoraite	$Ni_3Si_2O_5(OH_4)$			x		x	
Quartz/Chalcedony	SiO_2		x	x			
Sulfur	S					x	
Unspecified iron sulfate	$FeSO_4({*}XH_2O)$			x			

RFL: Reflected light microscopy.
TLM: Transmitted light microscopy.
SEM: Scanning electron microscopy by use of EDS analysis for qualitative and semi quantitative element abundances.
Raman: Raman spectroscopy.
XRD: Powder X-ray diffraction.
EMP: Electron microprobe analsysis.
EMP: Electron microprobe analsysis.
a Bischofite was not found as crystalline material.
b Lawrencite is not considered as a true mineral.
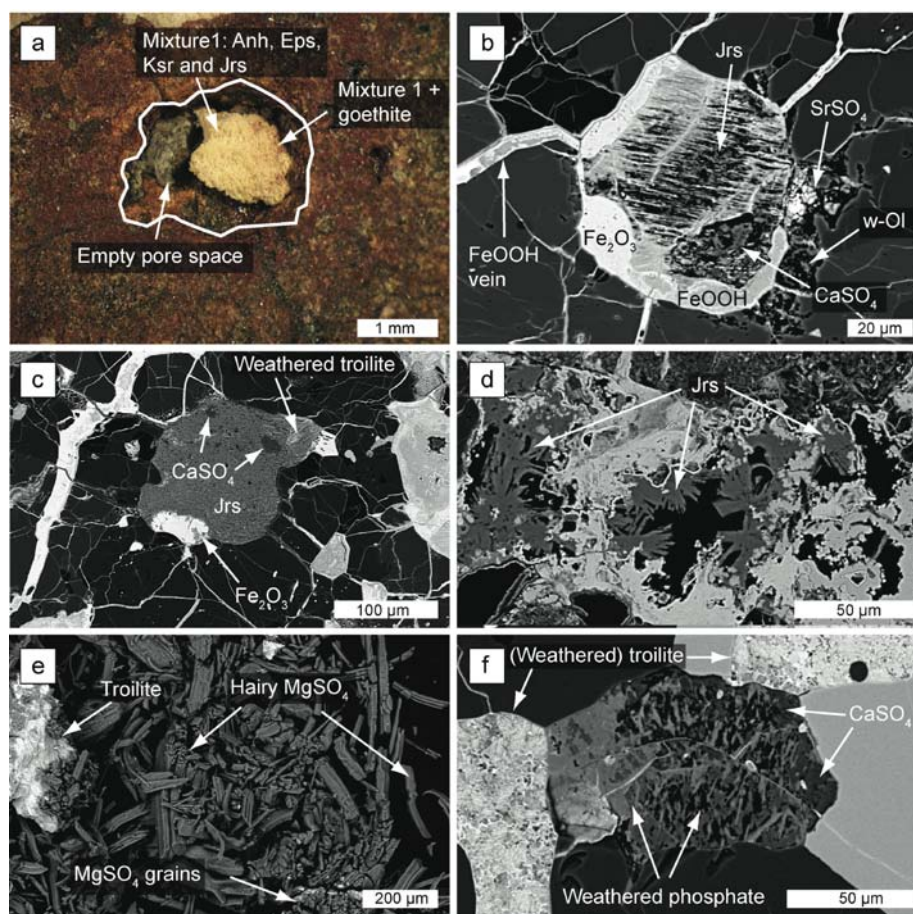
Figure 5.9. *Pore space fillings. a) Macroscopic view of a large partly filled pore in ordinary chondrites (OC) JaH 478. The whitish-yellowish area is a mixture of anhydrite (Anh), epsomite (Eps), kieserite (Ksr) and jarosite (Jrs). At the border of the pore filling some additional goethite causes rusty staining. Scale bar is 1 mm. b) BSE image of a weathered troilite grain in RaS 408. Most of the troilite is replaced by iron hydroxide (FeOOH). The iron oxides (Fe_2O_3) to the left might be from a former metal grain. Some of the mobilized iron is transported away to build up veins of iron oxides and iron hydroxides. Troilite is weathering along (001) twinning plains and, at latest stages of weathering, produces new pore space that is filled with Ca-sulfate and jarosite in this case. Terrestrial celestine ($SrSO_4$) precipitated in the neighborhood. The olivine grain to the right is slightly attacked (w-Ol). Scale bar is 20 μm. c) BSE image of a completely filled pore in RaS 408. The majority of the pore filling is jarosite (Jrs), which also produced veins that crack iron oxide veins. Close to a weathered troilite grain sparse Ca-sulfate occurs. Scale bar is 100 μm. d) BSE image of a weathered metal grain with jarosite efflorescence in RaS 395. Scale bar is 50 μm. e) BSE image of crystals gained from white salt efflorescence of a cut surface of an OC found in 2011 (1101_053). The minerals visible are Mg-sulfates with traces of Na, Cl and Ni occurring as hairy minerals and aggregates of small grains. The bright mineral at the left is troilite with attached silicate material that was accidentally picked. Scale bar is 200 μm. f) BSE image of a weathered phosphate grain in a JaH 091 sample (0703_335). The bright mineral in the neighborhood is partially weathered troilite. Some of the leached Ca^{2+} from the Ca-phosphate might have combined with sulfur released from troilite to form Ca-sulfate. A part of the Ca-phosphate is replaced by Fe-phosphate. Scale bar is 50 μm.*

5.4. DISCUSSION

5.4.1. Meteorite and soil temperature

In hot deserts extreme temperatures can occur. For example, in Sahara air temperature vary between -7°C and 57°C (Cooke and Warren, 1973) and sand surface temperatures can reach up to 83°C (Petrov, 1976). Air temperatures in Arabia are in summer commonly above 50°C with monthly averages of 41 to 42°C (Edgell, 2006). Black objects are usually hotter than surrounding sand as surface temperature measurements on black basalts (Walther, 1900), or on asphalt in Al Ain (UAE, close to Oman, 73°C) (McGreevy and Smith, 1982; Potocki, 1978) showed. Our maximum temperature measured inside the meteorite was 66.3°C, which is ~15°C hotter than air temperature. Maximal ΔT observed during a day is 46.5°C while the median ΔT per day is 34.3°C. These temperatures and their daily fluctuations have an influence on physical and chemical weathering. Due to different thermal conductivities (Yomogida and Matsui, 1983) and different volume expansions of the meteoritic minerals the diurnal temperature variations weakens the rocks physically (e.g. Gomez-Heras et al., 2006) and salts can be introduced into the meteorite. Freeze thaw cycles that are critical to rock disintegration (Ruedrich et al., 2011) were not observed during our temperature recording period but can occur during cold winter nights (Edgell, 2006). Due to the elevated temperatures chemical potential is higher and reactions are accelerated resulting in faster chemical weathering as compared to Antarctica. The observed temperature gradient between the dark meteorite and the soil is important for the evaporitic pumping of water through the meteorite.

Implications of temperature variations for potential microbial processes are discussed in chapter 5.4.10.

5.4.2. Source of the ions

The concentration of primary water-soluble salts is generally very low in freshly fallen ordinary chondrites (OC). This is in agreement with the low concentrations of dissolved ions observed in leaching experiments of Bensour (Lee et al., 2006) and Tamdakht (this study).

Most of the ions from these samples are likely dissolved due to weathering reactions (hydrolysis) of the relatively stable silicates and not due to primary water-soluble minerals (salts). Primary halite was detected in two meteorite falls that curiously occurred both in 1998 (Rubin et al., 2002). One is Monahans, a H5 chondrite fall in Texas (Grossman, 1998; Zolensky et al., 1999) and the other is Zag, a H3-6 regolith breccia fall in in Western Sahara (Grossman, 1999). Several arguments support a pre-terrestrial origin of the halite and sylvite grains in these meteorites: (1) these are falls that were recovered very soon after the fall events, (2) in both meteorites salt minerals are widely distributed in the matrix, (3) most of the halite grains are dark blue due to ionizing radiation, probably from solar and galactic cosmic rays and (4) the formation ages of halite obtained with Ar-Ar, Rb-Sr and I/Xe systematics yielded ages older than extant terrestrial rocks (Bogard et al., 2001; Rubin et al., 2002; Whitby et al., 2000; Zolensky et al., 1999). Nevertheless, the salt minerals in these two meteorites seem to be unique. Several studies determined the chlorine abundances in falls and obtained variable results. Garrison et al., (2000) calculated elemental chlorine concentrations of 132 samples from 94 meteorites (most of them finds, including some from Antarctica) using the nuclear reaction of ^{37}Cl (n,γ) ^{38}Ar achieved during neutron irradiation of meteorites. For ordinary chondrites they found 15 µg/g to 177 µg/g of chlorine. This is in partial agreement with 13 analyses of OCs by combustion ion chromatography of Tarter et al., (1980) yielding 9 µg/g to 345 µg/g of chlorine. Most of the studied samples were falls but no systematic enrichment of Cl in finds was observed. About 15 to 79 % of total Cl was water-soluble. This indicates the presence of a soluble Cl^--bearing phase (Tarter et al., 1980). Another explanation for the variation in the chlorine content, especially for the finds is sample contamination by Cl^- during handling (Garrison et al., 2000). During leaching experiments of Zag samples, a Cl^- excess relative to Na^+ was observed indicating the presence of another phase delivering Cl^-. The only other Cl^- bearing phase in Zag is chlorapatite that is why this mineral has to be dissolved during the water extraction (Bridges et al., 2004). The consensus of all these studies is the concentration of Cl^- in OCs is variable and ranges between 9 µg/g to 350 µg/g. We observed in our samples from Oman a range of 10.8 µg/g to 3367 µg/g with one outlier at 6036 µg/g. Most of the Oman samples are significantly higher than 177 µg/g, the upper limit of the Cl^- concentrations postulated by Garrison et al. (2000). The average Cl^- concentration of the MLO series is 721 µg/g and the median 356 µg/g. Such elevated Cl^- concentrations are for sure the result of terrestrial contamination. The soil where

the meteorites stayed hundreds to several ten thousand of years contains halite that can be transported into the meteorite and be accumulated. Sources for the halite in the soil are the weathered bedrock, saline layers in-between bedrock, evaporation of groundwater bringing salts from depth and wind-transported salt from sabkhat or sea spray (Chapman, 1980). Systematic studies of the halogen content in meteorite finds from Antarctica proves contamination of OC with terrestrial F^-, Cl^-, I^- and Br^-. The analyzed depth profiles of Antarctic H5 chondrites were enriched towards the meteorite surface with Cl^- whereas the analyzed meteorite falls Allende (CV3) and Holbrook (L6), had constant Cl^- concentrations (Langenauer and Krähenbühl, 1993a). The Cl^- contamination in Antarctic meteorites is slightly influenced by the location of recovery. Ice masses closer to the coast show higher Cl^- concentrations due to halogens transported inland by sea spray (Langenauer and Krähenbühl, 1993b). In contrast to Antarctic meteorites samples from Oman show a larger scatter in Cl^- and the contamination occurs in the interior of the samples and normally not in direct contact with the meteorite surface (Fig. 5.2c). This is in agreement with Cl^- depth profiles measured in three H5 chondrite finds from Western Australia (Krähenbühl and Langenauer, 1995). Their contamination patterns are random with lower values towards the meteorite surface. The measured maximum concentrations were 262 µg/g, 503 µg/g and 1528 µg/g. Also the minimal values are systematically higher than the results from analyses of meteorite falls. Therefore, contamination of hot desert meteorites with Cl^- is common.

The source of the measured Na and K contents could be due to the leaching of primary halite or sylvite, but they might also be from the desert soil. An alternative source could be meteoritic feldspar susceptible to weathering (Lee et al., 2006).

The interpretation of the origin of magnesium seems simpler. Extracts from the soil are low in Mg^{2+} whereas meteorites show high concentrations. Due to the fact that ordinary chondrites are composed of 50% to 75% of the Mg-rich minerals olivine and orthopyroxene (Dunn et al., 2010; Mason, 1965) which are relatively susceptible to weathering it is assumed that most of the detected Mg^{2+} is meteoritic in origin. As support we take white salts on Antarctic meteorites that were determined as Mg-carbonates with Na/Mg, K/Mg and Ca/Mg values closer to chondrites than Sea Water indicating a meteoritic origin (Velbel et al., 1991).

Less clear is the situation for calcium. It is abundant in the soil material (e.g. calcite, gypsum), rain water and also in meteorites (feldspar, Ca-rich pyroxenes and Ca-phosphates). But since the soil minerals are much richer in Ca and the meteoritic Ca-minerals are relatively

resistant against weathering, the majority of the analyzed Ca^{2+} likely has been transported from the soil into the meteorite. A similar behavior is evident for strontium. It is introduced in the meteorites and precipitates as celestine, a highly insoluble mineral, which accumulates over time.

The carbonate ions from the observed calcite within the meteorites are very unlikely to be derived from the meteorites itself because their carbon phases are highly resistant to oxidation (Abreu and Brearley, 2005). On the other hand, in a terrestrial environment, CO_2 is easily available from the atmosphere and from the soil in contact with the meteorite.

The source of sulfur in salt phases is the most difficult is to determine. A significant proportion is mobilized during weathering of troilite from the meteorite but occurs also in the soil. The sulfate found the in pore space could have a combined origin from the soil and the meteorite. In the vicinity of a weathered Ca-phosphate and a partly altered troilite an alteration assemblage of Ca-sulfate, Fe-phosphate and iron hydroxides was observed (Fig. 5.9f), which might be the result of spatial limited ion redistribution within the meteorite. However, contamination of hot desert meteorites by Ca-, Sr- and Ba-sulfates is common and occurs also in troilite poor meteorites such as lunar and martian meteorites (e.g. Crozaz and Wadhwa, 2001; Nazarov et al., 2004). Therefore, the major part of the sulfate within meteorites might be from the desert environment.

5.4.3. Mass balance

To interpret the relative abundance patterns of the water-soluble ions in the meteorites a mass balance approach was applied. The concentrations of water-soluble ions of the 15 Oman meteorites from the MLO series were converted to mmol/g of the meteorite. Then ions in proportions corresponding to the common salt minerals and hydrolysis reactions were subtracted in seven steps (Table 5.6a). After the mass balance the median values of the contribution of each constituents were calculated for the weathering grades $W \leq 2$, $W = 3$ and $W \geq 4$ (Table 5.6a). Step 1: Subtraction of NaCl. It is assumed that all Cl^- analyzed derived from the soil since OC falls generally have negligible concentrations as shown in the Tamdakht meteorite. In addition, primary halite could be leached out during early stage of weathering. Based on the analyzed soil extracts, we assume that chloride introduced into

meteorites was initially accompanied by Na and K with a molar Cl:Na:K ratio of 100:93:7. After subtraction of all Cl^- and corresponding amounts of Na and K, a negative balance for Na^+ results in 8 of 15 weathered meteorites. Extreme negative balance is found in samples of W=3 (Table 5.6b, see below). Step 2: Subtraction of the contribution from weathering of meteoritic feldspar. For this simplified mass balance approach it was assumed that all of the aluminum measured in the extracts is derived from feldspar since it is the only major Al-bearing mineral and artificial weathering experiments showed it is attacked (Lee et al., 2006).

Table 5.6.a. Mass balance results: Contribution during weathering.

Step	"Mineral"	Used formula	Derived from	W≤2	W=3	W≥4
1	Halite	$Na_{0.93}K_{0.07}Cl$	Cl^-	3.60	36.08	7.38
2	Feldspar	$Na_{0.10}K_{0.06}Ca_{0.84}Si_{2.16}Al_{1.84}O_8$	Al	0.03	0.03	0.04
3	Calcite	$CaCO_3$	HCO_3^-	0.14	0.14	0.71
4	Ca-sulfate	$CaSO_4$	Ca^{2+}	0.47	4.58	10.15
5	Olivine	$Fe_{0.2}Mg_{0.8}SiO_4$	Mg^{2+}	0.56	5.77	3.23
6	Metal	$Fe_{15}Ni$	Ni	4.44	7.39	0.47
7	Troilite	FeS	SO_4^{2-}	1.70	9.75	1.83

Number of samples: for W≤2 n=4, for W=3 n=5 and for W≥4 n=7.
Median values based on ion concentration in [mmol/g].

Table 5.6.b. Mass balance results: Balance.

Element	W≤2	W=3	W≥4	Explanation
Na^+	-1.79	-12.68	-5.42	Precipitation as jarosite? or lost as Na-sulfate?
K^+	-0.25	-1.38	-0.53	Precipitation of jarosite?
Fe	1.50	-1.09	-0.92	Precipitation of ironhydroxides
Si	-0.43	-7.98	-3.76	Precipitation of chalcedony
Balance	-0.97	-23.13	-10.63	Negative balance due to Na^+, Fe and Si underabundance.

All values in [mmol/g].

For the mass balance approach feldspar composition of $(Na_{0.10}K_{0.06}Ca_{0.84})(Si_{2.16}Al_{1.84})O_8$ was subtracted until Al reached a value of zero. Another Al-bearing mineral in OC would be chromite that is extremely resistant against weathering since it is preserved in fossil meteorites where all other minerals have been altered or replaced (Schmitz and Haggstrom, 2006; Thorslund et al., 1984). Step 3: All the measured alkalinity is interpreted to be derived from calcite dissolution, a contaminant from the environment. In this step pure calcite with the building blocks $1Ca^{2+}$ and $1HCO_3^-$ was removed in the mass balance approach. Its contribution is relatively small. Step 4: The residual Ca^{2+} is thought to be from terrestrial Ca-sulfates, which have precipitated in pore space as gypsum or anhydrite. Therefore, $Ca_1(SO_4)_1$ was removed in the mass balance. Besides feldspar, calcite and Ca-sulfate there might be additional sources for Ca^{2+} like Ca-rich pyroxenes or Ca-phosphates. But since these are minor minerals with their contribution was ignored. Calcium-phosphates are usually highly

weathered in finds from Oman (Fig. 5.9f) but their modal occurrence is typically <1% (Mason, 1965). The contamination with Ca-sulfates increases over weathering history. Step 5: All Mg^{2+} is supposed to be derived from the weathering of the meteorite. For simplicity, all magnesium was assumed to result from hydrolysis of olivine with an average composition of $(Fe_{0.2}Mg_{0.8})Si_1O_4$. Pyroxene hydrolysis was ignored, as olivine seems to be preferentially weathered as seen in thin section (Fig. 5.10).
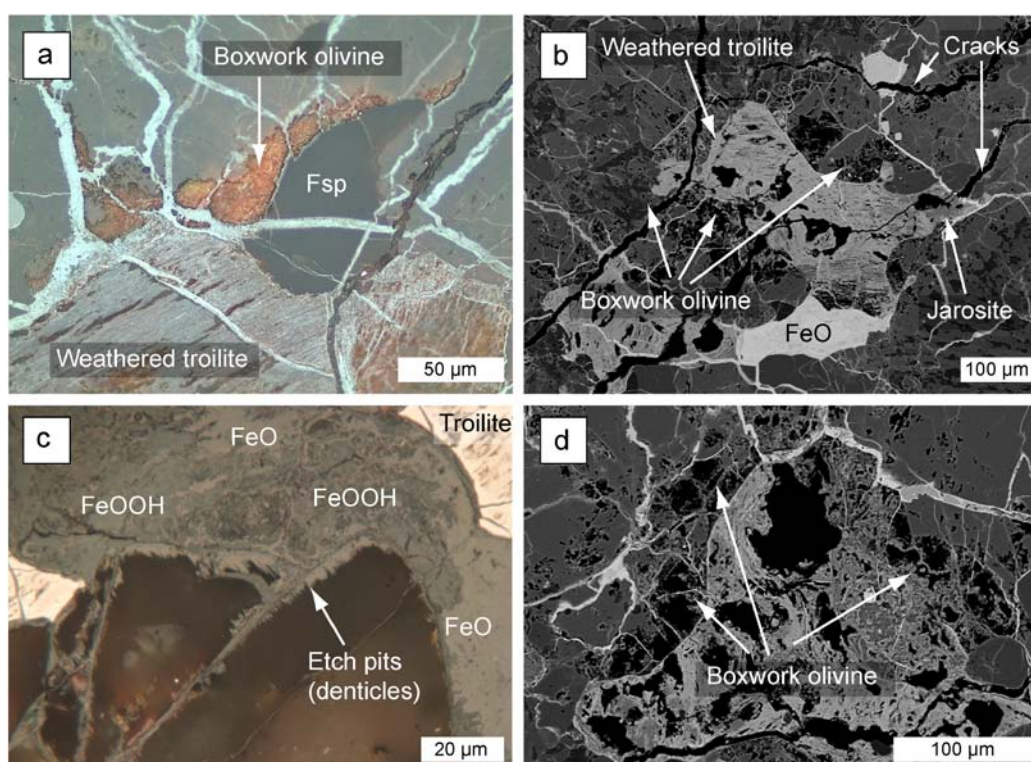
Figure 5.10. *Petrographical indications of leaching of meteoritic minerals. a) Reflected light (RFL) image of RaS 397. In vicinity of a weathered troilite olivine grains are attacked in boxwork style and iron hydroxides are produced. A feldspar grain (Fsp) is not attacked at all; only some fractures are filled with iron hydroxides. Scale bar is 50 µm. b) BSE image of RaS 316. This W4 chondrite is highly friable and is cross cut by several cracks. Olivines surrounding the weathered troilite are leached in boxwork style, producing new pore space. Troilite is altered to iron hydroxides and partly replaced by natrojarosite. A former metal grain is replaced by iron oxide (Fe_2O_3). Pyroxenes (dark grey) and feldspars (darkest grey) show no or only minor leaching. Scale bar is 100 µm. c) RFL image (oil immersion) of a JaH 091 sample (0603-249). A mafic silicate grain next to a mixture of iron oxides and iron hydroxides shows etch pits. The mineral with bright reflections is a partly altered troilite. Scale bar is 20 µm. d) BSE image of a weathered metal and troilite grain in RaS 316. Note the leached parts in the surrounding olivine. Scale bar is 100 µm.*

Step 6: Based on the measured Ni concentration the contribution derived from dissolution of metallic iron was subtracted. A metal composition of $Fe_{15}Ni_1$ was used. Step 7 at last, using the remaining excess of SO_4^{2-} the contribution of troilite (Fe_1S_1) oxidation was calculated. The results of these mass balance calculations are listed in Table 5.6a and illustrated in Figure 5.11. Table 5.6b shows the residuals. If we assume all Cl^- found in the meteorites was introduced as NaCl in proportions as it is present in the soil we have a strong deficit in Na^+ and to some extent K^+. The samples that are rich in Cl^- and show hygroscopic behavior are usually most depleted in Na^+. This issue is discussed later (5.4.7.). Also Si should have been detected in higher concentrations in the leachates; especially at W=3. But it is possible that silica mobilized by the weathering of the silicates precipitated as stable chalcedony and was not dissolved completely during the leaching procedure. In addition, Si could have built colloids together with Al, what would also have an influence on the estimated contribution of feldspar. Iron was measured in too high concentrations at W≤2, which could be due to artificial weathering during the leaching experiments. The slight under abundance of iron at W≥3 might be due to the precipitation of insoluble iron (oxi)hydroxides.

Figure 5.11. *Contribution of the most important ions represented as "minerals" of which proportion the ions occur during weathering history. Contamination constituents are to the left, while the contribution of weathering of meteoritic material is to the right. Contamination is over the whole history important and increases in general with weathering degree. Most ions are liberated from the meteorite during W=3.*
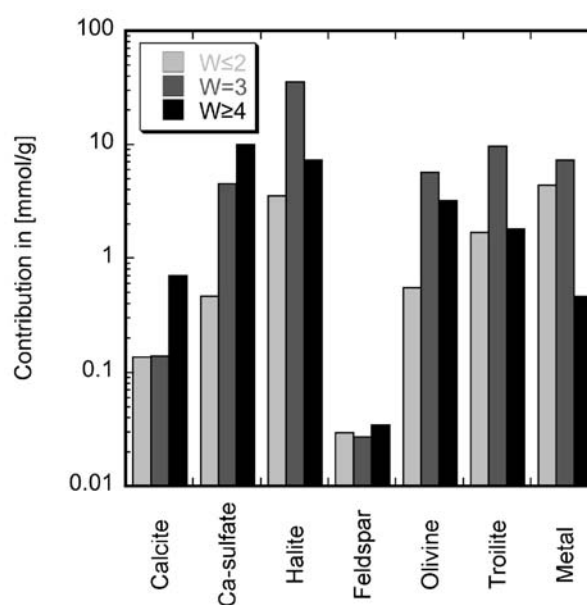
The input of terrestrial contaminants is significant and generally dominates over the ions mobilized from the meteorite by weathering (Table 5.6a, Fig. 5.11). Especially the input of Cl^- is highest during the W=3 stage. At the first stages of weathering (W≤2), weathering of metal and to a lesser degree of troilite are the main processes (e.g. Al-Kathiri et al., 2005). Contamination is present but minor. Weathering grade 3 is the most active part of weathering history. At this stage metal

and troilite oxidation are the dominant processes, but also olivine is attacked and a significant amount of ions are introduced from outside. At the latest stage of weathering (W≥4) the remaining troilite and metal is oxidized and olivine is leached. Contamination by Ca-sulfates gains importance and dominates the contamination. Weathering of feldspar is negligible and seems to be constant over the whole weathering history.

5.4.4. Weathering reactions

In this section we try to link the data of the water-soluble salts with the observed and/or inferred weathering reactions:

(i) The alteration of metal (kamacite, taenite) is always a multistage process including oxidation of zero-valent iron to mobile ferrous and finally ferric iron that mostly precipitates irreversibly as iron oxides or iron hydroxides (Buchwald and Clarke, 1989). Ferrous iron can be transported within the meteorites and even reach the meteorite surface where this effect often produces rusty encrustations, commonly incorporating sand grains. Within the meteorites a network of complex iron-oxides and iron-hydroxides is forming. As learned from thin sections studies of OCs from Oman, metal grains are first altered to fine grained iron hydroxides followed by iron oxides such as magnetite and maghemite at a later stage. Hematite occurs only rarely. Taking this into account we can write the following weathering reactions for the oxidation of iron:

$$3Fe^{0} + 2O_2 \rightarrow Fe^{II}Fe^{III}_2O_4 \qquad \text{(eq. 5.1)}$$

$$3Fe^{0} + H_2O \rightarrow Fe^{II}Fe^{III}_2O_4 + 4H_2 \qquad \text{(eq. 5.2)}$$

$$4Fe^{0} + 3O_2 \rightarrow 2Fe_2O_3 \qquad \text{(eq. 5.3)}$$

$$2Fe^{0} + 3H_2O \rightarrow Fe^{III}_2O_3 + 3H_2 \qquad \text{(eq. 5.4)}$$

$$4Fe^{0} + 2H_2O + 3O_2 \rightarrow 4\,Fe^{III}OOH \qquad \text{(eq. 5.5)}$$
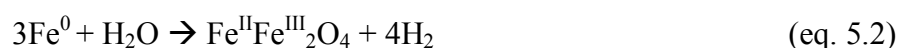
(ii) Weathering of troilite also starts with the oxidation of iron and sulfur and ends normally with the precipitation of iron-hydroxides. Sulfur can be mobile or precipitate as sulfate mineral. The reaction is best described as:

$$4FeS + 6H_2O + 9O_2 \rightarrow 4Fe^{III}OOH + 4SO_4^{2-} + 8H^+ \quad \text{(Hofmann et al., 2000)} \quad \text{(eq. 5.6)}$$
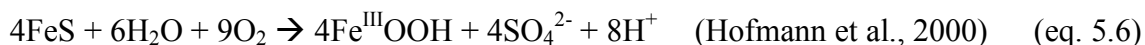
It is important to note that protons are produced by this reaction, lowering the pH, similar to pyrite oxidation in acid mine waste (e.g. Nordstrom, 2011). We measured pH values of 4 to 7 in meteorite leachates; most samples of the W3 were at pH 4. This might be an explanation why no serpentine is observed in weathered meteorites while in the nearby Oman Mountains forsterites of similar composition in ophiolitic rocks are altered to serpentine. In experimental weathering of enstatites no serpentinisation was observed at pH below 6 (Ohnishi and Tomeoka, 2007).

(iii) The weathering of mafic silicates (olivine and pyroxene treated together) is dominated by hydrolysis, here the example for forsterite:

$$Mg_2SiO_4 + 4H^+ \rightarrow 2Mg^{2+} + SiO_2 + 2H_2O \qquad \text{(eq. 5.7)}$$
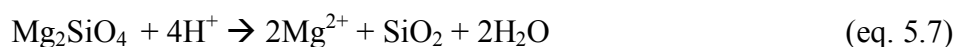
This reaction is important since it consumes protons. Weathering of troilite produces enough protons at W3 that are needed for dissolution of Mg^{2+} from olivine as calculated from the mass balance approach (Table 5.6a). We take higher degrees of weathering of olivines around altered troilites as support for this scenario (Figs. 5. 9b, 5.10a, b, c, d). The liberated Mg^{2+} forms together with Cl^- a hygroscopic brine that causes the "sweating" effect.

Weathering of the fayalitic part of the olivine is a multistage process, similar to the oxidation of troilite (Bland et al., 2006). The final, stable phase are iron-hydroxides, often with minor but significant amounts of silicon, as demonstrated by our EDS analyses and earlier work (e.g. Lee and Bland, 2004). Therefore we write the weathering equation as follows:

$$2Fe_2SiO_4 + O_2 + 2H_2O \rightarrow 4Fe^{III}OOH + 2SiO_2 \qquad \text{(eq. 5.8)}$$
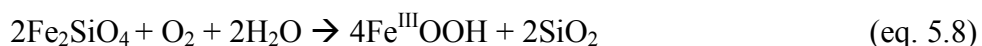
Weathered olivines occur mostly in the neighborhood of oxidized troilites (Figs. 5.9b, 5.10a). "Boxwork" olivines are very abundant where Mg^{2+} is leached out and a fine framework of

iron hydroxides is left behind (Figs. 5.10b and 5.10c). In vicinity, SiO_2 phases can occur in pore space or along cracks. In a few meteorites from Oman we found SiO_2 minerals. They are also described in meteorites from other find localities, as for example in the Wolf Creek iron meteorite (White et al., 1967) or the polymict ureilite EET 83309 (Beard et al., 2009; Beard et al., 2011; Downes et al., 2011). In contrast to the authors of the ureilite study, we interpret the occurrence of opal as low temperature terrestrial alteration. It forms typically at elevated weathering degrees, when the silicates start to be affected (W4) (Wlotzka, 1993).

5.4.5. Evolution of contamination

So far we have focused on the source of the ions. In this section we discuss the processes, which lead to the contamination. The ions have to be introduced into the meteorite by water. The analyses of the Oman rainwater yielded very low concentrations with $HCO_3^- > Ca^{2+} > Cl^- > SO_4^{2-} > Na^+$, comparable to other analyzed rainwaters from Arabia (Alabdula'aly and Khan, 2000). Over long periods of time and with extensive evaporation, rainwater might be sufficient to explain the observed contamination of meteorites by water-soluble salts. However, it is more reasonable that rainwater takes up ions from the soil and is then introduced into the meteorites by a combination of capillary forces and evaporative pumping. The saline water is distributed over most of the open pore space of the meteorites due to the activity of capillary forces (Chapman, 1980) and the introduced ions mix with preexisting salt concentrations by diffusion (Pel et al., 2003). Preferential heating of the dark meteorites as compared with the bright soil cause preferred evaporation from the meteorites, inducing more introduction of soil pore water into the meteorites. Figure 5.12 shows the concentration of major ions in rainwater, soil leachates, saline waters and the meteorite samples plotted against conservative Cl^-. It is evident that rainwater, soil leachates and saline waters have a Na/Cl ratio corresponding to sodium chloride dissolution line (halite Na/Cl=0.64, median Soil Na/Cl=0.94, median saline water Na/Cl=0.63) while meteorite leachates in most cases are depleted in Na (median meteorite Na/Cl=0.07) (Fig. 5.12). The evolution from dilute rainwater over soil leachates to saline water due to evaporation appears possible. Most meteorites have similar concentrations of ions like the saline waters, which represent rainwater plus ions from the soil, concentrated through evaporation (Fig. 5.12).
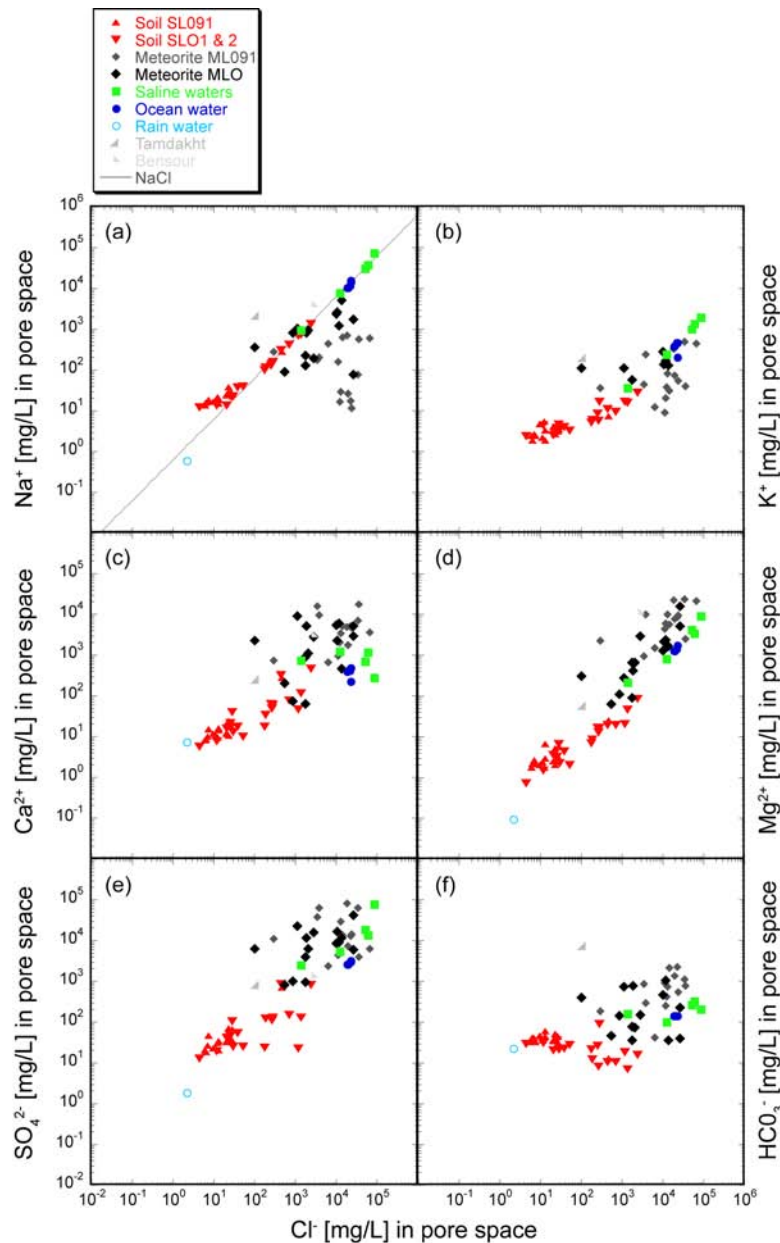
Figure 5.12. *Calculated concentrations of ions in assumed pore space of soil and of calculated pore space in meteorites and concentrations of ions in saline, ocean and rainwater plotted against Cl^-. NaCl is the halite dissolution line. All terrestrial samples plot close to this line, except soil samples at low concentrations. Weathered meteorites have a lower Na^+/Cl^- ratio. The meteorites with elevated Na^+/Cl^- ratios are Tamdakht and the W1 chondrite JaH 578. Here, the released sodium might be of primary meteoritic origin with only minor contamination by NaCl. Potassium shows a similar behavior as Na^+. Meteorites have slightly higher Ca^{2+}/Cl^- ratios. Magnesium to Cl^- ratios are similar for all kind of samples. Sulfate is richest in meteorites. HCO_3^- has no clear correlation. Since HCO_3^- is defined as alkalinity it is strongly dependent on the pH value and might not always represent the real bicarbonate content.*

The relations between ion concentrations and relative ion proportions in the reservoirs rain water, soil water, local saline water and meteorite extracts is consistent with the assumption that meteorites are contaminated by relatively dilute soil porewaters, followed by evaporative concentration within meteorites and water-rock (meteorite) reactions. From the highly concentrated brines in the meteorites several minerals precipitate, following their solubilities. First we would expect precipitation of carbonates, followed by sulfates and at the end chlorides, similar what is observed in terrestrial salt lakes where Mg rich salts precipitate at the latest stage (e.g. Kilic and Kilic, 2006). Then the brine becomes oversaturated in Mg^{2+}, Cl^- and SO_4^{2-} leading to the formation of hydrous Mg-sulfates and finally bischofite (Steiger et al., 2011).

Nickelbischofite, the nickel analogue of bischofite has been observed from alteration of ultramafic rocks from Dumont, Quebec, Canada and Liano County, Texas, USA, in the oxidized zone. In the Texas case, the chlorine might be derived from local chlorine-rich ground waters (Crook and Jambor, 1979). The extreme solubility and deliquescence of the hygroscopic nickelbischofite leads to the repeated crystallization and dissolution cycles (Crook and Jambor, 1979).

The evolution of the OC contamination is correlated to the degree of weathering as displayed in Figure 5.13, where the concentrations of the leached ions are plotted against weathering grade. Cations that are mainly introduced from the environment such as Ca^{2+} and Sr^{2+} increase with terrestrial residence time (Figs. 5.13a and 5.13b) because they precipitate in relative stable phases (Fig. 5.9b). The behavior of Na^+ is more complex (Fig. 5.13c), since it is introduced most likely as constituent of NaCl and then Na^+ is deficient in the leachates, possibly due to later loss as discussed below. The ions Mg^{2+} and Cl^- show a similar correlation to weathering grade indicating they are linked during the history of weathering (Figs. 5.13d and 5.13e). As discussed above, Cl^- has to be derived from outside and is accumulated from stages W1 to W3. Due to changing conditions within the meteorite Cl^- is continuously lost from stage W3 to W4. At the end of W3 and at W4 all of the troilite is oxidized and no more protons are produced leading to general neutral pH conditions. Similarly, Mg^{2+} is leached from olivine and pyroxene continuously from W1 to W3, the majority remaining in the meteorite, mainly in combination with Cl^-. Mg^{2+} is subsequently transported outwards as weathering proceeds from W3 to W4, where the mafic silicates, the main carriers of magnesium, are attacked. The weathering history of SO_4^{2-} is also complicated

(Fig. 5.13f). A part of the sulfate is introduced into the meteorites and precipitates as relative stable phases like $CaSO_4$, $BaSO_4$ or $SrSO_4$. Simultaneously, SO_4^{2-} is released during weathering of troilite (eq. 5.6) that starts at W1 but has it maximum during W3 to W4. Indeed we observe an increase of SO_4^{2-} up to late stage W3 but samples at W4 are significantly lower compared to high stage W3 samples indicating a loss of SO_4^{2-} during weathering stage W3 to W4. This result is in agreement with earlier studies where the release of sulfur during weathering of troilite and subsequent leaching from the meteorite was observed in bulk analyses (Al-Kathiri et al., 2005; Lee and Bland, 2004; Saunier et al., 2010). Only a minor amount of the released SO_4^{2-} remains in the meteorites, as component of weathering products such as jarosite, celestine, barite and Ca-sulfates. Buchwald and Clarke, (1989) detected traces of sulfur in terrestrial akaganéite within Antarctic meteorites. But the main part of the SO_4^{2-} anions might be lost together with Mg^{2+} and Cl^- as proposed above and also with Na^+ and K^+ as discussed in the next section (5.4.7.). At weathering stage W4 only low concentrations of soluble ions were detected. Most of the contamination minerals are precipitated as relative stable minerals and weathering of metal and troilite is terminated. Therefore, protons liberated by the weathering of troilite are consumed by dissolution of mafic silicates and the chemical environment within the meteorite reaches a near equilibrium, which slows down chemical weathering. Indeed, leachates of highly weathered samples yielded near neutral pH values. Most likely, the OCs reach a passive stage after W4 where chemical weathering is limited. During more than 10 years of meteorite searches in Oman we found only one meteorite at W5. On the other hand, physical weathering dominates the late history since cracks in the meteorites formed by the iron hydroxide veining and efflorescence of salts are subsequently filled with soil material blown in by wind. In addition, calcite veins can form and help to weaken further the meteorites and leading to fragmentation. Water-soluble salts are washed out at late stage of weathering. In addition, wind transported particles enhance erosion.
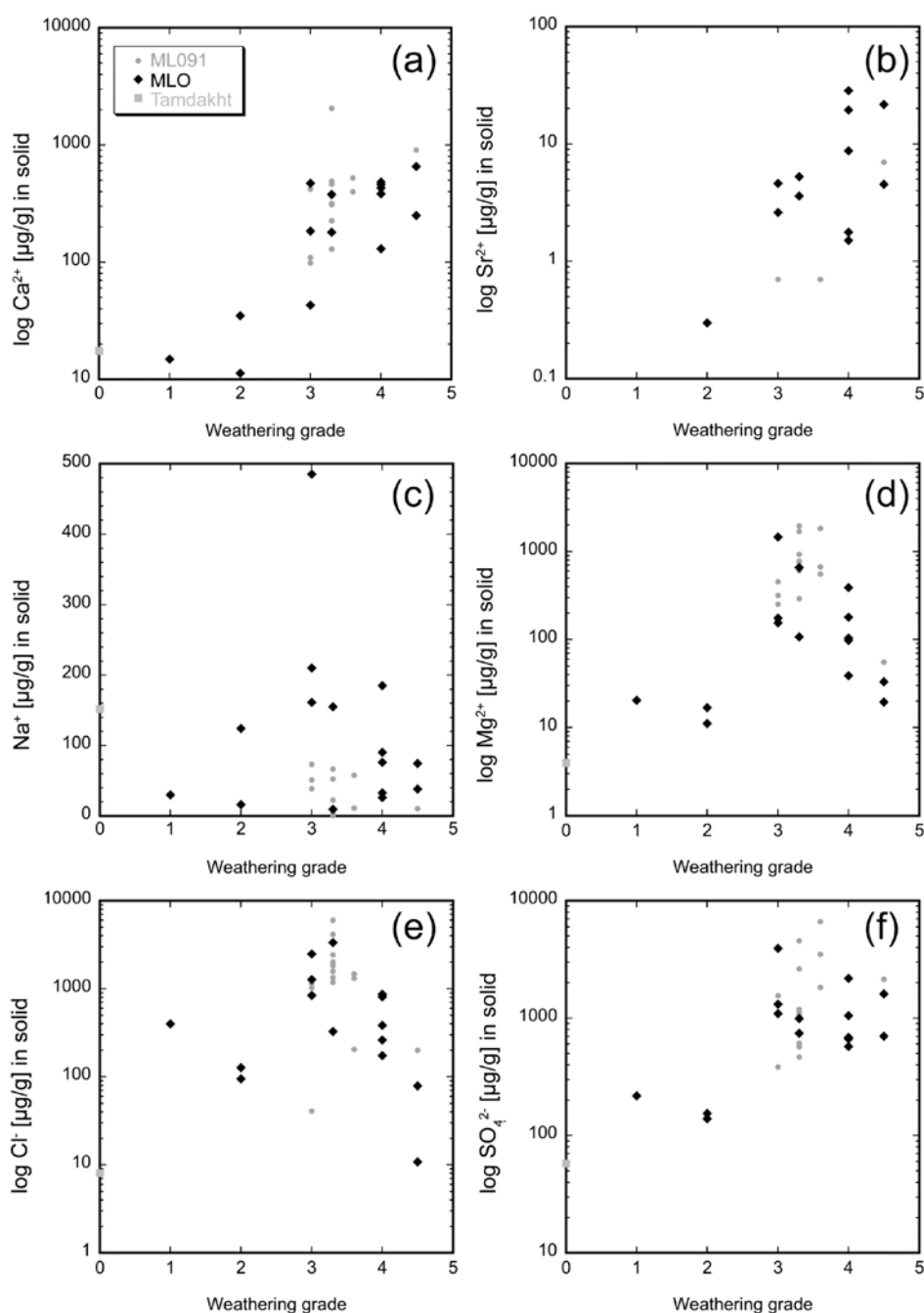
Figure 5.13. *Correlation of leached ions in solid with weathering degree (after Wlotzka, 1993 with slight modifications). a) The good correlation of Ca^{2+} to the weathering degree is the result of a continuous contamination with calcite and Ca-sulfate. b) The contamination of hot desert meteorites with Sr^{2+} is continuous with terrestrial residence time and therefore also with increasing degree of weathering. c) No strong correlation is observed between Na^+ and increasing degree of weathering. d) Most of the Mg^{2+} is leached at weathering stage W3. e) Samples at stage W3 have the highest Cl^- concentrations. f) The amount of SO_4^{2-} increases at higher degrees of weathering. At stage W3 there might be an increased contribution due to the weathering of the iron sulfide troilite.*

5.4.6. Place and timing of salt contamination

Meteorites are formed under conditions that are very different from the conditions prevailing on Earth. So weathering and contamination are supposed to be fast processes (Bland et al., 1998). Therefore water-soluble salts are also expected in lowly weathered samples. Indeed calcite was found in fragments of the diogenite Tatahouine collected 63 years after its fall in the Tunisian desert (Barrat et al., 1998). On a fragment of the CV3 chondrite Vigarano recovered one month after the fall precipitation of calcite veins was observed (Abreu and Brearley, 2005), implying this to be a really fast process. In OCs from Oman carbonate veins occur at early stages of weathering (W1-W3) but are also associated with iron-hydroxide veins at W4, i.e. the latest fillings of iron-hydroxide veins. "Pure" carbonate veins are usually observed starting at late W3 and W4, where they crosscut former iron-hydroxide veins (Fig. 5.14a). During radiocarbon dating of meteorites from OCs Oman also small samples of carbonates precipitated inside the meteorites were dated (Giscard et al., 2009). The "carbonate age" of meteorites with 10 to 25 ka show a positive correlation to the terrestrial ages of the meteorite and are relatively young (from recent ages to about 8 ka). Older meteorites have similar carbonate ages of around 30 ka (Giscard et al., 2010). But one has to be careful with those ages since they are from small samples (about 100 mg) and might be mixtures of several generations and the carbonates of the old meteorites are close to the limitations of ^{14}C dating method (Giscard et al., 2009). Oman meteorite samples with terrestrial ages of 0 ka to 10 ka show post-bomb carbonates implying recent or ongoing carbonate formation (Giscard et al., 2009).

Another question is, where happens the contamination? A meteorite partly embedded in Antarctic ice was significantly contaminated by Cl in the exposed part whereas the embedded proportion has a constant depth profile (Krähenbühl and Langenauer, 1994a). It is evident that the contamination in Antarctica can happen only on the exposed part since liquid water is only available during "hot" days in the cold desert of Antarctica (Schultz, 1986). It might be comparable in the hot desert: meteorites in Oman can be buried to 100% in the soil during their terrestrial history. Although they are in direct contact with the surrounding soil, the contamination might evolve more likely when they are partially exposed since then the temperature gradient between meteorite and surrounding soil is large enough to force

evaporating water that is loaded with salts from the soil to migrate through the meteorites and depose the transported ions in the pore spaces. This is in contrast to proposed process in more humid, temperate climates, where weathering occurs dominantly in the subsurface (Abreu and Brearley, 2005). In humid climates the water might penetrate the meteorites during percolation. Evidence for more extensive weathering of the exposed meteorite parts in comparison to buried pars was observed in several samples during this study. However, the position of meteorites can be changing during their terrestrial history. Due to evaporation water-soluble salts are concentrated in the top most part of the soil. Rain or wetting by morning fog affects only the top few millimeters to centimeters of the soil. The meteorite samples with the highest concentration of water-soluble salts, UaS 011 and 0703-703 (JaH 091) were not buried in the soil (Table 5.4a, c).
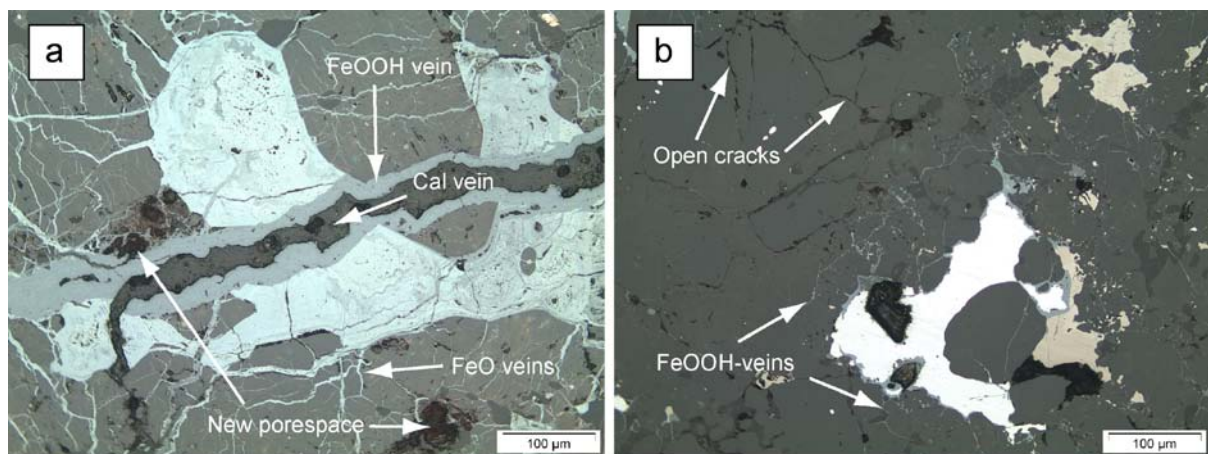
Figure 5.14. Evolution of pore space in ordinary chondrites during weathering. Scale bars are 100 μm. (a) Reflected light image of RaS 297, a highly weathered chondrite. All of the metal and troilite is oxidized and primary pore space is filled by an early set of bright grey iron oxide veins, mainly grown along grain boundaries. A second generation of grey iron hydroxide veins crosscuts minerals. A late stage dark grey calcite vein (Cal vein) partly follows iron hydroxide veins. Due to leaching of olivine additional new pore space is generated. (b) Reflected light image of the relatively fresh W1 meteorite Jah 578. Primary pore space along grain boundaries and open pore space due to shock events appears black, some are marked as "open cracks". Around a metal grain with a slightly oxidized rim a radiation of iron (oxy)hydroxide veins following primary pore space is visible. This effect is responsible for the low porosity of W1 to W2 (and partially W3) meteorites.

On the other hand, inspected terrestrial rocks showed no significant Cl^- contamination after treatment with $AgNO_3$. One reason might be the general lower porosity of the tested rocks like chert. In contrast, meteorites are relatively porous.

5.4.7. Loss of sodium

If we assume terrestrial contamination of the meteorites chlorine enters them primarily in combination with Na^+ and minor K^+ as shown by the leaching of soil samples. A small proportion of Cl^- might also derive from leaching of chlorapatite but its contribution is far too low to explain the observed under abundance of Na^+ relative to Cl^- (Fig. 5.12, Table 5.6a, 5.6b).

The lack of sodium could be interpreted as an artifact of the leaching experiments or analytical problems. This is not the case because the time series experiment showed increasing concentrations of Na, K and Cl at longer leaching time, but the Na/Cl and K/Cl ratios remained constant for all samples (Table 5.4c). IC and ICP-OES data are in agreement. We can also exclude the precipitation of a Na phase during leaching since the untreated IC measurements are in perfect agreement with the ICP-OES measurements where the precipitated minerals were dissolved by adding HNO_3. The question about the missing sodium remains. We have two hypotheses: (I) Precipitation of a low-water-soluble phase during weathering (e.g., magadiite, kenyaite, natrojarosite) and (II) precipitation of Na-salts on meteorite surfaces and successive erosion by wind or rain.

(I) A reason why we measured low Na^+ concentrations in the leachates of the meteorites could be that sodium precipitated during weathering in a mineral, which is insoluble in water. Possible candidates are the hydrous Na-silicates magadiite, $NaSi_7O_{13}(OH)_3 * 3H_2O$ and kenyaite, $Na_2Si_{22}O_{41}(OH)_8 * 6H_2O$, that were found precipitated from alkaline brines at Lake Magadi, Kenya (Eugster, 1967; Eugster and Jones, 1968). A hypothetical reaction (eq. 5.9) would be the hydrolysis of forsterite reacting with Na^+ and protons, most likely released from the weathering of troilite (eq. 5.6).

$$14Mg_2SiO_4 + 2Na^+ + 54H^+ \rightarrow 2NaSi_7O_{13}(OH)_3 * 3H_2O + 28Mg^{2+} + 18H_2O \qquad \text{(eq. 5.9)}$$
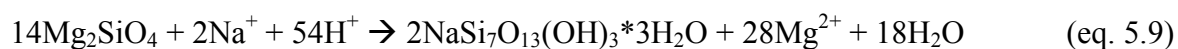
During this reaction also a lot of Mg^{2+} would be liberated what is observed in meteorites with high Na^+ depletion. However, no Na-silicate mineral was found through extensive survey of ordinary chondrite samples, neither during classification measurements at the EMP nor during special quests checking minerals in pores space or vein with the SEM. To store minor amounts of Na^+ a lot of olivine has to be weathered. Based on observations we rather think this reaction is unsubstantiated.

Another water insoluble sodium-bearing mineral is natrojarosite (eq. 5.10).

$$12FeS + 4Na^+ + 18H_2O + 27O_2 \rightarrow 4NaFe^{III}_3(SO_4)_2(OH)_6 + SO_4^{2-} + 12H^+ \qquad \text{(eq. 5.10)}$$
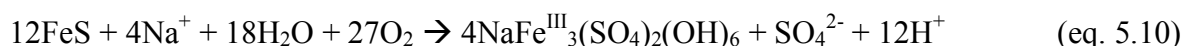
Jarosite forms generally at very acidic conditions, which can locally occur in the meteorites due to troilite oxidation. Indeed, in several altered remnants of troilites jarosite was found. However, 10 out of 12 samples were potassium jarosite with minor traces of sodium, and only in two cases natrojarosite was present. In samples having a Na^+ deficit as calculated during the mass balance approach, no natrojarosite was found. Therefore reaction 10 might explain to some degree the observed under abundance of K^+ in OCs compared to Cl^- but cannot explain fully the deficit in Na^+ (Table 5.6b).

(II) A second explanation is summarized equation 5.11. We postulate the formation of sodium sulfate efflorescence (mirabilite or related phases) on or near the meteorite surfaces while Mg^{2+} and Cl^- remain concentrated in brine or bischofite in more central parts of the meteorites. Iron hydroxides and silica are produced as additional phases.

$$Mg_2SiO_4 + (14+X)H_2O + 4NaCl + 4FeS + 20O_2 \rightarrow 2MgCl_2*6H_2O + 4FeOOH + SiO_2 +$$
$$4NaSO_4*X\ H_2O \qquad \text{(eq. 5.11)}$$
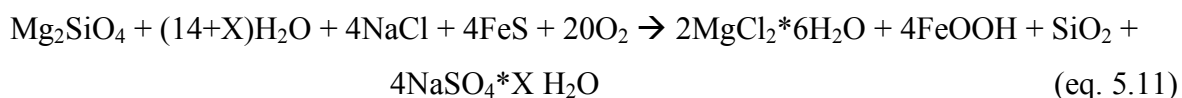
Efflorescence of white salts are described form terrestrial rocks in hot deserts (Walther, 1900). Indeed, several Omani OC stored in humidity- and temperature-controlled rooms showed efflorescence of white hairy minerals similar to descriptions of mirabilite salts from desert rocks or efflorescence of salts during rock disintegration experiments with sodium sulfate (e.g. Rodriguez-Navarro and Doehne, 1999; Walther, 1900). Nevertheless, all analyzed samples of such white hairy salts and aggregates of small grains showed them to be Mg-sulfates and Mg-carbonates, not Na-sulfates (Fig. 5.9e). The reason might be that Na^+

was already lost in the desert and these samples are oversaturated in Mg^{2+}. However, it might be a plausible process that Na^+ is introduced into the meteorite together with Cl^-, which then are separated. Chlorine rests in the meteorite while Na^+ is further transported in solution to the surface of the meteorites. There, the water evaporates at temperatures up to ~70°C and a highly concentrated brine enriched in sodium and sulfate is formed. When the meteorites cool down over night, efflorescence of mirabilite might occur, which then is removed the next day by wind erosion or it goes in solution since temperatures above 32.4°C are reached, where mirabilite is not stable anymore (Steiger and Asmussen, 2008; Witzke and Denk, 2011). Unfortunately we have never observed pure sodium sulfate salts on meteorites collected in Oman.

The most probable way to explain the deficit of water-soluble Na^+ in contaminated meteorites from Oman is a combination of both hypotheses. A small proportion is kept by water insoluble minerals such as jarosite and sparsely natrojarosite. The efflorescence of mirabilite on meteorite surfaces and subsequent erosion or out-washing might also contribute to the sodium loss. In addition, the same process could be responsible to some extend for the bulk loss of sulfur of weathered meteorites (Al-Kathiri et al., 2005; Lee and Bland, 2004; Saunier et al., 2010), even though sulfate ions are continuously introduced into the meteorites due to the contamination process. Efflorescence on the surface of an Antractic H5 chondrite contained significant proportion of Mg, Ca, Na, K and Rb indicating a redistribution of elements of meteoritic provenance (Velbel et al., 1991) and support our hypothesis.

5.4.8. Pore space and (salt) weathering

The study of porosity is important to understand the formation and behavior of asteroids (e.g. Flynn et al., 1999). Therefore processes that modify the porosity of meteorites have to be understood (Consolmagno et al., 2008). Porosity in ordinary chondrites occurs mostly as a network of micro cracks along grain boundaries and cutting through grains, produced by the passage of shock waves from collisions on the parent body (DeCarli et al., 2001). High porosity can also occur due to incomplete compaction because of the absence of late heavy shock events that was observed in some equilibrated chondrites (e.g. Sasso et al., 2009). The mean porosity of H chondrite falls is 7.0±4.9% and 5.6±4.7% for L chondrites falls

(Consolmagno et al., 2008). Generally it is assumed that weathering lowers pore space due to cementation of pores by iron hydroxides (Consolmagno et al., 2008) that can result in virtual zero porosity (Britt and Consolmagno, 2003). The porosities of our samples show a distinct picture: W0 meteorite Tamdakht has the highest porosity whereas W1 and W2 samples have the lowest. Interestingly, with increasing weathering degree, the porosity increases again (Fig. 5.15). At first glance, the observed difference in porosities might be due to the selection of the meteorite samples. In this study, OC from different classes (H and L) with unequal petrologic types and at various shock stages were investigated that had not the same initial porosities. However, the observed trend is real since the porosity of each meteorite was determined using different methods, which yielded similar results. For example, the porosities of Tamdakht obtained during leaching experiments (4.3%), using standard method on a large (297.375 g) sample (4.12%) and thin section investigation (5±2%) fit well together. A detailed study of the thin sections reveals the reason for the porosity variation during weathering history. First an initial decrease in pore space occurs due to sealing and clogging of micro cracks and other primary pore space by iron oxides and iron hydroxides (W1, W2 and partially W3; Fig. 5.14b). Volume increase can partially be buffered by the initial pore space (Al-Kathiri et al., 2005). The volume increase of metal transformation to iron hydroxide (~2.0x) is much higher compared to troilite alteration to iron hydroxide (~1.1x) (Al-Kathiri et al., 2005; Lee and Bland, 2004). In a second stage iron hydroxide- and calcite veins are formed (Fig. 5.14a) that can fracture the meteorites and produce new porosity. A similar conclusion was drawn by the study of the porosity of metal-rich enstatite chondrites where the initial porosity was not sufficient to absorb the volume increase caused by the alteration minerals (Macke et al., 2010). Weathering of metal and troilite is associated with leaching of mafic silicates (Figs. 5.11b and 5.14a) and produces a new generation of secondary pore space (W3 to W4).
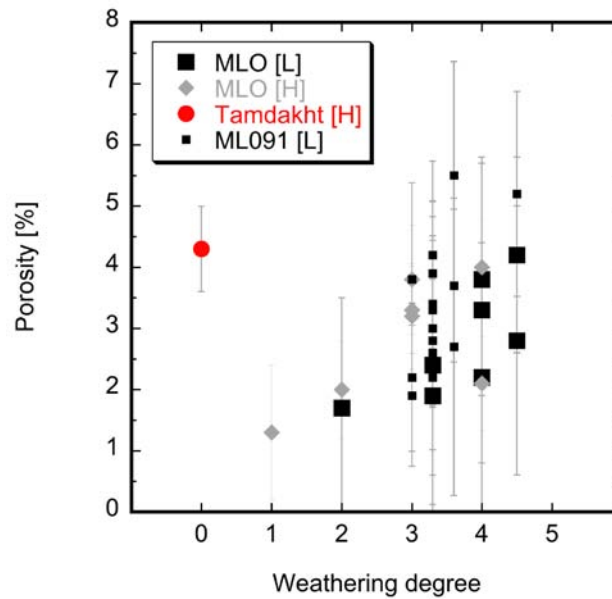
Figure 5.15. *Porosity of meteorites used for the leaching experiments correlated with degree of weathering. Fresh ordinary chondrite samples have relatively high porosities, 7.5% (H) and 5.6% (L) respectively. The only fall (W0) studied, the H5 chondrite Tamdakht, has a porosity of 4.3%, which is among the highest porosities determined in our study. Due to initial weathering a decrease in porosity occurs. With increasing weathering new pore space is produced.*

Salt weathering is certainly a potentially important process in disintegration of rocks from hot deserts since salts occur in desert soil, can be transported into the rocks and then precipitate due to evaporation (e.g. Goudie et al., 1997). But in meteorites the fragmentation due to the alteration of iron metal to iron hydroxides and oxides is certainly more important than the formation of cracks due to salt crystallization. During this work salts such as Ca- and Mg-sulfates that would have a potential to crack the meteorites (Charola et al., 2007; Winkler, 1987) were found in pores. However, these phases were mostly located in the center of pore space or within partially weathered metal grains where their crystallizations pressures could be buffered by the pore space. The iron hydroxide veins propagate mostly along grain boundaries and along small fissures formed by shock events, but can also penetrate mineral grains. In weathered samples cracks are abundant and some of them are only partially filled, mostly with Ca-carbonates or Ca-sulfates. Possibly they were formed due to sodium sulphate crystallization that has not survived cutting of the sample or thin section preparation. It is difficult to estimate the effect of salt weathering in meteorites since the iron-hydroxide vein

precipitation is certainly a major factor in the disintegration of meteorites. But the salt contamination is important for the chemical weathering, particularly the chlorides since they tend to attract water. The direct contribution of bischofite to physical weathering would be very minor since it hardly crystallizes under the given conditions (Steiger and Charola, 2011). Maybe salt weathering is even limited in Oman since moisture is abundant. In experimental simulations of rock weathering using conditions occurring in the Namib coastal desert, the greatest amount of breakdown was observed under conditions with relatively low fog moisture while high fog moisture reduced the rate of weathering by reducing opportunities for drying and related salt crystallization (Goudie and Parker, 1998).

In addition, the minerals that build up the meteorites have different thermal expansion coefficients (e.g. metal compared to olivine, Yomogida and Matsui, 1983), and therefore the anisotropic thermal expansion could weaken the rocks and help the contaminants or vein forming minerals penetrate into the meteorite. The most friable rocks used in this study were W4 rocks with abundant cracks, partially filled with Ca-carbonates and Ca-sulfates. They were found in the field disintegrated in to high number of fragments (Table 5.4c). But we have also found a lot of highly weathered (W4) meteorites that appear very stable even though they were penetrated by several generations of iron hydroxide veins. Such samples are found as single pieces and do not break apart during cutting in contrast to the friable samples with abundant Ca-sulfates and Ca-carbonate veins.

Once meteorites are collected and stored in rock archives or at exhibition, weathering of contaminated meteorites has not finished. Due to the hygroscopic force of the bischofite brines water is attracted even under relatively low humidity (~40%) conditions. We observed on some strongly salt-contaminated OC samples stored in the rock archive showed efflorescence of white Mg-rich minerals, identified as (hydrous) Mg-carbonates and Mg-sulfates with minor amounts of Cl^-. Subsequent precipitation of iron hydroxides or salts can cause cracks on the meteorite samples and lead to a disintegration of the pieces.

5.4.9. The role of salts in Oman meteorites as compared with Antarctica

Previous studies about contamination of meteorites from Antarctica focused either on the contamination with halogens which is interpreted to be sea spray sourced (Langenauer and Krähenbühl, 1993b) or the study of Mg-carbonate growth on ordinary chondrites (Velbel et al., 1991). The whitish efflorescence of salts on meteorites from Antarctica are dominated by evaporitic carbonates and sulfates, predominantly Mg and Ca bearing phases (Velbel et al., 1991). Minerals described are nesquehonite, $Mg(HCO_3)(OH)*2H_2O$; hydromagnesite, $Mg_5(CO_3)_4(OH)_2*4H_2O$; starkeyite, $MgSO_4*4H_2O$; epsomite, $MgSO_4*7H_2O$ and gypsum, $CaSO_4*2H_2O$. The efflorescence minerals must have grown rapidly since radiocarbon dating of such assemblages confirmed ages younger than A.D. 1950 since atomic bomb-produced ^{14}C was observed (Jull et al., 1988). Weathering only takes place when the meteorites are exposed from the ice (Velbel et al., 1991). The anions are thought to be derived from the atmosphere, since the ratios are distinct from seawater. The meteorites deliver the cations, predominately Mg (Velbel et al., 1991). In the meteorites from Oman, we observe a distinct picture. The soluble salts are also rich in Mg^{2+} but have a significant proportion of Ca^{2+}. The mineralogy of pore space fillings is dominated by Ba-, Ca-, Fe-, Mg- and Sr-sulfates, Ca-carbonates and Mg-chlorides. In general, a higher quantity and also diversity of ions is available in the hot desert environment and processes are faster due to the higher temperatures and abundance of water, resulting in higher concentrations of contaminants. Importantly, chloride is more abundant in meteorites from Oman and forms partly hygroscopic minerals. The attracted water forms highly concentrated corrosive brines in the pore space of meteorites that accelerate weathering. Another significant difference is the fact that in Oman the majority of the suitable surfaces for meteorite recovery are built of carbonates, which contribute to the contamination pattern.

Statistical studies showed that about 5 % of all ANSMET meteorites contain salts visible by naked eye (Losiak and Velbel, 2011; Velbel, 1988).

During the visual inspection of 269 individual OC samples from Oman we observed the presence of hygroscopic salts in 22.3% of the samples; most of these samples were of weathering grade W3. The majority of the samples showed macroscopically only minor efflorescence of hygroscopic salts, mainly dried residues. Among all inspected samples only

2.6% had extreme hygroscopic behavior as displayed in Figure 5.1. White pore space fillings, mostly Ca-sulfates and minor Ca-carbonates, were macroscopically observed in 27.4% of the samples from Oman. In meteorites from Australia terrestrial contamination minerals, described as calcite (but there might also be sulfates), was visible by naked eye in ~45% of samples (Bevan and Binns, 1989). The described population from Australia, with 34 notably smaller meteorites, might not be representative. However, contamination by water-soluble salts is more abundant in meteorites recovered in hot deserts compared to samples from cold deserts and has a significant influence in the way of weathering. The major ions involved in salt contamination, i.e. Mg^{2+}, Ca^{2+} and SO_4^{2-}, are very abundant in primary meteorites and partially derive from the meteorite itself, their depletion or accumulation might not be detectable in bulk composition analyses (Velbel, 1988).

The main difference between contaminated meteorites from hot deserts to Antarctica is the chemistry of contaminants and their abundance. Also worth mentioning is the fact that the chloride contamination in Antarctic meteorites displays well-defined depth profiles with the highest concentrations towards the exposed surfaces. A similar situation was found for Camel Donga eucrites from Nullarbor, Australia, with slightly elevated halogen concentrations on outer parts (Krähenbühl and Langenauer, 1994b). In contrast, OC from Oman have random patterns of Cl^- contamination, generally with the highest concentrations in the interior (Fig. 5.2).

5.4.10. Indications of microbial activity in meteorites

Hot desert are harsh environments for life due to the aridity, low abundance of organic matter and high daily temperature variations. Especially high temperatures up to the boiling point of water that were expected in meteorites would be adverse for life (Ash and Pillinger, 1995). In contrast, our temperature logging experiments yielded maximum ΔT during a day of 46.5°C and a maximum temperature of 66.3°C that might be survived for example by cyanobacteria (e.g. Rothschild and Mancinelli, 2001). Meteorites reach higher temperatures than observed by us but temperatures to the boiling point are not expected. Wind is often present and cools to a certain degree the meteorites. Therefore it is possible that microorganism can survive the rest in a desert meteorite.

Indeed, the presence of terrestrial microorganism in hot desert meteorites was verified, for example in fragments collected 63 years after fall of the Tatahouine diogenite from Tunisia (Barrat et al., 1999; Benzerara et al., 2006). Chondrites from Oman are contaminated by terrestrial amino acids derived from local soil (Martins et al., 2007), indicating the possible presence of bacteria in the meteorites. During our survey of water-soluble salts we detected traces of NH_4^+ in two OCs. A possible origin of ammonium is nitrate reduction by microbial activity (Shin and Cha, 2008). However, NH_4 can also be produced in absence of bacteria during oxidation of metallic iron (Till et al., 1998):

$$4Fe^0 + NO_3^- + 7H_2O \rightarrow 4Fe^{2+} + NH_4^+ + 10OH^- \qquad \text{(eq. 5.12)}$$
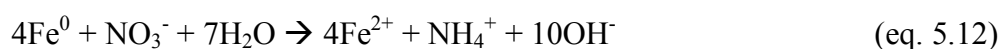
Microorganisms in meteorites have an influence on weathering of meteorites and can use ions liberated from the meteorites as nutrients. For example in cell walls of bacteria found in the weathered Tatahouine samples small crystals of NaCl and KCl were observed (Gillet et al., 2000). Another important nutrient for microbes is phosphate, occurring as Ca-phosphates that are usually extensively weathered in meteorites from Oman (Fig. 5.9f). During weathering of the Ca-phosphates some Cl^- is liberated. The assumption that the excess of Cl^- could be from the decomposition of Ca-phosphate seems also unlikely since they occur only as minor constituents and could not deliver the necessary amounts of Cl^-. Additionally, during decomposition of merrillite sodium would also be released.

Meteorites can be inhabited by (terrestrial) microorganisms that use ions from the meteorite and the environment as nutrients. Their influence on weathering is poorly studied since weathering studies of meteorites focused mainly on "inorganic" weathering so far.

5.5. CONCLUSIONS

Chondrites showing strongly hygroscopic behavior ("sweating") are only known from Oman so far. Ordinary chondrites recovered from the hot desert of Oman are contaminated by water-soluble salts residing in the pore space and can occur in high concentrations (up to 3400 µg/g of Cl^- and 9000 µg/g total soluble salts in bulk meteorite samples). The major ions are Mg^{2+}, Ca^{2+}, Cl^- and SO_4^{2-} and iron, originating as complex mixtures of ions derived from rainwater, soil and the meteorites. The observed salt concentrations and relative ion

abundances are controlled by weathering. Highest concentrations are reached during W3, a stage that is generally the most active stage in the meteorite weathering history, which is dominated by the oxidation of troilite that leads to local acidic microenvironments in the meteorites as proven by the occurrence of jarosite. Concomitantly a significant part of olivine is leached and metal is further oxidized. Chloride is reaching high concentrations in the pore space while sodium is strongly depleted, either by efflorescence as sulfate on meteorite surfaces and subsequent erosion by wind or occasional rain, or by formation of Na-bearing jarosite. Other prominent contamination minerals in meteorites are Ca-carbonate and Ca-sulfate. Therefore, the concentrations of water-soluble Ca^{2+} and Sr^{2+} increase with increasing weathering degree. Meteorites at W4 chemically reach a relatively stable state with ongoing slow silicate hydrolysis. Some W4 meteorites are physically weakened, mostly due to precipitation of calcite veins. Fracturing of the meteorites and leaching of olivine produce new pore space resulting in an increase in porosity at higher weathering degrees. Observed diurnal temperature variations in an OC are in average 34.3°C. Minimal temperature observed is 4.8°C and the maximal 66.3°C, respectively. Even though we found variable concentrations of water-soluble ions in soil samples, their magnitude only has a minor influence on the salt contamination in associated meteorites. Rather, the propagation of weathering controls the amount and pattern of salts found in OC from Oman.

This first data set of water-soluble salts and temperature variations in OC from hot desert has enlighten some dark areas. But we are far away from understanding all processes such as the fact why only meteorites from Oman are heavily contaminated by salts and meteorites from other hot desert areas with similar present and past climate histories, similar soil compositions and weathering rates of the meteorites seem to be not affected or at least to a lesser degree.

5.6. Acknowledgments

5.7. REFERENCES

Abed, R. M. M., Dobrestov, S., Al-Kharusi, S., Schramm, A., Jupp, B., and Golubic, S., 2011. Cyanobacterial diversity and bioactivity of inland hypersaline microbial mats from a desert stream in the Sultanate of Oman. *Fottea* 11: 215-224.

Abreu, N. M. and Brearley, A. J., 2005. Carbonates in vigarano: Terrestrial, preterrestrial, or both? *Meteoritics & Planetary Science* 40: 609-625.

Al-Kathiri, A., Hofmann, B. A., Jull, A. J. T., and Gnos, E., 2005. Weathering of meteorites from Oman: Correlation of chemical and mineralogical weathering proxies with ^{14}C terrestrial ages and the influence of soil chemistry. *Meteoritics & Planetary Science* 40: 1215-1239.

Alabdula'aly, A. I. and Khan, M. A., 2000. Chemistry of rain water in Riyadh, Saudi Arabia. *Archives of Environmental Contamination and Toxicology* 39: 66-73.

Alsaaran, N. A., 2008. Origin and geochemical reaction paths of sabkha brines: Sabkha Jayb Uwayyid, eastern Saudi Arabia. *Arabian Journal of Geosciences* 1: 63-74.

Ash, R. D. and Pillinger, C. T., 1995. Carbon, nitrogen and hydrogen in Saharan chondrites: The importance of weathering. *Meteoritics* 30: 85-92.

Barrat, J. A., Gillet, P., Heulin, T., Lesourd, M., Blichert-Toft, J., Achouak, W., Guyot, F., and Benzerara, K., 1999. Mineralogical, chemical, and biological effects of 63 years of terrestrial residence in the Tatahouine meteorite. *Meteoritics & Planetary Science* 34: A10-A10.

Barrat, J. A., Gillet, P., Lecuyer, C., Sheppard, S. M. F., and Lesourd, M., 1998. Formation of carbonates in the Tatahouine meteorite. *Science* 280: 412-414.

Beard, A. D., Downes, H., and Howard, K., 2009. Hydrated silica (opal) in a polymict ureilite, EET83309. *Meteoritics & Planetary Science* 44: A31-A31.

Beard, A. D., Downes, H., and Howard, K. T., 2011. Significane of opal in ureilites-Delivery of H(2)O to the inner Solar System? *Meteoritics & Planetary Science* 46: A15-A15.

Benzerara, K., Chapon, V., Moreira, D., Lopez-Garcia, P., Guyot, F., and Heulin, T., 2006. Microbial diversity on the Tatahouine meteorite. *Meteoritics & Planetary Science* 41: 1249-1265.

Bevan, A. W. R. and Binns, R. A., 1989. Meteorites from the Nullarbor region, Western Australia. 2. Recovery and classification of 34 new meteorite finds from the Mundrabilla, Forrest, Reid and Deakin areas. *Meteoritics* 24: 135-141.

Bland, P. A., Sexton, A. S., Jull, A. J. T., Bevan, A. W. R., Berry, F. J., Thornley, D. M., Astin, T. R., Britt, D. T., and Pillinger, C. T., 1998. Climate and rock weathering: A study of terrestrial age dated ordinary chondritic meteorites from hot desert regions. *Geochimica et Cosmochimica Acta* 62: 3169-3184.

Bland, P. A., Zolensky, M. E., Benedix, G. K., and Sephton, M. A., 2006. Weathering of chondritic meteorites. In: Lauretta, D. S. and McSween, H. Y. (Eds.), *Meteorites and the Early Solar System II*. University of Arizona Press, Tucson.

Bogard, D. D., Garrison, D. H., and Masarik, J., 2001. The Monahans chondrite and halite: Argon-39/argon-40 age, solar gases, cosmic-ray exposure ages, and parent body regolith neutron flux and thickness. *Meteoritics & Planetary Science* 36: 107-122.

Bridges, J. C., Banks, D. A., Smith, M., and Grady, M. M., 2004. Halite and stable chlorine isotopes in the Zag H3-6 breccia. *Meteoritics & Planetary Science* 39: 657-666.

Britt, D. T. and Consolmagno, G. J., 2003. Stony meteorite porosities and densities: A review of the data through 2001. *Meteoritics & Planetary Science* 38: 1161-1180.

Buchwald, V. F. and Clarke, R. S., 1988. Akaganeite, not lawrencite, corrodes antarctic iron-meteorites. *Meteoritics* 23: 261-261.

Buchwald, V. F. and Clarke, R. S., 1989. Corrosion of Fe-Ni alloys by Cl-containing akaganéite (beta-FeOOH) - The Antarctic meteorite case. *American Mineralogist* 74: 656-667.

Changela, H. G. and Bridges, J. C., 2010. Alteration assemblages in the nakhlites: Variation with depth on Mars. *Meteoritics & Planetary Science* 45: 1847-1867.

Chapman, R. W., 1980. Salt weathering by sodium chloride in the Saudi Arabian desert. *American Journal of Science* 280: 116-129.

Charola, A. E., Puhringer, J., and Steiger, M., 2007. Gypsum: a review of its role in the deterioration of building materials. *Environmental Geology* 52: 207-220.

Chennaoui-Aoudjehane, H., Jambon, A., Denise, M. B., Boudouma, O., Gattacceca, J., Weber, P., and Bonte, P., 2009. Tamdakht meteorite: The last Moroccan fall. *Meteoritics & Planetary Science* 44: A50-A50.

Consolmagno, G. J. and Britt, D. T., 1998. The density and porosity of meteorites from the Vatican collection. *Meteoritics & Planetary Science* 33: 1231-1241.

Consolmagno, G. J., Britt, D. T., and Macke, R. J., 2008. The significance of meteorite density and porosity. *Chemie Der Erde-Geochemistry* 68: 1-29.

Cooke, R. and Warren, A., 1973. *Geomorphology in Deserts*. Batsford Ltd, London.

Crook, W. W. and Jambor, J. L., 1979. Nickelbischofite, A new nickel chloride hydrate. *Canadian Mineralogist* 17: 107-109.

Crozaz, G. and Wadhwa, M., 2001. The terrestrial alteration of Saharan shergottites Dar al Gani 476 and 489: A case study of weathering in a hot desert environment. *Geochimica et Cosmochimica Acta* 65: 971-977.

DeCarli, P. S., Bowden, E., and Seaman, L., 2001. Shock-induced compaction and porosity in meteorites. *Meteoritics & Planetary Science* 36: A47.

Downes, H., Smith, C. L., Beard, A. D., and Ross, A. J., 2011. Early Solar System processes revealed by an integrated study of ureilite meteorites. *Meteoritics & Planetary Science* 46: A60-A60.

Dunn, T. L., Cressey, G., McSween, H. Y., Jr., and McCoy, T. J., 2010. Analysis of ordinary chondrites using powder X-ray diffraction: 1. Modal mineral abundances. *Meteoritics & Planetary Science* 45: 123-134.

Edgell, H. S., 2006. *Arabian deserts*. Springer, Dordrecht.

Eugster, H. P., 1967. Hydrous sodium silicates from Lake Magadi, Kenya - Precursors of bedded chert. *Science* 157: 1177-&.

Eugster, H. P. and Jones, B. F., 1968. Gels composed of sodium-aluminium silicate, Lake Magadi, Kenya. *Science* 161: 160-&.

Fisher, M., 1994. Another look at the variability of desert climates, using examples from Oman. *Global Ecology and Biogeography Letters* 4: 79-87.

Fleitmann, D. and Matter, A., 2009. The speleothem record of climate variability in Southern Arabia. *Comptes Rendus Geoscience* 341: 633-642.

Flynn, G. J., Moore, L. B., and Klock, W., 1999. Density and porosity of stone meteorites: Implications for the density, porosity, cratering, and collisional disruption of asteroids. *Icarus* 142: 97-105.

Fookes, P. G. and Lee, M. E., 2009. Desert environments of inland Oman. *Geology Today* 25: 226-231.

Garrison, D., Hamlin, S., and Bogard, D., 2000. Chlorine abundances in meteorites. *Meteoritics & Planetary Science* 35: 419-429.

Gillet, P., Barrat, J. A., Heulin, T., Achouak, W., Lesourd, M., Guyot, F., and Benzerara, K., 2000. Bacteria in the Tatahouine meteorite: Nanometric-scale life in rocks. *Earth and Planetary Science Letters* 175: 161-167.

Giscard, M. D., Jull, A. J. T., and Hewitt, L. R., 2009. Terrestrial carbonates of meteorites from Chile, Oman, Northwest Africa and Saudi Arabia. *Meteoritics & Planetary Science* 44: A78-A78.

Giscard, M. D., Jull, A. J. T., Hofmann, B. A., Valenzuela, V. M., and Gnos, E., 2010. ^{14}C terrestrial ages and carbonate ages of meteorites from the Atacama Desert (Chile) and the Omani Desert. Unpublished Master report, University of Arizona, Tucson.

Gnos, E., Eggimann, M., Al-Kathiri, A., and Hofmann, B. A., 2006. The JaH 091 strewnfield. *Meteoritics & Planetary Science* 41 Suppl.: A64.

Gnos, E., Lorenzetti, S., Eugster, O., Jull, A. J. T., Hofmann, B. A., Al-Kathiri, A., and Eggimann, M., 2009. The Jiddat al Harasis 073 strewn field, Sultanate of Oman. *Meteoritics & Planetary Science* 44: 375-387.

Goede, A., Harmon, R. S., Atkinson, T. C., and Rowe, P. J., 1990. Pleistocene climatic change in southern Australia and its effects on speleothem deposition in some Nullarbor caves. *Journal of Quaternary Science* 5: 29-38.

Gomez-Heras, M., Smith, B. J., and Fort, R., 2006. Surface temperature differences between minerals in crystalline rocks: Implications for granular disaggregation of granites through thermal fatigue. *Geomorphology* 78: 236-249.

Gooding, J. L., Wentworth, S. J., and Zolensky, M. E., 1991. Aqueous alteration of the Nakhla meteorite. *Meteoritics* 26: 135-143.

Goudie, A. S. and Parker, A. G., 1998. Experimental simulation of rapid rock block disintegration by sodium chloride in a foggy coastal desert. *Journal of Arid Environments* 40: 347-355.

Goudie, A. S., Viles, H. A., and Parker, A. G., 1997. Monitoring of rapid salt weathering in the central Namib Desert using limestone blocks. *Journal of Arid Environments* 37: 581-598.

Grossman, J. N., 1998. The Meteoritic Bulletin, No. 82, 1998 July. *Meteoritics & Planetary Science* 33: A221-A239.

Grossman, J. N., 1999. The Meteoritical Bulletin, No. 83, 1999 July. *Meteoritics & Planetary Science* 34: A169-A186.

Hofmann, B. A., Nystrom, J. O., and Krähenbühl, U., 2000. The Ordovician chondrite from Brunflo, central Sweden III. Geochemistry of terrestrial alteration. *Lithos* 50: 305-324.

Jull, A. J. T., Cheng, S., Gooding, J. L., and Velbel, M. A., 1988. Rapid growth of magnesium-carbonate weathering products in a stony meteorite from Antarctica. *Science* 242: 417-419.

Jupp, B. P., Eichenberger, U., and Cookson, P., 2008. The microbial domes of Wadi Muqshin pools, Sultanate of Oman. *International Journal of Environmental Studies* 65: 685-703.

Kilic, Ö. and Kilic, A. M., 2006. Recovery of salt co-products during the salt production from brine. *Desalination* 186: 11-19.

Krähenbühl, U. and Langenauer, M., 1994a. ALH-82102 - An Antarctic meteorite embedded partly in ice. *Meteoritics* 29: 651-652.

Krähenbühl, U. and Langenauer, M., 1994b. Distribution of halogens in eucrites and their weathering compared to chondrites. *Meteoritics* 29: 486-486.

Krähenbühl, U. and Langenauer, M., 1995. Comparison of the distribution of halogens in chondrites from Antarctica and from Western Australia. In: Schultz, L., Annexstad, J. O., and Zolensky, M. (Eds.) *Workshop on meteorites from hot and cold deserts*, Nördlingen.

Langenauer, M. and Krähenbühl, U., 1993a. Depth-profiles and surface enrichment of the halogens in 4 Antarctic H5 chondrites and in 2 non-Antarctic chondrites. *Meteoritics* 28: 98-104.

Langenauer, M. and Krähenbühl, U., 1993b. Halogen contamination in Antarctic H5 and H6 chondrites and relation to sites of recovery. *Earth and Planetary Science Letters* 120: 431-442.

Lee, M. R. and Bland, P. A., 2004. Mechanisms of weathering of meteorites recovered from hot and cold deserts and the formation of phyllosilicates. *Geochimica et Cosmochimica Acta* 68: 893-916.

Lee, M. R., Smith, C. L., Gordon, S. H., and Hodson, M. E., 2006. Laboratory simulation of terrestrial meteorite weathering using the Bensour (LL6) ordinary chondrite. *Meteoritics & Planetary Science* 41: 1123-1138.

Losiak, A. and Velbel, M. A., 2011. Evaporite formation during weathering of Antarctic meteorites--A weathering census analysis based on the ANSMET database. *Meteoritics & Planetary Science* 46: 443-458.

Macke, R. J., Consolmagno, G. J., Britt, D. T., and Hutson, M. L., 2010. Enstatite chondrite density, magnetic susceptibility, and porosity. *Meteoritics & Planetary Science* 45: 1513-1526.

Martins, Z., Hofmann, B. A., Gnos, E., Greenwood, R. C., Verchovsky, A., Franchi, I. A., Jull, A. J. T., Botta, O., Glavin, D. P., Dworkin, J. P., and Ehrenfreund, P., 2007. Amino acid composition, petrology, geochemistry, C-14 terrestrial age and oxygen isotopes of the Shisr 033 CR chondrite. *Meteoritics & Planetary Science* 42: 1581-1595.

Mason, B., 1965. The chemical composition of olivine-bronzite and olivine-hypersthene chondrites. *American Museum Noviatates* 2223: 1-38.

McGreevy, J. P. and Smith, B. J., 1982. Salt weathering in hot deserts - Observations on the design of simulation experiments. *Geografiska Annaler Series a-Physical Geography* 64: 161-170.

Nazarov, M. A., Demidova, S. I., Patchen, A., and Taylor, L. A., 2004. Dhofar 311, 730 and 731: new lunar meteorites from Oman *Lunar and Planetary Science XXXV, Abstract Nr. 1233*.

Nininger, H. H., 1929. Notes on oxidation of certain meteorites: The formation of meteorodes. *Transactions of the Kansas Academy of Science* 32: 63-67.

Nordstrom, D. K., 2011. Mine waters: Acidic to circumneutral. *Elements* 7: 393-398.

Ohnishi, I. and Tomeoka, K., 2007. Hydrothermal alteration experiments of enstatite: Implications for aqueous alteration of carbonaceous chondrites. *Meteoritics & Planetary Science* 42: 49-61.

Pachur, H.-J., 1980. Climatic history in the Late Quaternary in southern Libya and the western Libyan desert. In: Salem, M. J. and Busrewil, M. T. (Eds.), *The Geology of Libya*. Academic Press.

Pel, L., Huinink, H., and Kopinga, K., 2003. Salt transport and crystallization in porous building materials. *Magnetic Resonance Imaging* 21: 317-320.

Petrov, M. P., 1976. *Deserts of the World*. Wiley and Sons, New York.

Pilson, M. E. Q., 1998. *An introduction to the chemistry of the sea*. Prentice Hall, Upper Saddle River, New Jersey, USA.

Potocki, F. P., 1978. Road temperatures and climatological observations in the Emirate of Abu Dhabi. *U.K. Transport and Road Research Laboratory* Supp. Rept. 412.

Rodriguez-Navarro, C. and Doehne, E., 1999. Salt weathering: Influence of evaporation rate, supersaturation and crystallization pattern. *Earth Surface Processes and Landforms* 24: 191-209.

Rothschild, L. J. and Mancinelli, R. L., 2001. Life in extreme environments. *Nature* 409: 1092-1101.

Rubin, A. E., Zolensky, M. E., and Bodnar, R. J., 2002. The halite-bearing Zag and Monahans (1998) meteorite breccias: Shock metamorphism, thermal metamorphism and aqueous alteration on the H-chondrite parent body. *Meteoritics & Planetary Science* 37: 125-141.

Ruedrich, J., Kirchner, D., and Siegesmund, S., 2011. Physical weathering of building stones induced by freeze-thaw action: a laboratory long-term study. *Environmental Earth Sciences* 63: 1573-1586.

Sasso, M. R., Macke, R. J., Boesenberg, J. S., Britt, D. T., Rivers, M. L., Ebel, D. S., and Friedrich, J. M., 2009. Incompletely compacted equilibrated ordinary chondrites. *Meteoritics & Planetary Science* 44: 1743-1753.

Saunier, G., Poitrasson, F., Moine, B., Gregoire, M., and Seddiki, A., 2010. Effect of hot desert weathering on the bulk-rock iron isotope composition of L6 and H5 ordinary chondrites. *Meteoritics & Planetary Science* 45: 195-209.

Sawyer, D. J., McGehee, M. D., Canepa, J., and Moore, C. B., 2000. Water soluble ions in the Nakhla martian meteorite. *Meteoritics & Planetary Science* 35: 743-747.

Schlüter, J., Schultz, L., Thiedig, F., Al-Mahdi, B. O., and Abu Aghreb, A. E., 2002. The Dar al Gani meteorite field (Libyan Sahara): Geological setting, pairing of meteorites, and recovery density. *Meteoritics & Planetary Science* 37: 1079-1093.

Schmitz, B. and Haggstrom, T., 2006. Extraterrestrial chromite in Middle Ordovician marine limestone at Kinnekulle, southern Sweden - Traces of a major asteroid breakup event. *Meteoritics & Planetary Science* 41: 455-466.

Schultz, L., 1986. Allende in Antarctica: Temperatures in Antarctic meteorites (abstract). *Meteoritics* 21: 505.

Shin, K.-H. and Cha, D. K., 2008. Microbial reduction of nitrate in the presence of nanoscale zero-valent iron. *Chemosphere* 72: 257-262.

Sjøgren, A. and Buchwald, V. F., 1991. Hydrogen plasma reactions in a D.C. mode for the conservation of iron meteorites and antiquities. *Studies in Conservation* 36: 161-171.

Steiger, M. and Asmussen, S., 2008. Crystallization of sodium sulfate phases in porous materials: The phase diagram $Na_2SO_4-H_2O$ and the generation of stress. *Geochimica et Cosmochimica Acta* 72: 4291-4306.

Steiger, M. and Charola, A. E., 2011. Weathering and deterioration. In: Siegesmund, S. and Snethlage, R. (Eds.), *Stone in Architecture*. Springer-Verlag, Berlin Heidelberg.

Steiger, M., Linnow, K., Ehrhardt, D., and Rohde, M., 2011. Decomposition reactions of magnesium sulfate hydrates and phase equilibria in the $MgSO_4$-H_2O and Na^+-Mg^{2+}-Cl^--SO_4^{2-}-H_2O systems with implications for Mars. *Geochimica et Cosmochimica Acta* 75: 3600-3626.

Stöffler, D., Keil, K., and Scott, E. R. D., 1991. Shock metamorphism of ordinary chondrites. *Geochimica et Cosmochimica Acta* 55: 3845-3867.

Tarter, J. G., Evans, K. L., and Moore, C. B., 1980. Chlorine in meteorites (abstract). *Meteoritics* 15: 373-374.

Thorslund, P., Wickman, F. E., and Nystrom, J. O., 1984. The Ordovician chondrite from Brunflo, central Sweden, 1. General description and primary minerals. *Lithos* 17: 87-100.

Till, B. A., Weathers, L. J., and Alvarez, P. J. J., 1998. Fe(0)-supported autotrophic denitrification. *Environmental Science & Technology* 32: 634-639.

Van Schmus, W. R. and Wood, J. A., 1967. A chemical-petrologic classification for the chondritic meteorites. *Geochimica et Cosmochimica Acta* Acta, 31: 747-765.

Velbel, M. A., 1988. The distribution and significance of evaporitic weathering products on Antarctic meteorites. *Meteoritics* 23: 151-159.

Velbel, M. A., Long, D. T., and Gooding, J. L., 1991. Terrestrial weathering of Antarctic stone meteorites: Formation of Mg-carbonates on ordinary chondrites. *Geochimica et Cosmochim. Acta* 55: 67 - 76.

Walther, J., 1900. *Das Gesetz der Wüstenbildung* Dietrich Reimer (Ernst Vohsen), Berlin.

Weisberg, M. K., Smith, C., Benedix, G., Folco, L., Righter, K., Zipfel, J., Yamaguchi, A., and Aoudjehane, H. C., 2009. The Meteoritical Bulletin, No. 95. *Meteoritics & Planetary Science* 44: 429-462.

Whitby, J., Burgess, R., Turner, G., Gilmour, J., and Bridges, J., 2000. Extinct I-129 in halite from a primitive meteorite: Evidence for evaporite formation in the early solar system. *Science* 288: 1819-1821.

White, J. S., Henderso.Ep, and Mason, B., 1967. Secondary minerals produced by weathering of Wolf Creek meteorite. *American Mineralogist* 52: 1190-&.

Winkler, E. M., 1987. Weathering and Weathering Rates of Natural Stone. *Environmental Geology and Water Sciences* 9: 85-92.

Witzke, T. and Denk, M., 2011. Eine temporäre Mirabilit-Mineralisation bei Teutschenthal, Sachsen-Anhalt. *Der Aufschluss* 62: 353-360.

Wlotzka, 1993. A weathering scale for the ordinary chondrites. *Meteoritics* 28: 460.

Yomogida, K. and Matsui, T., 1983. Physical-properties of ordinary chondrites. *Journal of Geophysical Research* 88: 9513-9533.

Zolensky, M. E., Bodnar, R. J., Gibson, E. K., Nyquist, L. E., Reese, Y., Shih, C. Y., and Wiesmann, H., 1999. Asteroidal water within fluid inclusion-bearing halite in an H5 chondrite, Monahans (1998). *Science* 285: 1377-1379.
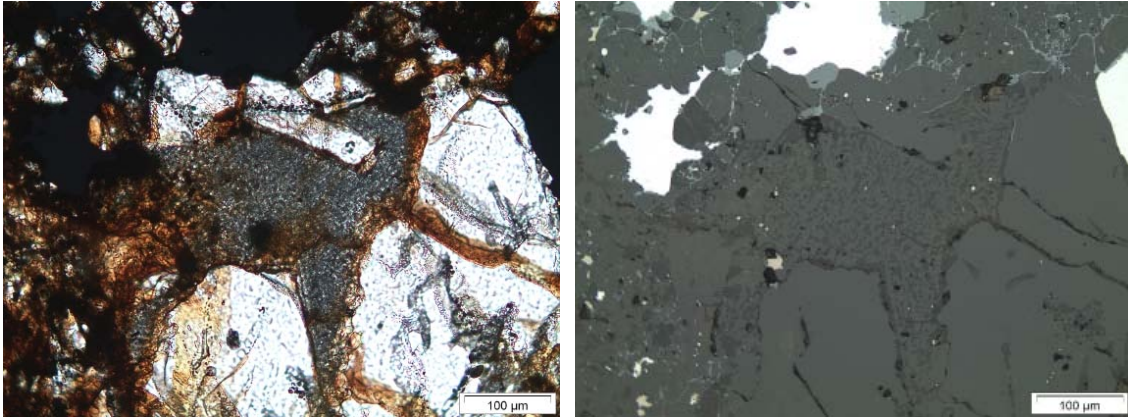
Micro-camel composed of feldspar with a rusty leash in JaH 578, H6 S2 WD1.0.

Left: transmitted light, right: reflected light.

Chapter 6

Terrestrial age estimation of ordinary chondrites from Oman based on a refined weathering scale and other physical and chemical weathering parameters

Terrestrial age estimation of ordinary chondrites from Oman based on a refined weathering scale and other physical and chemical weathering parameters

Florian J. ZURFLUH[1]*, Beda A. HOFMANN[2], Edwin GNOS[3] and Urs EGGENBERGER[1] and A. J. Timothy JULL[4]

[1]Institut für Geologie, Universität Bern, Baltzerstrasse 1 + 3, CH-3012 Bern, Switzerland
[2]Naturhistorisches Museum der Burgergemeinde Bern, Bernastrasse 15, CH-3005 Bern, Switzerland
[3]Muséum d'histoire naturelle de la Ville de Genève, 1 Route de Malagnou, CP 6434 CH-1211 Genève 6, Switzerland
[4]NSF-Arizona AMS Laboratory, The University of Arizona, 1118 East Fourth St., Tucson, Arizona 85721, USA
* Corresponding author. E-mail address: florian.zurfluh@geo.unibe.ch

Abstract - Over 100 ^{14}C dated ordinary chondrites from Oman (n=101, so far unpublished: n=51; corrected for pairing) were investigated for macroscopically visible weathering parameters, for thin section based weathering classification and for chemical parameters analyzed with handheld XRF (HHXRF). Macroscopic weathering parameters are based on: i) fusion crust conservation on exposed surfaces (ES); ii) wind ablation on ES; iii) salt contamination on cut surfaces (CS); iv) attached sand on ES; v) filled pores on CS and vi) color difference between ES and the buried surface (BS). The weathering degree (WD) is evaluated in thin section using a refined weathering scale based on the current W0 to W6 classification (Wlotzka, 1993), with newly included intermediate steps WD3.0, WD3.3 and WD3.6 as well as WD4.0 and WD4.5. Chemical parameters used are the contamination of Sr on CS, Sr on ES, Ba on natural surface (NS), V on ES, the enrichment of Mn on NS relative to Mn on CS and the Fe/Mn ratio on CS. Back-calculations of terrestrial ages based on weathering parameters for 55 ^{14}C-dated samples show a good correlation between the age estimate based on the mean of all weathering parameters for individual meteorites and the respective ^{14}C age (median relative deviation: 13%, mean relative deviation: 31%, r=0.77). Based on the correlations of these weathering parameters, terrestrial ages are estimated for meteorites found during fieldwork in 2009 and 2010. The comparison of ^{14}C ages and estimated ages demonstrates that is it possible to estimate terrestrial ages of Oman meteorites based on weathering parameters alone. The correlation between terrestrial age and the newly defined weathering subclasses WD3.0 to WD4.5 demonstrates that the addition of these classes is meaningful and improves terrestrial age estimation.

6.1. INTRODUCTION

The study of meteorites is of fundamental interest for understanding the early history of our solar system. The majority of available meteorites are finds, affected in variable magnitude by terrestrial weathering. Most of these meteorites are recovered from hot deserts where weathering rates are lower than in more humid areas. Several studies have been performed to quantify terrestrial alteration of hot desert meteorites by Mössbauer spectroscopy (e.g. Bland et al., 1998), geochemical investigations (Al-Kathiri et al., 2005; Crozaz et al., 2003; Hezel et al., 2011) or iron isotope analyses (Saunier et al., 2010). These methods for quantification of weathering are all relatively sophisticated, expensive and time consuming and thus not applicable to large numbers of hot desert meteorites. To obtain weathering information for larger datasets, several schemes for classification of weathering were invented using simple and fast methods. A need for relatively simple ways to quantify weathering by several methods was originally proposed by Gooding (1986) due to the large amounts of samples found in Antarctica. These meteorites are classified by a weathering index, using the macroscopically visible degree of rustiness into categories A, B and C (Cassidy, 1980). For meteorites with evaporitic deposits a lower-case "e" was proposed (Velbel, 1988). This scheme allows a rapid estimation of the weathering degree, but the resulting classification is vague and depends on the person doing the classification. Also, the physical meaning of the weathering categories is not clear (Gooding, 1989; Ikeda and Kojima, 1991; Losiak and Velbel, 2011). Later, as large numbers of meteorites were recovered from hot deserts, classification of the weathering was proposed using thin sections with a scales ranging from A to C (Jull et al., 1990), A to E (Jull et al., 1991) or A to D (Jull et al., 1993). A slight modification was then proposed with weathering grades W0 to W6 (Wlotzka, 1993), and this system is currently in use for non-Antarctic meteorites. However, as the original publication is a not peer-reviewed abstract and contains several ambiguities, in this study, a refined weathering degree is used, which is based on the Wlotzka (1993) weathering grade.

The determination of the terrestrial ages is crucial for understanding weathering rates. Meteorites from hot deserts survive shorter time spans than meteorites from Antarctica (e.g. Jull, 2006) and can therefore be dated by the use of cosmogenic ^{14}C, that was produced in situ during travel in space (e.g. Jull, 2006). Terrestrial age dating of meteorites also allows

determining minimum ages of accumulation areas and geomorphological studies can be supported by terrestrial ages of meteorites. If a large population from an accumulation area is dated, calculation of meteorite flux is possible (Zolensky et al., 2006). Since meteorites record conditions from the environment, paleoclimatic studies would be likely to perform on meteorites since their pre-terrestrial composition is well-defined by falls and they are found in all areas on Earth (Bland, 2006). One of the features recognized is the contamination of hot desert meteorites with terrestrial Sr and Ba (Al-Kathiri et al., 2005; Crozaz et al., 2003; Nazarov et al., 2004; Saunier et al., 2010; Shih et al., 2002; Stelzner et al., 1999). Initial concentrations in ordinary chondrites are 9 µg/g to 11 µg/g Sr and 3 µg/g to 5 µg/g Ba (Wasson and Kallemeyn, 1988). Even within a short time, the concentrations of these elements can be doubled as it was observed in samples of the Holbrook 1912 fall collected in 1968 (Gibson and Bogard, 1978). Previous studies of bulk chemistry and weathering grades of ^{14}C dated meteorites showed a correlation of weathering features with terrestrial age of meteorites from Oman (Al-Kathiri et al., 2005).

We have developed a relatively simple and, as compared to ^{14}C method, quick way to estimate the terrestrial age of ordinary chondrites using a combination of macroscopically visible weathering features, weathering degree determined in thin section and chemical contamination measured with simple, quick and non-destructive handheld XRF analyses (Zurfluh et al., 2011). Previously, the dating of meteorites from Antarctica by their degree of contamination with fluoride was attempted (Krähenbühl et al., 1998; Noll et al., 2003). Because we have access to many samples (whole rocks, not only thin sections or cut slices) from the find location through classification to storage allows us to perform studies on weathering and contamination including macroscopic, microscopic, environmental and chemical parameters and also to identify patterns that are dependant on local geography situation or geology.

In a first step of this study, we evaluate methods to estimate the terrestrial age of ordinary chondrites (OC) from Oman based on correlations between weathering parameters and ^{14}C ages. In a second step, the ages of ^{14}C-dated samples are then back-calculated to demonstrate the feasibility of the approach and to estimate its levels of uncertainty. In a third step, the method is applied to all OC samples found during our 2009 and 2010 field campaigns.

6.2. SAMPLES AND ANALYSES

6.2.1. Ordinary chondrites from Oman

For this study, ordinary chondrites (OC) found in the hot desert of Oman by the Omani-Swiss Meteorite Search expeditions (e.g. Hofmann, 2004) were investigated. Some of these meteorites (found 2001 to 2003) were part of an earlier study (Al-Kathiri et al., 2005). Meteorites are carefully documented in the field including a description of the soil surface. Samples are packed without touching in polypropylene bags for transportation. Unpacking is performed wearing gloves to avoid contamination. Samples are cleaned from attached soil using pressurized air. Meteorites were cut using isopropanol and polished thin sections were prepared. They were investigated under optical microscope and electron microscopes (scanning electron microscope, SEM with EDS: Zeiss EVO50 and electron microprobe, EMP: Jeol JXA-8200) at the Institute of Geological Sciences, University of Bern.

6.2.2. Terrestrial age determination

The terrestrial ages of the meteorites were calculated from the content of cosmogenic ^{14}C in 0.04 g to 2.4 g (typically 0.5 g) subsamples of ordinary chondrites. Radiocarbon concentrations were analyzed using methods described elsewhere (Bland et al., 1998; Jull, 2006; Jull et al., 1989; 1990; 1993; 1998). To remove terrestrial carbon contamination, samples were cleaned with 85% phosphoric acid (to remove terrestrial carbonates) and heated to 500°C in air (to remove terrestrial low temperature components). All ^{14}C analyses were performed at the NSF-Arizona AMS Laboratory, University of Arizona, Tucson.

6.2.3. Description of macroscopic weathering features

Macroscopically visible weathering effects were estimated for all radiocarbon-dated meteorites and all samples collected during field campaigns 2009 and 2010 using a simple intensity scale ranging from 0 to 3 for each parameter (Table 6.1). The following parameters were determined: i) The degree of preservation of fusion crust (FC) on exposed surface (ES); ii) intensity of wind ablation (Fig. 6.1a); iii) abundance of salt efflorescence/hygroscopic behavior due to the contamination with water-soluble salts, as visible on cut surfaces (CS); iv) occurrence of attached sand on exposed surface (ES, Fig. 6.1b, c); v) the amount of filled pore pace as seen on CS (Fig. 6.1c) and vi) color difference between ES and buried surface (BS), mainly due to the development of a reddish coloration of the BS.

Table 6.1. Macroscopic weathering parameters

Intensity Code	Abbreviation	N = 0	N = 1	N = 2	N = 3
Wind ablation on [ES]	WA	No wind ablation visible	FC/rock surface with cavities/mild wind-polishing	"Monadnocks"/strong polishing	Ventifact, striation visible
Sand on [ES]	Sand	No attached sand	Some isolated sand grains attached	Some isolated sand-grain-aggregates attached	Abundant sand-grain-aggregates attached
Fusion crust (FC) on [ES]	FC	No FC [<2%] preserved	Some FC remnants [2-20%]	FC partly eroded [20-80%]	FC preserved [>80%]
Salt on [CS]	Salt	No salts or hygroscopic behavior visible	Few isolated droplets of hygroscopic salts	Some spots of hygroscopic salts	Extreme salt efflorescence/hygroscopic behavior
Pore space on [CS]	PO	No macroscopic pore space	Empty pores	Pore space partially filled	All pore space filled
Red [BS]	Red	Same as [ES]; rock-color chart: if FC present: N1, fresh and broken samples: N3 to N5, weathered and broken samples: 5YR 2/2	Small area of [BS] has slightly reddish color; rock-color chart: 5YR 2/2 to 5YR 3/4	Abundant red, >10% of BS; rock-color chart: 5YR 3/4 to 5YR 5/6	Bright rusty/red, >75% of BS; rock-color chart: 5YR 4/6 to 5YR (3 to 5)/4

CS: Cut surface, BS: Buried surface, ES: Exposed surface.

The color difference is established using the rock color chart (Goddard, 1948). Surfaces of fresh meteorites are either black at regions with FC (N1) or grey on broken surfaces (N3 to 5). With increasing weathering, the alteration mineralogy is responsible for a dark, dusky brown color (5YR 2/2) of the meteorites. If a "red BS" evolves, the part of the meteorite buried in the soil attains a light brown color of 5YR (4 to 5)/6 or 5YR (3 to 5)/4 (Table 6.1,

Fig. 6.1d). These effects are examined by naked eye and with the use of a binocular microscope. All samples were investigated independently by at least two persons to reduce personal bias. The criteria are defined in Table 6.1 and Figure 6.1. In addition to these six macroscopic weathering parameters (MWP), we have explored others such as the amount of greenish staining due to Ni-serpentine precipitation on BS (Al-Kathiri et al., 2005), the amount of cracks due to weathering and the infiltration of soil material into such cracks, the preservation of FC on BS, the amount of attached caliche or calcite on BS, the abundance of metal grains on CS and the coverage of the meteorites with lichen. The correlation of all parameters with terrestrial age was evaluated.
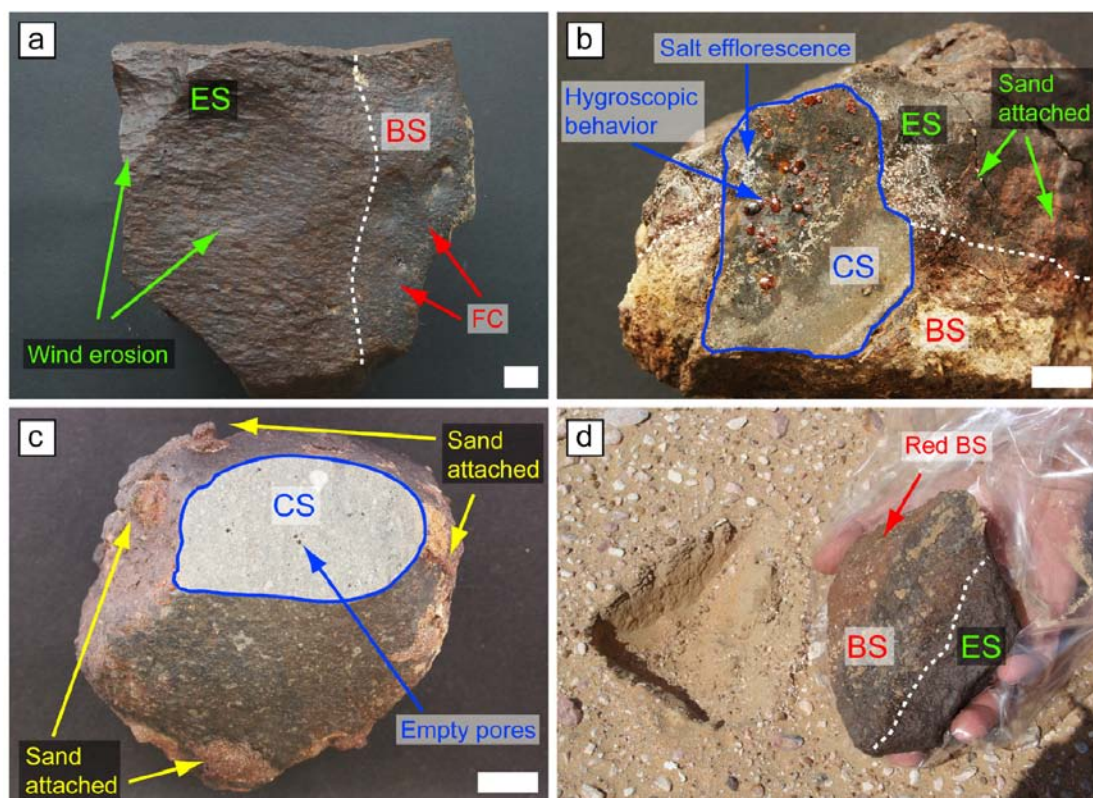
Figure 6.1. *Macroscopically visible weathering parameters. a) RaS 381, L6 S3 WD3.3, shows prominent wind erosion on the exposed surface (ES). The buried part (BS) has still some remnants of fusion crust (FC). b) The cut surface (CS) of JaH 100, H4-5 S1 WD3.0, shows efflorescence due to contamination with hygroscopic salts. Salt efflorescence also occurs on the exposed surface (ES) and some sand grains are attached due to precipitation of iron hydroxides on ES. The buried surface (BS) has attached caliche. c) Meteorite RaS 401, L3.8 S2 WD3.3, recovered near dunes displays patches of attached sand. Empty pores are visible on cut surface (CS). Scale bar of a, b and c is 1 cm. d) The buried part of RaS 284, LL5 S1 WD 3.3, has a slightly reddish color and is distinct in color to that of ES.*

6.2.4. Classification of weathering degree

The grade of weathering of meteorites is currently reported using thin-section observation and the scale defined by Wlotzka (1993). This classification scheme was published in an abstract and some of the steps are not well-defined, in particular W3 (Fig. 6.2a). Following Wlotzka (1993) W3 is defined as "heavy oxidation of metal and troilite, 60-95% being replaced". It remains unclear whether the percentage refers to the sum of troilite+metal or to each phase individually. Because weathering degree W2 just takes into account the oxidation of metal, depending on interpretation, this results in an undefined gap for meteorites with >60% of metal and <60% of combined metal+troilite altered. This is particularly relevant because many meteorites recovered in Oman show metal oxidation close to 95 % while troilite is still relatively fresh, i.e. altered <20%. It is well established that metal is oxidized first in meteorites under hot desert conditions whereas the alteration of troilite is slower (e.g. Al-Kathiri et al., 2005; Lee and Bland, 2004). There are only a few exceptions where troilite is weathered preferentially compared to metal. Examples are two L chondrites from Western Australia at initial stages of weathering (Bevan et al., 2001; Ruzicka, 1995). Samples from Antarctica often show no or only minor alteration of troilite (Lee and Bland, 2004). We therefore introduce intermediate steps to the weathering grades W3 and W4 and a more detailed description of the altered phase (Table 6.2). Our scale is named weathering degree (WD). Due to incomplete definition of the W2 to W3 boundary by Wlotzka (1993) in the original publication, we consider the upper limit of W2 (60% metal oxidation) as the lower limit for W3 (Fig. 6.2). W3 is further divided into WD3.0, WD3.3 and WD3.6 based on troilite oxidation of <20%, 20% to 60% and >60%, respectively. The boundary to W4 remains at 95% oxidation of metal and 95% oxidation of troilite. We include an additional extension WD4.5 to account for samples where essentially no metal and troilite is left (if not fully enclosed in silicates). The Wlotzka (1993) definition of W5 is actually problematic, as we often observe beginning alteration of mafic silicates in samples belonging to W3 based on metal and troilite oxidation (Fig. 6.3). We have only one sample classified as WD5.0 and the definition of this step remains vague. Stage WD6.0 was not observed in our collection and is adopted unmodified (Table 6.2).

Table 6.2. The refined weathering degree classification

Weathering degree	Metal oxidation [vol%]	Troilite oxidation [vol%]	Comments
WD0.0	0	0	Fresh, some iron-hydroxide staining possible
WD1.0	<20	≥0	Minor oxide rims around metal and troilite, small iron oxides and iron hydroxide veins might be already present
WD2.0	20 to 60	<20	Onset of veining with iron oxides and iron hydroxides
WD3.0	>60	<20	Strong oxidation of metal, troilite shows only minor alteration
WD3.3	>60	20-60	Strong oxidation of metal, troilite moderately altered. Usually a few troilites are completely oxidized
WD3.6	>60[§]	>60[§]	Strong oxidation of metal and troilite. Most troilites are oxidized or show reduced reflectivity.
WD4.0	>95	>95	Nearly complete oxidation of metal and troilite, usually some troilite remnants are visible
WD4.5	100	100	All metal and troilite oxidized, only minor remnants of metal and troilite as inclusions in silicates
WD5.0*	100	100	Metal and troilite 100% oxidized, major alteration of silicates, mainly olivine.
WD6.0[#]	100	100	Massive replacement of silicates by clay and oxides

[§] When metal and troilite both individually are oxidized >95vol% the sample is classified as WD4.0, but a sample with 100 vol% metal alteration and 90 vol% troilite alteration is still a WD3.6.
* Since we have only one WD5.0 sample in our collection, the definition of this step is still vague.
[#] WD6.0 if fully adopted from Wlotzka (1993) since we have no such sample in our collection.
Classification guide:
i) Weathering degree is designed for ordinary chondrites but might be used for other metal-, troilite- and silicate bearing meteorites.
ii) The thin section should be prepared from a representative part of the interior of the sample. If several stages are visible take the mean.
iii) Troilite and metal inclusions in shock veins, shock melts or other protected grains have to be excluded for classification.

W3 actually comprises the major part of the alteration history of ordinary chondrites. Our refined scale for weathering degree (WD) classification is compatible with the previous scale e.g. a previous W3 meteorite will remain at the same stage but could be either a WD3.0, WD3.3 or WD3.6 (Fig. 6.2b). The stages W0, W1 and W2 were adopted unmodified. To take also in account the preferred weathering of troilite as observed in Australian chondrites (Bevan et al., 2001; Ruzicka, 1995) further division of weathering stages W1 and W2 similar to W3 to WD3.0, WD3.3 and WD3.6 might be applied. Since we have no such sample in our collection and the general weathering trend worldwide never appears to reach this stages, we have not included them into our scheme. However, if such a weathering path is found, we would propose to use criteria for those stages analogous to WD3.X. Weathering degree 1.X has always metal oxidation <20%. At stage WD1.0 troilite is also <20%, at stage WD1.3 troilite is between 20 to 60% and for WD1.6 troilite is altered >60%. Samples at WD2.X have metal oxidation of 20 to 60%. The most meteorites have troilite oxidation of <20% and are classified as WD2.0. If higher alteration of troilite occurs, WD2.X could be divided in

WD2.3 for troilite alteration of 20 to 60% and WD2.6 for troilite oxidation of >60% (dashed lines in Fig. 6.2b).
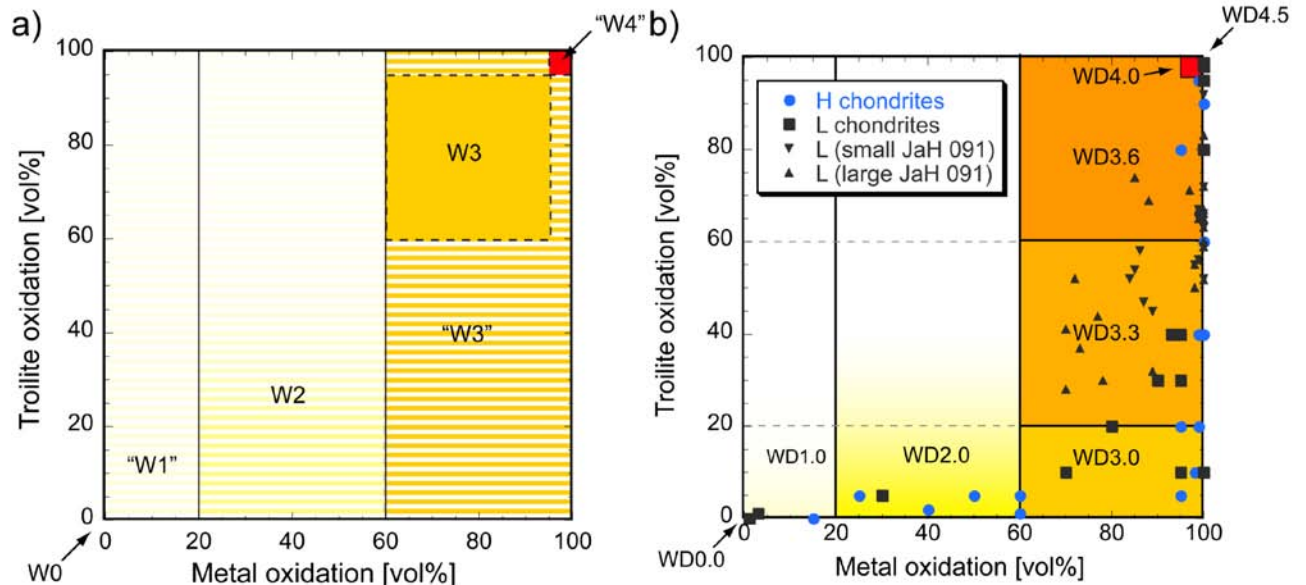
Figure 6.2. *Graphical display of the weathering classification scales. a) Interpretation of the weathering grade classification by Wlotzka (1993). Metal oxidation of 20-60% defines W2. If the text for W3 is interpreted as referring to the percentage of metal and troilite that are altered both individually to 60-95%, only the area represented by the square outlined with dashed lines corresponds to W3. If "W1" and "W3" are defined by exclusion of well-defined W2, the "W3" is indicated the horizontally striped field including the W3 square and "W1" would indicate all samples with metal oxidation <20%. "W4" is interpreted to be >95% alteration of metal and troilite individually. b) Our refined classification of weathering degrees divides W3 into three intermediate steps based on oxidation of troilite (WD3.0, WD3.3 and WD3.6) The dashed lines indicate possible further subdivisions for WD1.X and WD2.X samples (not realized in our samples). Plotted data is from ordinary chondrite samples from Oman indicating typical weathering paths (Al-Kathiri et al., 2005).*
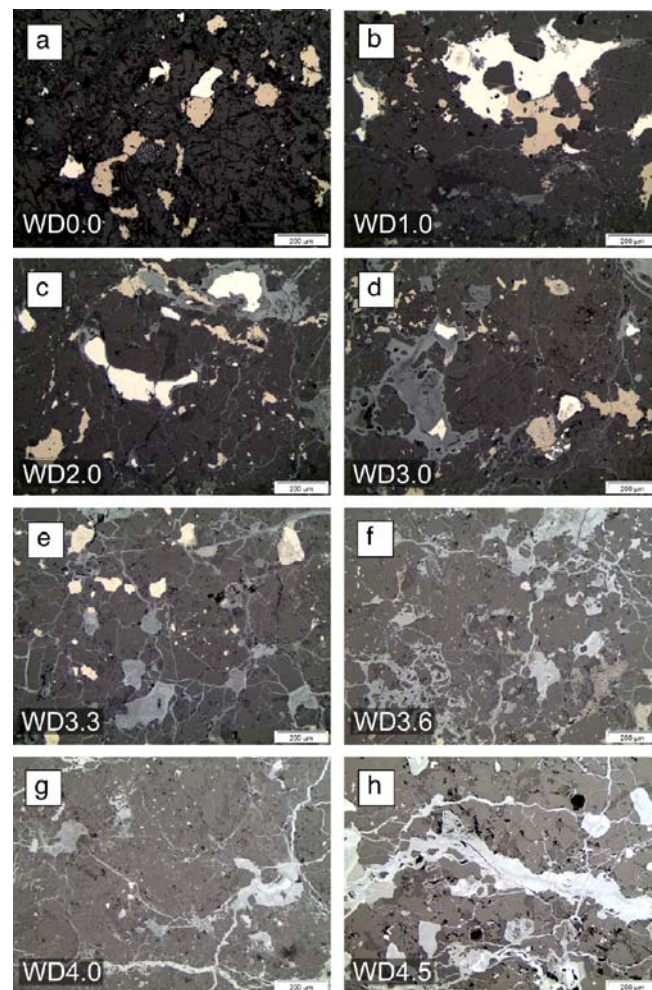
Figure 6.3. *Reflected light photomicrographs of ordinary chondrites from Oman showing different weathering degrees. Note the continuous alteration of Fe-Ni-metal (white) and yellowish troilite to grey iron oxides and iron hydroxides and the onset of iron hydroxide and iron oxide veins. Scale bar at bottom right is 200 µm. a) SaU 424, L6 S3 WD0.0 b) JaH 578, H6 S2 WD1.0 c) RaS 311 H4-6 S3 WD2.0 d) Al Huqf 069, H4/5 S2 WD3.0 e) RaS 304, H6 S2 WD3.3 f) RaS 114, H5 S1/2 WD3.6 g) RaW 022, H5 S3 WD4.0 h) RaW 041, H6 S1 WD4.5*

6.2.5. Quantification of terrestrial elemental contamination

All ^{14}C dated meteorites and all meteorites found in 2009 and 2010 were non-destructively analyzed for their chemical composition with a Thermo Scientific NITON XL3t-600 handheld energy dispersive X-ray Fluorescence (HHXRF) analyzer placed in a mobile test stand. To obtain proper results for meteorites a slightly adjusted calibration of the "mining mode" was used (Zurfluh et al., 2011). Elements of interest are K, Ca, Ti, V, Cr, Mn, Fe, Co,

Ni, Zn, As, Sr, Mo, Ba and Pb. Measurements were performed on exposed surfaces (ES), buried surfaces (BS) and cut surfaces (CS). Since it is not possible to reconstruct the find situation of each meteorite, the more general term "natural surface" (NS) is used for unspecified surfaces. NS represents also the mean of ES and BS integrated over the whole meteorite. Each surface was measured at least three times and the median values of all measurements on one surface were taken for further calculations. All elements of interest were evaluated for their correlation with terrestrial age. We call them chemical parameters (CP).

6.3. RESULTS AND AGE ESTIMATIONS

6.3.1. C-14 ages

The terrestrial ages of 50 meteorites from Oman were reported by Al-Kathiri et al., (2005). Additional data were determined by Jull et al., (2008) and Giscard et al., (2009). 51 new terrestrial ages are reported in this paper (Table 6.3). Meteorites for terrestrial age determination (after the first set of 50 analyses) were selected using the following criteria: (1) all individual samples found on the Jabin plateau (21° 0-24'N 28° 22-26'E) west of the Wahibah sands in the meteorite recovery area Ramlat al Wahibah (RaW), an area underlain by lithified dune sands with a maximum age of about 120 ka (Preusser et al., 2002; Radies et al., 2004); (2) all LL chondrites of the campaigns from 2001 to 2009; and (3) selected samples covering a profile from the Arabian sea coast to inland including all stages of the modified weathering degree. Meteorites with weights between 200 g and 2000 g were selected and samples from meteorite showers were avoided. The 51 new ages comprise 8 LL, 17 L and 26 H chondrites. Overall, the ages range from <1 ka up to the limit of the ^{14}C method (>38.5 ka, depending on sample size). New and so far unpublished samples are summarized in Table 6.3. The mean age of the newly-dated meteorites is 19.6 ka (median: 17.9 ka; st. dev.: 10.2 ka), which is congruent to the mean of the previous population, 21.5 ka (median 17.9 ka; st. dev.: 13.0 ka; Al-Kathiri et al., 2005). For all dated meteorites, the mean

terrestrial age is 19.9 ka whereas the percentage of samples 0 to 10 ka is 19% and of samples >30 ka is 25%.

Table 6.3. Classification and new terrestrial ages of OC from Oman.

Name	N [°]	E [°]	Class	P	S	WD	^{14}C [dpm kg^{-1}]	^{14}C error [dpm kg^{-1}]	TA [ka]	TA error [ka]
Al Huqf 063	19.4453	57.0234	L	6	S2	3.6	3.0	0.8	23.4	2.6
Al Huqf 065	19.3209	57.2298	L	6	S5	2.0	49.4	2.0	0.3	1.3
Al Huqf 069	19.2680	57.1341	H	4/5	S2	3.0	0.7	0.3	34.3	3.5
JaH 343	19.7517	56.5798	LL	6	S3	1.0	24.5	1.0	6.7	1.3
JaH 413	19.8299	56.5770	H	4	S1	3.0	10.1	1.0	12.6	1.5
JaH 416	19.7872	56.4216	L	6	S5	4.0	2.9	0.8	23.8	2.7
JaH 418	19.7923	56.4262	H	4	S3	3.6	1.9	1.0	26.2	4.5
JaH 423	19.7833	56.4139	H	4	S3	3.3	5.3	0.6	18.0	1.6
JaH 474	19.8142	56.4456	LL	3.7-6	S2	3.0	27.7	1.1	5.7	1.3
JaH 493	19.7845	56.4167	L	6	S3-4	3.3	2.5	0.8	25.0	3.1
JaH 498	19.7922	56.4098	L	6	S4	3.6	1.7	0.8	28.9	4.0
JaH 578	19.7642	56.2989	H	6	S2	1.0	10.1	0.4	12.6	1.3
JaH 579	19.3542	56.7529	L	4-6	S3-5	3.3	7.3	0.5	15.3	1.4
JaH 620	19.3713	55.3692	L	6	S4	2.0	14.4	0.7	9.7	1.4
QaM 001	21.3702	57.7291	LL	4-6	S2	3.0	25.6	0.6	6.3	1.3
RaS 242	20.0180	56.4180	LL	4	S3	3.0	2.8	0.6	24.5	2.3
RaS 262	20.0135	56.4070	LL	6	S3	1.0	25.6	0.9	6.4	1.3
RaS 267	20.5971	56.1509	LL	6	S1	4.0	1.4	0.7	30.5	4.4
RaS 281	20.5709	56.3885	H	3.4-6	S2	3.0	5.3	0.3	17.9	1.4
RaS 290	20.5234	55.5307	L	6	S4	3.3	5.4	0.4	17.7	1.4
RaS 292	20.5983	55.5240	L	6	S2	3.0	14.1	0.3	9.8	1.3
RaS 295	20.6697	55.4281	H	4	S2	3.0	18.6	1.0	7.5	1.4
RaS 297	20.6675	55.3172	L	6	S4	4.5	2.2	0.3	25.1	1.7
RaS 302	20.1448	56.2409	H	4	S2	3.6	0.7	0.4	35.0	5.7
RaS 304	20.4380	56.1028	H	6	S2	3.3	6.2	0.4	16.6	1.4
RaS 316	20.8949	55.5061	L	5	S3	4.5	6.5	0.3	16.3	1.4
RaS 322	20.9190	55.4119	H	3.7	S1	3.0	13.7	0.3	10.1	1.3
RaW 002	21.3703	58.4046	H	4-5	S2	2.0	8.1	0.9	14.4	1.6
RaW 005	21.2251	58.4116	H	5	S3	4.0	0.7	1.2	34.2	13.1
RaW 007	21.1746	58.4092	H	5	S2	4.0	2.0	0.8	25.9	3.5
RaW 008	21.1683	58.3914	L	4	S2	3.0	2.3	0.8	25.5	3.2
RaW 010	21.1383	58.3636	H	4	S2-3	4.0	2.3	1.2	25.0	4.4
RaW 014	21.0598	58.4043	H	5	S2	2.0	20.2	0.9	6.9	1.3
RaW 015	21.1728	58.4217	H	5	S3	3.0	9.1	0.8	13.4	1.5
RaW 016	21.1664	58.4103	L	6	S4-5	4.5	1.0	0.6	32.5	5.4
RaW 017	21.1584	58.3892	H	5	S2	3.0	19.6	1.1	7.1	1.4
RaW 019	21.2127	58.3864	H	6	S1	4.5	0.9	0.8	32.2	7.1
RaW 021	21.1520	58.4139	H	5	S1	4.0	1.4	1.1	28.9	6.4
RaW 024	21.3763	58.4277	H	5	S2	1.0	32.7	1.2	2.9	1.3
RaW 027	21.2601	58.3915	H	5	S2-3	4.5	0.5	0.9	37.0	13.5
RaW 031	21.2733	58.3965	H	4	S2	3.0	3.3	0.9	22.0	2.7
RaW 034	21.3623	58.4118	LL	3-5	S2	0.0	23.9	1.0	6.9	1.3
RaW 035	21.3686	58.3977	H	5	S2	3.6	2.3	1.3	24.9	4.9
RaW 032	21.3380	58.4115	L	6	S4	4.5	n.a.	n.a.	>38.5	
RaW 038	21.3705	58.4140	H	5	S2	4.5	n.a.	n.a.	>34.8	
SaU 420	20.9224	56.8868	LL	6	S2	3.3	12.2	0.9	12.5	1.4
SaU 523	20.4153	56.6655	L	6	S4	3.3	6.5	1.1	16.3	1.9
Shalim 008	18.8680	55.4507	H	5	S3	2.0	5.8	0.3	17.2	1.4
UaS 009	21.0649	56.4819	L	6	S4	4.0	0.9	0.4	32.5	3.6
UaS 011	21.3760	56.2911	H	4	S1	3.0	3.1	0.4	22.4	1.6
UaS 013	21.3728	56.3138	L	6	S4	2.0	7.8	0.3	14.8	1.3

P: Petrologic type.
S: Shock level.
WD: Weathering degree.
TA: Terrestrial age.
n.a.: Not available.

6.3.2. Macroscopic weathering parameters

All previously described macroscopic weathering parameters were evaluated for their correlation with the ^{14}C terrestrial age. The following ones were found to be useful for terrestrial age estimation: i) the degree of preservation of fusion crust on ES; ii) the degree of wind ablation on ES; iii) the amount of salt contamination; iv) the quantity of attached sand; v) the degree of filling of the pore space; and vi) the color difference between BS and ES (Fig. 6.4). The other parameters show no evident correlation with terrestrial age (Greenish staining due to Ni-serpentine precipitation on BS, cracks and crack fillings, calcite deposition on BS), are not recorded from a sufficient number of samples (metal flakes visible on CS, coverage of meteorite by lichen) or are already included in other parameters (FC on BS is similar to FC on ES, metal on CS is comparable to the weathering degree). The age dependence of the macroscopically visible weathering parameters was evaluated using the median ^{14}C ages of each weathering category (Fig. 6.4). With decreasing amounts of FC the terrestrial age increases (Fig. 6.4a). Wind ablation is more pronounced with increasing terrestrial age (Fig. 6.4b). Hygroscopic salts and attached sand are only present on OC with terrestrial ages between approximately 5 and 30 ka, with a maximum at ~15 ka. The intensity of pore infill increases with age and the color difference between BS and ES becomes much more pronounced for older meteorites (Fig. 6.4). Based on these observations, equations for a calculation of estimated terrestrial ages for each parameter were extracted using the linear regression of the medians of each category. The resulting equations are rather similar for the individual parameters. Equation 6.1 is the correlation of FC on ES with terrestrial age, eq. 6.2 for the wind ablation, eq. 6.3 for pore space filling and eq. 6.4 for red BS.

$$T_{(FC)} = -5.5N_{(FC)} + 26.56 \qquad \text{(eq. 6.1)}$$

$$T_{(WA)} = 4.6N_{(WA)} + 15.6 \qquad \text{(eq. 6.2)}$$

$$T_{(PO)} = 4.3N_{(PO)} + 15.3 \qquad \text{(eq. 6.3)}$$

$$T_{(Red)} = 4.5N_{(Red)} + 17.0 \qquad \text{(eq. 6.4)}$$
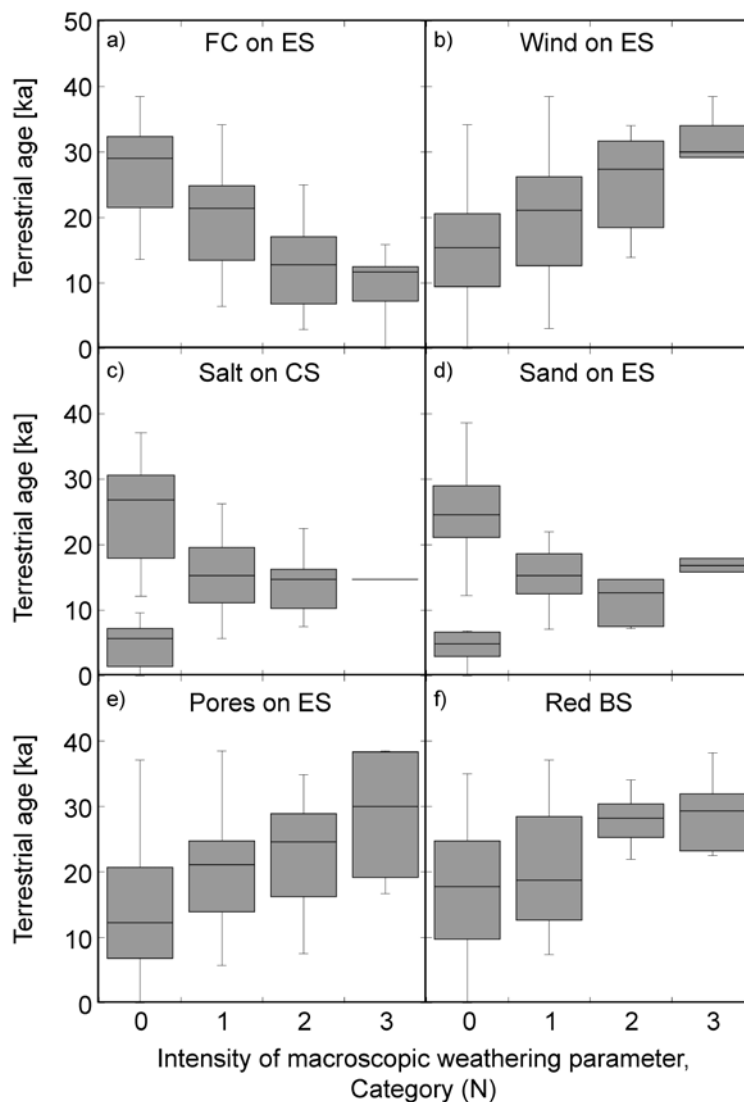
Figure 6.4. *Summary of terrestrial ages as a function of macroscopically visible weathering parameters for ordinary chondrites. The grey box represents 50% of the data whereas the horizontal line within the box marks the median value. The thin vertical lines display the full range of the data.*

Where T is the estimated age in ka based on N (number of the category, e.g. FC for fusion crust, 0 to 3).

The level of salt contamination and amount of attached sand are not linearly dependent on age (Fig. 6.4). To ascertain terrestrial ages for those two parameters, the number of the category (N, 0 to 3) has to be replaced with the median age value of the corresponding category as visible in Figure 6.4. For salt contamination $N_{(Salt)} = 1$ a terrestrial age, $T_{(Salt, N = 1)}$,

of 15.3 ka is estimated, 2 = 14,8 ka and 3 = 15.0 ka. Sand category, $N_{(Sand)}$ 1 = 15.5 ka, 2 = 12.6 ka and 3 = 16.9 ka. If a sample has $N_{(Salt)} = 0$ or $N_{(Sand)} = 0$ it can either be a very young or a very old meteorite (Fig. 6.4). Young meteorites have often still some FC preserved, show only minor wind ablation, have no reddish BS and metal flakes are present on CS. Therefore, if a sample has $N_{(Salt)} = 0$ or $N_{(Sand)} = 0$ and $N_{(FC)} \leq 1$, $N_{(W)} \geq 1$, $N_{(Red)} \geq 1$ and fresh metal is visible on CS (WD ≤ 2.0) an age estimation for $N_{(Salt)} = 0$ of $T_{(Salt)} = 6.9$ ka and $N_{(Sand)} = 0$ of $T_{(Sand)} = 4.0$ ka is used. Meteorites with $N_{(Salt)} = 0$ or $N_{(Sand)} = 0$ and $N_{(FC)} \geq 1$, $N_{(W)} \leq 1$ and no visible metal flakes on CS (WD ≥ 3.6) have an estimated terrestrial age of 28.0 ka for $N_{(Salt)} = 0$ and 24 ka for $N_{(Sand)} = 0$. If one of those criteria ($N_{(FC)}$, $N_{(W)}$, $N_{(Red)}$ and metal flakes on CS) does not clearly indicate the meteorite to be very young or very old, the age estimation is too uncertain and cannot be applied for $N_{(Salt)} = 0$ and $N_{(Sand)} = 0$.

Back-calculating estimated ages for the ^{14}C-dated samples using a combination of the six macroscopic weathering parameters yields a relatively narrow range of estimated terrestrial ages ($T_{(MWPA)}$). Only ages between 11.5 ka and 27.8 ka are covered using just macroscopic weathering parameters (Fig. 6.5) because the criteria used are weakly sensitive for very young or very old meteorites (Fig. 6.4). The correlation of the estimated ages with the ^{14}C terrestrial age is acceptable (r=0.73) but the slope is very steep, resulting in an overestimation of young and underestimation of high ages. Based on the fact of an existing correlation and known (^{14}C) terrestrial ages for this group, we applied an empirical correction to the data by forcing the regression line of the $T_{(MWPA)}$ through the origin and the centroid of the regression line ($\bar{y} = \bar{x}$) to reach a slope close to 1 (Fig. 6.5). Then, using the corrected correlation, the back-calculated ages were compared with the ^{14}C ages. The first estimated weathering age ($T_{(MWPA)}$) has to be corrected with equation 6.5:

$$T_{(MWPA\_corr)} = 2T_{(MWPA)} - 19.49 \qquad \text{(eq. 6.5)}$$

Using this equation the corrected macroscopic weathering parameter age ($T_{(MWPA\_corr)}$) is determined from the macroscopic weathering parameter age ($T_{(MWPA)}$). By applying this correction, the back-calculated age estimates obtained from macroscopic weathering ages range from 4.2 ka to 34.5 ka.
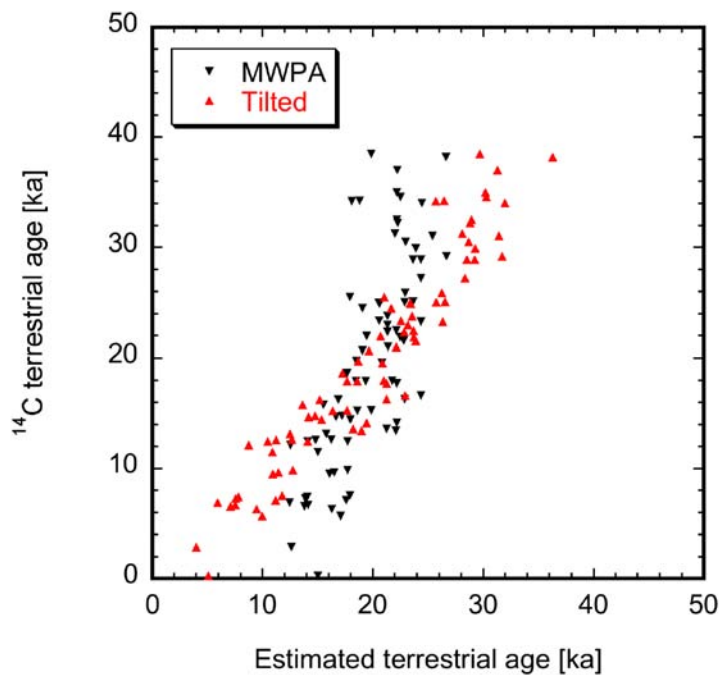
Figure 6.5. *Correlation of macroscopic weathering parameters ages (MWPA) with ^{14}C ages before (inverted triangles) and after (triangles) a correction consisting of forcing the correlation through the origin and the centroid. For age estimation the corrected relation has to be used.*

6.3.3. Weathering degree and terrestrial age

The weathering degree (WD) was determined for all newly dated meteorites and all previously ^{14}C dated meteorites from Oman with our refined scale. We observe a positive correlation of the refined weathering scale, notably for stages WD3.0 to WD4.5, with ^{14}C terrestrial age (Fig. 6.6). Since all three ordinary chondrite groups show similar weathering rates, the terrestrial age based on weathering degree (T_{WDA}) can be estimated using the linear regression of all data points (eq. 6.6):

$$T_{(WDA)} = 6.8N_{(WD)} - 1.28 \qquad\qquad \text{(eq. 6.6)}$$

Based on this relation e.g. a WD3.3 sample has an estimated terrestrial age of 21.2 ka. Age estimations ($T_{(WDA)}$) range from -1.3 ($\approx$0) ka (WD0.0) to 29.3 ka (WD4.5).
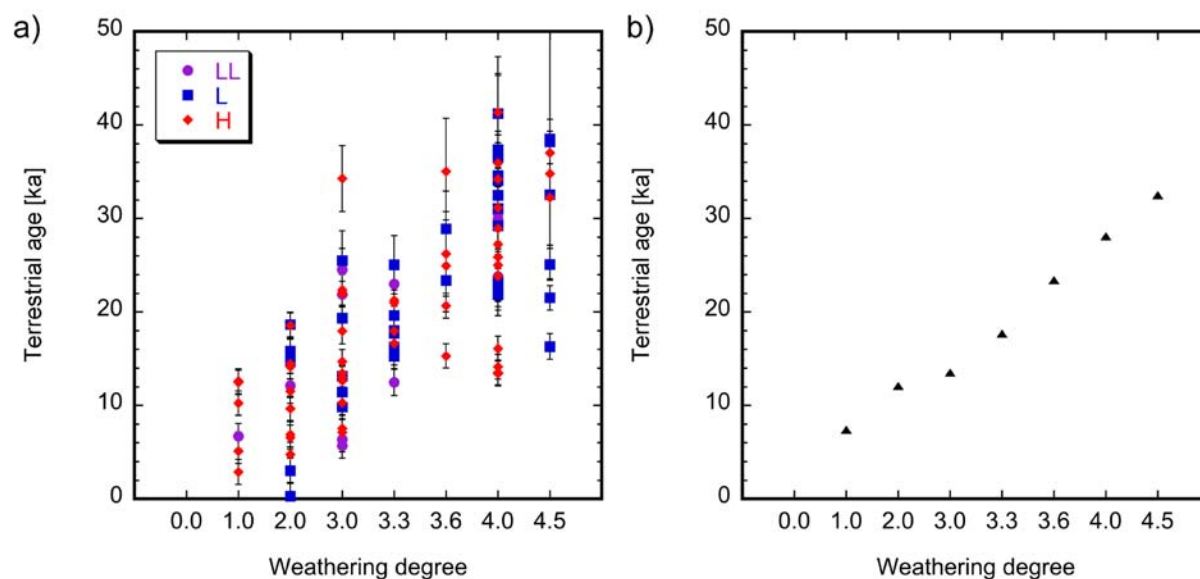
Figure 6.6. *Relation between terrestrial ages and weathering degrees of OC from Oman. a) In general, OC with longer terrestrial residence times are weathered to higher degrees. b) Median terrestrial ages of all ^{14}C dated OC from Oman showing the similar weathering speed of the three OC groups. Note the systematic increase of terrestrial ages among the newly defined weathering subgroups WD3.0-WD4.5.*

6.3.4. Chemical parameters

From the meteorites collected in Oman, 368 meteorites were examined by handheld XRF (HHXRF). In total, 5586 measurements were evaluated. The most prominent contamination elements are Sr and Ba. Highly-contaminated meteorites have interior (CS) concentrations of Sr and Ba of about 30 times the initial concentration. The highest concentration on CS is 888 µg/g for Sr and 554 µg/g for Ba, respectively. On natural surfaces of the meteorites, the contamination is usually much higher. Profiles measured through cut slabs of several meteorites showed relatively constant concentrations inside and highly elevated concentrations either on one or both of the natural surfaces (ES or BS; Fig. 6.7). In most analyzed meteorites, the accumulation of Sr and Ba, as well as of Mn and V, elements typically associated with desert varnish, is similar on ES and BS. Maximum values detected on natural surfaces (comprising ES and/or BS) are ~3500 µg/g for Sr and ~650 µg/g for Ba.
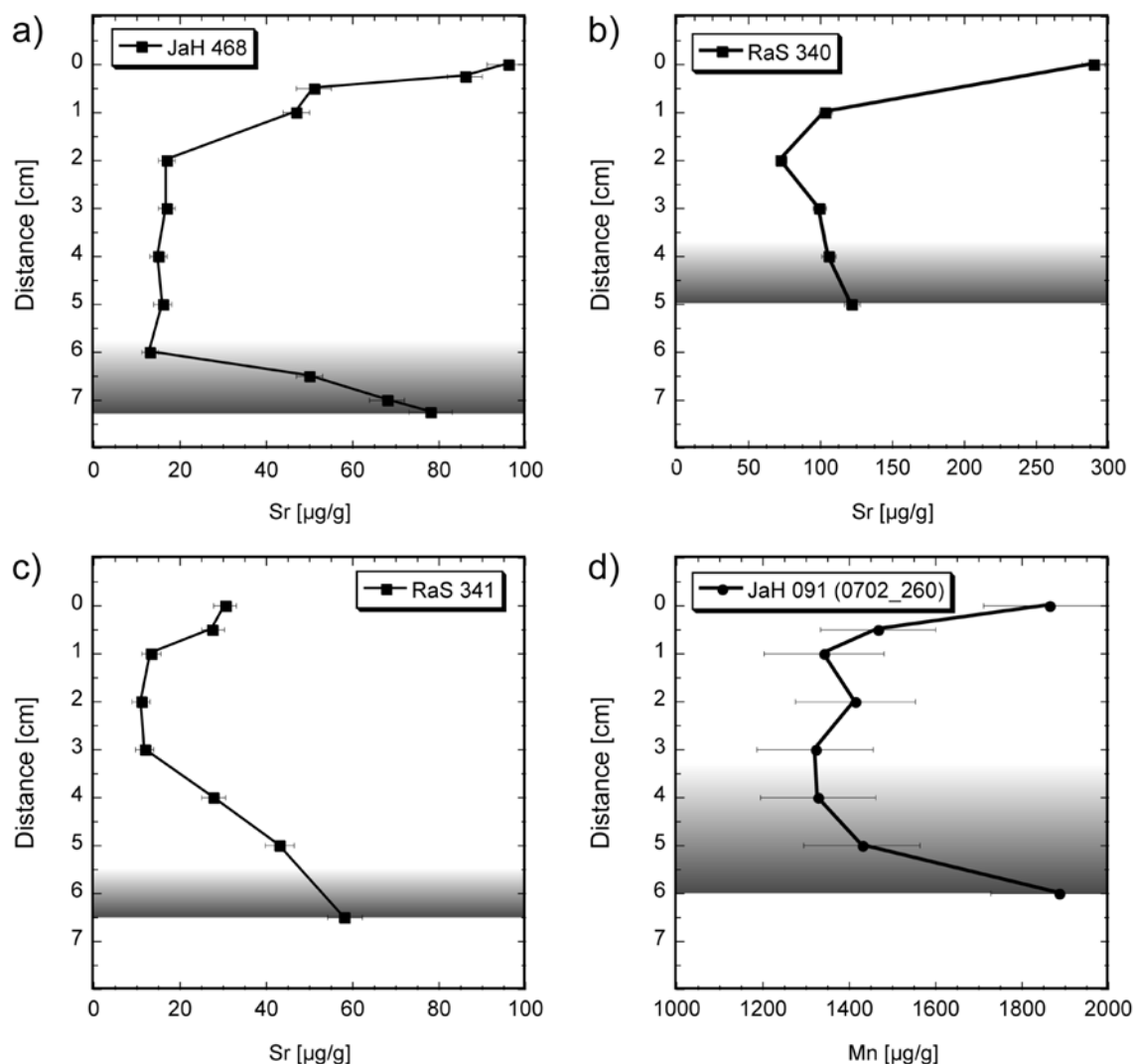
Figure 6.7. Profiles of Sr and Mn concentrations through cut surfaces of OC measured with HHXRF. Each measuring spot has a diameter of 8 mm. Point 0 is a spot measured on the exposed surface. The lowest point was obtained on BS. The gradient indicates the part of the meteorite that was buried in the soil. a) JaH 468, L6 S3 WD2.0, shows Sr enrichment on ES and BS as compared to CS. b) Meteorite RaS 340, L6 S4 WD4.0, has only Sr enrichment on ES. c) The BS part of meteorite RaS 341, L6 S1 WD1.0, yields higher Sr contamination. d) A sample from the JaH 091 meteorite shower, L5 S2, has Mn enrichment on ES and BS.

To test for a correlation of contamination with terrestrial age, the degree of contamination was quantified for 98 ^{14}C dated chondrites (14 LL, 34 L and 50 H). A special focus was placed on the Sr and Ba contamination since their accumulation during terrestrial residence is very prominent and well-established (e.g. Al-Kathiri et al., 2005). The best correlations with terrestrial age show the Sr contamination on CS and ES, Ba on NS, V on ES, the

accumulation of Mn on NS compared to Mn on CS and the Fe/Mn ratio determined on CS (Fig. 6.8). All other elements of interest show either no significant variation through terrestrial history as analyzed by HHXRF on the surfaces (K, Ca, Ti, Cr, Co and Ni), or can not be analyzed accurately enough by HHXRF or are below limit of detection (Zn, As, Mo and Pb). For elements with the best correlations, linear regression curves were calculated using the median values of 5 ka age steps (<5, 5 to 10, 10 to 15, 15 to 20, 20 to 25, 25 to 30, 30 to 35 and >35 ka). The resulting equations are eq. 6.7 for Sr on CS, eq. 6.8 for Sr on ES, eq. 6.9 for Ba on NS, eq. 6.10 for V on ES, eq. 6.11 for Mn on NS/Mn on CS, eq. 6.12 for Fe on CS/Mn on CS for H chondrites, eq. 6.13 for Fe on Cs/Mn on CS of L chondrites and eq. 6.14 for Fe on CS/Mn on CS of LL chondrites.

$$T_{(Sr\ CS)} = 0.25N_{(Sr\ CS)} + 1.2 \qquad\qquad \text{(eq. 6.7)}$$

$$T_{(Sr\ ES)} = 0.06N_{(Sr\ ES)} + 2.9 \qquad\qquad \text{(eq. 6.8)}$$

$$T_{(Ba\ NS)} = 0.18N_{(Ba\ NS)} - 11.2 \qquad\qquad \text{(eq. 6.9)}$$

$$T_{(V\ ES)} = 0.11N_{(V\ ES)} - 6.8 \qquad\qquad \text{(eq. 6.10)}$$

$$T_{(Mn\ NS/Mn\ CS)} = 46.6N_{(Mn\ NS/Mn\ CS)} - 33.1 \qquad\qquad \text{(eq. 6.11)}$$

$$T_{(Fe\ CS/Mn\ CS\ H)} = 1.27N_{(Fe\ CS/Mn\ CS\ H)} - 115.2 \qquad\qquad \text{(eq. 6.12)}$$

$$T_{(Fe\ CS/Mn\ CS\ L)} = 1.80N_{(Fe\ CS/Mn\ CS\ L)} - 127.1 \qquad\qquad \text{(eq. 6.13)}$$

$$T_{(Fe\ CS/Mn\ CS\ LL)} = 1.37N_{(Fe\ CS/Mn\ CS\ LL)} - 89.9 \qquad\qquad \text{(eq. 6.14)}$$

For the terrestrial age estimation based on chemical parameters (CPA) the mean of the six ages is taken, resulting in a estimated age range from ~3 to >70 ka.
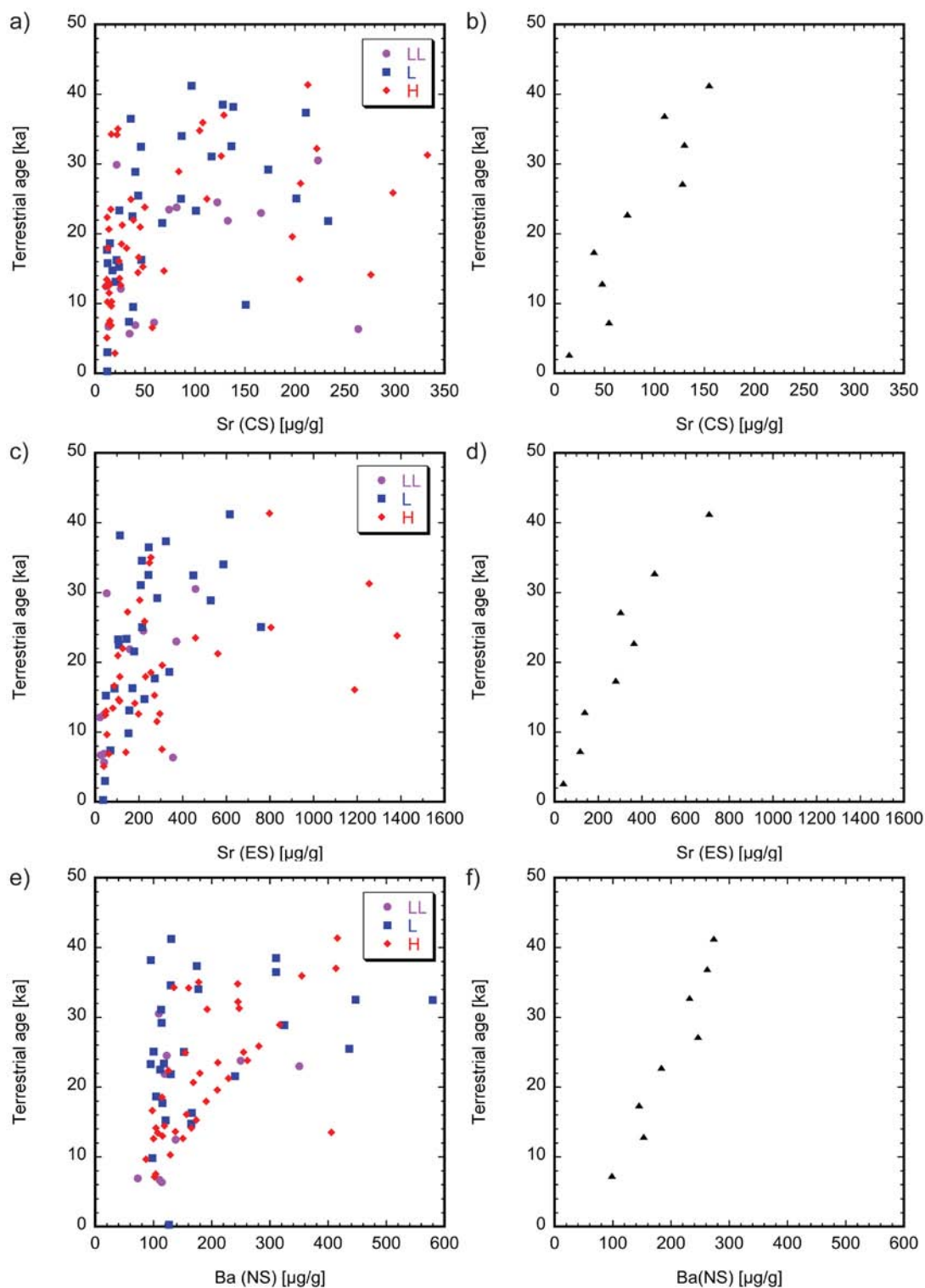
Figure 6.8. *Data used for age estimations with chemical parameters. The plots a), c), e), g), i) and k) are data as analyzed by HHXRF. Each data point represents the median of at least three measurements. At right, the median element concentrations of 5 ka age steps of all OC groups are displayed in b), d), f), h), j) and l).*
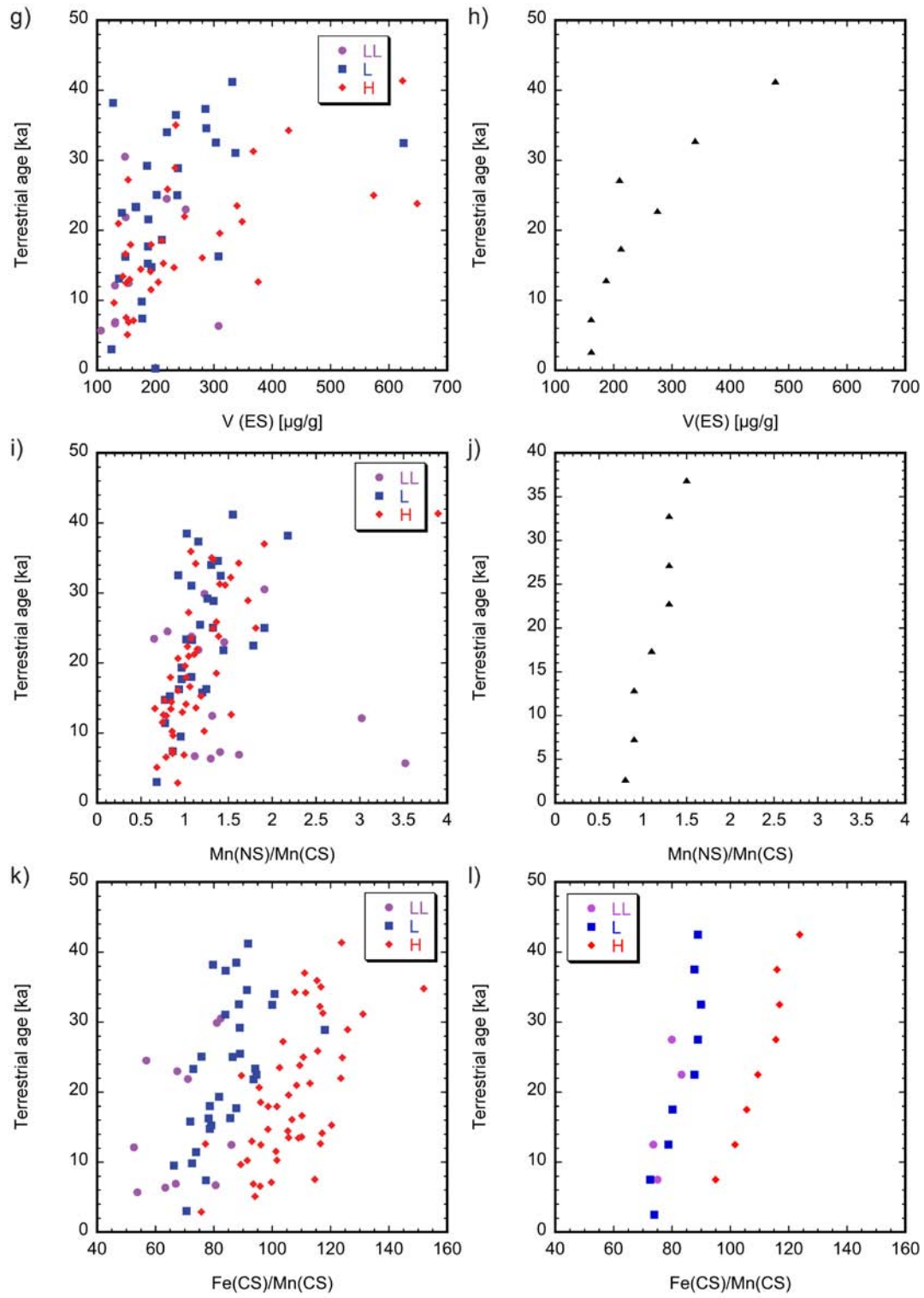
Figure 6.8. *Continued.*

6.4. DISCUSSION

6.4.1. New ^{14}C terrestrial ages

The newly-obtained terrestrial ages (Table 6.3) confirm the general trend observed in Oman with a mean ^{14}C age around 20 ka and a prominent lack of young (<10 ka) samples (Al-Kathiri et al., 2005; Jull, 2006). Also the selected meteorite populations (all RaW and all LL samples) show a similar age pattern with a lack of young and old (>40 ka) meteorites, even though those two populations are less representative due to the low number of samples. The reason for the age distribution with a prominent lack of young (<10 ka) meteorites remains unclear. This is one of the motivations to find parameters allowing for terrestrial age estimation for the whole population of Oman meteorites. We further discuss the ^{14}C dated samples in a later chapter 6.4.4. with estimated terrestrial ages from meteorites found in 2009 and 2010.

6.4.2. Terrestrial age estimations

6.4.2.1. Macroscopic weathering age

The combination of all six macroscopic weathering parameters allows a relatively good estimation of the terrestrial age ($T_{(14C)} = 0.94 T_{(MWPA\_corr)} + 1.5$, r = 0.72; median relative deviation: 21%; Fig. 6.9a), even though the individual parameters scatter strongly. The best dependence shows the preservation of FC, the degree of wind ablation, the contamination of hygroscopic salts and the attached sand. For rough age estimation these four values might be sufficient but for better statistics we recommend the use of all six parameters.
Freshly-fallen meteorites usually are covered by fusion crust, which is gradually lost during terrestrial residence by wind erosion and other physical weathering processes such as cracking due to daily temperature variation and salt weathering. Physical weathering is typically slower than chemical weathering and dominates the late weathering history of

meteorites (e.g. Al-Kathiri et al., 2005; Lee and Bland, 2004). Wind ablation occurs in every meteorite recovery region of Oman but is stronger at areas where fine-grained material (mostly dune sand) is available. Meteorites with strong wind ablation features are found dominantly in Ramlat as Sahmah (RaS) or Sayh al Uhaymir (SaU) regions while meteorites from Al Huqf or Shalim show only minor wind ablation. However, wind erosion is also recognizable on meteorites from those regions and the parameter can be used for age estimation. Hygroscopic salts occur dominantly in samples of about 15 ka, but are not found in all samples of these ages. A detailed discussion of salts in OC from Oman is given elsewhere (Zurfluh et al., in review). The attached sand occurs at similar time span as the hygroscopic salts and both parameters might be linked. The efflorescence of iron hydroxides cement sand grains from the environment (mostly dune sand) to the meteorites. Calcite can also occur as cement. Attached sand is preferentially found on meteorites recovered between dunes for example in the RaS region, but is also observed on meteorites from dune free areas such as the Jiddat al Harasis (JaH). Due to wind erosion, sand is only sparsely found on old meteorites. After oxidation of all metal (and troilite) no more iron hydroxides are present for renewing sand cementation. With increasing terrestrial time the meteorites are contaminated by terrestrial material that can precipitate within pore space. However, not all meteorites have macroscopically visible porosity. That is why the estimated ages using this parameter are less robust as compared for example to FC on ES. Iron-rich stony meteorites and mesosiderites with stable position (no turning) during their terrestrial residence in Oman tend to develop a reddish (rusty) color on the lower side (buried or partly buried in soil) in contrast to the exposed upper side that has usually a relatively dark brown color. Since meteorites can have unstable positions during their terrestrial history weathering patterns such a red BS might never evolve.

Since all the individual parameters scatter with terrestrial age and only four categories are defined, the best estimation is reached when all six macroscopically visible weathering parameters are combined. The scale might be refined using more than four categories, e.g. a new category for meteorites with "fresh" FC on ES, but, even though the categories were strictly defined, at the end they are dependant on the experience of the persons doing the classification. Due to the lack of samples <5 ka and >35 ka the strong criteria for such meteorites were not extractable.
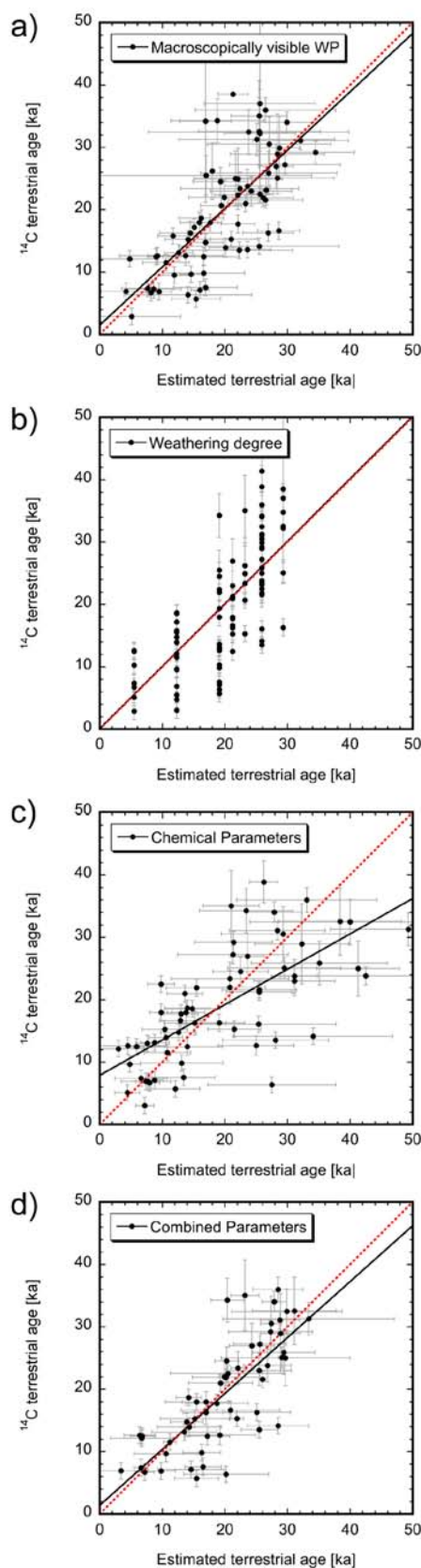
Figure 6.9. *Comparison of estimated terrestrial ages with* ^{14}C *terrestrial ages. The dashed line is the 1:1 correlation; the solid line is the linear correlation. a) Macroscopically visible weathering parameters age (r=0.72). b) Weathering degree age (r=0.73). c) Chemical parameters age (r=0.69). d) The combination of all three estimated ages (r=0.77).*

6.4.2.2. Weathering degree age

The estimated terrestrial age based on the modified weathering degree is relatively good ($T_{(14C)} = 1.00T_{(WDA)} + 0.03$, r=0.73, median relative deviation: 22%; Fig. 6.9b). This relation clearly benefits from the refinement of the stages W3 into WD3.0, WD3.3 and WD3.6 and W4 into WD4.0 and WD4.5. However, since only eight categories (i.e. weathering degrees) can occur in periods >10 ka, this parameter can only be used for a rough division of the samples into relative age groups. Weathering rates are similar for all OC groups, even though H chondrites have higher kamacite contents (which is attacked first) compared to L and especially LL chondrites. Towards the coast (Al Huqf, Shalim), humidity is slightly higher as compared to inland desert (e.g. RaS, SaU) but no significant difference of weathering speed was observed comparing meteorites from different meteorite recovery areas over the whole Oman. The weathering degree scheme is developed based on observations on OC and was calibrated for age estimation using OC samples. Since our H, L and LL samples show a similar WD to terrestrial age correlation, it might be also applicable to other meteorite groups with similar mineralogy and regions with comparable geology and climatic conditions.

6.4.2.3. Chemical parameter age

Due to the large scatter in the data used for estimation of the terrestrial age with chemical parameters, the age estimations have larger errors than $T_{(WDA)}$ and $T_{(MWPA)}$ ($T_{(14C)} = 0.57T_{(CPA)} + 7.9$, r=0.69; median relative deviation: 27%; Fig. 6.9c). The combination of all 6 chemical parameters yields ages from 3 up to 70 ka. Individual chemical age parameters can also result in negative ages or ages above 100 ka. The major problem with the chemical parameters is that in general they are not distributed homogenous on a sample, either on a natural surface (ES, BS, NS) or inside (CS). In addition, contamination profiles are not linear and the amount of contamination occurs not linear with time since it is dependant on porosity of the sample, which is can be closed and reopened during weathering history (Bland et al., 1998; Britt and Consolmagno, 2003; Consolmagno et al., 2008; Macke et al., 2010, Zurfluh et al., in review), and the availability of water. Thin coatings (desert varnish like) of contaminants on natural surfaces, dominantly ES, can be lowered by leaching during rain events or are continuously eroded by sand blasting. Wind ablation is a strong physical weathering process and nearly all (older) meteorites from Oman show polishing or erosion. Therefore, Sr on ES, Ba on NS and V concentrations on ES show a wide variation. Best estimations are reached by use of Mn accumulation on NS compared to Mn on CS and the Fe/Mn ratio measured on CS. The higher MnNS/MnCS ratios for older meteorites indicate Mn accumulation due to desert varnish formation. Researchers have tested dating of petroglyphs by measuring the Mn concentrations of varnished country rock and the scratched part of the petroglyph with HHXRF (Lytle, 2009; Lytle et al., 2000; Pingitore and Lytle, 2003; Pingitore et al., 2004). Similar to us, they used the accumulation of Mn on desert rocks over time as age estimation. The differences in Fe/Mn ratios on CS of the distinct age groups seem to be a result of the analytical method applied. When metal flakes are present in a meteorite X-rays are preferentially absorbed and influence the measurement. To minimize these effects, the instrument was calibrated using powders and hand specimens (Zurfluh et al., 2011). Since the effect was observed in all groups, even in metal-poor LL chondrites, the parameter can be used for age estimation. Other analytical problems concern the element Ba. Line interference of Ti $K\alpha$ with Ba $L\alpha$ can occur at high Ba concentrations (>400 µg/g), which is, however not problematic in most of the OC samples from Oman. In addition, the limit of detection is relatively high with 100 µg/g. Initial Ba concentration of OC are between

3 µg/g to 5 µg/g (Wasson and Kallemeyn, 1988). For samples with Ba below limit of
detection this parameter could not be used.

6.4.3. Combined estimated terrestrial age

The mean of the three ages $T_{(MWPA\_corr)}$, $T_{(WDA)}$ and $T_{(CPA)}$ (actually a combination of a total
of 13 individual age estimations: $T_{(FC)}$, $T_{(WA)}$, $T_{(PO)}$, $T_{(Red)}$, $T_{(Salt)}$, $T_{(Sand)}$, $T_{(WDA)}$, $T_{(Sr\ CS)}$, $T_{(Sr}$
$_{ES)}$, $T_{(Ba\ NS)}$, $T_{(V\ ES)}$, $T_{(Mn\ NS/Mn\ CS)}$ and $T_{(Fe\ CS/Mn\ CS)}$) provides a relatively robust age estimation
($T_{(14C)} = 0.90T_{(COMB)} + 1.4$, $r = 0.77$; median relative deviation: 13%; Fig. 6.9d). Because all
three, respectively 13, estimated ages have to be used for the combined age, only 55 $T_{(COMB)}$
estimated terrestrial ages of complete datasets of ^{14}C dated meteorites could be obtained. An
age range from 3.4 to 33.4 ka was determined for this group (mean: 19.9 ka, median: 20.2 ka,
st. dev.: 7.6 ka), which is very similar to the range of the ^{14}C dated samples (2.9 ka to 41.4 ka,
mean: 19.9 ka, median: 19.0 ka, st. dev.: 9.8 ka) used for calibration. Using the minimal or
maximal values (i.e. category or composition that yields the youngest or oldest estimated age)
of each parameter, an age range of 2.3 ka to 50.6 ka would have been possible. Although the
parameters used for the age estimation can be determined quite quickly, the whole procedure
is relatively time consuming, but still much faster than dating by ^{14}C. In particular, the
method can be applied to a larger set of samples. The determination of the macroscopically
visible weathering parameters and thin section observation are relatively quick if an
experienced and trained person does the classification. Instead, the collection of the chemical
data needs time, because a single measurement takes 300 s (if Ba is desired) and every
surface (CS, ES and BS) has to be measured at least 3 times for an accurate determination.
For simplification, one can also use just the $T_{(MWPA\_corr)}$ and $T_{(WDA)}$ for terrestrial age
estimation. This combination gives the age equation ($T_{(14C)} = 1.02T_{(MWPAWDA)} - 0.02$, r=0.75,
median relative deviation: 20%) but is less accurate than the combination of all three
estimated ages. The minimum of parameters that should be used for age estimation are FC on
ES, salt on CS and sand on ES; the weathering degree; MnNS/MnCS and FeCS/MnCS. We
see a good potential in this age estimation procedure to obtain a terrestrial age estimate for
each meteorite recovered during our campaigns and thus an age distribution for the whole

population, which is impossible using ^{14}C technique due to the large number of recovered meteorites (>700 different fall events).

6.4.3.1. Limitation of the age estimation

Due to local influences of geography, geology and climate, the age estimations presented here are just applicable to meteorites from Oman. The macroscopic parameters "FC on ES", "wind ablation ES" and to some degree "filled pores on CS" are valid for all ordinary chondrites and may also be applicable for other meteorite groups. Parameters like "sand ES", "salt CS", "red BS" and WD can only be used for meteorites with significant amounts of metal, troilite and mafic silicates such as ordinary chondrites, enstatite chondrites, primitive achondrites, some carbonaceous chondrites (CR, CV, CH and CB) and metal-poor mesosiderites (e.g. JaH 203 and paired stones). The chemical age is designed for OC and is dependent on the group (H, L or LL). A whole age estimation scheme could be developed for other chondrite or achondrite groups. But at the moment, not enough samples from the different meteorite groups or classes are dated or available for a refined chemical age classification scheme.

The surface types show slight variation over the whole of Oman. For example, the amount of moving surface sand and of silty material in the soil is variable for different areas of Oman, resulting in likely differences of the importance of wind ablation in different areas. The bulk composition (especially Sr and Ba concentrations) of soils is relatively homogeneous over the whole meteorite recovery areas of Oman. In contrast, the concentration of water-soluble salts is variable (Zurfluh et al. in review). However, salt contamination occurs also in meteorites found in areas with low concentrations of water-soluble salts in soil (Zurfluh et al., in review).

The application of the terrestrial age estimation method as presented here for Oman to other hot desert accumulation areas would require a calibration for each specific area and for each parameter. In areas with similar geology and climate history such as the Sahara (Schlüter et al., 2002) similar factors might occur. Meteorites from United Arab Emirates (Hezel et al., 2011) can be regarded as belonging to the same "weathering group" as Oman meteorites. In contrast, meteorites from the Atacama desert or Australia apparently show no correlation of weathering degree with terrestrial age (Gattacceca et al., 2011; Jull et al., 2010).

6.4.4. Terrestrial age distribution of ^{14}C dated and estimated ages

The presented terrestrial age estimation was applied to all OC (n=295) found during fieldwork in 2009 and 2010. Some samples had to be excluded from age determination, e.g. small samples cannot be examined for macroscopic parameters and chemical contamination data is not meaningful for such samples. Sorting them out, ages for 169 samples were estimated. Corrected for pairing, 122 individual falls are represented, recovered in nearly all important meteorite find areas of Oman with the exception of Dhofar and Shisr. Since we have included all the OC found, no bias due to sample selection is present as might be possible for the subgroup of ^{14}C-dated meteorites. Hence, our 2009/2010 recovered meteorite selection is considered representative for the whole population of OC from Oman. Comparing the frequency of weathering degree and estimated terrestrial ages of the meteorites from 2009 and 2010 (Fig. 6.10) with the weathering degree and terrestrial ages for all ^{14}C dated samples from Oman (Fig. 6.10) a similar distribution is observed: A lack of fresh (WD0.0 to WD2.0) and consequently young (<10 ka) samples is obvious. As observed earlier, W3/4 samples and meteorites with terrestrial ages of 15 ka to 25 ka are very abundant (Al-Kathiri et al., 2005). Highly weathered (WD≥4.5) and very old samples (≥40 ka) are also missing among the group with estimated ages. The similar age distribution of ^{14}C dated samples and estimated terrestrial ages of the whole 2009/2010 population also demonstrates that a representative sample suite was selected for radiocarbon dating. A similar terrestrial age (and weathering grade) distribution was observed for a smaller OC population (n=21) from the United Arab Emirates (UAE), found in the same geological environment as the meteorites from Oman (Hezel et al., 2011). Since the weathering grade shows a correlation with terrestrial age for OC from Oman, we can also take this parameter for a rough estimation of the terrestrial age of all our finds. Including all collected OC since 2001 (corrected for pairing, not all reclassified for refined weathering degree) we still observe a dramatic lack of samples at low weathering grades (W≤2) or heavily weathered (only one W5 sample!). The same situation applies for the population of OC collected by other groups in Oman with independently determined weathering degrees (Meteoritical Society Database). A reason for the lack of OC with long terrestrial histories might the limit of the dating method. However, only six of the investigated meteorites had not enough cosmogenic ^{14}C for a proper dating of the terrestrial age. Meteorites of weathering degrees >4.5 might be missing due to the

neutralization and passivation that occurs at WD4.0 (Bland et al., 1998; Zurfluh et al., in review). Due to the cementation of pore space, washing out of salts and neutral to basic pH conditions after completion of troilite oxidation, chemical weathering is slowed down in ordinary chondrites and physical weathering, most prominently wind ablation, dominates the late weathering history of OC from Oman. However, it remains unclear what we would expect a very old (>>50 ka) ordinary chondrite from the Oman desert to look like. Probably wind erosion removes them relatively quickly.
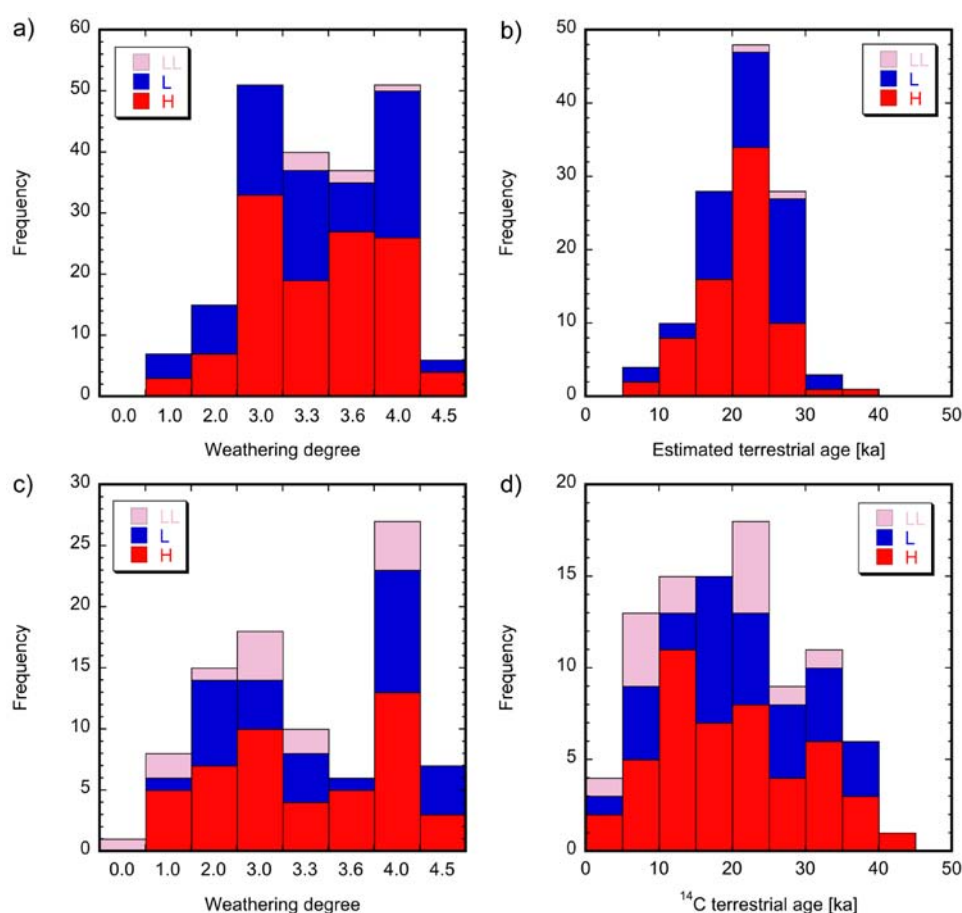
Figure 6.10. Histograms of weathering degree (a) and estimated terrestrial ages (b) for pairing-corrected samples (n=122) recovered during fieldwork in 2009 and 2010. Frequency of weathering degree (c) and terrestrial age of the ^{14}C dated (d) samples (n=93). Six meteorites had ^{14}C concentrations below limit of detection and might have ages older than 40 ka. They are not displayed. Both populations show a deficit of unaltered (WD<2) respectively young (<10 ka) samples.

The absence of very young OC is even more difficult to explain. We have no plausible explanation for this absence. Possible scenarios might be: (i) selective removal by recent fast weathering; (ii) selective collection of unaltered meteorites by humans; (iii) selective burial of fresh falls in the soil; (iv) recent change of the meteorite flux. These scenarios are discussed in the following: (i) If weathering has removed almost the entire population of young meteorites it is not explainable why older meteorites would have survived. The climatic conditions have an influence on weathering rates (Bland et al., 1998). The meteorite recovery areas of Oman experienced periods of more humid climatic conditions around 10 to 5 ka ago (Fleitmann and Matter, 2009; Preusser, 2009), which might have caused higher weathering rates. However, the last 5 ka were dominated by relatively dry conditions and the few young samples found show no evidence of accelerated weathering. (ii) If humans had preferentially collected young meteorites (e.g. as source of iron or for fire-making) one should find traces of their use such as tools made of meteoritic material. In addition, an efficient removal of a significant part of unweathered meteorites from large areas of Oman by earlier populations appears quite unlikely. However, we plan to further explore this possibility by analysis of archeological artifacts. (iii) After each meteorite find, we document the degree of burial in the soil. Several samples are buried up to 90% in the soil and it is plausible that the meteorites were completely covered by soil or dune sand for a significant part of their terrestrial residence time. Attached sand commonly observed on ES might be the result of earlier complete coverage of the meteorite by soil. However, we see no reason why young meteorites should be preferentially buried completely in the soil. Most of the meteorites found with terrestrial ages <5 ka were buried less than 20% in the soil. (iv) Based on present day fireball observations and studies of old meteorite populations dated for terrestrial age, e.g. from Antarctica (Zolensky, 1998), it is assumed that meteorite flux was constant over the period meteorites have accumulated in Oman (Bland et al., 1996; Halliday et al., 1989; Zolensky et al., 2006). In addition, the infall rate of meteorites is assumed to be equal all over the world (Halliday et al., 1989). If the flux was higher 15 ka ago, similar patterns had to be observed in other recovery areas, which is not observed. The meteorite population from western Australia have a higher percentage of young samples and show an expected age distribution, i.e. decreasing abundances of samples with increasing terrestrial age (Jull et al., 2010). Also, meteorites from Algeria show an approximately exponential drop-off of number of meteorites with increasing terrestrial age, similar to the population

from Australia (Jull, 2006). The high abundance of meteorites with terrestrial ages of 20 ka to 25 ka in Oman remains mysterious. A similar situation is observed in the Roosevelt Co recovery areas, New Mexico (Jull, 2006).

6.5. CONCLUSIONS

Several macroscopic, microscopic and chemical weathering features observed in ordinary chondrites from Oman show a correlation with the ^{14}C terrestrial age of the respective meteorites. We show that these weathering features can be used for an estimation of the terrestrial age, resulting in age estimations with a median deviation from the ^{14}C age of 13-27 rel%, depending on the parameters used. The procedure is relatively simple, needs no sophisticated analytical tools and can therefore be quickly applied to a large number of samples. The weathering parameters used include macroscopically visible weathering features such as the preservation of fusion crust, the degree of wind erosion, salt contamination in the interior, the presence of attached sand on exposed natural surfaces of the meteorite, the degree of pore infill and the color difference between the buried and exposed part of the meteorite.

The weathering degree as recorded in thin sections gives a good rough estimation of the terrestrial age. To reach a better correlation with terrestrial age we have modified the weathering scale proposed by Wlotzka (1993) by including intermediate steps at weathering grade W3 and W4 that are now unambiguously defined.

The most advanced weathering parameters used are chemical measurements performed by HHXRF. However, the chemical parameters show the weakest correlations with terrestrial age and might be excluded for rapid estimations.

The updated dataset of 101 ^{14}C dated ordinary chondrite fall events from Oman as well as the data set of 122 additional estimated ages from Oman both show an under abundance of very young samples (<10 ka) or old samples (>40 ka). Both datasets are corrected for pairing. The reason for the lack of meteorites with low terrestrial ages in Oman remains unclear and is subject of further studies.

6.6. Acknowledgments

6.7. REFERENCES

Al-Kathiri, A., Hofmann, B. A., Jull, A. J. T., and Gnos, E., 2005. Weathering of meteorites from Oman: Correlation of chemical and mineralogical weathering proxies with ^{14}C terrestrial ages and the influence of soil chemistry. *Meteoritics & Planetary Science* 40:1215-1239.

Bevan, A. W. R., Downes, P. J., and Thompson, M., 2001. Little Minnie Creek, a L4(S2) ordinary chondritic meteorite from Western Australia. *Journal of the Royal Society of Western Australia* 84:149-152.

Bland, P. A., 2006. Terrestrial weathering rates defined by extraterrestrial materials. *Journal of Geochemical Exploration* 88:257-261.

Bland, P. A., Berry, F. J., Smith, T. B., Skinner, S. J., and Pillinger, C. T., 1996. The flux of meteorites to the Earth and weathering in hot desert ordinary chondrite finds. *Geochimica et Cosmochimica Acta* 60:2053-2059.

Bland, P. A., Sexton, A. S., Jull, A. J. T., Bevan, A. W. R., Berry, F. J., Thornley, D. M., Astin, T. R., Britt, D. T., and Pillinger, C. T., 1998. Climate and rock weathering: A study of terrestrial age dated ordinary chondritic meteorites from hot desert regions. *Geochimica et Cosmochimica Acta* 62:3169-3184.

Britt, D. T. and Consolmagno, G. J., 2003. Stony meteorite porosities and densities: A review of the data through 2001. *Meteoritics & Planetary Science* 38:1161-1180.

Cassidy, W. A., 1980. Discovery of the Allan Hills A77, Antarctica, meteorites. In: Graham, A. L. (Ed.), *The Meteoritical Bulletin No. 57*. The meteoritical society.

Consolmagno, G. J., Britt, D. T., and Macke, R. J., 2008. The significance of meteorite density and porosity. *Chemie Der Erde-Geochemistry* 68:1-29.

Crozaz, G., Floss, C., and Wadhwa, M., 2003. Chemical alteration and REE mobilization in meteorites from hot and cold deserts. *Geochimica et Cosmochimica Acta* 67:4727-4741.

Fleitmann, D. and Matter, A., 2009. The speleothem record of climate variability in Southern Arabia. *Comptes Rendus Geoscience* 341:633-642.

Gattacceca, J., Valenzuela, M., Uehara, M., Jull, A. J. T., Giscard, M., Rochette, P., Braucher, R., Suavet, C., Gounelle, M., Morata, D., Munayco, P., Bourot-Denise, M., Bourles, D., and Demory, F., 2011. The densest meteorite collection area in hot deserts: The San Juan meteorite field (Atacama Desert, Chile). *Meteoritics & Planetary Science* 46:1276-1287.

Gibson, E. K., Jr. and Bogard, D. D., 1978. Chemical alterations of the Holbrook chondrite resulting from terrestrial weathering. *Meteoritics* 13.

Giscard, M. D., Jull, A. J. T., and Hewitt, L. R., 2009. Terrestrial carbonates of meteorites from Chile, Oman, Northwest Africa and Saudi Arabia. *Meteoritics & Planetary Science* 44:A78-A78.

Goddard, E. N., Trask, P. D:, De Ford, R. K., Rove, O. N., Singewald, J. T., Jr., and Overbeck, R. M., 1948. Rock-color chart. Boulder, Colorado. *Geological Society of America.* :11 p.

Gooding, J. L., 1986. Weathering of stony meteorites in Antarctica. *International Workshop on Antarctic Meteorites,*

Gooding, J. L., 1989. Significance of terrestrial weathering effects in Antarctic meteorites. In: Marvin, U. B. and MacPhearson, G. J. (Eds.), *Field and Laboratory Investigations of Meteorites from Victoriay Land and the Thiel Mountains Region, Antarctica, 1982-1983 and 1983-1984*. Smithsonian Contrib. Earth Sci.

Halliday, I., Blackwell, A. T., and Griffin, A. A., 1989. The flux of meteorites on the Earth's surface. *Meteoritics* 24:173-178.

Hezel, D. C., Schlüter, J., Kallweit, H., Jull, A. J. T., Al-Fakeer, O. Y., Al-Shamsi, M., and Strekopytov, S., 2011. Meteorites form the United Arab Emirates: Description, weathering, and terrestrial ages. *Meteoritics & Planetary Science* 46:327-336.

Hofmann, B. A., Gnos, E. Al-Kathiri, A., 2004. Harvesting meteorites in the Omani desert: Implications for astrobiology. *Proceedings of the Third European Workshop on Exo-Astrobiology.*

Ikeda, Y. and Kojima, H., 1991. Terrestrial alteration of Fe-Ni metals in Antarctic ordinary chondrites and the relationship to their terrestrial ages. *Proc. NIPR Symp. Antarct. Meteorites* 4:307-318.

Jull, A. J. T., 2006. Terrestrial ages of meteorites. In: Lauretta, D. S. and McSween, H. Y. (Eds.), *Meteorites and the Early Solar System II*. University of Arizona Press, Tucson.

Jull, A. J. T., Cloudt, S., and Cielaszyk, E., 1998. ^{14}C terrestrial ages of meteorites from Victoria Land, Antarctica, and the infall rate of meteorites. In: McCall, G. J., Hutschison R., Grady, M. M., and Rothery, D. (Eds.), *Meteorites: Flux with time and impact effects*. Geological Society of London Special Publication #140, London.

Jull, A. J. T., Donahue, D. J., Cielaszyk, E., and Wlotzka, F., 1993. Carbon-14 terrestrial ages and weathering of 27 meteorites from the southern high-plains and adjacent areas (USA). *Meteoritics* 28:188-195.

Jull, A. J. T., Donahue, D. J., and Linick, T. W., 1989. Carbon-14 activities in recently fallen meteorites and Antarctic meteorites. *Geochimica et Cosmochimica Acta* 53:2095-2100.

Jull, A. J. T., Leclerc, M. D., Biddulph, D. L., McHargue, L. R., Burr, G. S., Al-Kathiri, A., Gnos, E., and Hofmann, B., 2008. Radionuclide studies of meteorites from Ramlat al Wahibah and other omani desert locations. *Meteoritics & Planetary Science* 43:A69-A69.

Jull, A. J. T., McHargue, L. R., Bland, P. A., Greenwood, R. C., Bevan, A. W. R., Kim, K. J., LaMotta, S. E., and Johnson, J. A., 2010. Terrestrial ages of meteorites from the Nullarbor region, Australia, based on ^{14}C and ^{14}C-^{10}Be measurements. *Meteoritics & Planetary Science* 45:1271-1283.

Jull, A. J. T., Wlotzka, F., and Donahue, D. J., 1991. Terrestrial ages and petrologic description of Roosevelt County meteorites *Lunar and Planetary Science XXII,,*

Jull, A. J. T., Wlotzka, F., Palme, H., and Donahue, D. J., 1990. Distribution of terrestrial age and petrologic type of meteorites from western Libya. *Geochimica et Cosmochimica Acta* 54:2895-2898.

Krähenbühl, U., Noll, K., Dobeli, M., Grambole, D., Herrmann, F., and Tobler, L., 1998. Exposure of Allan Hills 84001 and other achondrites on the Antarctic ice. *Meteoritics & Planetary Science* 33:665-670.

Lee, M. R. and Bland, P. A., 2004. Mechanisms of weathering of meteorites recovered from hot and cold deserts and the formation of phyllosilicates. *Geochimica et Cosmochimica Acta* 68:893-916.

Losiak, A. and Velbel, M. A., 2011. Evaporite formation during weathering of Antarctic meteorites--A weathering census analysis based on the ANSMET database. *Meteoritics & Planetary Science* 46:443-458.

Lytle, F., 2009. How old are petroglyphs? Prove it. *Nevada Rock Art Foundation meeting, Mesquite NV*.

Lytle, F. W., Pingitore, N. E., Lytle, N. W., Ferris-Rowley, D., and Reheis, M. C., 2000. Determination of growth rate of desert varnish: Application to dating petroglyphs. *Workshop on Synchrotron Radiation in Art and Archaeology, SSRL*.

Macke, R. J., Consolmagno, G. J., Britt, D. T., and Hutson, M. L., 2010. Enstatite chondrite density, magnetic susceptibility, and porosity. *Meteoritics & Planetary Science* 45:1513-1526.

Nazarov, M. A., Badyukov, D. D., Lorents, K. A., and Demidova, S. I., 2004. The flux of lunar meteorites onto the Earth. *Solar System Research* 38:49-58.

Noll, K., Dobeli, M., Krahenbuhl, U., Grambole, D., Herrmann, F., and Koeberl, C., 2003. Detection of terrestrial fluorine by proton induced gamma emission (PIGE): A rapid quantification for Antarctic meteorites. *Meteoritics & Planetary Science* 38:759-765.

Pingitore, N. E. and Lytle, F. W., 2003. Desert varnish: Relative and absolute dating using portable X-ray fluorescence. *EOS Trans. AGU* 84.

Pingitore, N. E., Lytle, F. W., Rowley, P. D., and Ferris, D. E., 2004. Absolute dating of desert varnish using portable X-ray fluorescence: Calibration and testing. *American Geophysical Union, Fall Meeting 2004*:abstrct #B33B-0266.

Preusser, F., 2009. Chronology of the impact of Quaternary climate change on continental environments in the Arabian Peninsula. *Comptes Rendus Geoscience* 341:621-632.

Preusser, F., Radies, D., and Matter, A., 2002. A 160'000-year record of dune development and atmospheric circulation in southern Arabia. *Science* 296:2018-2020.

Radies, D., Preusser, F., Matter, A., and Mange, M., 2004. Eustatic and climatic controls on the development of the Wahiba Sand Sea, Sultanate of Oman. *Sedimentology* 51:1359-1385.

Ruzicka, A., 1995. Nullarbor-018 - A new L6 chondrite from Australia. *Meteoritics* 30:102-105.

Saunier, G., Poitrasson, F., Moine, B., Gregoire, M., and Seddiki, A., 2010. Effect of hot desert weathering on the bulk-rock iron isotope composition of L6 and H5 ordinary chondrites. *Meteoritics & Planetary Science* 45:195-209.

Schlüter, J., Schultz, L., Thiedig, F., Al-Mahdi, B. O., and Abu Aghreb, A. E., 2002. The Dar al Gani meteorite field (Libyan Sahara): Geological setting, pairing of meteorites, and recovery density. *Meteoritics & Planetary Science* 37:1079-1093.

Shih, C.-Y., Nyquist, L. E., Reese, Y., Wiesmann, H., Nazarov, M. A., and Taylor, L. A., 2002. The choronology and petrogenesis of the mare basalt clast from lunar meteorite

Dhofar 287: Rb-Sr and Sm-Nd isotopic studies. *Lunar and Planetary Science XXXIII, Abstract #1344,*

Stelzner, T., Heide, K., Bischoff, A., Weber, D., Scherer, P., Schultz, L., Happel, M., Schron, W., Neupert, U., Michel, R., Clayton, R. N., Mayeda, T. K., Bonani, G., Haidas, I., Ivy-Ochs, S., and Suter, M., 1999. An interdisciplinary study of weathering effects in ordinary chondrites from the Acfer region, Algeria. *Meteoritics & Planetary Science* 34:787-794.

Velbel, M. A., 1988. The distribution and significance of evaporitic weathering products on Antarctic meteorites. *Meteoritics* 23:151-159.

Wasson, J. T. and Kallemeyn, G. W., 1988. Compositions of chondrites. *Philosophical Transactions of the Royal Society of London Series a-Mathematical Physical and Engineering Sciences* 325:535-544.

Wlotzka, F., 1993. A weathering scale for the ordinary chondrites. *Meteoritics* 28:460.

Zolensky, M. E., 1998. The flux of meteorites to Antarctica. In: McCall, G. J., Hutschison R., Grady, M. M., and Rothery, D. (Eds.), *Meteorites: Flux with time and impact effects.* Geological Society of London Special Publication #140, London.

Zolensky, M. E., Bland, P. A., Brown, P., and Halliday, I., 2006. Flux of extraterrestrial materials In: Lauretta, D. S. and McSween, H. Y. (Eds.), *Meteorites and the Early Solar System II.* University of Arizona Press, Tucson.

Zurfluh, F. J., Hofmann, B. A., Gnos, E., and Eggenberger, U., 2011. Evaluation of the utility of handheld XRF in meteoritics. *X-Ray Spectrometry* 40:449-463.

Zurfluh, F. J., Hofmann, B. A., Gnos, E., and Eggenberger, U., in review. "Sweating meteorites" - water-soluble salts and temperature variation in ordinary chondrites and soil from the hot desert of Oman. *Meteoritics & Planetary Science*.

Chapter 7: Synopsis and outlook

In this concluding chapter, a typical terrestrial history of an ordinary chondrite that fell in Oman is presented. It is mainly based on the results of the research papers of this thesis. Since not all questions could be answered, some ideas for future investigations are proposed.

7.1 Terrestrial history of an ordinary chondrite in Oman

The history starts 40 ka ago, when an ordinary chondrite reaches Earth's atmosphere. There, the first interaction of the extraterrestrial material with Earth occurs during the formation of fusion crust that gives the meteorite a black appearance. Inside, its color is bright grey (Fig. 7.1a and b). Terrestrial weathering of the meteorite starts immediately after it's fall. Humidity from fog in the morning or sparse rain wet the meteorite and causes oxidation of metal grains resulting in rusty haloes around metal grains (Fig. 7.1c and d).

In the first 10 ka of its terrestrial history, the oxidation of metal is the main process. Macroscopically, the meteorite appears more and more rusty and the fusion crust is slowly removed by wind erosion and by thermal stress caused by daily temperature variation (Fig. 7.1b to 7.1d). In thin section, weathering degrees between WD0.0 and WD2.0 would be observed. Metal is altered and iron hydroxide veins close pores and cracks. At this weathering stage chemical analyzes (e.g. with handheld XRF, HHXRF) yield only minor Sr contamination on natural surfaces. Rain events cause soil movements (Fig. 7.1e) and the dense meteorite might be buried into the soil (Fig. 7.1f) or at least be turned over. Deflation by wind will re-expose the meteorite.

The following thousands of years are the most dramatic. When a meteorite has stayed 10 to 25 ka in Oman, it usually becomes rust-impregnated completely rusted (Fig. 7.1e to 7.1h). Mild wind erosion and probably daily temperature fluctuations of >30°C cause removal of large parts of the fusion crust (Fig. 7.1b, d and i). When most of the metal is oxidized alteration of troilite becomes more important. The weathering of troilite causes local acidic conditions and release of sulfate. The olivines in vicinity of weathered troilite are attacked and Mg^{2+} is mobilized. In addition, due to capillary forces and heating of the meteorite,

which causes a pumping effect, water containing ions from the soil is transported into the meteorite (Fig. 7.1g and h). Ions from soil (mainly Ca^{2+}, SO_4^{2-} and Cl^-) and meteorite (mainly Mg^{2+}, SO_4^{2-} and iron) react and form highly concentrated brines and salts. High concentrations of salt can occur at this stage within the meteorite and some of the salts are highly hygroscopic. Mobilization of iron and formation of iron hydroxide veins continues. Some iron hydroxides effloresce on the surfaces of the meteorites. In these weathering-rind sand-grains from the soil are cemented on the surface of the meteorite. Contamination by Sr and Ba continues. At this weathering stage HHXRF analyzes of Sr (and Ba) show that contamination is also significant inside the meteorites (Fig. 7.1h). The Sr/Ba-ratios of the contamination in the meteorites is similar to the Sr/Ba ratio of the soil. On exposed surface, Mn enrichment might be detectable due to fine desert varnish coating (Fig. 7h).

After about 25 ka in desert, all metal and most of the troilite is oxidized and chemical weathering is slowed down. At this stage, chemical weathering only plays a minor role and physical weathering is more important (Fig. 7.1i). As a result, the early salt contamination is partly lost. Due to wind erosion, fusion crust is completely eroded and some meteorites are shaped to ventifacts (Fig. 7.1j). Also most of the attached sand is removed and accumulated chemical contamination (Mn, Sr and Ba) is removed to some extent (Fig. 7.1i). However, elemental contamination is a continuous process and therefore remains at a certain level or slightly increases, depending on the intensity of wind erosion. Meteorites with stable positions have a reddish buried surface compared to the dark brown exposed surface. Most of the meteorites show evidence for overturning since Mn, Sr or Ba concentrations are elevated on both exposed and buried surfaces. Also attached sand grains cemented with iron hydroxides or calcite may be observed on both surfaces. Due to the higher volumes of the oxidation phases and probably also due to daily temperature fluctuations and probably also due to precipitation of salts in cracks and pore space, some of the meteorites are fragmented in to several pieces (Fig. 7.1i and j).
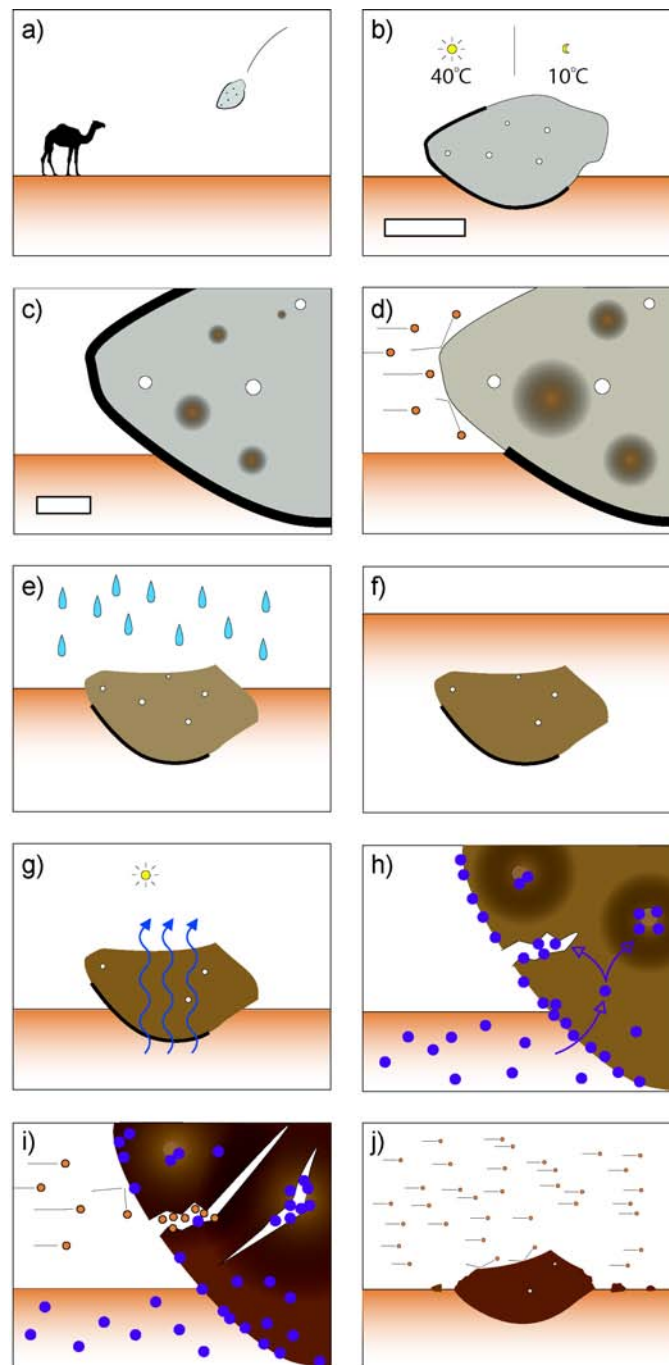
Figure 7.1. *Comic strip showing a typical terrestrial history of an ordinary chondrite in Oman. The fall of the meteorite a) is placed 40 ka ago. Black bold line represents fusion crust that is gradually lost (a to g) due to thermal stress of daily temperature differences (b) and wind erosion, which is displayed with orange-black circles representing sand grains (d, i and j). Capillary forces, heating of the meteorite and evaporation causing a pumping effect (g) that transports ions into the meteorite (h). Chemical contamination is illustrated as purple spots and includes, among others, Cl, S, Ca, Mn, Sr and Ba. Scale bar in b) is 5 cm and is similar for e, f, g and j. Scale bar in c) is 1 cm and is similar for d, h and i. Modified drawings by Matthias Bieri.*

It remains obscure how the history continues because we did not find many ordinary chondrites much older than 50 ka (no detectable ^{14}C). Since we only find minor alteration of silicates in the oldest meteorites, fragmentation, wind erosion and distribution of small fragments by wind cause the unspectacular end of the terrestrial history of an ordinary chondrite that fell to the hot desert of Oman.

Our studies have shown that HHXRF is a well-suited tool to detect chemical contamination. In combination with macroscopic alteration parameters and especially with refined microscopic weathering parameters it is possible to determine the weathering stage of a meteorite and to estimate how long the meteorite stayed in the desert.

7.2 Possible further investigations

At the final stage of this project, the PIN detector of the handheld XRF (HHXRF) was replaced by a new silicon drift detector, which permits to analyze light elements such as Si, Al or Mg not detectable with the PIN detector. In addition, precision and detection limits for several elements have improved. The addition of Si, Al and Mg expand the possibilities for classification of meteorites, especially achondrites. For chemical weathering studies the better capability for the detection of S could be helpful. First tests did not confirm a better detection of Ba. However, the instrument has a high potential in meteoritics.

The survey of water-soluble salts in ordinary chondrites from Oman has to be regarded as a pioneer study, which was aimed to define the diversity of salts and concentrations of salts. Further tests could use meteorite powders for the extraction of water-soluble salts or the leaching of samples that are disintegrated by high voltage discharge pulses in sealed containers (SelFrag). These methods would likely result in slightly higher salt concentrations since they permit to open closed pore spaces not accessible by the applied leaching experiments using meteorite cubes. But the risk for leaching meteoritic ions by weathering reactions is also higher when using powders or electrodynamical processed samples as compared to leaching by out-diffusion experiments of meteorite cubes. To prevent leaching of meteoritic ions, the leaching times have to be adjusted when using powders or SelFrag processed samples. Oxidation of the samples has to be avoided.

The identification of minerals (salts) in the pores can be improved using thin sections that are prepared without the usage of water. Microanalyical techniques such as μ-XRD could help to determine mineralogy of fine-grained aggregates. Sulfur isotope analyzes might help to better define the source of S. This may help to answer the question whether sulfur in contamination minerals such as barite, celestine, gypsum or jarosite is derived from soil or from alteration of troilite in the meteorite.

To predict additional processes occurring during interaction of brines with soil and meteorite material, computer modeling might be a powerful tool. Pathways of the brines could be tested by transport modeling and thermodynamical modeling might help to find the most plausible chemical reactions. Artificial weathering experiments might help to identify or check processes involved in weathering and contamination at the presence of salts.

Currently, the data logger recording in situ temperatures in the meteorite and soil is still active at the same locality as described in Chapter 5. In addition, relative humidity is recorded. These data will help to better understand the conditions affecting a meteorite in the hot desert.

The proposed method for terrestrial age estimation could be improved by better or expanded definitions of the parameters. For example the preservation of fusion crust might yield better results if it is investigated in more detail. The state of the pores (no pores, empty pores, partly filled or filled) was defined to be able to interpret the results of HHXRF analyzes. If also the kind of pore space filling is taken into account, the age resolution might be improved. A strong parameter is the weathering degree determined in thin section. The abundance of unweathered metal could also be included in the suite of macroscopic weathering parameters and could help to reach better age estimations. The precursor study of weathering effects and terrestrial ages observed a change in color of meteorite powders with increasing weathering. This effect was not investigated during this study since no powders were prepared. However, color changes are also detectable on hand specimens and might be used as macroscopic weathering parameter.

The proposed age estimation method should be applied to all meteorites, or at least to all meteorites undergoing classification procedure. This would give a more robust basis for statistical evaluation of the terrestrial age distribution, weathering speed or meteorite flux rate

over time. Effects of climate could be tracked in a more focused way. If for example the alteration mineralogy of a large group of meteorites from different geographical localities in Oman would be studied in more detail one could better estimate the influence of the climate or soil composition on weathering. It was, for example, observed that some samples close to the coast contained more magnetite than others. The influence of microbes in weathering of meteorites remains also mostly unexplored.

Appendix A: Database of Omani-Swiss meteorite search and research project

A1. Introduction

A database (DB) was created to improve access to all relevant data produced during the Omani-Swiss Meteorite search and research project. In this chapter, the intent, structure and contents of the DB as well as some problems and possible expansions are presented.

The ongoing meteorite search project started in 2001 and yielded an immense amount of data. As of August 2012, 5637 meteorites are found that belong to 759 fall events. During every field season a set of data was recorded for every meteorite find and corresponding soil samples (Chapters 1.10, 2, 4, 5 and 6). These field records are dispersed over the field books of several persons. During classification (Appendix B) and examination additional data was produced including the precise weights and chemical composition of minerals. Selected samples were dated with ^{14}C method, analyzed with HHXRF and described for their macroscopically visible weathering effects (Chapters 4 and 6). The main data of the meteorites, which were needed for submission to the Meteoritical Society to assign a name, were compiled and stored so far in separate excel sheets, the so called "master lists". But all additional data such as the ages, chemical data and weathering parameters were stored in individual excel sheets. To combine all data a FileMaker based database was created. This allows a quick search for certain parameters or a quick compilation of relevant data for investigations. In the following, the most important points regarding the database are mentioned. In Table A1 the contents and formats of the different data fields and an example exported from the DB are listed.

A2. Structure and content

The fundament of the database is the main table (i), which basically is the collection of the master lists with some additional information (marked with "Main_" in Table A1). Further,

the database contains five relational tables that are all linked via the field number of the meteorite (and soil/terrestrial) samples. The field number is a unique character in the main table. It is formatted as "0902_098" (underline, and not as earlier used "-"). The first two letters represent the year, the third and the fourth the month of the meteorite find. The numbers after the underline is a serial number, which has to have the same number of digits as the highest number occurring during the same campaign (Table A1, Chapter 1.9). The relational tables linked with the (i) main table contain information about: (ii) meteorite_weights, (iii) meteorite_age, (iv) meteorite_WP and (v) meteorite_niton_XRF (Table A1).

(i) The main table includes the most relevant information of each sample (field number, "FieldNo"). It combines data recorded during fieldwork (e.g. find date, distance of recognition, degree of burial, etc) and results from laboratory analyses (e.g. total weight, classification, mineral chemistry, etc).

(ii) Meteorite_weights is the list where the exact weight of the meteorite fragments as determined after cleaning in the lab is recorded. In the database, total mass and the mass of the five heaviest fragments are included. The total mass and the mass of the largest fragment are needed for the fragmentation index (FI; Al-Kathiri et al., 2005). This weathering parameter was evaluated for terrestrial age estimation but was excluded since the correlation of FI with terrestrial age is too weak.

(iii) Meteorite_age is the collection of terrestrial age determination by Prof. Dr. A. J. T. Jull, University of Arizona. This compilation includes the running number (label) of the ^{14}C analyses, field number, weights and ^{14}C content of the sample used for dating and the age including standard deviation. The most important column is "Age" where the valid ages are summarized as numbers. Not included in this column are ages of paired samples, samples at the limit of the method and obviously misdated samples. Some meteorites were analyzed more than once.

(iv) Meteorite_WP summarizes selected weathering parameters that are macroscopically visible and described in Chapters 4 and 6.

(v) Meteorite_Niton_XRF is the collection of HHXRF measurements. Most of the samples contain several HHXRF records. The most important features are field number, LOCATION, INSPECTOR and the chemical elements. LOCATION describes the physical state of the sample, if it was performed, for example, on a hand specimen or a powder sample.

INSPECTOR is used to discriminate between the measured surfaces types on a rock. CS: cut surface, ES: exposed surface, BS: buried surface or NS: natural surface. This table includes also measurements on standard samples, soil samples and terrestrial rocks. For more details see Table A1.

As of September 2012, the database contains 5808 records in the main table, 5193 weights are recorded in the meteorite_weight table. The meteorite_age table contains 151 age entries, 6870 HHXRF measurements are collected and 404 weathering parameter descriptions are available. Not included are the meteorites found during 2011 and 2012, as their classification was not completed.

A3. Remarks

In the following section possible problems and restrictions are mentioned.

1) Large weathered meteorites are often fragmented into hundreds of pieces, which can be buried in the soil and it is impossible to collect all fragments. When such a find place is visited during a following campaign, new fragments can appear on the surface due to deflation by wind. The new numbers of fragments and weights are not updated in all fields of the database consequently. E.g. the fragments of 0603_235 collected in 2010 have not been included into the database. It remains open, if one should just correct the main entry or include a new entry? The best way would be to correct the main entry and note the modification in the field "Main_CommentSample".

2) HHXRF measurements below limit of detection are stored in excel export from Niton software as "<LOD". During import into the database, it might be converted to "0", which gives false information. Since there is no valid way to calculate the concentration (e.g. using the detection limit), the usage of "0", is, however, the most proper way. It is useful to discriminate between analyzed and not analyzed. If the fields were kept empty it would imply "not analyzed" what is also not the truth.

3) Some ^{14}C-dated samples were analyzed twice. In the database, both data are recorded, but when doing an export, only one number appears together with the main data. To avoid this, the field "Age" was created, where the most reliable age is recorded. In some cases (when the

ages are within 2σ), the mean of both ages is taken, which may not be compatible with the single set of recorded ^{14}C activity (dpm/kg)!

4) Beside samples from Oman, the database includes also samples from Australia having southern hemisphere latitudes. Since the coordinates are stored as numbers and not coordinates, a negative value is used for the southern hemisphere.

5) To study the correlation of petrologic type with another parameter, a number for petrologic type is assigned. Some samples are breccias and this information is stored as text. Breccias ("-") are covered with the petrologic type schema and are not included in the "Petro_Nr" field; transitional samples ("/") are recorded as number in-between (e.g. 4/5 -> 4.5). Shock grades are treated similarly.

6) Some entries in the main list (excel sheets) were highlighted with special formats, e.g. the main mass of a pairing group was marked bold. Such formats are lost in the DB.

7) Paired meteorites are fragments belonging to a single meteorite fall that were separated during atmospheric passage or during terrestrial history (Benoit et al., 2000). They commonly have identical classification (petrography, shock stage, mineralogy, mineral chemistry), same terrestrial age but can have different degrees of weathering and are contaminated to various amounts (Benoit et al., 2000; Gnos et al., 2009, Chapter 5). The identification of paired meteorites is a difficult issue, especially in dense meteorite accumulation areas. Further more, the recent meteorite shower of Almahata Sitta showed that a single meteorite fall can contain very distinct lithologies such as ureilites and EL chondrites (Bischoff et al., 2010). Therefore, the sentence of Benoit et al., (2000) is accurate: "pairing is more an art than a science". In the DB, meteorites can be sorted easily for its pairing group (PG). Usually, the largest mass is the main piece of a pairing group. This piece was noted in the main lists (excel) as "PG"-number minus 0.0001, e.g. the main mass of the JaH 091 (PG=86) sample had an entry of 85.9999. Often, a "new" or even the "true" main mass is found in subsequent fieldwork, e.g. the initial mass of JaH 091 was found in 2001, while the (current) main mass was found in 2006. In the DB, all pairing numbers (PG) are noted as natural number and the main mass of a pairing group is noted in the field "pairing" (Table A1).

A4. Future perspectives

The database can be expanded to include other data:

a) Beside the median value and the range, the standard deviation (STD) and the number of electron microprobe (EMP) analyses are required for classification. Currently, the median is recorded as well as the minimum and maximum values, i.e. the range. Eventually, one has to create a new field where STD and the number of analyses are noted. The field "comment_min" is designed for this; however, in the comment field one should only note extraordinary data or problems concerning analytics such as calcium-rich pyroxene analyzes or bad totals of the EMP analyses.

b) Oxygen isotopes are recorded for only a few meteorites. One could expand the database for these few numbers or include them into the column "comments_sample".

c) In the recent version, chemical data is recorded only from HHXRF analyses in the DB. Since chemical data is available for several other methods, an additional table could be introduced. A key for the kind of analyses has to be introduced then (e.g. 0=literature, undefined, 1=FUS-ICP, 2=FUS-MS, 3=XRF, 4=FUS Na2O2, 5=INNA, 6=ICP-MS, 7=ICP-OES, 8=HHXRF_PIN, 9=HHXRF_SDD). The HHXRF table has to be expanded since the updated instrument (now with silicon drift detector, SDD) records additional elements that are not scheduled in the current version.

d) Surface characterization and corresponding soil samples are described for several localities but not included in the DB. It could be interesting for further studies with the focus on interaction between meteorites and soil to have these data stored and linked in the database.

e) The database would be an excellent method to keep the overview of the samples. This section would include the available kind of samples (main mass, fragments, type specimen, how many thin sections, powders etc.) and for recording loans to other institutions.

f) Density is determined for some samples. If a systematic survey of density measurements would be planed, this section could also be included into the DB.

g) It would be interesting to have a tool, where all publications of a certain sample are linked.

h) A part of the DB could be made accessible via Internet. Collectors and meteorite enthusiast might be interested in pictures. Micrographs and cathode luminescence images are

included in a separate DB, which is linked with the current DB. For complete documentation, scans of thin section, field images and backscatter electron images could be included.

A5. Acknowledgements

A6. References

Al-Kathiri, A., Hofmann, B. A., Jull, A. J. T., and Gnos, E., 2005. Weathering of meteorites from Oman: Correlation of chemical and mineralogical weathering proxies with ^{14}C terrestrial ages and the influence of soil chemistry. *Meteoritics & Planetary Science* 40:1215-1239.

Benoit, P. H., Sears, D. W. G., Akridge, J. M. C., Bland, P. A., Berry, F. J., and Pillinger, C. T., 2000. The non-trivial problem of meteorite pairing. *Meteoritics & Planetary Science* 35:393-417.

Bischoff, A., Horstmann, M., Pack, A., Laubenstein, M., and Haberer, S., 2010. Asteroid 2008 TC3-Almahata Sitta: A spectacular breccia containing many different ureilitic and chondritic lithologies. *Meteoritics & Planetary Science* 45:1638-1656.

Gnos, E., Lorenzetti, S., Eugster, O., Jull, A. J. T., Hofmann, B. A., Al-Kathiri, A., and Eggimann, M., 2009. The Jiddat al Harasis 073 strewn field, Sultanate of Oman. *Meteoritics & Planetary Science* 44:375-387.

Table A1. Database fields and an example of a full record from the database.

Header in Database	Example from database	Format in database	Description of content
Main_FieldNo	0902_098	Text	As registered in the field (YYMM_runningNr, always use the same amount of digits with the runningNr. (at least per campaign) e.g. "0901_003" and not "0901-3"). The field number is unique in the main list of the database. Surface soil samples collected in 2009/2010 are named "_Surf" or" _REF" (2001 to 2008) and "_SUM" for soils under meteorites.

Header in Database	Example from database	Format in database	Description of content
Main_Name	Shalim_008	Text	Official meteorite name, empty if unassigned, generic name for non-meteoritic samples. Use underline instead of empty space.
Main_MB	S+	Number/Text	Meteoritical bulletin Nr in which the meteorite was published. S+: meteorite is submitted but not official yet, S: meteorite is classified but has to be submitted, empty: not classified yet.
Main_Area	W of Nimr	Text	Generic area name.
Main_Pairing	Shalim_008	Text	Here the official name or, if not available, the field Nr of the main sample of the pairing group is mentioned, bold for main sample (formats are lost in the database) of pairing group, empty or unpaired for unpaired meteorites.
Main_PG	488	Number	Pairing group Nr of the meteorite, the absolute number and sequence has no meaning, all numbers must be used.
Main_Met	1	Number	Code for fast sorting of desired sample population: 0: Oman, terrestrial samples. 1: Oman, meteorites. 2: Saudi Arabia, terrestrial. 3: Saudi Arabia, meteorites. 4: Sahara, terrestrial. 5: Sahara, meteorites. 6: Australia, terrestrial. 7: Australia, meteorite. 8: Standard, terrestrial. 9: Standard, meteorite. Examples for terrestrial samples are: soil samples, cherts or "meteorite wrongs". Standards are used for calibration of HHXRF. Terrestrial standards are for example KAI230R or MPI olivine. A meteorite standard is Allende. No terrestrial soil is included so far.
Main_FDate	13/02/2009	Date	Date of find. The format used is DD/MM/YYYY. Note that Excel uses two types of dates, one starting in 1900 and one starting 1904. To be compatible with the Met Soc templates, here we use the 1900 format (the

Appendix A

Header in Database	Example from database	Format in database	Description of content
			standard on Mac's is 1904). In order to test check the first search day (22/01/2001), this should be day 36913. The difference between the two formats is 1462 days.
Main_FTime	16:30:00	Time	Time of find (local time).
km	71.5	Number/Text	Kilometers driven at the day until the meteorite was found. (sometimes several drives per day; one drive may take several days)
			FFS: Meteorites found during „free" foot searches? (eventually add reason for foot search: e.g. find additional samples from 1002-156 and strewn field 1002-155?)
			SFS: For systematic foot searches? (and add the „official" name of the area, e.g. „CO_1"?)?
			Or keep empty when meteorite was found during foot search.
Main_Finders	UE,EG,EJ,FZ	Text	Initials of finders
Main_°N	18	Number	Latitude degrees.
Main_min_N	52.077	Number	Latitude minutes.
Main_°E	55	Number	Longitude degrees.
Main_min_E	27.044	Number	Longitude minutes.
Main_N_dec	18.868	Number	Latitude in decimal format.
Main_E_dec	55.45073333	Number	Longitude in decimal format.
Main_Lat_MB	1852.077	Text	Latitude in Meteoritical Bulletin format.
Main_Long_MB	5527.044	Text	Longitude in Meteoritical Bulletin format.
Main_Mass_tot	323.489	Number	Total mass of find in grams.
Main_Mass_BE	323.489	Number	Mass of sample arrived in Bern.
Main_Mass_others		Number	Mass stored elsewhere?
Main_Mass_Oman		Number	Mass stored in Oman initially after search campaign.
Main_FragBE	1	Number	Number of fragments, "real" number of fragments as counted during unpacking in Bern.
Main_FragApprox	1	Text	Number of fragments as counted/estimated in the field, if too many fragments, <X is noted.
Main_Class	H	Text	Classification of Sample, use "A_" for achondrites (e.g. "A_ureilite"), for chondrites use: H, L, LL, CO, etc; (no numbers); Terrestrial samples start with Terr_ and then the type of sample: Terr_chert.

Header in Database	Example from database	Format in database	Description of content
Main_Petro	5	Text	Petrologic type, use "-" for breccias and "/" for transitional samples.
Main_PetroNr	5	Number	Only one number for the petro. Type (breccias etc. are empty).
Main_Shock	S3	Text	Shock grade. Breccias "-", transitional "/".
Main_ShockNr	3	Number	Shock grade number (no breccias -> empty).
Main_WG	WD2.0	Text	Weathering grade as in the old list.
Main_WGNr	2.0	Number	Weathering grade as single number, no "-"; use weathering degree classification Chapter 6.
Main_Fa_XRD		Number	Fayalite content of olivine as determined by XRD.
Main_Fa_med	18.3	Number	Fayalite content of olivine as determined by electron microprobe analysis, use the median value.
Main_Fa_min		Number	Minimal fayalite content of olivine as determined by electron microprobe analysis, important for low petrologic type meteorites.
Main_Fa_max		Number	Maximal fayalite content of olivine as determined by electron microprobe analysis, important for low petrologic type meteorites.
Main_Fs_med	16.3	Number	Ferrosilite content of Ca-poor pyroxene as determined by electron microprobe analysis, use median value.
Main_Fs_min		Number	Minimal ferrosilite content of Ca-poor pyroxene as determined by electron microprobe analysis, important for low petrologic meteorites.
Main_Fs_max		Number	Maximal ferrosilite content of Ca-poor pyroxene as determined by electron microprobe analysis, important for low petrologic meteorites.
Main_Wo_med	1.3	Number	Wollastonite content of Ca-poor pyroxene as determined by electron microprobe analysis, use median value.
Main_Wo_min		Number	Minimal wollastonite content of olivine as determined by electron microprobe analysis, important for low petrologic meteorites.
Main_Wo_max		Number	Maximal wollastonite content of Ca-poor pyroxene as determined by electron microprobe analysis, important for low petrologic type meteorites.

Appendix A

Header in Database	Example from database	Format in database	Description of content
Main_CommentMin		Text	Comments on mineralogy: - "br" for breccias; - "CL" observations from cathode luminescence analyses, e.g. color or homogeneous pattern; - "EMP": observations from electron microprobe analyses, e.g. number of analyses, problems, Ca-rich pyroxene composition; - "SEM": observations from scanning electron microscope, e.g. semi-quantitative analyses, texture; - Microscopic observations e.g. ringwoodite, special weathering features; - XRD analyses - other comments.
Main_CommentSample		Text	Comments on sample history, macroscopic observations, special find situation, etc.
Main_MagnSusc		Number	Magnetic susceptibility, determined with SM30
Main_Distance	6	Number	Distance in [m] from which the meteorite was recognized, "seen from".
Main_Burial	50	Number	Degree of burial in % of the meteorite volume, as estimated in the field.
Main_Fe AV	0	-	Average of Fe from HHXRF list, relict of older calculation.
Main_ListeXRF	?	-	Relict of older calculation.
Main_CurrSerNum	1002_170	-	Relict of older calculation.
Main_SrM_CS		Summary	Summary field, the median of a chemical element is calculated form the HHXRF data.
Main_BaM_CS		Summary	Ditto
Main_FeM_CS		Summary	Ditto
Main_NiM_CS		Summary	Ditto
Main_MnM_CS		Summary	Ditto
Main_CrM_CS		Summary	Ditto
Main_CaM_CS		Summary	Ditto
Main_KM_CS		Summary	Ditto
Main_TiM_CS		Summary	Ditto
Main_VM_CS		Summary	Ditto
Main_SrM_BS		Summary	Ditto
Main_BaM_BS		Summary	Ditto
Main_FeM_BS		Summary	Ditto
Main_NiM_BS		Summary	Ditto
Main_MnM_BS		Summary	Ditto
Main_CrM_BS		Summary	Ditto
Main_CaM_BS		Summary	Ditto
Main_KM_BS		Summary	Ditto
Main_TiM_BS		Summary	Ditto
Main_VM_BS		Summary	Ditto
Main_SrM_ES		Summary	Ditto
Main_BaM_ES		Summary	Ditto
Main_FeM_ES		Summary	Ditto

Header in Database	Example from database	Format in database	Description of content
Main_NiM_ES		Summary	Ditto
Main_MnM_ES		Summary	Ditto
Main_CrM_ES		Summary	Ditto
Main_CaM_ES		Summary	Ditto
Main_KM_ES		Summary	Ditto
Main_TiM_ES		Summary	Ditto
Main_VM_ES		Summary	Ditto
Main_SrM_NS		Summary	Ditto
Main_BaM_NS		Summary	Ditto
Main_FeM_NS		Summary	Ditto
Main_NiM_NS		Summary	Ditto
Main_MnM_NS		Summary	Ditto
Main_CrM_NS		Summary	Ditto
Main_CaM_NS		Summary	Ditto
Main_KM_NS		Summary	Ditto
Main_TiM_NS		Summary	Ditto
Main_VM_NS		Summary	Ditto
Meteorite_Age::Run	R3691	Text	Number of the C-14 dating series.
Meteorite_Age::FieldNo	0902_098	Text	Field number to link with main table.
Meteorite_Age::Name		Text	Official name.
Meteorite_Age::Weight	0.09437	Number	Weight of C-14 sample.
Meteorite_Age::Fm	3.45	Number	
Meteorite_Age::FMstd	0.054	Number	
Meteorite_Age::CO2	0.016	Number	
Meteorite_Age::Dilted	0.016	Number	
Meteorite_Age::C14atoms	1024157.604	Number	
Meteorite_Age::C14g	10852576.07	Number	
Meteorite_Age::dpmkg	2.49733621	Number	
Meteorite_Age::dpmkgStd	0.392101983	Number	
Meteorite_Age::Saturated	46.4	Number	
Meteorite_Age::AgeC14Values	24.15971454	Number	C-14 terrestrial age.
Meteorite_Age::AgeC14Std	1.837164911	Number	Error of C-14 age.
Meteorite_Age::Age10Be		Number	Be-10 corrected age.
Meteorite_Age::AgeC14		Text	C-14 age as text field, includes also ">" ages.
Meteorite_Age::Age		Number	Summarized age.
Meteorite_Age::CommentAge	too old	Text	Comment to age -> what type is noted in the "Age" field.
Meteorite_Niton_XRF::Reading No	2286	Number	Number of HHXRF measurement.
Meteorite_Niton_XRF::Time	14:58:00	Time	Time of HHXRF analysis.
Meteorite_Niton_XRF::Type	MINING	Text	Type of analyses: "MINING" or "SOIL" mode.
Meteorite_Niton_XRF::Duration	300.5	Number	Duration of analyze [s].
Meteorite_Niton_XRF::Units	ppm	Number	Unit of analyzes [ppm] or [%].
Meteorite_Niton_XRF::Sequence	Final	Number	Entry from analysis.
Meteorite_Niton_XRF::Sample	0901-98	Text	Sample ID.
Meteorite_Niton_XRF::FieldNo	0902_098	Text	Field number.
Meteorite_Niton_XRF::Name		Text	Official name.
Meteorite_Niton_XRF::LOCATION	HS	Text	Type of sample: "HS": Hand specimen, "cs": small pieces of rocks, used for thin section preparation, "PH": sample holder, "PP": press pill, "pp": press pill small, used for Sr&Ba standards, "PS": plastic bag (soil samples).
Meteorite_Niton_XRF::INSPECTOR	CS	Text	Measured surface: CS Cut surface,

Appendix A

Header in Database	Example from database	Format in database	Description of content
			cs: Small samples, ES: Exposed surface, BS: Buried surface, NS: Natural surface, ES_FC: When fusion crust (FC) was measured on an exposed part of the meteorite, P: powder sample, 0.15: for soil samples, sieved fraction <0.15 mm.
Meteorite_Niton_XRF::FeMn	93.23663787	Number	Calculated Fe/Mn ratio from HHXRF data.
Meteorite_Niton_XRF::FeNi	24.39704144	Number	Calculated Fe/Ni ratio from HHXRF data.
Meteorite_Niton_XRF::SrBa		Number	Calculated Sr/Ba ratio from HHXRF data.
Meteorite_Niton_XRF::Flags	ModCF Meteorit-8mm	Text	Used analyze program and spot size: "cM": mining Cu-Zn mode, "tM": Ta/Hf mining, "S" soil, "Meteorit": corrected for meteorite samples, uses cM mode.
Meteorite_Niton_XRF::Sr	15.49	Number	Elements as detected by HHXRF, <LOD: below limit of detection.
Meteorite_Niton_XRF::Sr Error	1.41	Number	Reported error of HHXRF analyzes.
Meteorite_Niton_XRF::Ba	0	Number	Ditto
Meteorite_Niton_XRF::Ba Error	87.47	Number	Ditto
Meteorite_Niton_XRF::Fe	242439.5	Number	Ditto
Meteorite_Niton_XRF::Fe Error	3484.51	Number	Ditto
Meteorite_Niton_XRF::Ni	9937.25	Number	Ditto
Meteorite_Niton_XRF::Ni Error	209.49	Number	Ditto
Meteorite_Niton_XRF::Mn	2600.26	Number	Ditto
Meteorite_Niton_XRF::Mn Error	138.7	Number	Ditto
Meteorite_Niton_XRF::Cr	4133.97	Number	Ditto
Meteorite_Niton_XRF::Cr Error	122.36	Number	Ditto
Meteorite_Niton_XRF::Ca	15030.21	Number	Ditto
Meteorite_Niton_XRF::Ca Error	511.2	Number	Ditto
Meteorite_Niton_XRF::K	1140.45	Number	Ditto
Meteorite_Niton_XRF::K Error	442.84	Number	Ditto
Meteorite_Niton_XRF::Ti	606.72	Number	Ditto
Meteorite_Niton_XRF::Ti Error	75.8	Number	Ditto
Meteorite_Niton_XRF::Pb	0	Number	Ditto
Meteorite_Niton_XRF::Pb Error	9.16	Number	Ditto
Meteorite_Niton_XRF::Bal	722028.5	Number	Ditto
Meteorite_Niton_XRF::Bal Error	6534	Number	Ditto
Meteorite_Niton_XRF::Sn	0	Number	Ditto
Meteorite_Niton_XRF::Sn Error	26.84	Number	Ditto
Meteorite_Niton_XRF::Zn	59.47	Number	Ditto
Meteorite_Niton_XRF::Zn Error	12.38	Number	Ditto
Meteorite_Niton_XRF::Zr	8.02	Number	Ditto
Meteorite_Niton_XRF::Zr Error	2.46	Number	Ditto
Meteorite_Niton_XRF::Mo	9.06	Number	Ditto
Meteorite_Niton_XRF::Mo Error	4.01	Number	Ditto
Meteorite_Niton_XRF::Cu	97.11	Number	Ditto
Meteorite_Niton_XRF::Cu Error	37.27	Number	Ditto
Meteorite_Niton_XRF::Ag	0	Number	Ditto
Meteorite_Niton_XRF::Ag Error	4.87	Number	Ditto
Meteorite_Niton_XRF::S	15694.7	Number	Ditto
Meteorite_Niton_XRF::S Error	4689.62	Number	Ditto
Meteorite_Niton_XRF::Co	0	Number	Ditto
Meteorite_Niton_XRF::Co Error	382.23	Number	Ditto

Header in Database	Example from database	Format in database	Description of content
Meteorite_Niton_XRF::Sb	0	Number	Ditto
Meteorite_Niton_XRF::Sb Error	21.17	Number	Ditto
Meteorite_Niton_XRF::Cd	0	Number	Ditto
Meteorite_Niton_XRF::Cd Error	7.62	Number	Ditto
Meteorite_Niton_XRF::Pd	0	Number	Ditto
Meteorite_Niton_XRF::Pd Error	2.62	Number	Ditto
Meteorite_Niton_XRF::Nb	8.13	Number	Ditto
Meteorite_Niton_XRF::Nb Error	3.03	Number	Ditto
Meteorite_Niton_XRF::Rb	0	Number	Ditto
Meteorite_Niton_XRF::Rb Error	2	Number	Ditto
Meteorite_Niton_XRF::Bi	0	Number	Ditto
Meteorite_Niton_XRF::Bi Error	6.8	Number	Ditto
Meteorite_Niton_XRF::As	0	Number	Ditto
Meteorite_Niton_XRF::As Error	4.58	Number	Ditto
Meteorite_Niton_XRF::Se	0	Number	Ditto
Meteorite_Niton_XRF::Se Error	5.93	Number	Ditto
Meteorite_Niton_XRF::W	0	Number	Ditto
Meteorite_Niton_XRF::W Error	108.86	Number	Ditto
Meteorite_Niton_XRF::V	119.25	Number	Ditto
Meteorite_Niton_XRF::V Error	54.96	Number	Ditto
Meteorite_Niton_XRF::Re		Number	Ditto
Meteorite_Niton_XRF::Re Error		Number	Ditto
Meteorite_Niton_XRF::Ta		Number	Ditto
Meteorite_Niton_XRF::Ta Error		Number	Ditto
Meteorite_Niton_XRF::Hf		Number	Ditto
Meteorite_Niton_XRF::Hf Error		Number	Ditto
Meteorite_Niton_XRF::Fe_av	244236.7109	Number	Average of Fe for all samples with the same field numbers, inspectors and locations. Relict of an older version.
Meteorite_Niton_XRF::Mn_av	2837.736	Number	Average of Mn for all samples with the same field numbers, inspectors and locations. Relict of an older version.
Meteorite_Niton_XRF::Calculus	137.86 151.1 175.06 203.52	-	Calculus field, used for median calculation.
Meteorite_Niton_XRF::MEd	163.08	-	Calculus field, used for median calculation
Meteorite_weights::FieldNo	0902_098	Text	Field number.
Meteorite_weights::Name	Shalim_008	Text	Official name.
Meteorite_weights::MassTot	323.489	Number	Total weight [g].
Meteorite_weights::Frag1	323.489	Number	Weight of the largest fragment [g].
Meteorite_weights::FI	1	Number	Fragmentation index, weight of the largest fragment divided by the total mass.
Meteorite_WP::FieldNo	0902_098	Text	Field number.
Meteorite_WP::Salt_CS	1	Number	Salt efflorescence visible on cut surface (chapter 5). Code see chapter 4 and 6.
Meteorite_WP::Porefill_CS	1	Number	State of pores on cut surface.
Meteorite_WP::Red_dorso_BS	0	Number	Color difference of buried to exposed surface.
Meteorite_WP::Ni_green_stain_BS	0	Number	Greenish staining on buried surface present?
Meteorite_WP::FC_BS		Number	Preservation of fusion crust on buried surface.
Meteorite_WP::CC_BS	1	Number	Calcite precipitation on

Appendix A

Header in Database	Example from database	Format in database	Description of content
			buried surface.
Meteorite_WP::FC_ES	1	Number	Preservation of fusion crust on exposed surface.
Meteorite_WP::Wind_ES	0	Number	Amount of wind erosion on exposed surface.
Meteorite_WP::FeSand_ES	1	Number	Attached sand on exposed surface?
Meteorite_WP::Cracks_ES	1	Number	Amount and width of cracks visible on exposed surface.
Meteorite_WP::lichen	0	Number	Coverage by lichen.

Appendix B: Classification of meteorites found in 2009 and 2010

In Table B1 the classifications of all meteorites collected during fieldwork in 2009 and 2009/2010 are listed. Their classification is crucial for the weathering studies presented in chapters 4, 5 and 6. The ordinary chondrites were assigned to the classes H, L and LL using fayalite content of olivine and ferrosilite content of low-Ca pyroxene as defined by Brearley and Jones, (1998, references therein). Quantitative mineral chemistry was determined on polished thin sections using a Jeol JXA-8200 electron microprobe (EMP) with wavelength-dispersive spectrometers at the Institute of Geological Sciences, University of Bern. Beam conditions were 15 kV, 20 nA and spot size varied between 1 and 5 µm. Natural or synthetic silicate and oxide standards were used for calibration. Mineral chemistry of equilibrated chondrites is plotted in Figure B1a. Petrologic type (Van Schmus and Wood, 1967), shock (Stöffler et al., 1991) and weathering degree (Chapter 6) were determined in thin section with optical microscopy techniques. Some obviously paired samples were not examined in thin section. For verification, fayalite content of olivine was determined by X-ray diffraction (XRD) in those samples. The EMP and XRD results are in agreement with each other for equilibrated chondrites (Fig. B1b). Values obtained with XRD are slightly higher than EMP analyses. Cathodoluminescence (CL) analyses for determination of subtype 3 (petrologic type) were performed on a cold CL OPEA32J instrument equipped with a Leica DMLB microscope at the Natural History Museum, Geneva. The measurements were carried out at a 15 keV accelerating voltage and a 43–45 mA beam current. Division in subtypes was done based on luminescence color of matrix and mesostasis (Akridge et al., 2004; Huss et al., 2006).
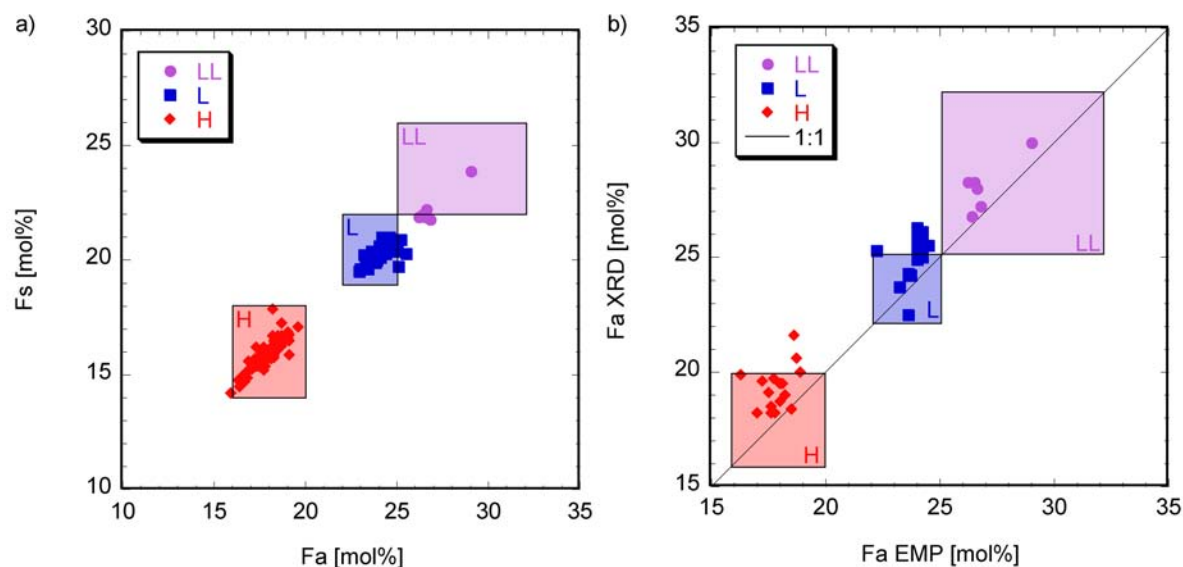
Figure B1. *Classification of ordinary chondrites found in 2009 and 2010 by mineral chemistry. a) Equilibrated chondrites (petrologic types 4 to 6) are classified by fayalite (Fa) and ferrosilite (Fs) content determination in olivine and pyroxene, respectively. Each data point is the median of more than ten analyses. b) Fa contents were determined in equilibrated ordinary chondrites with XRD and EMP. Excluded from both graphs (a, b) are unequilibrated (petrologic type 3) and variable petrologic type 4 meteorites.*

References

Akridge, D. G., Akridge, J. M. C., Batchelor, J. D., Benoit, P. H., Brewer, J., DeHart, J. M., Keck, B. D., Jie, L., Meier, A., Penrose, M., Schneider, D. M., Sears, D. W. G., Symes, S. J. K., and Zhang, Y. H., 2004. Photomosaics of the cathodoluminescence of 60 sections of meteorites and lunar samples. *Journal of Geophysical Research-Planets* 109.

Brearley, A. J. and Jones, R. H., 1998. Chondritic meteorites. In: Papike, J. J. (Ed.), *Planetary Materials*. Mineralogical Society of America, Washington D. C.

Huss, G. R., Rubin, A. E., and Grossman, J. N., 2006. Thermal metamorphism in chondrites. In: Lauretta, D. S. and McSween, H. Y. (Eds.), *Meteorites and the Early Solar System II*. University of Arizona Press, Tucson.

Stöffler, D., Keil, K., and Scott, E. R. D., 1991. Shock metamorphism of ordinary chondrites. *Geochimica et Cosmochimica Acta* 55:3845-3867.

Van Schmus, W. R. and Wood, J. A., 1967. A chemical-petrologic classification for chondritic meteorites. *Geochimica et Cosmochimica Acta* 31:747-765.

Table B1. Classification of Omani-Swiss meteorites found in 2009 and 2010.

Field number	Official name	PG	N [°]	E [°]	Mass [g]	Frag.	Class	P	S	WD	Fa (XRD)	Fa [mol%]	Fs [mol%]	Wo[mol%]
0901_002	SaU 505	26	20.5640	56.6655	109.962	1	L	4-5	S2	1.0		25.1	19.7	1.2
0901_003	RaS 281	429	20.5709	56.3885	203.727	1	H	3.4-6	S2	3.0		18.7	17.3	0.8
0901_004	RaS 282	429	20.5781	56.3949	132.046	1	H	3.4-5	S2	3.0		17.6	16.0	0.9
0901_005	RaS 283	430	20.7878	56.4711	447.657	3	H	4	S1	4.0		19.1	15.9	1.0
0901_006	UaS 008	431	21.0058	56.4692	290.271	3	L	6	S3	4.0		24.4	20.3	1.6
0901_007	UaS 009	432	21.0649	56.4819	3989	1	L	6	S4	4.0		24.2	21.0	1.6
0901_008	SaU 506	433	21.2545	56.5030	356.726	10	H	4-5	S1	3.3		18.6	16.4	1.2
0901_009	UaS 010	434	21.3489	56.1619	251.663	1	H	4	S3	3.0		18.3	16.5	1.1
0901_010	UaS 011	435	21.3760	56.2911	790.5	1	H	4	S1	3.0		18.4	16.6	1.0
0901_011	UaS 012	435	21.3802	56.2908	1354.8	1	H	4	S1	3.0		18.4	16.6	1.0
0901_012	UaS 013	436	21.3728	56.3138	205.566	1	L	6	S4	2.0		24.7	20.6	1.4
0901_013	UaS 014	435	21.3739	56.3137	1713.8	1	H	4	S1	4.0		18.4	16.6	1.0
0901_014	SaU 507	437	21.2900	56.5809	665.7	1	L	6	S1	3.0		24.3	20.5	1.5
0901_015	SaU 508	438	21.2001	56.7355	373.869	1	H	6	S3	3.3		18.7	16.3	1.4
0901_016	SaU 509	439	21.0122	56.7796	182.658	1	H	5	S3	2.0		17.7	15.8	1.3
0901_017	SaU 510	440	20.9393	56.9045	257.62	1	L	6	S3	3.0		24.4	20.7	1.3
0901_018	SaU 511*	441	20.8961	56.9261	266.202	2	Ureilite					21.2	17.9	10.1
0901_019	SaU 512	442	20.9062	56.9489	1606.9	1	H	4-5	S2	3.0		17.5	15.8	1.2
0901_020	RaS 284	443	20.5195	55.8010	1489.6	1	LL	5	S1	3.0	28.0	26.6	22.2	1.6
0901_021	RaS 285	444	20.5157	55.7903	269.303	11	L	6	S4	4.0		24.2	20.8	1.6
0901_022	RaS 286	445	20.5079	55.7755	4445.2		H	4-5	S1	3.0		17.6	16.0	1.3
0901_023	RaS 287*	446	20.4768	55.5279	1961.961	2	Diogenite						27.6	2.2
0901_024	RaS 288	447	20.4571	55.4914	73.263	1	L	4-6	S1	2.0		23.3	19.9	1.4
0901_025	RaS 289	448	20.5135	55.5274	123.461	1	H	4	S2	3.0		18.2	16.1	0.9
0901_026	RaS 290	449	20.5234	55.5307	446.822	2	L	6	S4	3.3		24.2	20.5	1.6
0901_027	RaS 291	450	20.5283	55.5298	138.233	9	L	4	S2	4.5		24.1	20.6	1.4
0901_028	RaS 292	451	20.5983	55.5240	1991.656	5	L	6	S2	3.0		24.6	20.4	1.4
0901_029	RaS 293	452	20.6284	55.5312	30.966	1	H	5-6	S2	4.0	20.0	18.9	16.7	1.2
0901_030	RaS 294	453	20.6928	55.4922	52.868	1	L	6	S3	3.0	25.5	24.5	20.4	1.4
0901_031	RaS 295	454	20.6697	55.4281	227.695	1	H	4	S2	3.0		18.2	16.3	0.9
0901_032	RaS 296	455	20.6684	55.3401	49.32	6	L	6	S4	4.0	24.8	18.5	16.6	1.4
0901_033	RaS 297	455	20.6675	55.3172	706.937	20	L	6	S4	4.5		25.2	20.9	1.5
0901_034	RaS 298	455	20.6671	55.3157	389.242	2	L	6	S4	4.0		25.0	20.4	1.7
0901_035	RaS 299	455	20.6675	55.3159	53.132	2	L	6	S4	4.0		25.5	20.3	1.8
0901_036	RaS 300	455	20.6664	55.3140	419.894	1	L	6	S4	4.0		24.4	20.5	1.4
0901_037	RaS 301	456	20.0373	56.2742	86.751	1	L	4	S2	4.0		23.9	20.1	1.2
0901_038	RaS 302	457	20.1448	56.2409	161.675	1	H	4	S2	3.6		17.2	15.7	1.1
0901_039	RaS 303	458	20.4472	56.1209	102.966	1	H	4	S2	4.0		18.3	16.1	1.1

Field number	Official name	PG	N [°]	E [°]	Mass [g]	Frag.	Class	P	S	WD	Fa (XRD)	Fa [mol%]	Fs [mol%]	Wo[mol%]
0901_040	RaS 304	459	20.4380	56.1028	373.441	2	H	6	S2	3.3		19.0	16.8	1.5
0901_041	RaS 305	460	20.4149	56.0794	130.781	1	L	6	S4	4.0		24.4	20.4	1.4
0901_042	RaS 306	461	20.4898	56.0363	165.2	1	H	6	S2	4.0		17.4	15.4	1.2
0901_043	RaS 307	462	20.5263	55.9060	327.537	5	H	3.9-6	S3	3.0		16.8-21.5 (18.8)	15.3-18.0 (16.8)	0.6-1.9 (1.8)
0901_044	RaS 308	463	20.4879	55.8205	1352	1	H	4	S2	3.3		16.9	15.6	1.4
0901_045	JaH 568	464	19.7013	56.3671	3248.999	63	H	4-6	S2	4.0		16.6-18.8 (18.2)	14.8-20.1 (16.0)	0.5-1.7 (1.4)
0901_046	JaH 569	340	19.7404	56.3396	159.31	3	H	4-6	S2	4.0		18.8	16.5	1.3
0901_047	JaH 570	340	19.7524	56.3304	4747.94	17	H	4-6	S2	4.0		18.4	16.2	1.3
0901_048	JaH 571	340	19.7507	56.3309	802.551	4	H	4-6	S2	3.3		13.5-19.9 (17.6)	11.9-17.3 (16.6)	0.7-1.3 (1.2)
0901_049	JaH 572	340	19.7509	56.3311	417.591	1	H	5-6	S2	4.0		17.8	15.9	1.4
0901_050	JaH 573	340	19.7517	56.3306	28.889	1	H	4-6	S2	3.0		18.6	16.4	1.3
0901_051	JaH 574	340	19.7538	56.2969		42	H	4-6	S2	4.0		15.3-18.6 (18.1)	6.7-16.2 (15.6)	0.1-1.3 (0.7)
0901_052	JaH 575	328	19.7599	56.2861	190.419	2	H	6	S1	3.0		18.8	16.6	1.2
0901_053	JaH 576	328	19.7487	56.3201	284.621	3	H	5/6	S1	4.0		19.0	16.9	1.3
0901_054	JaH 577	465	19.7375	56.3073	81.63	2	H	4/5	S3	4.0		17.6	15.6	1.2
0901_055	JaH 578	466	19.7642	56.2989	1064.3	1	H	6	S2	1.0		19.6	17.1	1.7
0901_056	Al Huqf 067	467	19.2260	57.5406	61.568	2	H	4	S2	4.0		17.6	15.5	1.0
0901_057	Al Huqf 068	468	19.1403	57.5843	165.444	4	L	3.8	S2	3.6		9.4-28.6 (24.0)	7.3-13.1 (10.1)	0.6-3.0 (1.6)
0901_059	Al Huqf 069	469	19.2680	57.1341	250.483	1	H	4/5	S2	3.0		17.8	15.8	1.1
0901_060	JaH 579	470	19.3542	56.7529	475.106	27	L	4-6	S3-5	3.3		23.4	19.6	0.6
0902_061	JaH 580	471	19.4202	56.7016	1929	1	H	5	S2	3.0		18.3	16.2	1.4
0902_062	JaH 581	471	19.4220	56.6991	375.118	1	H	5	S2	4.0		18.5	16.4	1.3
0902_063	JaH 582	472	19.4221	56.6994	1647.5	1	L	6	S5	4.0		23.9	20.1	1.4
0902_064	JaH 583	471	19.4207	56.6993	1272.547	20	H	5	S2	4.0		18.5	16.4	1.4
0902_065	JaH 584	473	19.7067	56.7513	715.161	5	H	6	S3	3.0		19.1	16.5	1.4
0902_066	SaU 513	519	20.1254	56.5534	154.244	6	H	5	3	3.6		18.5	16.7	1.3
0902_067	SaU 514	520	20.7128	57.1216	1145.125	2	L	5	S3	3.0		24.3	20.4	1.5
0902_068	SaU 515	66	20.7272	57.1074	549.906	1	H	4	S2	3.0		17.9	15.7	0.7
0902_069	JaH 585	521	19.4387	56.6775	408.73	1	H	5	S3	3.0		18.5	16.4	1.8
0902_070	JaH 586	206	19.7429	56.6506	3568.46	3	H	5	S3	3.0		18.3	16.2	1.4
0902_071	JaH 587	206	19.8049	56.6705	1721.5	1	H	5	S3	3.0		18.6	16.6	1.4
0902_072	JaH 588	474	19.6236	56.8788	165.346	1	L	6	S4	3.3		24.2	20.4	1.4
0902_073	Al Huqf 070	475	19.1880	57.1098	2632.834	61	L	3.7-3.9	S3	4.0	24.6	23.6-26.9 (24.4)	19.5	0.3-1.9 (0.7)
0902_075	JaH 589	476	19.3358	56.9379	666.6	1	H	5	S1	3.0		18.2	16.7	1.0
0902_076	JaH 590	471	19.4225	56.7002	1044	1	H	5	S2	3.0		18.4	16.2	1.4
0902_077	JaH 591	471	19.4221	56.7003	103.253	1	H	5	S2	4.0		18.3	16.1	1.2
0902_078	JaH 592	471	19.4205	56.6996	423.229	2	H	5	S2	3.0		18.4	16.4	1.3

Field number	Official name	PG	N [°]	E [°]	Mass [g]	Frag.	Class	P	S	WD	Fa (XRD)	Fa [mol%]	Fs [mol%]	Wo[mol%]
0902_079	JaH 593	471	19.4200	56.7033	1725.1	1	H	5	S2	2.0		18.4	16.2	1.4
0902_080	JaH 594	471	19.4184	56.6964	201.289	1	H	5	S2	4.0		18.3	16.2	1.4
0902_081	JaH 595	477	19.5088	56.6464	929.1	1	L	5	S3	3.6		23.6	19.9	1.3
0902_082	JaH 596	478	19.6615	56.4393	336.365		L	3.2	S2	3.0	28.5	9.2-38.6(25.6)	10.5-24.2(17.1)	0.4-9.6(1.0)
0902_083	JaH 597	479	19.6561	56.3718	51.284	1	H	4	S2	2.0		16.4	14.8	0.9
0902_084	JaH 598	70	19.8277	55.6734	39.181	1	L	6	S4	4.0		24.3	20.4	1.3
0902_085	JaH 599	70	19.7965	55.6827	169.744	1	L	6	S4	3.0		24.0	20.4	1.3
0902_086	JaH 600	70	19.7955	55.6831	5750.77	3	L	6	S4	3.0		24.1	20.4	1.4
0902_087	JaH 601	70	19.6442	55.7396	59.804	1	L	6	S4	4.0		23.7	20.2	1.5
0902_088	JaH 602	480	19.6783	55.8646	39.952	1	H	6	S1	3.0		18.6	16.6	1.3
0902_089	JaH 603	481	19.7046	55.8819	29.442	1	H	5	S2	3.0		17.8	15.9	1.6
0902_090	JaH 604	482	19.7896	55.9762	754.008	19	H	4-6	S2	3.0		18.6	16.2	1.2
0902_091	JaH 605	483	19.8629	56.0060	58.466	1	L	6	S1	2.0		24.4	20.3	1.6
0902_092	JaH 606	484	19.9294	55.9235	114.662	14	H	5	S3	3.6		18.7	16.4	1.1
0902_093	JaH 607	485	19.9080	55.9086	1317.6	1	L	6	S4	3.0		23.9	20.3	1.5
0902_094	JaH 608	482	19.8590	55.9404	120.648	4	H	5	S2	4.0		17.3	15.6	1.1
0902_095	JaH 609	486	19.8598	55.9464	442.891	23	L	6	S3	4.0		24.1	20.3	1.6
0902_096	JaH 610	482	19.8724	55.9809	457.503	1	H	3.2-5	S2	3.3		8.9-20.7(18.1)	14.4-18.4(16.2)	0.8-1.6(1.3)
0902_097	JaH 611	487	19.9576	56.0606	109.517	1	H	4	S1	4.0		17.3	15.4	0.7
0902_098	Shalim 008	488	18.8680	55.4507	323.489	1	H	5	S3	2.0		18.3	16.3	1.3
0902_099	Shalim 009	489	18.8725	55.4759	9472.157		L	6	S5	3.0		23.9	20.4	1.6
0902_100	Shalim 010	489	18.8887	55.4379	291.61	7	L	6	S5	4.0		24.0	20.6	1.5
0902_101	Shalim 011	490	18.9002	55.5935	201.199	2	H	4	S1	3.0		16.4	14.5	1.1
0902_102	Shalim 012	491	18.9426	55.6314	101.945	1	H	4	S2	4.0		18.0	16.1	1.1
0902_103	Shalim 013	490	18.9865	55.5865	405.788	22	H	4	S1	3.3		15.9	14.2	0.9
0902_104	Shalim 014	492	18.9993	55.4952	34.103	1	L	6	S5	4.0		23.0	19.6	1.1
0902_105	JaH 612	493	19.0097	55.3431	179.684	1	H	6	S2	3.0		16.7	14.8	1.4
0902_106	JaH 613	494	19.0092	55.3340	241.029	8	H	4/5	S2	4.0		16.7	14.8	1.2
0902_107	JaH 614	494	19.0106	55.3126	3532.863	3	H	4/5	S2	3.3		16.7	14.7	1.2
0902_108	JaH 615	495	19.1551	55.4312	111.275	2	H	5	S1	3.0		18.5	16.2	1.5
0902_109	JaH 616	496	19.1714	55.4217	360.512	2	H	4	S2	3.0		18.1	16.0	1.1
0902_110	JaH 617	495	19.1940	55.4172	128.437	1	H	5	S1	3.0		18.6	16.4	1.3
0902_111	JaH 618	497	19.2400	55.3702	42.947	1	H	3.9	S4	3.0		14.6-17.9(16.5)	14.1-15.4(14.6)	0.4-3.9(0.7)
0902_112	JaH 619*	498	19.3263	55.3659	14.541	1	CO	3.2	S1			0.7-38.6(12.5)	0.9-44.6(8.9)	0.3-3.2(1.9)
0902_113	JaH 620	499	19.3713	55.3692	244.566	3	L	6	S4	2.0		24.1	20.4	1.6
0902_114	JaH 621	500	19.3852	55.3774	43.429	1	L	6	S1	3.0		24.6	20.7	1.4
0902_115	JaH 622	501	19.4217	55.3686	76.519	1	H	5	S2	4.0		17.9	16.0	1.3
0902_116	JaH 623	502	19.4310	55.3640	22.056	1	H	4	S1	4.0		18.3	15.9	1.0
0902_117	JaH 624	499	19.4320	55.3634	34.226	1	L	6	S3	3.0		23.8	20.3	1.4

Field number	Official name	PG	N [°]	E [°]	Mass [g]	Frag.	Class	P	S	WD	Fa (XRD)	Fa [mol%]	Fs [mol%]	Wo[mol%]
0902_118	RaS 309*	503	20.7658	55.4359	1428.376	3	Brachinite					33.1	27.5	2.2
0902_119	RaS 310	504	20.7831	55.4433	1223.241	6	H	3.2-6	S3	2.0		2.7-19.9 (18.6)	6.4-22.2 (16.1)	0.2-1.6 (1.3)
0902_120	RaS 311	504	20.7839	55.4479	20.279	1	H	4-6	S3	2.0		18.7	16.7	1.4
0902_121	RaS 312	505	20.7982	55.4715	472.659	1	H	6	S4	3.3	18.2	17.8	16.1	1.6
0902_122	RaS 313	505	20.7989	55.4720	111.275	1	H	6	S4	3.3	17.7	0.0		
0902_123	RaS 314	505	20.8016	55.4732	218.951	2	H	6	S4	3.6	19.5	0.0		
0902_124	RaS 315	505	20.8018	55.4736	2.885	1	H	6	S4	4.0	18.2	17.6	15.9	1.6
0902_125	RaS 316	506	20.8949	55.5061	2706.034		L	5	S3	4.5	24.2	23.7	20.1	1.4
0902_126	RaS 317	506	20.8933	55.4938	237.216	1	L	5	S3	4.0	24.2	23.6	20.4	1.4
0902_127	RaS 318	506	20.8934	55.4936	1172.393	3	L				24.1			
0902_128	RaS 319	507	20.8819	55.4345	948.412	3	H	5	S2	4.0		18.3	16.5	1.3
0902_129	RaS 320	508	20.8728	55.4277	1002.311	2	L	6	S5	2.0		24.3	20.9	1.4
0902_130	RaS 321	509	20.8847	55.4210	171.871	1	H	5	S1	4.0		17.5	15.6	1.7
0902_131	RaS 322	510	20.9190	55.4119	264.422	1	H	3.7	S1	3.0		1.3-25.9 (16.9)	6.6-20.1 (14.6)	0.-3.2 (0.9)
0902_132	RaS 323	511	20.7991	55.4247	161.776	35	L	3.7-6	S3	3.6	23.3	6.2-31.5 (24.2)	0.4-22.7 (20.0)	0.3-2.1 (1.5)
0902_134	RaS 324	512	20.1186	56.2943	63.217	1	L	6	S4	3.6		24.0	20.3	1.4
0902_135	RaS 325	513	20.2604	56.4902	850.8	1	L	6	S4	3.0		24.0	20.2	1.5
0902_136	SaU 516	514	20.3565	56.5489	115.535	1	H	5	S2	4.0		17.9	15.9	1.6
0902_137	SaU 517	515	20.3564	56.5514	1.731	1	L	4	S2	4.0		23.8	19.9	0.6
0902_138	SaU 518	516	20.3715	56.5108	390.325	14	L	5	S3	4.0		23.9	20.3	1.6
0902_139	SaU 519	516	20.3717	56.5102	403.23	18	L	5	S3	4.0		23.9	20.1	1.7
0902_140	RaS 326	517	20.4063	56.4753	65.443	2	H	4	S4	3.6		18.0	16.1	1.1
0902_141	RaS 327	335	20.4136	56.4782	198.974	1	L	6	S3	3.0		23.9	20.1	1.3
0902_142	RaS 328	335	20.4209	56.4999	1732.697	100	L	6	S4	3.0		24.6	21.0	1.7
0902_143	SaU 520	336	20.4209	56.5003	30.185	10	H	5	S3	3.0		18.3	16.1	1.5
0902_144	SaU 521	160	20.4043	56.6421	350.097	1	H	5	S3	3.0		18.4	16.3	1.5
0902_145	SaU 522	348	20.4070	56.6523	977.837	8	L	6	S4	3.3		24.2	20.4	1.4
0902_146	SaU 523	348	20.4153	56.6655	265.209	1	L	6	S4	3.3		23.2	20.2	1.4
0902_147	SaU 524	342	21.0371	57.2311	1485.7	1	L	6	S4	3.0		24.4	20.5	1.3
0912_001	Al Huwaysah 001	522	22.8049	55.3274	3150.518	237	LL	6	S3	4.0	28.2			
0912_002	Al Huwaysah 002	522	22.7985	55.3167	690.5	1	LL	6	S3	3.6	27.2	26.8	21.8	1.6
1001_003	Al Huwaysah 003	523	22.7486	55.3732	273.047	1	L	4-6	S2-4	3.3		23.7-26.8 (25.5)	19.9-22.3 (21.1)	0.5-6.0 (1.9)
1001_004	Al Huwaysah 004	524	22.7473	55.3952	141.51	1	H	5	S2	3.3		17.5	15.6	1.3
1001_005	Al Huwaysah 005	525	22.7334	55.3312	1228.119	27	L (LL)	3.5-3.7	S3	2.0		3.3-38.5 (23.4)	2.2-33.3 (16.4)	0.2-6.2 (0.9)
1001_006	Al Huwaysah 006	526	22.7374	55.3191	16.412	1	L	6	S2	3.3		24.1	20.3	1.6

Field number	Official name	PG	N [°]	E [°]	Mass [g]	Frag.	Class	P	S	WD	Fa (XRD)	Fa [mol%]	Fs [mol%]	Wo [mol%]
1001_007	Al Huwaysah 007	527	22.7339	55.3204	1.563	1	L	6	S4	3.3		23.7	19.9	1.5
1001_008	Al Huwaysah 008	528	22.7380	55.3213	356.202	127	H	4	S3	4.5		17.0	15.11-18.2 (15.4)	1.0-3.1 (1.2)
1001_009	Al Huwaysah 009	529	22.7575	55.4140	3407.797	119	H	6	S3	3.3	19.4			
1001_010	Al Huwaysah 010*	530	22.7487	55.4722	1411.791	2	UG				16.0	15.9	10.7	45.1
1001_011	Al Huwaysah 011	531	22.7598	55.3908	112.76	1	L	4-5	S4	1.0		21.4-23.6(22)	18.8	1.3
1001_012	Al Huwaysah 012	532	22.6775	55.3403	4694.9	1125	H	5	S1	4.0		17.9	15.8	1.4
1001_013	Al Huwaysah 013	533	22.6842	55.3365	55.512	1					19.5			
1001_014	Al Huwaysah 014	533	22.6860	55.3209	45.522	1	H	6	S1	3.3	19.0	18.2	17.9	1.4
1001_015	Al Huwaysah 015	533	22.6892	55.3209	35.295	1					19.0			
1001_016	Al Huwaysah 016	534	22.6981	55.3336	1330.939	332	H	5	S4	3.6		17.7	15.5	1.4
1001_017	Al Huwaysah 017	535	22.7385	55.3625	439.58	1	L	6	S4	1.0		22.9	19.5	2.3
1001_021	UaS 015	536	21.3453	55.4630	395.655	2	L	6	S1	4.5		24.2	20.3	1.7
1001_022	UaS 016	537	21.3439	55.4571	3.856	1	H	5	S2	4.5	19.9			
1001_023	UaS 017	537	21.3442	55.4551	61.312	1	H	3.2-6	S2	3.6	18.7	4.7-33.6 (17.8)	2.3-39.2 (15.9)	0.2-6.4 (1.4)
1001_024	UaS 018	538	21.2294	55.5169	97.48	2	H	5	S2	4.0	16.2			
1001_025	UaS 019	539	21.2295	55.5209	3.157	1	L	6	S4	3.0	24.9			
1001_026	UaS 020	540	21.2316	55.5211	1.362	1	L	6	S4	4.0		23.7	20.0	1.8
1001_027	UaS 021	538	21.2351	55.5348	101.979	10	H	5	S2	4.0	19.6			
1001_028	UaS 022	541	21.1382	55.5249	20.778	4	H	3.9	S2	3.6		17.4-18.4 (17.0)	15.7	1.1
1001_030	UaS 023	542	21.1427	55.5391	144.383		L	6	S4	2.0		23.4	20.1	1.4
1001_031	UaS 024*	543	21.1264	55.5261	406.812	1	Eucrite						62.5	5.5
1001_032	UaS 025	542	21.1254	55.5270	305.981	1	L	6	S4	2.0	25.1			
1001_033	UaS 026	542	21.1264	55.5370	255.825	1	L	6	S5	2.0	25.0			
1001_034	UaS 027	542	21.1130	55.5408	2907	1	L	6	S4	3.0	24.7			
1001_035	UaS 028	542	21.1133	55.5410	123.641	1	L				25.0			
1001_036	UaS 029	542	21.1107	55.5315	24.706	1	L	6	S4	2.0	25.4	23.7	16.3-23.2 (20.0)	1.2-1.7 (1.4)
1001_037	UaS 030	544	21.0917	55.5110	10.063	1	H	4-6	S3	3.0		17.1-20.7 (17.7)	15.5	1.0
1001_038	UaS 031	545	21.0236	55.5630	212.693	11	H	6	S2	3.6	19.7	17.7	15.2	1.4

Field number	Official name	PG	N [°]	E [°]	Mass [g]	Frag.	Class	P	S	WD	Fa (XRD)	Fa [mol%]	Fs [mol%]	Wo[mol%]
1001_039	UaS 032	546	21.0483	55.5737	4335.153	8	H	4	S2	1.0		17.0	15.3	1.1
1001_040	RaS 332	547	20.8042	55.4489	123.742	6	H	5	S2	3.6		17.7	15.7	1.6
1001_041	RaS 333	548	20.8023	55.4439	100.683	18	H	3.6	S1	4.5		17.7-19.7 (18.1)	7.3-24.3 (15.9)	0.5-4.2 (0.8)
1001_042	RaS 334	549	20.7827	55.4267	80.478	1	L	6	S2	3.3	25.9	24.2	20.3	1.7
1001_043	RaS 335	511	20.8010	55.4306	9.794	3	L	3.9	S3	4.0		14.2-26.5 (22.7)	4.5-29.5 (19.7)	0.4-2.8 (1.7)
1001_044	RaS 336	550	20.8085	55.4543	4.917	1	H	6	S3	3.3		18.6	16.4	1.5
1001_045	RaS 337	548	20.8140	55.4618	1119.842	8	H	3.6	S2	3.6	21.6	17.2-20.1 (18.1)	6.9-19.1 (10.6)	0.2-2.6 (0.5)
1001_046	RaS 338	548	20.8027	55.4668	934.7	1	H	3.6	S2	3.3		6.3-19.3 (18.1)	5.3-19.0 (12.9)	0.3-2.0 (0.7)
1001_047	RaS 339	551	20.7988	55.4621	1035.808	2	H	3.6-6	S3	1.0	18.7	0.5-28.2 (18.0)	6.5-17.9 (15.7)	0.3-1.9 (1.4)
1001_048	RaS 340	552	20.7932	55.4649	414.116	1	L	6	S4	4.0	26.1	24.2	20.5	1.5
1001_049	RaS 341	553	20.7872	55.4548	325.37	1	L	6	S1	1.0	25.9	24.0	20.2	1.9
1001_050		503	20.7658	55.4368	7.054	1	Brachinite				34.7			
1001_051	RaS 342	554	20.7603	55.4334	519.308	1	H	4	S1	4.5		17.1	15.3	1.2
1001_053	RaS 343	555	20.4952	55.5244	1192.001	7	H	5	S2	3.3		17.4	15.7	1.4
1001_054	RaS 344	556	20.4702	55.5262	41.493	1	H	5	S1	4.5		17.8	15.7	1.3
1001_055	RaS 345	557	20.4739	55.5179	226.85	1	H	6	S1	3.0	20.2			
1001_056	RaS 346	448	20.4948	55.5363	178.931	64	H	4	S2	3.6		17.7	16.0	1.2
1001_057	RaS 347	558	20.4941	55.5590	37.667	1	H	6	S6	3.6	19.9			
1001_058	RaS 348	559	20.4377	55.8837	30.995	1	L	6	S4	4.0	24.1			
1001_059	RaS 349	560	20.3861	55.7903	16.97	1	H	7	S1	4.0	18.3	17.7	16.2	3.7
1001_060	RaS 350	561	20.3843	55.7013	47.708	1	H	5	S2	3.0		17.6	15.7	1.2
1001_061	RaS 351	562	20.3833	55.7036	5.18	1	L	6	S4	3.3		23.7	20.1	1.4
1001_062	RaS 352	563	20.3837	55.7042	34.895	1	L	6	S2	3.6	24.3	23.6	20.1	1.4
1001_063	RaS 353	564	20.3609	55.6722	143.602	1	H	5	S2	3.3	17.9			
1001_064	RaS 354	565	20.3178	55.5940	3873.793	12	H	6	S1	3.0	19.6	17.2	15.4	1.3
1001_065	RaS 355	566	20.3409	55.5512	61.021	1	H	5	S3	2.0	18.5	17.6	15.4	1.3
1001_066	RaS 356	567	20.4215	55.5630	39.13	9	L	5	S3	3.0	24.8			
1001_067	RaS 357	568	20.4318	55.5332	2781.181	2	L	6	S3	3.0	25.3	22.2	18.1	1.4
1001_068	RaS 358	569	20.4492	55.5737	17.631	1	L	6	S3	3.3	24.7			
1001_069	RaS 359	570	20.4545	55.5823	4.913	1	H	6	S3	3.0		18.6	16.6	1.3
1001_070	RaS 360	571	20.4760	55.5943	5.507	1	H	4	S1	4.0		17.6	15.7	1.2
1001_071	RaS 361	572	20.4814	55.5951	229.648	2	L	5	S3	3.3	26.1	24.1	20.4	1.5
1001_072	RaS 362	573	20.5051	55.7614	69.762	2	L	6	S3	3.6	24.5			
1001_073	RaS 363	574	20.5058	55.8318	611.62	9	H	6	S1	4.0	19.2			
1001_074	RaS 364	574	20.5089	55.8360	334.458	2	H	6	S1	4.0	19.0			
1001_075	RaS 365	575	20.5111	55.8379	229.46	7	H	5	S2	4.0	20.0			
1001_076	RaS 366	576	20.5211	55.8526	15.8	1	L	4-5	S3-6	3.0		20.2-24.3 (22.9)	18.5-21.1 (19.3)	0.8-1.9 (1.2)

Field number	Official name	PG	N[°]	E[°]	Mass [g]	Frag.	Class	P	S	WD	Fa (XRD)	Fa [mol%]	Fs [mol%]	Wo[mol%]
1001_077	RaS 367	577	20.5194	55.8529	352.778	4	H	4-6	S3	3.6		17.8-21.4 (18.6)	16.3	1.4
1001_078	RaS 368	575	20.5102	55.8357	172.467	2	H	5	S1	3.6	18.0			
1001_079	RaS 369	575	20.5121	55.8362	129.431	2	H	5	S1	4.0	17.6			
1001_080	RaS 370	443	20.5063	55.8251	182.417	1	LL	6	S2	3.6	28.3	26.2	21.9	2.0
1001_081	RaS 371	443	20.5042	55.8291	61.029	3	LL	6	S2	4.0	28.3	26.5	21.9	2.1
1001_082	RaS 372	575	20.5060	55.8285	123.772	5	H	5	S2	4.0	18.4	18.5	16.1	1.6
1001_083	RaS 373	443	20.5080	55.8271	52.292	2	LL	6	S2	3.3	26.8	26.4	22.0	1.7
1001_084	RaS 374	575	20.5002	55.8343	156.482	4	H	3.7	S2	4.0	20.0	16.5-19.3 (18.4)	14.1-17.2 (16.2)	0.5-1.7 (1.6)
1001_085	RaS 375	576	20.4949	55.8511	31.944	1	L	3.9-5	S2-6	3.0		21.8-24.2 (22.9)	19.6	1.3
1001_086	RaS 376	578	20.5253	55.9686	193.773	3	H	6	S1	2.0	19.1	17.5	15.6	1.5
1001_087	RaS 377	579	20.5463	56.0137	416.268	1	H	4	S1	4.0		16.4	14.5	0.7
1001_088	RaS 378	580	20.5726	56.0550	1649.207	3	H	5	S2	3.0		17.6	15.7	1.2
1001_089	RaS 379	581	20.5760	56.0505	126.733	1	L	6	S3	3.3	24.3			
1001_090	RaS 380	582	20.5880	56.1226	457.881	1	H	5	S3	2.0	19.3			
1001_091	RaS 381	583	20.5681	56.2814	1628.1	1	L	6	S3	3.3		23.8	20.2	1.5
1001_092	RaS 382	584	20.1309	56.2763	11.332	1	L	6	S3	4.0		24.0	20.3	1.5
1001_093	RaS 383	585	20.1179	56.3945	266.014	8	H	3.6	S5 / S2	3.0		13.5-28.7 (17.6)	1.9-17.2 (15.8)	0.2-4.6 (1.2)
1001_094	SaU 532	586	20.1345	56.5898	99.668	9	L	6	S4	4.0	25.4	24.0	20.1	1.5
1001_095	SaU 533	587	20.2665	56.5165	146.352	1	L	6	S3	4.0		23.8	20.2	1.7
1001_096	SaU 534	588	20.3806	56.5934	49.658	1	L	6	S5	3.3		23.6	20.1	1.3
1001_097	SaU 535	160	20.4014	56.6383	318.213	1	H	5-6	S2	3.0	18.1	10.7-37.9 (29.7)		
1001_098	JaH 642	589	19.4258	56.5948	219.724	19	LL	3-6	S3	3.3	27.7		24.4	2.5
1001_099	JaH 643	590	19.6059	56.6998	132.809	1	LL	6	S2	3.3	30.0	29.0	23.9	2.1
1001_100	JaH 644	591	19.8122	56.6706	2272.814	4	L	6	S6	3.0	25.0	24.2	20.5	1.7
1001_101	RaS 384	145	20.0049	56.4047	5026.679	29	Mesosiderite							
1001_102	RaS 385	592	20.0547	56.4619	2275.314	5	LL	3.3	S1	3.6	31.0	2.3-40.7 (22.4)	2.6-29.6 (18.9)	0.2-10.6 (1.3)
1001_103	RaS 386	593	20.0587	56.4649	254.271	1	H	6	S3	3.0	18.2			
1001_104	JaH 645	594	19.4383	56.6080	3030.051	15	H	5	S1	3.3	20.3			
1001_105	JaH 646	595	19.5188	56.6660	3020.51	35	H	4	S2	3.6		17.1-20.7 (18.0)	15.8	1.2
1001_106		86	19.6790	56.6396	1342.3	1	L				25.5			
1001_107	JaH 647	596	19.8200	56.6604	365.596	7	L	6	S4	4.0	26.3	24.0	20.4	1.5
1001_108	JaH 648	597	19.4018	56.5659	1577.866	35	H	4	S2	3.6		17.6	15.5	1.1
1001_109	JaH 649	598	19.4694	56.5578	15.946		L	6	S4	4.0		23.9	20.0	1.8
1001_110	JaH 650	599	19.5054	56.5433	868	1	H	5	S2	3.3	17.9			
1001_111	JaH 651	600	19.6811	56.4510	207.619	1	H	3.9	S1	3.6		16.6	15.0	1.2
1001_112	JaH 652	601	19.6810	56.4512	242.352	1	H	4-6	S2	3.6		18.5	16.4	1.3

Field number	Official name	PG	N [°]	E [°]	Mass [g]	Frag.	Class	P	S	WD	Fa (XRD)	Fa [mol%]	Fs [mol%]	Wo[mol%]
1001_113	JaH 653	602	19.7328	56.3829	57.604	1	H	5	S3	3.3		18.0	15.9	1.5
1001_114	RaS 387	603	20.0160	55.6151	49.648	14	H	4	S1	4.5		17.1	15.3	0.7
1001_115		603	20.0166	55.6171	0.759	1								
1001_116	RaS 388	604	20.0132	55.6190	3.46	2	L	6	S4	4.0	20.4	23.4	20.0	1.4
1001_117		603	20.0134	55.6193	1.323	1								
1001_118	RaS 389	605	20.0513	55.6306	785.1	1	L	4-6	S2-3	3.0		22.1-27.1 (22.45)	18.8-21.6 (19.45)	0.8-1.9 (1.3)
1001_119	RaS 390	606	20.0949	55.6932	0.686	1	H	3.8-6	S3	3.0		17.9	15.7	1.3
1002_120	RaS 391	607	20.0944	55.6862	21.954	1	H	6	S1	4.0	20.6	18.7	16.6	1.4
1002_121			20.1454	55.7085	0.27	1								
1002_121A		608	20.1455	55.7083	0.519	1								
1002_121B		608	20.1455	55.7084	0.343	1								
1002_121C		608	20.1458	55.7085	0.613	2								
1002_121D		608	20.1457	55.7086	0.231	1								
1002_121E		608	20.1457	55.7085	1.104	1								
1002_121F		608	20.1458	55.7087	0.125	1								
1002_121G		608	20.1455	55.7089	1.007	1								
1002_121H	RaS 392	609	20.1450	55.7095	0.399	1	H	4	S2	3.6		17.3	16.2	1.2
1002_121I	RaS 393	610	20.1460	55.7094	2.243	1	H	6	S2	3.6		18.5	16.3	1.3
1002_121J		608	20.1457	55.7092	0.344	1								
1002_121K		608	20.1464	55.7086	0.151	1								
1002_121M		608	20.1466	55.7097	0.394	1								
1002_121N	RaS 394	609	20.1472	55.7096	0.182	1	H	4	S3	3.6		18.0	16.0	1.3
1002_123	RaS 395	608	20.1469	55.7092	982.476	3	L	6	S5	4.0	23.4			
1002_124	RaS 396	611	20.1469	55.7091	30.291	1	H	4	S2	3.3		17.8	15.9	1.1
1002_125	RaS 397	608	20.1465	55.7091	1118.758	273	L	6	S5	4.0	23.7	23.2	20.2	1.9
1002_126	RaS 398	608	20.1467	55.7098	289.633	23	L	6	S5	4.0	22.5	23.6	20.1	1.9
1002_127	RaS 399	612	20.1512	55.7093	6319	1	L	6	S2	3.3		24.1	20.5	1.5
1002_128	RaS 400	613	20.1919	55.6796	11.61	1	H	6	S4	4.0		18.3	15.8	1.7
1002_129	RaS 401	614	20.1876	55.6676	473.786	1	L	3.8	S2	3.3		19.6-24.5 (23.5)	19.7	0.8
1002_130	RaS 402	615	20.1451	55.7680	100.936	1	H	4	S3	3.3	19.5	18.1	15.9	1.3
1002_131		615	20.1440	55.7682	185.058	1	H				18.6			
1002_132		615	20.1440	55.7683	75.463	2	H				19.0			
1002_133		615	20.1442	55.7689	0.178	1	H				18.5			
1002_134		615	20.1455	55.7683	27.896	1	H				18.4			
1002_135		615	20.1421	55.7656	208.248	1	H				18.7			
1002_136		615	20.1451	55.7667	81.134	1	H				19.0			
1002_137		615	20.1454	55.7668	25.226	1	H				18.6			
1002_138	RaS 403	616	20.2173	56.0167	1.253	1	H	4	S3	3.6		16.8	14.9	1.0
1002_139	RaS 404	617	20.2208	56.0201	0.609	1	H	6	S2	4.0		19.0	16.7	1.5
1002_140	RaS 405	618	20.2200	56.0204	0.264	1	L	6	S5	3.3		23.9	20.2	1.3
1002_141	RaS 406	619	20.2191	56.0209	0.512	1	H	5	S2	3.6		16.9	15.2	1.1

Field number	Official name	PG	N [°]	E [°]	Mass [g]	Frag.	Class	P	S	WD	Fa (XRD)	Fa [mol%]	Fs [mol%]	Wo[mol%]
1002_142	RaS 407	617	20.2206	56.0207	0.684	1	H	6	S2	4.0		19.0	16.6	1.4
1002_143	RaS 408	617	20.2179	56.0212	0.368	1	H	6	S2	4.0		18.7	16.5	1.3
1002_144	RaS 409	617	20.2176	56.0213	0.269	1	H	5	S2	4.0		19.1	16.8	1.4
1002_145	RaS 410	619	20.2167	56.0217	0.281	1	H	5	S2	3.6		18.0	16.0	1.3
1002_146	RaS 411	620	20.2024	56.0326	1.021	1	H	5	S2	3.3	19.1			
1002_147	RaS 412	619	20.2027	56.0323	0.257	1	H	5	S2	3.6		18.1	15.7	1.1
1002_148	RaS 413	621	20.3312	56.1962	149.983	1	L	5	S4	3.3	25.5	24.0	20.3	1.9
1002_149	RaS 414	622	20.3414	56.2058	212.821	1	H	5	S2	3.0		18.4	16.5	1.4
1002_150	RaS 415	623	20.3351	56.2024	1.018	1	H	4	S2	3.6		17.8	15.4	1.5
1002_151	RaS 416	623	20.3353	56.2026	385.761	3	H	5	S1	3.6	19.5	18.0	15.9	1.4
1002_152	RaS 417	623	20.3341	56.2037	297.922	1	H	5		4.0	18.2	17.0	14.7-17.5	1.1-2.2
									S2				(15.2)	(1.3)
1002_153	RaS 418	624	20.3936	56.2200	28791.143	917	L	6	S5	4.0	24.9	24.0	20.2	1.7
1002_154	RaS 419	625	20.4469	56.2549	122.209	1	L	6	S3	2.0		24.1	20.1	1.7
1002_155	RaS 420	624	20.4195	56.2737	1556.572	19	L				25.6			
1002_156	RaS 420*	626	20.4171	56.2749	70.298	1	Ureilite					20.2	16.8	8.0
1002_157		624	20.4164	56.2745	1162.608	6	L				24.8			
1002_158		624	20.4161	56.2750	1050.336	74	L				24.7			
1002_159		624	20.4228	56.2763	301.48	2	L				24.1			
1002_160	RaS 421	624	20.4246	56.2782	2840.625	187	L	6	S5	3.3	25.5			
1002_161		624	20.4415	56.3008	198.397	27	L				24.6			
1002_162		624	20.4411	56.3000	196.52	13	L				25.1			
1002_163		624	20.4410	56.3052	173.201	1	L				24.7			
1002_164		624	20.4525	56.3159	361.932	1	L				24.7			
1002_165	RaS 422	627	20.5052	56.4844	3878.815	4	H	3.7-5	S3	3.6	19.5	6.4-27.4 (18.1)	4.4-21.0 (16.1)	0.3-5.3 (1.5)
1002_166	RaS 423	627	20.4992	56.4982	230.3	2	H	3.4-5	S3	3.6		0.4-26.7 (17.7)	2.1-24.1 (16.4)	0.3-3.3 (0.5)
1002_167	SaU 536	628	20.5374	56.9892	412.784	3	H	5	S2	3.6	18.7	18.0	16.0	1.6
1002_168	Hayy 001	629	20.8413	57.6300	4208.471	231	H	5	S3	3.6		17.9	15.9	1.3
1002_169	RaW 045	630	21.3686	58.3955	85.275	1	H	6_IM	S6	3.6	19.9	16.3	14.8	1.1
1002_170	RaW 046	631	21.3374	58.4024	136.987	1	L	6	S4	3.0	25.8	24.2	20.4	1.3

PG: Pairing number, each pairing group has an individual number.
Frag.: Number of fragments, counted during unpacking.
P: Petrologic type, S: Shock classification, WD: Weathering degree.
Fa (XRD) is in [mol%].
UG: Ungrouped.
IM: Impact melt.
* See Meteoritical Society database for more details (http://www.lpi.usra.edu/meteor/metbull.php).

Erklärung

gemäss Art. 28 Abs. 2 RSL 05

Name/Vorname: Zurfluh/Florian J.

Matrikelnummer: 03-131-885

Studiengang: Doktorat Phil.-nat. (Erdwissenschaften)

    Dissertation

Titel der Arbeit: Quantification of terrestrial weathering and contamination in
Meteorites recovered in the Sultanate of Oman

Leiter der Arbeit: PD Dr. Beda A. Hofmann
PD Dr. Edwin Gnos
Dr. Urs Eggenberger

Ich erkläre hiermit, dass ich diese Arbeit selbständig verfasst und keine anderen als die angegebenen Quellen benutzt habe. Alle Stellen, die wörtlich oder sinngemäss aus Quellen entnommen wurden, habe ich als solche gekennzeichnet. Mir ist bekannt, dass andernfalls der Senat gemäss Artikel 36 Absatz 1 Buchstabe o des Gesetzes vom 5. September 1996 über die Universität zum Entzug des auf Grund dieser Arbeit verliehenen Titels berechtigt ist.

…………………………………..
Ort/Datum

....
Unterschrift

Curriculum vitae

Personal Information

Full name:	Florian J. Zurfluh
Date of birth:	March 05, 1984
Place of birth:	Schattdorf, UR
For a portrait see:	http://imca.cc/insights/2011/IMCA-Insights09.htm

Education

Since 2008	Doctorate	Geology, University of Bern „Quantification of terrestrial weathering and contamination in meteorites recovered in the Sultanate of Oman"
2006 – 2008	Master	Geology, University of Bern „Meteorites in the Sultanate of Oman – Effects of terrestrial weathering in the Jiddat al Harasis (JaH) 091 Strewnfield"
2003 – 2006	Bachelor	Geology, University of Bern „Vergleich der beiden Niedermendiger Lavaströme, Osteifel (D)"
1997 – 2003	Matura	Physics and applied mathematics, Kantonale Mittelschule Uri, Altdorf

Publications

Peer-reviewed articles

Zurfluh F. J., Hofmann B. A., Gnos E., and Eggenberger U. (2011) Evaluation of the utility of handheld XRF in meteoritics. *X-Ray Spectrometry* 40, 449-463.

Zurfluh, F. J., Hofmann, B. A., Gnos, E., and Eggenberger, U., in review. "Sweating meteorites" - water-soluble salts and temperature variation in ordinary chondrites and soil from the hot desert of Oman. *Meteoritics & Planetary Science*.

Zurfluh, F. J., Hofmann, B. A., Gnos, E., Eggenberger, U., and Jull, A. J. T., in review. Terrestrial age estimation of ordinary chondrites from Oman based on a refined weathering scale and other pysical and chemical weathering parameters. *Meteoritics & Planetary Science*.

Popular article

Zurfluh F. J., Hofmann B. A., Gnos E., Eggenberger U., Greber N. D., and Villa I. M. (2012) Weathering and Strontium Contamination of Meteorites Recovered in the Sultanate of Oman. *Meteorite* 18, 34-38.

Conference presentations (Talks and posters):

Zurfluh, F. J., Hofmann, B. A., and Gnos, E., 2008. Effects of terrestrial weathering in the JaH 091 strewnfield in Oman – water-soluble salts. *Paneth Colloquium.*

Zurfluh, F. J., Hofmann, B. A., Gnos, E., and Eggenberger, U., 2009. Applications of handheld XRF analysis in meteoritics. *72th Annual Meeting of the Meteoritical Society.*

Zurfluh, F. J., Hofmann, B. A., Gnos, E., Eggenberger, U., and Opitz, C., 2009. Approximate terrestrial age dating of meteorites by use of handheld XRF. *7th Swiss Geoscience Meeting.*

Zurfluh, F. J., Hofmann, B. A., Gnos, E., and Eggenberger, U., 2010. What stories tell us 300 s measurements of meteorite surfaces with HandheldXRF (HXRF)? *Paneth Colloquium.*

Zurfluh, F. J., Hofmann, B. A., Gnos, E., and Eggenberger, U., 2010. Water-soluble salts and temperature variation in meteorites recovered in the hot desert of Oman. *8th Swiss Geoscience meeting.*

Zurfluh, F. J., Hofmann, B. A., Gnos, E., Eggenberger, U., Janots, E., and Greenwood, R. C., 2010. RaS 309: The first Brachinite from the Sultanate of Oman. *Paneth Colloquium.*

Zurfluh, F. J., Hofmann, B. A., Gnos, E., Eggenberger, U., and Preusser, F., 2011. Whend did the large meteorite shower Jiddat al Harasis 091 arrive on Earth? *9th Swiss Geoscience Meeting.*

Zurfluh, F. J., Hofmann, B. A., Gnos, E., Eggenberger, U., Villa, I. M., Greber, N. D., and Jull, A. J. T., 2011. New Insights into the Strontium Contamination of Meteorites. *Meteoritics & Planetary Science* 46:A264. *74th Annual Meeting of the Meteoritical Society.*

Zurfluh, F. J., Hofmann, B. A., Gnos, E., Eggenberger, U., Villa, I. M., Greber, N. D., and Jull, A. J. T., 2012. Chemical and physical weathering of meteorites recovered in the desert of the Sultanate of Oman. *International Conference on the Geology of the Arabian Plate and the Oman Mountains.*
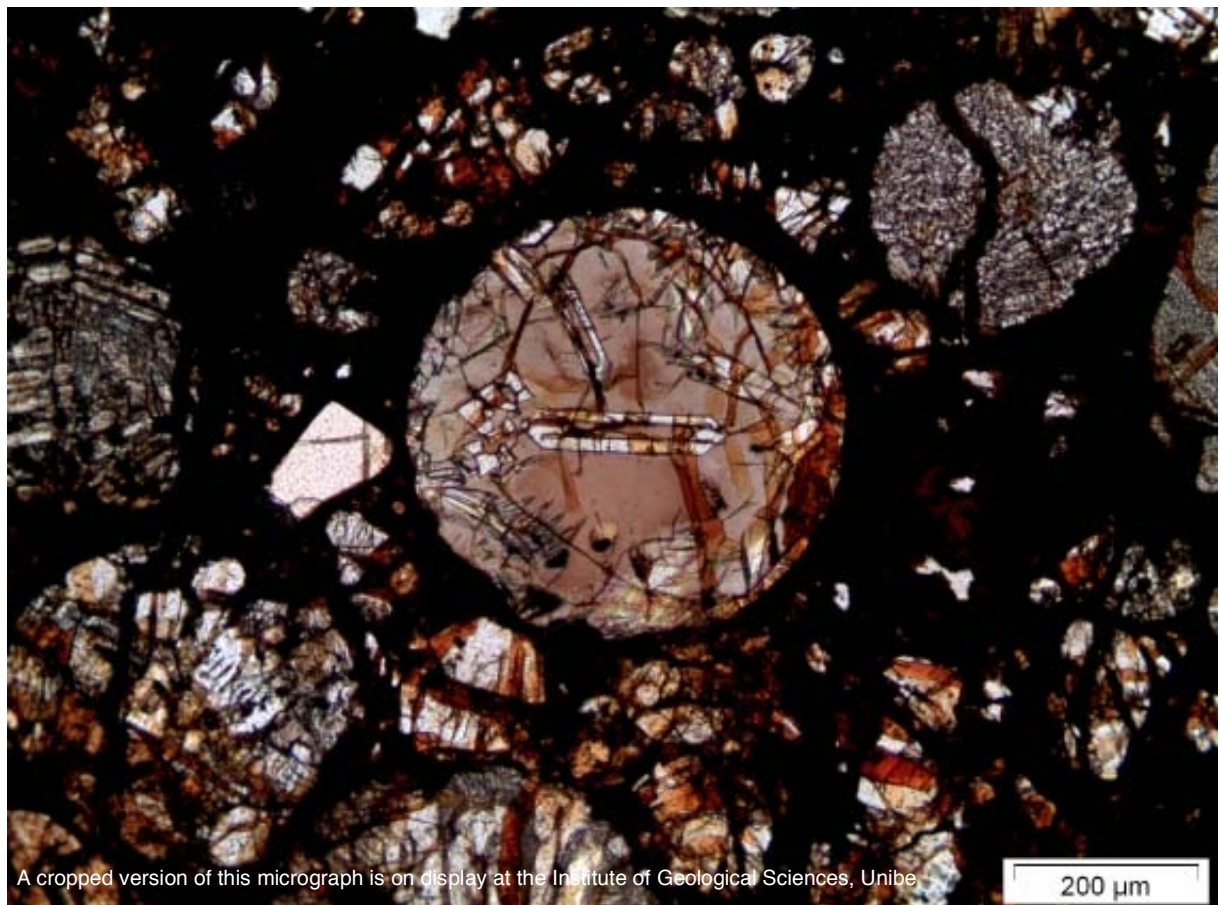
A cropped version of this micrograph is on display at the Institute of Geological Sciences, Unibe

200 µm

Transmitted light microscopy image of a glass bearing chondrule of RaS 337, H3.6 S2 WD3.6.

The photo will be used in the new meteorite-exhibition at the Natural History Museum of Vienna

What stories can tell us RaS 399, L6 S2 WD3.3?